SCUOLA NORMALE SUPERIORE

Classe di Scienze

Corso di perfezionamento in

Neuroscienze

XXXIII ciclo

Pupillometry measures for tracking brain function in health and disease

Candidato

dr.ssa Aurelia Viglione

A mamma, papà e ai miei fratelli

Contents

Preamble and object of the thesis

The size of our pupils changes continuously in response to variations in ambient light levels to regulate the amount of light that reaches the retina for optimizing vision. However, even when exposed to isoluminant conditions, fluctuations in pupil size can be influenced by attention and cognitive processes (Granholm et al. 2004; Kahneman et al. 1966; Nassar et al. 2012; Schmidt et al. 1982). Pupillary dilation has been indeed documented for nonvisual factors such as fear or empathy (Harrison et al. 2007; Korn et al. 2017; Leuchs et al. 2017), arousal (the level of vigilance and alertness during wakefulness) and attention (whether one is focused on a task or not) (Binda et al. 2014; Hoeks et al. 1993). More in general it is possible to affirm that any stimulus able to activate the mind, or anything that increases the mind's 'processing load' causes the pupil to dilate (Beatty 1982; Mathôt 2018). Even the pupillary light reflex, i.e. the constriction of the pupil in response to brightness and the dilation of the pupil in response to darkness, has been shown to be influenced by factors related to the selection, processing, and interpretation of visual input (Castaldi et al. 2021; Mathôt et al. 2017; Mathôt et al. 2015). These findings demonstrate that pupillary constriction typically reflects the interpretation of light within a visual scene, extending beyond the simple quantification of physical light energy entering the eye (Binda et al. 2013b). Neurology first exploited the usefulness of monitoring changes in pupil size as a way to identify specific pathological processes within the nervous system. Recently, pupillometry, the science of measuring pupil size and its dynamic variations, has raised attention for its capacity to unravel several intriguing phenomena and holds significant promise for assessing directly and non-invasively the activity of the brain.

This doctoral thesis focuses on a comprehensive exploration of pupillometry, seeking to elucidate its role as a pivotal tool in understanding diverse aspects of cognition, emotion, and health. In particular, in my research I tried to explore the diverse aspects that make pupillometry a compelling area of study:

- Objective Measure: Pupil responses are objective and quantifiable, reducing the potential for subjective bias in research. This makes pupillometry a valuable tool for obtaining reliable data in the study of brain activity.
- Non-Invasive and Real-Time: Pupillometry is non-invasive and allows for real-time monitoring of brain activity. Unlike other methods, such as functional magnetic resonance imaging (fMRI) or positron emission tomography (PET) scans, which require significant equipment and can be uncomfortable for participants, pupillometry can be conducted with relatively simple and portable equipment.
- Autonomic Nervous System Reflection: The pupil is mainly controlled by the autonomic nervous system, which consists of the sympathetic and parasympathetic pathways. Changes

in pupil size reflect the balance between these two pathways. The sympathetic system dilates the pupils, while the parasympathetic system constricts them. This makes pupillometry a direct indicator of the autonomic nervous system activity.

- Neurotransmitter Activity: Pupillometry can provide insights into the activity of specific neurotransmitter systems. For instance, the dilation of pupils is associated with the release of norepinephrine in the brain. By measuring pupil responses, it is possible to indirectly assess the activity of these neurotransmitter systems and their role in brain function.
- Cognitive and Emotional Processes: Pupil size changes in response to cognitive and emotional stimuli. For example, when people engage in mentally demanding tasks or experience emotional arousal, their pupils tend to dilate. Conversely, during relaxation or low cognitive load, the pupils tend to constrict. These responses are known to be related to changes in neurotransmitter activity.
- Clinical Applications and Disease Diagnosis: Pupillometry shows promising results as a biomarker for various neurological and psychiatric disorders. Abnormal pupil responses have been reported in conditions such as traumatic brain injury, Alzheimer's disease, Parkinson's disease, and schizophrenia. These findings have the potential to aid in early diagnosis and monitoring of disease progression, offering valuable insights for clinical and preclinical studies.

I investigated these aspects in the first part of the thesis (Part I) as three different projects:

i The first study focused on the creation of a cutting-edge deep learning tool, called MEYE. MEYE is capable of real-time detection and quantification of alterations in pupil size and applies to both humans and mice across different experimental conditions. Notably, MEYE's innovation lies in the seamless integration of artificial intelligence algorithms into standard web browsers, affording non-technical operators the capacity to conduct cost-effective pupillometry assessments in clinical and pre-clinical research settings.

ii Several findings highlight the potential of pupillometry as a biomarker for neurological and psychiatric conditions, including arousal alterations in attention deficits (e.g. ADHD) and autism spectrum disorder (ASD). Therefore, my research investigated pupillary abnormalities in a mouse model of Cyclin-dependent kinase-like 5 (Cdkl5) deficiency disorder (CDD), a severe neurodevelopmental condition, characterized by early-onset seizures, intellectual disability, motor, and social impairment, providing insights into the functional implications of CDKL5 protein deficiency on attention and arousal. Moreover, the non-invasive nature of pupillometry and its applicability to non-collaborative and preverbal subjects make it a valuable tool for longitudinally evaluating disease progression and therapeutic efficacy in both preclinical and clinical investigations.

iii Finally, I explored the potential of pupillometry as a complementary method for the assessment and quantification of conditioned fear responses and as a non-invasive approach

to evaluate neural plasticity. In particular, I examined fear memories in mice lacking the cartilage link protein 1 (Crtl1) gene in the central nervous system, a condition that results in attenuated perineuronal nets (PNNs) but unchanged overall levels of chondroitin sulfate proteoglycans (CSPGs) in the adult brain. The study aimed to investigate whether preventing the aggregation of CSPGs into PNNs is sufficient to induce fear memory susceptible to erasure, while also evaluating the corresponding activation pattern. These results also contributed to a comprehensive understanding of the employment of pupillometry in studying neuronal and behavioral responses.

For the initial study, I contributed as a co-author (Mazziotti et al. 2021), while for the subsequent two studies, I held a co-first-authorship position (Viglione, Sagona et al. 2022, Poli, Viglione et al. 2023).

All these data have been published and the full articles are available at these links:

- MEYE: Web App for Translational and Real-Time Pupillometry.
- Behavioral Impulsivity is Associated with Pupillary Alterations and Hyperactivity in CDKL5 Mutant Mice.
- Selective Disruption of Perineuronal Nets in Mice Lacking Crtl1 is Sufficient to Make Fear Memories Susceptible to Erasure.

After establishing the critical importance of preserving the integrity of PNNs for memory maintenance in the first part of this thesis, the second part (Part II) delves into an exploration of the potential molecular and epigenetic mechanisms underlying their dynamic regulation. Previous work has demonstrated that during postnatal development, a specific family of microRNAs (miRNAs), the miR-29 family, experiences a dramatic upregulation with aging (Napoli et al. 2020; Mazziotti et al. 2017a). The miR-29a-3p, specifically, was the microRNA with the largest age-dependent upregulation. This upregulation has been linked with reduced plasticity in the visual cortex. Notably, the targets of the miR-29a are enriched in categories associated with the extracellular matrix, PNNs composition, and transcriptional regulation. In this study, I investigated the role of miR-29a in influencing the persistence of fear memories, with a specific focus on its modulation of the epigenetic landscape.

This part of the thesis represents a novel project that is still ongoing.

Introduction

0.1 Anatomy and neural correlates of the pupil

Light reaches the retina via the pupil, a central opening within the iris. The iris, the structure that determines eye color, contains the muscles responsible for regulating pupil size. As a dynamic structure, the pupil responds mainly to variation in light conditions by constricting or dilating. In bright sunlight, the pupil constricts to reduce the amount of light entering the eye (miosis), whereas when brightness decreases, it dilates to enable greater light admission (mydriasis). This phenomenon is referred to as pupillary light reflex (PLR). However, the pupil also reacts to near fixation (known as the pupillary near response) and dilates in response to heightened cognitive activity (Mathôt 2018). The diameter of the human pupil varies between 2-8 mm, while in mice pupil diameter varies between 0.4-2 mm.

The diameter of the pupil is controlled by two sets of muscles, the iris sphincter muscle constricts the pupil while the iris dilator muscle promotes pupil dilation. The iris sphincter muscle and the iris dilator muscle are controlled by two interconnected pathways of the autonomic nervous system: the parasympathetic constriction pathway and the sympathetic dilation pathway (Figure 0.1A). In the PLR, these circuits operate in response to changes in light levels. Specifically, pupil constriction primarily occurs due to parasympathetic activation, while in response to darkness, dilation is mainly driven by sympathetic activation. Light signals are transmitted by a class of photosensitive retinal ganglion neurons directly to the pretectal olivary nucleus in the brainstem (Hattar et al. 2002), which controls pupil size primarily via its projections to the Edinger–Westphal nucleus (EWN) (Steiger et al. 1979). In the EWN, cholinergic preganglionic motoneurons project to the ciliary ganglion of the third cranial nerve from which the ciliary nerve controls the iris sphincter muscle (Ruskell 1990; Strassman et al. 1987). Activation of projecting neurons in the EWN nucleus drives contraction of the iris sphincter muscle and constriction of the pupil while inhibition of EWN neurons relaxes the iris sphincter muscle, permitting dilation. The pupil dilation pathway is a subcortical pathway that starts at the hypothalamus and the locus coeruleus (LC). The dilator pathway comprises sympathetic innervation of the pupil, originating from neurons located in the intermediolateral cell column of the cervical and thoracic spinal cord (Strack et al. 1990). This input leads to the activation of the superior cervical ganglion, which subsequently provides direct innervation to the dilator muscle.

Notably, the pupil's function extends beyond its role as a mere regulator of light; it also undergoes changes associated with emotional states like fear or empathy (Leuchs et al. 2017; Harrison et al. 2007; Korn et al. 2017), mental states such as attention levels and arousal (Hoeks et al. 1993; Binda et al. 2014), and unexpected environmental stimuli (Figure 0.1B). These alterations in pupil size are believed to be influenced, at least in part, by neuromodulators like norepinephrine (NE), acetylcholine, dopamine, and serotonin (5-HT). Rather than driving

neuronal activity directly, these neurotransmitters act as modulators, regulating the ongoing neural processes. Consequently, fluctuations in pupil size that coincide with environmental factors or behavioral states are often considered indicative of neuromodulator levels within the brain.

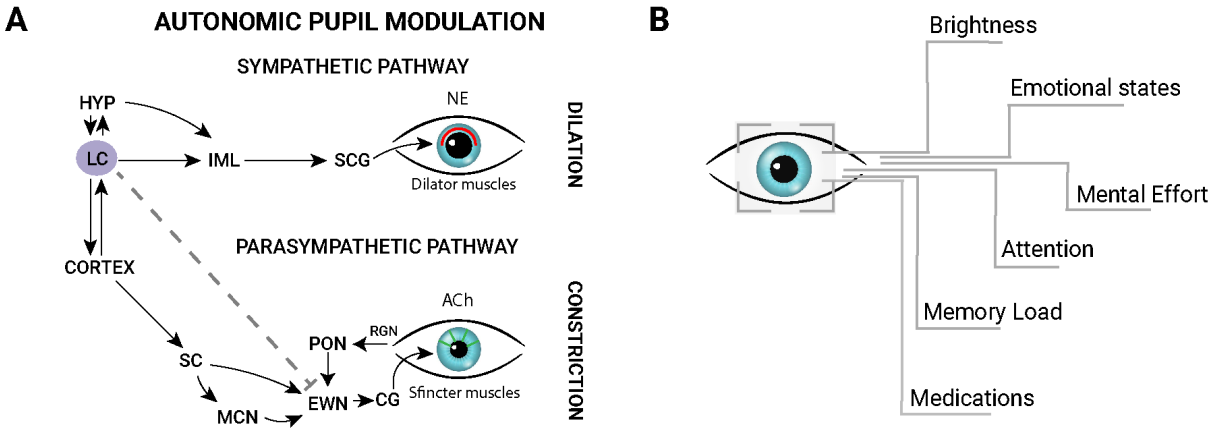

Figure 0.1: **Sources of pupil size modulation**. **(A)** The pupil constriction and dilation pathways. The iris of the eye contains two muscles that control its size: the sphincter muscle and the dilator muscle. The size of the iris is regulated by two interconnected neural pathways: the parasympathetic constriction pathway and the sympathetic dilation pathway. The parasympathetic constriction pathway originates in the EWN, which via cholinergic preganglionic motoneurons, sends its axons to synapse on the sphincter muscle. This pathway causes sphincter muscle contraction, leading to constriction of the pupil. The Superior Colliculus also controls pupil constriction through both a direct and indirect pathway: Certain SC neurons project directly to the EWN, while a second indirect pathway involves SC projections to the mesencephalic cuneiform nucleus, which influences parasympathetic tone via projections to the EWN. The sympathetic dilation pathway originates in the SCG and sends axons to synapse on the dilator muscle. This pathway causes the dilator muscle relaxation, leading to pupil dilation. The LC plays a key role in regulating the sympathetic nervous system, including the sympathetic dilation pathway that controls pupil size. The LC is responsible for releasing the neurotransmitter NE, which acts on the dilator muscle and regulates pupil size. Activation of the LC leads to the dilation of the pupil, and inhibition of the LC leads to constriction of the pupil. Additionally, studies have shown that the LC-NE system regulates the pupillary light reflex, which is the automatic response of the pupil to changes in light intensity. **(B)** Exogenous factors influencing pupil size. PON, pretectal olivary nucleus; RGN, retinal ganglion neurons; HYP, hypothalamus; LC, locus coeruleus; SC, superior colliculus; MCN, mesencephalic cuneiform nucleus; EWN, Edinger-Westphal nucleus; CG, ciliary ganglion; IML, intermediolateral cell column of the spinal cord; SCG, superior cervical ganglion; NE, norepinephrine; ACh, acetylcholine; Figure adapted from Viglione et al. 2023

0.1.1 Noradrenergic control of pupil size

The LC is a small nucleus located in the dorsal tegmentum with a high level of complexity in terms of its molecular, cellular, and regional targets. As all neurons in the LC contain NE, the LC serves as the foremost source of NE in the forebrain, projecting widely to both cortical and subcortical regions (Szabadi 2013; Benarroch 2018). The widespread distribution of noradrenergic fibers in the neocortex indicates that the projections from the LC exert a broad influence on this area (Morrison et al. 1979). This extensive LC modulation of the cortex underlies the role of the LC in controlling brain state, such as arousal (Carter et al. 2010;

Susan J Sara et al. 2012), locomotion (Polack et al. 2013), exploration (Gompf et al. 2010), and attention (Bouret et al. 2004).

The LC controls pupil dilation by directing projects to the IML region, facilitating excitatory sympathetic activation through α1 adrenergic receptors (Szabadi 2018; M. S. Smith et al. 1999). Additionally, the LC can exert indirect sympathetic influence by reciprocal connections with the hypothalamus, which, in turn, projects to the IML (Szabadi 2018; Nunn et al. 2011) (Fig. 1A). It has also been proposed that LC could act directly on neurons in the EWN, with NE (Breen et al. 1983) binding the inhibitory α2-adrenergic receptors (M C Koss 1986). However, the existence of a direct pathway is still controversial (Nieuwenhuis et al. 2011).

There is extensive evidence of functional relationships between LC activity and pupil dilation which can occur in the absence of the PLR. In humans, fMRI studies combined with pupillometry measures have shown that LC activity increases together with pupil size during behavioral tasks and in resting (Gee et al. 2017). In another fMRI study involving humans performing an oddball task, changes in pupil size were observed to covary with the blood-oxygen-level-dependent (BOLD) signal localized in the LC (Murphy et al. 2014). Moreover, the electrical stimulation of LC in anesthetized and awake animals evokes pupil dilation (Joshi et al. 2016; Reimer et al. 2016; Privitera et al. 2020) (Figure 0.2B). These data support the idea of a direct coupling between the LC and pupil diameter. A recent study has investigated the accuracy by which pupil size can be used to index LC activity in mice (Megemont et al. 2022). The authors recorded spiking activity from LC neurons optogenetically tagged and pupil diameter in head-fixed mice trained to perform a tactile detection task. Although pupil diameter was found to have a positive and monotonic relationship with LC spiking activity, they found that identical optical LC stimulations evoked variable pupil responses on each trial (Megemont et al. 2022). This variability in the LC-pupil coupling may be linked to the involvement of other brain areas or neuromodulatory systems in controlling pupil fluctuations (Joshi et al. 2016; Reimer et al. 2016) (Figure 0.2A-B). For example, sustained activity in cholinergic axons is observed during longer-lasting pupil dilations, such as those occurring during locomotion (Reimer et al. 2016) (Figure 0.2B-C). In addition, phasic stimulation of the dorsal raphe serotonergic nuclei can also regulate pupil size and reactivity to sensory stimulation (Cazettes et al. 2021). Other studies suggest that pupil fluctuations can be influenced by hormonal changes (Leknes et al. 2013; Prehn et al. 2013). Several medications and drugs of abuse [such as selective serotonin reuptake inhibitors (SSRI) and Opioids] may affect pupillary size and spontaneous fluctuations (J. A. J. Schmitt et al. 2002; Dhingra et al. 2019). These factors must be taken into account when interpreting results, in particular in non-drug-free clinical populations. Task-related variables can also influence pupillary variability. Pupil dilation can occur in response to unexpected stimuli (orienting response), expectation violation, and cognitive processes (Kahneman et al. 1966; Qiyuan et al. 1985; Alnæs et al. 2014; Gee et al. 2014; C.-A. Wang et al. 2014) (Figure 0.1C). Transient pupil dilations are typically linked to phasic LC firing (Aston-Jones et al. 1994), but some factors, such as stimulus salience, are associated with shifts of attention and likely also related to superior colliculus activation (C.-A. Wang et al. 2012). Additionally, other cortical regions like the anterior cingulate cortex and the orbitofrontal cortex are involved in pupil dynamics (Hayden et al. 2011; Padoa-Schioppa et al. 2017). However, LC activation reliably anticipates changes in pupil diameter with an early

latency compared with other regions showing a similar relationship with pupil size (Joshi et al. 2016). The interconnectivity between these regions and the LC suggests that fluctuations in pupil size could be a result of the LC regulation of neural activity across those areas of the brain.

0.1.2 Other sources of neuromodulatory control

Cholinergic neurons in the basal forebrain, much like NE neurons, exhibit activity during various physiological events, including pupil dilation, transitions between sleep and wakefulness, moments of whisking in rodents, and following mildly aversive stimuli like an air puff (Larsen et al. 2018). Similarly, the activity of cholinergic neurons, measured using calcium indicators expressed in cortical cholinergic axons, increases during pupil dilation and decreases during constriction (Nelson et al. 2016; Reimer et al. 2016). Several lines of research have also paved the way for investigating dopamine's involvement in regulating pupil size. Studies conducted across non-human animal models, patient cohorts, and adult neuroimaging investigations have collectively established connections between reward-related striatal dopamine activity and the alteration observed in pupil diameter (Eckstein et al. 2017; Tummeltshammer et al. 2019; Muhammed et al. 2016; Sg et al. 2015). In addition, pupil abnormalities have been frequently documented in people affected by Parkinson's disease (Micieli et al. 1991; You et al. 2021). Nevertheless, the exact nature of dopamine's influence on pupil responses remains to be clarified. These modulations may occur through interactions with the LC. The LC and dopaminergic midbrain structures exhibit dense reciprocal connections and receive a shared top-down projection from the prefrontal cortex (Susan J. Sara 2009). Moreover, both systems play distinct yet significant roles in reward learning and motivational behavior (Varazzani et al. 2015). A recent study has demonstrated an association between 5-HT and pupil dilation during goal-directed behaviors. In this study, Cazettes et al. (Cazettes et al. 2021) trained head-fixed mice to forage for water from two sources. Mice could decide to drink from one of two resource sites. In particular, mice were trained to remain still during licking and to run on a treadmill to switch from one site to another. Reward delivery at a given site was probabilistic. They observed transient pupil dilations during various conditions, including stillness, locomotion, and licking. Interestingly, optogenetic stimulation of 5-HT neurons in the dorsal raphe nucleus resulted in reliable pupil dilations, particularly when temporally aligned with lick periods. Their model revealed that pupil size changes were associated with stimulation, regardless of arousal or global indicators of brain state. To investigate further, the researchers examined the impact of reward uncertainty on pupil size changes induced by 5-HT stimulation. They manipulated reward uncertainty in a foraging task, finding that 5-HT stimulation caused larger transient pupil dilations in low-uncertainty conditions compared to high-uncertainty conditions. This suggested that the effect of 5-HT on pupil size acts as a prediction-error signal, and is modulated by uncertainty. While locomotion also influenced pupil size, it was not dependent on 5-HT stimulation. Fluctuations in pupil size, along with locomotion, have conventionally been used to assess arousal levels. However, recent evidence suggests that these pupil fluctuations carry additional information related to cognitive factors beyond mere arousal (Jepma et al. 2011; Nieuwenhuis 2011; Filipowicz et al. 2020). These cognitive aspects, such as expectation violation and prediction error, are associated with neural computations in regions like the prefrontal and cingulate cortex (Matsumoto et al. 2007; Tervo

et al. 2014). Some of these brain regions are connected with neuromodulatory centers like LC and dorsal raphe nucleus (Arnsten et al. 1984), allowing them to influence pupil size. However, further research is needed to decode these fluctuations and reliably distinguish between the various factors influencing pupil size.

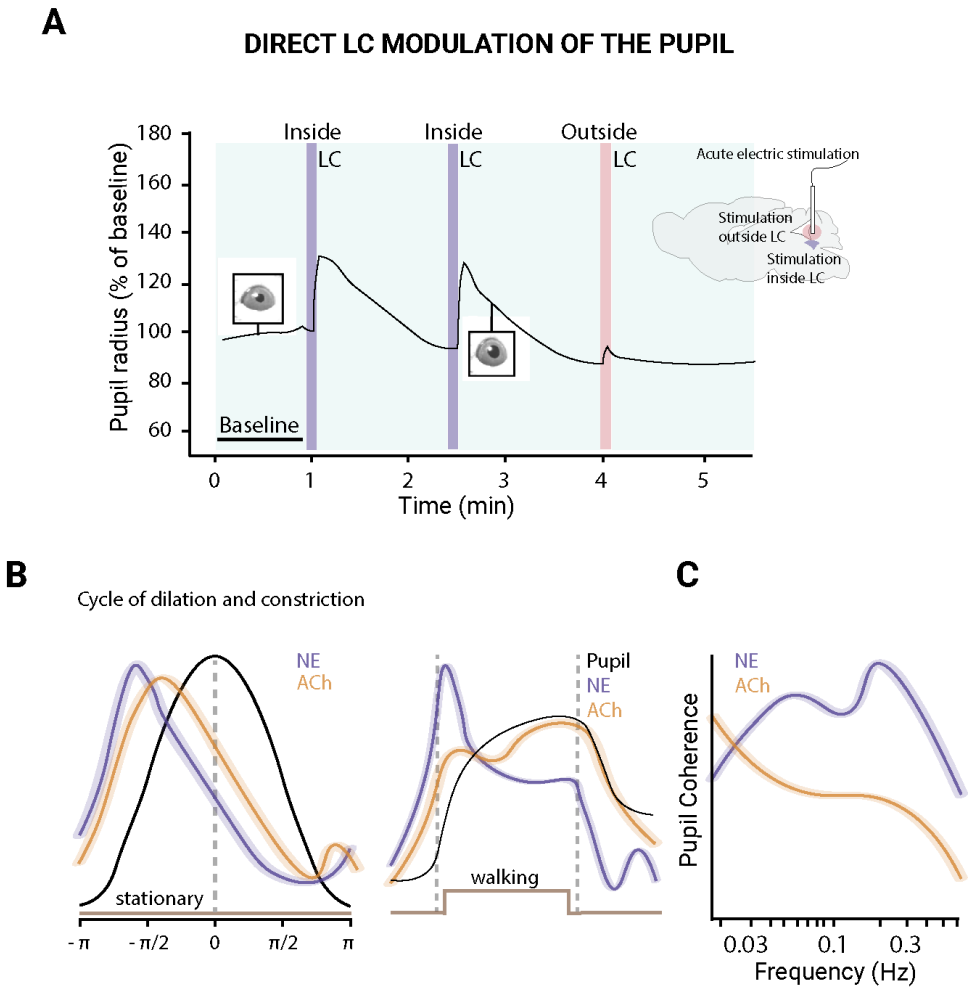

Figure 0.2: **LC-pupil relationship**. **(A)** The acute electric stimulation of the LC can evoke pupillary dilations in mice. **(B)** Noradrenergic versus cholinergic control of pupil size. The left panel shows ACh (orange) and NE (violet) dynamics during the dilation (values < 0) and constriction (values > 0) phases in the absence of locomotion. The right panel illustrates NE and ACh activity during locomotion onset and offset. NE activity levels were higher and had a shorter latency than ACh activity preceding the peak of dilation. These findings suggest that both neuromodulatory systems regulate pupil size changes during quiet wakefulness, with NE playing a more prominent role in rapid and transient pupil responses. During locomotion, phasic noradrenergic axonal activity (violet) is closely linked to rapid pupil dilations, while sustained cholinergic axonal activity (orange) is associated with longer-lasting dilations (left). **(C)** Coherence of NE and ACh in pupillary oscillations: NE levels display coherence with pupillary fluctuations across a wide frequency range. In contrast, ACh exhibits coherence primarily at lower frequencies, indicating distinct roles of the two neuromodulatory systems in the initiation and maintenance at different time scales. LC, locus coeruleus; ACh, acetylcholine; NE, norepinephrine. Figure adapted from Viglione et al. 2023

0.2 Exploring the relationship between pupil size and cortical plasticity

Since pupil dilations coincide with changes in neuromodulatory signaling, pupillometry appears to be a promising technique for estimating the degree of residual plasticity. In a recent study conducted on humans, Binda et al. 2017 demonstrated that monocular deprivation affects spontaneous slow pupil oscillation at rest (Binda et al. 2017), called hippus (J. P. Diamond 2001). The authors measured pupillary oscillations before and after monocular deprivation and found an increased hippus amplitude after visual deprivation. Moreover, participants with more pronounced pupillary fluctuations also showed stronger ocular dominance changes in binocular rivalry dynamics, an index of ocular dominance plasticity in humans (Steinwurzel et al. 2020). In a binocular rivalry experiment, incompatible images are presented to each eye simultaneously, but instead of perceiving a combination of the two images, people typically experience slow and irregular perceptual alternations of the two stimuli. They also hypothesized that the relationship between pupillary hippus and plasticity lies within the neural circuits that regulate the balance between inhibition and excitation in the cortex, where NE plays a key role. Moreover, hippus amplitude is thought to depend on the interplay between noradrenergic and cholinergic transmission (Michael C. Koss et al. 1984), with pupil dilations correlating with activity in the LC (Joshi et al. 2016). The LC-NE system, indeed, has been extensively studied in the cortical plasticity framework (Kasamatsu et al. 1976; Bear et al. 1983; Marzo et al. 2009; Shepard et al. 2015), starting from the discovery that NE plays a pivotal role in the developmental plasticity of the visual cortex (Kasamatsu et al. 1976; Kasamatsu et al. 1979; Kasamatsu et al. 1981). As a promising index of cortical plasticity, pupil size has been used to study switches between alternative percepts. Existing results reveal transient pupil dilations accompanying perceptual switches (Einhäuser et al. 2008; Hollander et al. 2018). In a recent study, Brascamp et al. demonstrated that perceptual changes were marked by a complex pupil response that could be decomposed into two components: a dilation linked to task execution and plausibly indicative of an arousal-linked NE surge and an overlapping constriction linked to the perceptual transient and plausibly a marker of altered visual cortical representation (Brascamp et al. 2021). Constriction, but not dilation, amplitude systematically depended on the time interval between perceptual changes, possibly providing an overt index of neural adaptation (Brascamp et al. 2021). The findings indicate that the size of the pupil reflects the activity of interacting but dissociable neural mechanisms during perceptual multistability and suggest that the release of arousal-related neuromodulators may affect behavior but not perception.

In the mouse, the oscillations of pupil constriction and dilation provide an efficient means of monitoring the cortex's reaction to sensory stimuli (Reimer et al. 2014; C. R. Lee et al. 2016). Specifically, the dilation of the pupil is associated with desynchronized activity within neural populations and heightened sensitivity to visual/somatosensory stimulation. Both these responses are correlated with activity alteration in various categories of inhibitory interneurons (Reimer et al. 2014). Moreover, they are also linked to signaling within the NE and ACh systems(Reimer et al. 2016). Jordan et al. 2023, recently have demonstrated that the LC-NE system in mice is involved in prediction errors and that LC activity promotes learning by

contributing to sensorimotor cortical plasticity. The study also found a significant correlation between LC axon activation in different somatosensory cortical regions and changes in pupil size (Jordan et al. 2023). Overall, these findings open up for further investigation into the use of pupil fluctuations as a proxy for cortical plasticity.

0.3 Pupillometry to measure fear conditioned responses

Due to its sensitivity to arousal, the pupil responds with dilation to salient or threatening stimuli. For this reason, pupil dilations have gained interest as a measure of conditioned fear responses. Fear conditioning is one of the most used experimental procedures to study the neurophysiology of aversive learning across different species (S. Maren 2001). During fear conditioning, an initially neutral stimulus is repeatedly paired with an aversive unconditioned stimulus (US), such as a mild electric stimulation. After learning the neutral stimulus becomes a conditioned stimulus (CS+) which can predict the aversive event and can elicit fear responses. In humans, several studies have demonstrated a pronounced pupil dilation in responses to the CS+ compared to CS- (a neutral stimulus never paired with the US) (Reinhard et al. 2002; Reinhard et al. 2006; Visser et al. 2015; Visser et al. 2013). In most pupillometry-based fear conditioning investigations, changes in pupil diameter are typically assessed over the entire stimulus duration (Visser et al. 2013; Visser et al. 2016; Visser et al. 2015; Reinhard et al. 2002; Reinhard et al. 2006; Hopkins et al. 2015), while in others the average pupil diameter is calculated during the stimulus presentations (Voogd et al. 2016). Another approach is to test pupillary reflexes during CS presentations. Numerous studies have demonstrated that pupillary constriction in response to light stimuli is less marked during states of perceived threat (Bitsios et al. 2004; Hourdaki et al. 2005). Other physiological measures, such as the fear-potentiated startle reflex (Alfons O Hamm et al. 1991; Weike et al. 2007) and skin conductance response (SCR) (Pineles et al. 2009; Luck et al. 2016), show differences between CS+ and CS-, and are usually used as readouts of fear learning. The SCR is considered valence-unspecific, while the startle reflex is influenced by emotional valence. Awareness of CS-US contingencies seems crucial for SCR (Sevenster et al. 2014; Weike et al. 2007), while the startle response can occur without conscious awareness (A O Hamm et al. 1996). Thus, different physiological measures may represent different aspects of fear learning. Compared to SCR and startle responses, pupil responses are influenced by several cognitive-affective processes. Indeed, pupillometry measures can show distinct temporal patterns during fear learning (Jentsch et al. 2020; Yamada et al. 2022; Leuchs et al. 2019), which allow one to discern different influences given by the above processes. Moreover, pupil responses may directly provide information about the influence of the LC-NE on learning and memory. Recently, It has been proposed that NE dynamically modulates fear conditioning and extinction, thereby either enhancing or impairing aversive learning processes depending on the level of behavioral arousal. Specifically, an intriguing review (Giustino et al. 2018) suggests that during high-stress conditions, the LC enhances cued fear learning by intensifying amygdala function while simultaneously attenuating prefrontal function. Conversely, under conditions of low arousal, the LC promotes medial prefrontal cortex function, facilitating the inhibition of the amygdala and promoting the extinction of cued fear. Additionally, the LC-NE system shows

significance in the acquisition, consolidation, and extinction of contextual fear memories, via the dense expression of adrenoceptors in the hippocampus, and the regulatory role of NE in long-term potentiation (LTP) in this region. The pupil's ability to mirror arousal levels plays a crucial role in evaluating the significance of arousal in fear memory and extinction, with clinical implications for post-traumatic stress disorder studies (Giustino et al. 2018).

In mice, conventional behavioral responses like freezing remain the preferred readout for investigating fear conditioning (S. Maren 2001). However, pupillometry for studying fear learning in rodents merits further exploration. For example, in head-fixed animals, the direct measurement of the classical definition of freezing is usually challenging. Some researchers have bypassed this limitation by testing animals in a classical fear conditioning apparatus before head-fixing them for subsequent cue presentations under neural imaging setups (Ross et al. 2018; Wood et al. 2022). However, this approach carries the risk of measuring a neural activation pattern that is disconnected from the corresponding behavioral response. To directly measure fear conditioning responses during head fixation, other studies have employed lick suppression. In these experiments, water-restricted mice are trained to lick a spout to obtain water. The reduction in licking behavior during the CS+ serves as a measure of conditioning response (Ahmed et al. 2020; Lovett-Barron et al. 2014; Rajasethupathy et al. 2015; Kaifosh et al. 2013). Also this approach presents problems, it is an indirect measure of fear, necessitates training and introduces confounding factors like water restriction. In contrast, pupil dilation serves as a direct and temporally precise quantifier of fear responses. Its application is non-invasive and does not interfere with concurrent measurements. Furthermore, pupil dilation offers valuable insights into the cognitive states associated with fear responses.

0.4 Pupil alterations in neurodevelopmental disorders

The dysregulation of the LC-NE system has been linked to the development of various brain disorders. Decreased noradrenergic activity, for instance, has been observed in individuals with depression and is commonly treated with selective noradrenergic reuptake inhibitors (Brunello et al. 2002). Conversely, an increase in noradrenergic activity has been observed in patients with anxiety (Vismara et al. 2020). The LC-NE system also plays a role in the pathogenesis of other brain disorders such as post-traumatic stress disorder, schizophrenia, substance use disorders, and neurodegenerative disorders like Alzheimer's disease (Weinshenker et al. 2006; Fitzgerald 2014; David et al. 2022). Pupillary alterations have been reported for all these pathologies, and pupillometry has shown promise in the early detection and tracking of various brain disorders, in early development and adult subjects (Iadanza et al. 2020; Blaser et al. 2014; Frost et al. 2017; Chougule et al. 2019; Winston et al. 2020; El Ahmadieh et al. 2021). In the realm of neurodevelopmental disorders, in particular, pupillometry has emerged as a promising biomarker. Pupillometry is non-invasive, can be performed on non-collaborative and preverbal subjects (like infants), promoting early diagnosis, and can be easily combined with other clinical measurements. Brain development and maturation require incredible plasticity. Such plasticity is particularly pronounced during critical periods, specific temporal windows during which the neural circuitry is highly sensitive to both internal and external modulations (Wiesel et al. 1963;

Barkat et al. 2011). The importance of NE in regulating neural development (Lovell 1982; Gustafson et al. 1987) is supported by studies that have shown noradrenergic fibers developing before the emergence of cortical neurons in the cerebral and cerebellar cortices (Lauder et al. 1974; Sievers et al. 1981; Kolk et al. 2022). During brain development, NE participates in the shaping and wiring of the nervous system (Felten et al. 1982; Gustafson et al. 1987; Golovin et al. 2016) by creating an opportunity for early life experiences to influence neuronal circuits and cause permanent changes in performance (Herlenius et al. 2004). Early alterations in NE transmission have significant implications for behavior, cognition, and mental health across the lifespan. In rodents, for instance, modifications in the expression of critical genes that regulate NE transmission during vulnerable developmental stages can affect adult circuits involved in emotional behavior, leading to the emergence of anxiety and depression-like symptoms later in life (Schramm et al. 2001; Lähdesmäki et al. 2002; Shishkina et al. 2004; Shishkina et al. 2002).

It has been shown that the PLR in infancy can predict the severity of autism spectrum disorders (ASDs) (Nyström et al. 2018). In children with ASD, the degree of relative constriction (but not latency) is associated with the extent of sensory dysfunction (Nyström et al. 2018), and infants with a high risk for ASD demonstrated larger PLR compared to low-risk control infants with no family history of ASD. This study shows a significant role of abnormal sensory processing in the etiology of ASD and proposes that measuring changes in the size of the pupils may aid in identifying infants at risk for ASD. Recent studies also suggest that pupil size may be a potential biomarker for attentional states in individuals with attention-deficit/hyperactivity disorder (ADHD), due to the central role of the LC-NE system in regulating attention (Wainstein et al. 2017). Pupil size variations have been found to indicate alterations in performance during a visuospatial working memory task, which is typically impaired in ADHD patients (Wainstein et al. 2017). Additionally, changes in pupil size have been observed during the presentation of attentionally relevant cues, and have been shown to correlate with individual performance variability and the administration of methylphenidate (Wainstein et al. 2017).

The development of mouse models of neurodevelopmental disorders is a crucial aspect of understanding the molecular and cellular mechanisms involved in brain development, as well as how genetic variance can impact the development of the CNS. Animal models make it possible to study the molecular pathways involved in the pupillary alterations observed in patients. In a recent study, Artoni et al. 2020 reported that mouse models of idiopathic or monogenic ASD display a signature of broadly distributed pupil sizes. Moreover, they have shown that in cholinergic circuits the select.ive expression of MeCP2 could rescue the pupillary deficit of MeCP2-deficient mice. Despite the direct involvement of neuropathological changes in the LC-NE system in ASD remains controversial, and there is much evidence to support the presence of autonomic dysregulation.

Pupillometry as a biomarker is not without challenges. Variability in measurement protocols and equipment, as well as inter-individual variability, must be carefully considered. Future research should focus on standardizing pupillometry procedures and exploring its potential in combination with other neuroimaging techniques, such as fMRI and electroencephalography, to enhance diagnostic accuracy.

0.5 The future of pupillometry measures: advancement of high-throughput pupillometry systems

The use of commercially available eye trackers and open-source tools has made performing pupillometry measurements relatively easy (i.e. Tobii Pro, Smart Eye Pro, or Eyelink). However, these commercial options can be costly and are mainly dedicated to human gaze tracking and/or pupillometry. Recently, open-source methods based on computer vision and deep learning approaches have been implemented. An open-source platform called PupilEXT allows performing pupillometry using single and stereo cameras, enabling high-resolution and gaze-corrected pupil measurements (Zandi et al. 2021). In mice, one study (Privitera et al. 2020) evaluated pupil size fluctuations using DeepLabCut (Mathis et al. 2018), a 3D markerless pose estimation technique based on transfer learning with neural networks. This approach requires minimal programming knowledge as the user needs to train the neural network with a small dataset labeled with user-defined key points of the eye before starting pupillometry. These custom-built systems are typically applied to awake, head-fixed animals; however, many behavioral experiments require animals to move freely in specific experimental settings. For these reasons, more complex equipment has been proposed, allowing for pupillometry in small animals while moving freely and performing multiple physiological recordings (e.g. microendoscopy, chronic electrophysiology) and sensory stimulation. These approaches are based on miniaturized head-implanted infrared cameras (Sattler et al. 2020; Huang et al. 2022), paving the way for further research in more ecologically relevant conditions and characterizing more complex cognitive abilities. Pupillometry would also be a promising tool in the recently growing field of telemedicine. The progress in pupillary response research and its applications relies on the availability of pupillometry for patients. Recent efforts have attempted to bring pupillometry into patients' homes using smartphones (Piaggio et al. 2021; Barry et al. 2022). However, this approach faces challenges related to controlling ambient light, particularly for tests that cause only slight pupil dilation, such as cognitive battery tests, where a strong light stimulus may obscure the results. Despite these limitations, the ability to conduct pupillometry in patients' homes with greater frequency and in a more comfortable setting is highly desirable. This could allow for studies on how life stress and environmental factors affect pupil-based biomarkers.

Part I

Translational and real-time pupillometry for studying cognitive and emotional processing

1 MEYE: Web App for Translational and Real-Time Pupillometry

1.1 Summary

Pupil dynamics alterations have been found in patients affected by a variety of neuropsychiatric conditions, including autism. Studies in mouse models have used pupillometry for phenotypic assessment and as a proxy for arousal. Both in mice and humans, pupillometry is non-invasive and allows for longitudinal experiments supporting temporal specificity, however its measure requires dedicated setups. In this study, we introduced a Convolutional Neural Network that performs on-line pupillometry in both mice and humans in a web app format. This solution dramatically simplifies the usage of the tool for non-specialist and non-technical operators. Because a modern web browser is the only software requirement, this choice is of great interest given its easy deployment and set-up time reduction. The tested model performances indicate that the tool is sensitive enough to detect both spontaneous and evoked pupillary changes, and its output is comparable with state-of-the-art commercial devices.

1.2 Introduction to the project

Pupillometry, the measurement of pupil size fluctuations over time, provides useful insights into clinical settings and basic research activity. Light level is the primary determinant of pupil size, although non-light-driven pupil fluctuations, widely assumed as an indicator of arousal through locus coeruleus activity, can be used to index brain state across species (McGinley et al. 2015b; C. R. Lee et al. 2016; Reimer et al. 2016). Higher cognitive and emotional processes are also able to evoke tonic or phasic pupillary changes, such as attention (Binda et al. 2013a), memory load (Wierda et al. 2012), novelty (Angulo-Chavira et al. 2017; Krebs et al. 2018; Montes-Lourido et al. 2021), pain (Connelly et al. 2014; Azevedo-Santos et al. 2018; Charier et al. 2019), and more general cortical sensory processing (Binda et al. 2013b; C. R. Lee et al. 2016) in humans and in animal models.

A growing body of work shows how pupillometry can be used as a possible biomarker for numerous neurologic and psychiatric conditions in early development and adult subjects (Aleman et al. 2004; Blaser et al. 2014; Rorick-Kehn et al. 2014; Frost et al. 2017; Nyström et al. 2018; Chougule et al. 2019; Gajardo et al. 2019; Oh et al. 2019; Artoni et al. 2020; Burley et al. 2020; Iadanza et al. 2020; Obinata et al. 2020; Winston et al. 2020; El Ahmadieh et al. 2021). Spontaneous and voluntary modulation of pupil fluctuations has also been used to facilitate human–computer interaction in normal subjects (Mathôt et al. 2016; Beggiato et al. 2018; Ponzio et al. 2019) and patients with severe motor disabilities. For example, pupil dynamics is used to

assess communication capability in locked-in syndrome, a crucial factor for the determination of a minimally conscious state (Olivia et al. 2013; Stoll et al. 2013). Pupillometry is also becoming a valuable tool for child neurology, to facilitate risk assessment in infants. For example, the pupil light reflex (PLR) during infancy seems to predict the later diagnosis and severity of autism spectrum disorders (ASDs; Nyström et al. 2018). Intriguingly, pupil alterations are also present in several ASD mouse models (Artoni et al. 2020).

Pupillometry has several advantages compared with other physiological methods: it is non-invasive and can be performed by nonspecialized personnel on noncollaborative and preverbal subjects (like infants), allowing the design of longitudinal experiments to permit temporal specificity. More importantly, it can be conducted similarly across different species from mice to humans, guaranteeing maximal translatability of the protocols and results (Aleman et al. 2004; Rorick-Kehn et al. 2014; Artoni et al. 2020). Given these assumptions, it is vital to introduce a simple, versatile tool used in a range of settings, from the laboratory to the clinical or even domestic environment. Available open-source methods require complicated steps for the installation and configuration of custom software not suitable for nontechnical operators. Moreover, these tools were tested exclusively in one species [mice (Privitera et al. 2020), humans (Yiu et al. 2019)], and none of them were applied in cognitive experiments that usually involve small pupil changes associated with high variability.

In this work, we have developed a deep learning tool called MEYE, using convolutional neural networks (CNNs) to detect and measure real-time changes in pupil size both in humans and mice in different experimental conditions. Furthermore, the MEYE web app, performs pupil area quantification and blink detection, all within a single network. By embedding artificial intelligence algorithms in a web browser to process real-time webcam streams or videos of the eye, MEYE can be used by nontechnical operators, opening the possibility to perform pupillometry widely, cost-effectively, and in a high-throughput manner. This architecture is resistant to different illumination conditions, allowing the design of basic neuroscience experiments in various experimental settings, such as behavior coupled with electrophysiology or imaging such as two-photon microscopy. To describe the performance of the MEYE web app in different settings, we tested the app in both mice and humans. In mice, we recorded both running speed and pupil size during visual and auditory stimulation (AS). In humans, we tested MEYE capabilities to detect the PLR. Furthermore, we performed a visual oddball paradigm (Liao et al. 2016; Aggius-Vella et al. 2020; LoTemplio et al. 2020), comparing pupil size and eye position measurements obtained from MEYE with one of the most used commercial eye-tracker systems: the EyeLink 1000. Finally, we released a dataset of 11,897 eye images that can be used to train other artificial intelligence tools.

1.3 Declaration of author contributions

Here I summarize, for clarity, the details of my specific personal contribution to this project. All of the conceptual, experimental and analytical tasks are grouped according to the level of my involvement in three categories as follows:

- I was the only/main contributor

  - Designing and conducting experiments on mice

- I collaborated in the tasks
  - Conceptualization of the project
  - Manual segmenentation of the pupil in the pictures used for the CNN training
- Task performed by other people or institutions
  - The Institute of Information Science and Technologies (ISTI) developed the CNN
  - The Pisa Vision Laboratory performed the human experiments
  - Data analysis

2 Results

2.1 Pupillometry in Head-Fixed Mice

We tested our CNN-based pupillometer in two behavioral experiments involving locomotion-induced and stimulus-evoked pupillary changes. Pupil size was simultaneously recorded with running speed from head-fixed mice free to run on a circular treadmill (Figure 2.1A).

We employed two different stimulation protocols: auditory stimulation (AS), and visual stimulation while the animal is freely exploring virtual reality (VR). The VR experiment included an initial period of habituation in which the animal navigated inside a virtual corridor for 5 minutes. After this period a squared visual stimulus was presented in the binocular portion of the visual field (20 s duration, interstimulus of 120 s for 10 times, Figure 2.1A-B). The AS experiment was carried out with the same structure of the VR experiment and using auditory stimulus previously used to induce a defensive behavior detectable as a pupillary and behavioral response (Hersman et al. 2020; Z. Li et al. 2021; H. Wang et al. 2019; Xiong et al. 2015). An initial period of habituation was followed by auditory stimulation using two tones (Tone1: 3 kHz, Tone2: 4kHz, 20 s duration, 120 s interstimulus, Figure 2.2A-B). We first set out to evaluate if CNN can detect event-related pupil transients (ERT) due to sensory stimulation in the VR. We averaged pupil size and running velocity during a 15 s temporal window centered on visual stimulation (Figure 2.2C). We detected a significant pupillary dilation after the onset of the visual stimulus, and no changes in evoked locomotion (Pupil: P-value: <0.001, Post hoc: 1.2 to 2.7 s adjusted P-values <0.05, 2 way ANOVA RM, Velocity: P-value: 0.96, 2 way ANOVA RM). This ERT is an orienting-related pupil response and a proxy of the arousal change due to stimulus detection (Montes-Lourido et al. 2021; C.-A. Wang et al. 2015). In the AS experiment, we also found an increase in pupil size, but dilation was associated with a significant increase in stimulus-induced locomotor activity (Pupil: P-value: <0.001, Post hoc: 1 to 10 s adjusted P-values <0.05, 2 way ANOVA RM, Velocity: P-value: <0.01, Post hoc: 3 to 5.3 s adjusted P-values <0.05, 2 way ANOVA RM, Figure 2.1C). Finally, we calculated pupil size during baseline periods before sensory stimulation both in the VR and the AS experiments. We found that during locomotion the pupil was significantly larger than in stationary periods both in the AS (P-value < 0.01, Paired T-Test,Figure 2.1D) and in the VR (P-value < 0.01, Paired T-Test,Figure 2.2D) experiment. These results demonstrate that CNN pupillometry can detect the mouse locomotion-induced and stimulus-evoked pupillary changes and can be used to monitor behavioral state change during head fixation experiments.

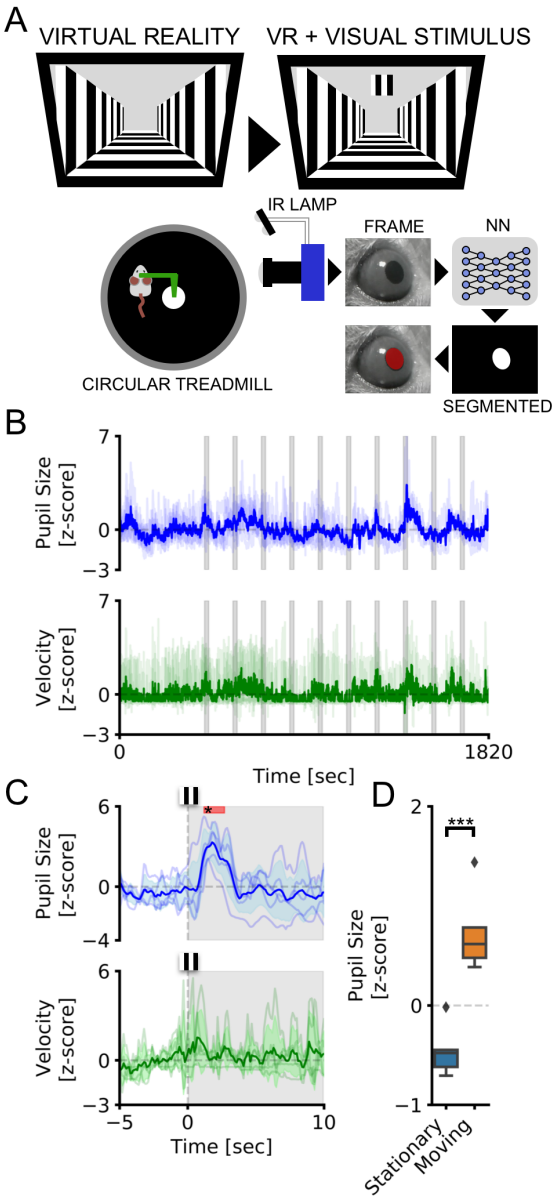

Figure 2.1: **Pupillometry and VR in head-fixed mice**. **(A)** Setup for head-fixed pupillometry in VR in the awake mouse. Showing the habituation phase (left) in which only the virtual corridor is shown, and the stimulation phase in which a visual stimulus appears above the virtual corridor, in the binocular portion of the visual field. **(B)** The average fluctuations of pupillometry and velocity in all experimental mice. Dashed gray areas represent the onset and duration of auditory stimuli. **(C)** Average event-related transients for both pupil size and velocity. Colored areas represent stimulus onset and duration. Red areas in the upper part of the plot represent statistically significant data points. **(D)** Sensibility of the system to detect locomotor-induced arousal fluctuations. Average pupil size is significantly affected by the behavioral states of the animal. During running epochs (Moving) the pupil is significantly more dilated than during the resting state (Stationary).

2.2 Web-Browser Application to Perform Real-Time Pupillometry Experiments

To greatly expand the use of our CNN-based pupillometer, we implemented the CNN in a web browser (MEYE, Figure 2.3A) and we tested whether it could be used also in humans. To

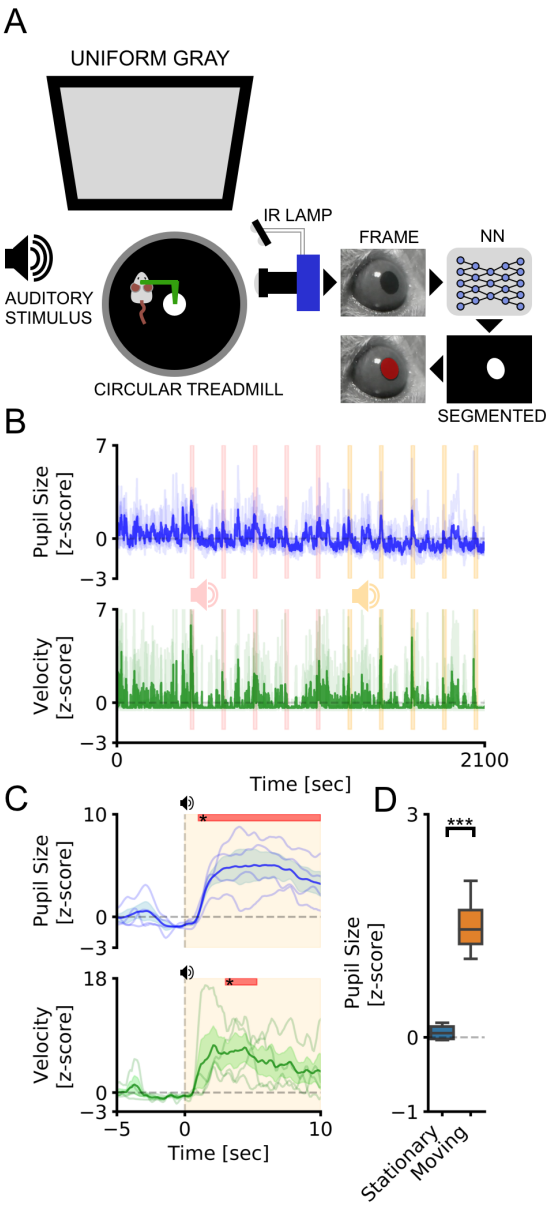

Figure 2.2: **Pupillometry in head-fixed mice**. **(A)** Setup for head-fixed pupillometry in the awake mouse. The mouse is head-fixed to a custom made metal arm equipped with a 3D printed circular treadmill to monitor running behavior. In the meantime, pupillometry is performed using CNN. **(B)** The average fluctuations of pupillometry and velocity in all experimental mice. Dashed pink and yellow areas represent the onset and duration of auditory stimuli. Evoked peaks in both pupil size (blue line) and velocity (green line) are clearly noticeable during auditory stimulation. **(C)** Average event-related transients for both pupil size and velocity. Colored areas represent stimulus onset and duration. Red areas in the upper part of the plot represent statistically significant data points. **(D)** Sensibility of the system to detect locomotor-induced arousal fluctuations. Average pupil size is significantly affected by the behavioral states of the animal. During running epochs (Moving) the pupil is significantly more dilated than during the resting state (Stationary).

test this possibility, we designed a simple experiment aimed to measure PLR evoked by brief flashes of light on the human eye. The experiment included 10 flash events with an interstimulus of 5 s (dashed vertical lines in Fig. Figure 2.3C). The results showed a clear light-induced modulation of pupil size in correspondence with each flash onset. Aligning and averaging all the

traces along with the events, PLR can be quantified in both the raw (44.53%±0.67% change from baseline) and z-scored (14.59±2.05 st.dev. from baseline) trace (Figure 2.3D-E). To detect if it is possible to measure cognitively driven pupil signals using the MEYE tool reliably, we performed pupillometry while participants executed an oddball task, a commonly used paradigm for cognitive and attentional measurement. This task is based on the principle by which pupil dilation is stronger in response to rare stimuli and can be used as a physiological marker for the detection of deviant stimuli (Liao et al. 2016). This experiment has been carried out recording the same eye using both the MEYE tool and an EyeLink 1000 system. According to Google Scholar, the Eyelink system is one of the most utilized eye trackers in psychology, psychophysics, and neuroscience, with more than 17K scientific publications mentioning this tool. During the oddball experiment, the subject was instructed to maintain fixation on a small dot presented in the center of the screen, pushing a button only when the Target stimulus appears on the screen and not responding to the Standard stimulus (Figure 2.4A). Averaging and comparing the responses to Standard and Target gratings results in significantly stronger pupil dilation for the Target stimulus than the Standard stimulus, that is detected by both the recording systems (MEYE: P-value < 0.001, T-Test Paired, EyeLink: P-value < 0.001, T-Test Paired, Figure 2.4B-C). No differences have been found for the responses evoked by the Target stimulus between the MEYE tool and the EyeLink system (P-value:0.327, T-test Paired, Fig. 4 B-inset). Moreover, the single-subject pupillary evoked amplitudes show a significant positive correlation between the two techniques (ρ:0.88, P-value:0.01, Spearman Correlation) with more than 75% of the variability explained by the linear model. Pupil size is known to covary with eye position in video-based measurements (Hayes et al. 2016), producing foreshortening of the pupillary image because the camera is fixed but the eye rotates. To overcome this issue, there are several possible solutions: the most simple one requires constant fixation throughout each trial, but, if this requirement cannot be satisfied (such as in sentence reading), the position of the pupil at each sample can be used to correct and mitigate the estimation error. Thus, we decided to quantify the agreement between positional outputs provided by MEYE and Eyelink for horizontal eye movements. We designed two tasks: in the first task, a dot smoothly traveled horizontally on the screen from left to right and vice versa at a velocity of 8 deg/s and spanning 20 degrees, producing slow and smooth pursuit eye movements. In the other experiment, a dot jumped every 5 s from a position to the other (spanning 20 degrees), producing large, fast, and abrupt saccades. Results (Figure 2.3D) show that smooth pursuit movements generate a sinusoidal change of position with a good agreement between both systems (MAE: 0.04). The second task, inducing saccades, produces a slightly larger error (MAE: 0.073). This error is mainly due to the much lower sampling rate of MEYE (MEYE:15 fps; Eyelink: 1000 fps). This means that even if MEYE provides the exact positional information for each sample, it has a lower performance in adequately describing fast eye movements, such as saccades. Thus, MEYE provides the data required for post-hoc correction of pupil measures although it should be used with caution for measuring saccades.

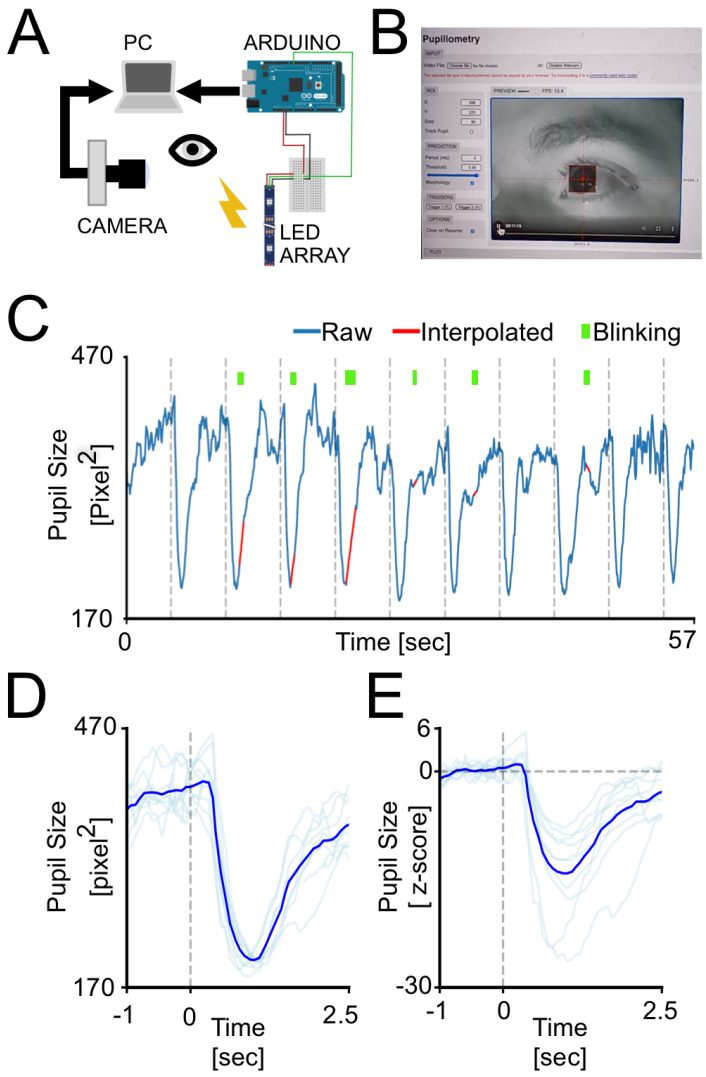

Figure 2.3: **Web-browser Pupillometry Experiment**. **(A)** Experimental setup for running the PLR stimulation and in the meantime perform pupillometric recordings. The PC is connected to the internet running an instance of MEYE tool in the web browser. A USB camera, equipped with an IR light source, is focused on the eye of the subject. The photic stimulus is delivered using a LED array driven by an Arduino Due. The Arduino is connected to the PC emulating a keyboard and sending keystroke stimulus triggers to the MEYE tool. **(B)** A picture of MEYE graphical user interface. The subject during the recording is visualized as a streaming video. A ROI is used to locate the eye and a preview of the estimation of the pupil is superimposed to the image of the subject. The GUI allows to set different parameters of post-processing (map thresholding and refinement via mathematical morphology). **(C)** Raw trace of the experiment (blue). Dashed lines locate the onset of flash stimuli. The green rectangles locate the onset and duration of blinks. The samples corresponding to blinks are removed and linearly interpolated (in red). **(D)** Average event related transient to flash stimulation in raw values. After the onset of the stimulus (dashed line) a strong constriction of the pupil is observed (44.53%). **(E)** Z-score of the average event related transient seen in D. The average nadir amplitude is 14.59 standard deviations from baseline.

2.3 Web-Browser Application to Perform Pupillometry on Videos

MEYE can also be used as an offline tool to analyze pupillometry videos in various file formats, depending on the video codec installed in the web browser. To demonstrate the feasibility to

perform pupillometry on videos captured in a variety of situations and in both mice and humans, we sampled 3 videos with a duration of 40 s from different experiments carried in our laboratory. Each video can be loaded as a demo in the web app to reproduce the same plots seen in Fig. 6. Three conditions were analyzed. The first condition can be found by pressing the 'Mouse' button in the DEMO section of the GUI. It depicts a head-fixed mouse running on a circular treadmill under IR illumination and watching a uniform gray screen at 10 cd/m^2 (Figure 2.5A). The second is a mouse under a 2-photon microscope (button '2P mouse'), walking on a cylindrical treadmill and showing clear dilation events due to locomotion (Figure 2.5B). The third is found pressing the button 'Human' is a 40 s footage of a human subject wearing VR goggles projecting a uniform gray at 15 cd/m^2 (Figure 2.5C). These results show that offline pupillometry can be performed in various conditions and in both mice and humans.

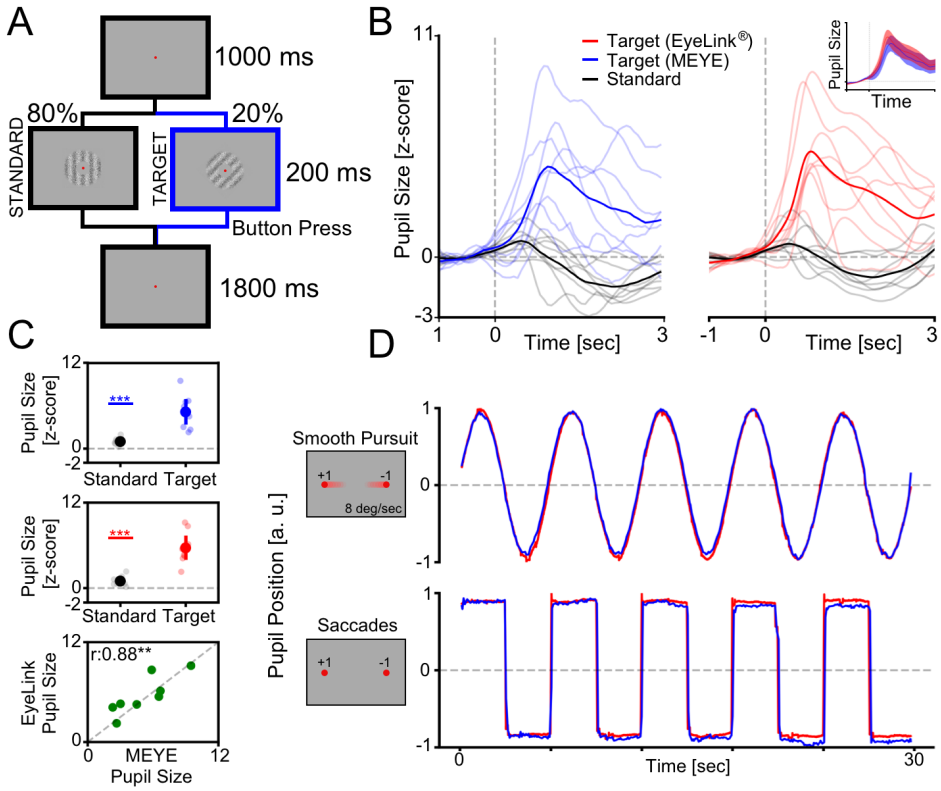

Figure 2.4: **Cognitively driven pupillary changes**. **(A)** Visual Oddball procedure. The participant is instructed to fixate a small red dot placed at the center of the screen and to push a button only when the Target visual stimulus appears. **(B)** Average Pupil waveforms. Average pupil response to Standard and Target stimulus for both MEYE (blue, left) and EyeLink (red, right). In the inset is represented the comparison between the evoked response to the Target stimulus in both setups. **(C)** Average pupil response. Difference between the Standard and Target stimuli recording using MEYE (uppermost) and Eyelink (middle). The lowermost graph represents the correlation between MEYE and Eyelink data. D: Eye movements data. Comparison between the MEYE tool (blue) and Eyelink system (red) during smooth pursuit task (upper) and saccades (lower).

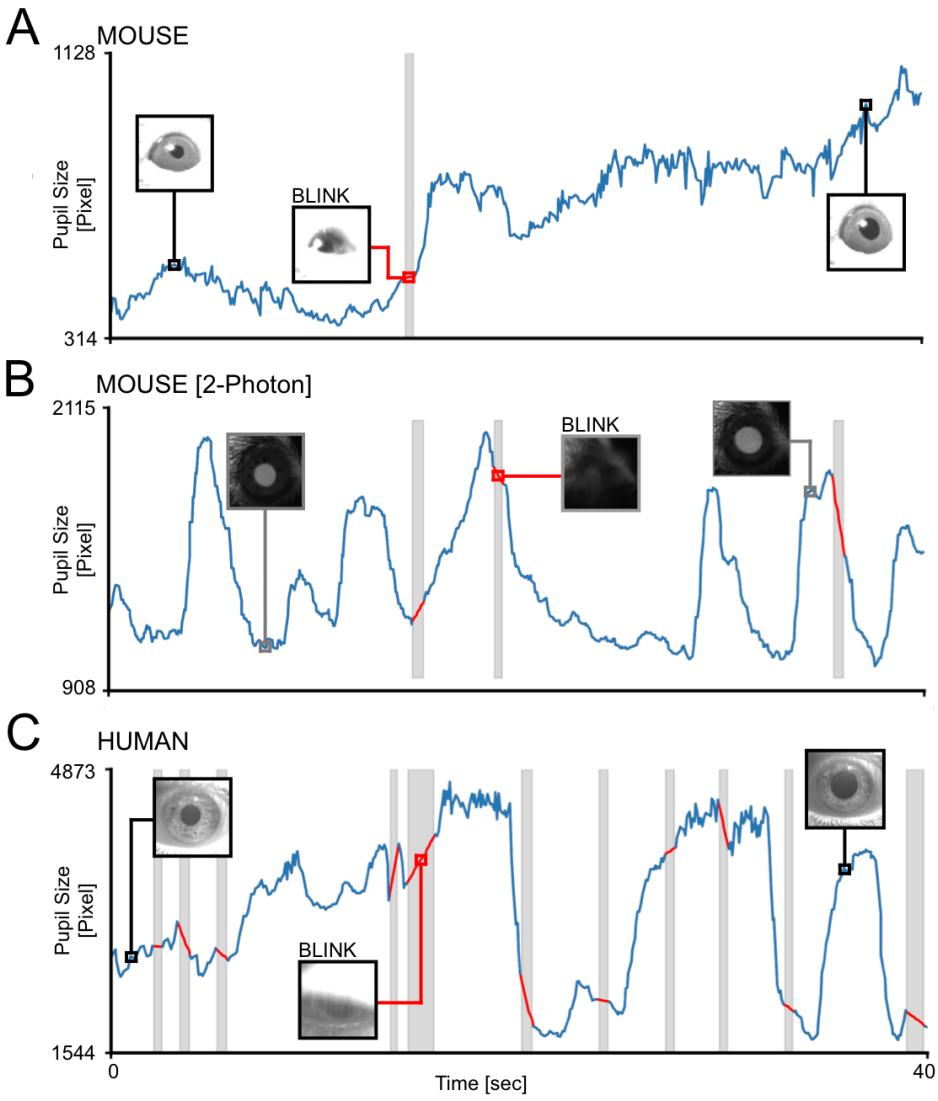

Figure 2.5: **Offline Movies Analysis**. **(A)** Awake Head-fixed mouse running on a treadmill, recorded for 40 s. The grey area represents a blink, the trace of the blink is removed and linearly interpolated (red line). **(B)**Awake mouse during 2-photon calcium imaging. Here is clearly visible a brighter pupil with respect to A. Blinking epochs are removed and linearly interpolated. **(C)** Pupillometry performed on a human subject, with a higher blinking rate with respect to mice. In all figures the insets images represent the ROIs.

3 Discussion

In this work, we demonstrated that MEYE is a sensitive tool that can be used to study pupil dynamics in both humans and mice. Furthermore, by providing eye position MEYE allows post-hoc control of possible effects of eye movements on pupil measures (Hayes et al. 2016). MEYE can detect both spontaneous and evoked pupil changes in a variety of conditions: mice with black pupils in normal illumination conditions, and mice with bright pupils resulting from laser infrared illumination. This flexibility allows the use of MEYE in combination with 2-photon, wide-field imaging, and electrophysiological techniques widely adopted in the awake or anesthetized mice. Furthermore, MEYE can be employed to design standalone experiments using cost-effective hardware with performance comparable with that of state-of-the-art commercial software. In this experiment, we used a USB webcam with a varifocal objective that allows focal adjustment concentrated on the eye. The cost of the imaging equipment is less than 50 euros and requires no knowledge of coding to set up. The flashing stimulus apparatus requires a basic understanding of Arduino boards and can be assembled at a price lower than 50 euros. The overall cost of the apparatus is less than 100 euros. Our code can be used in two different ways, to satisfy many needs. One way relies on the standalone web browser tool, that allows running MEYE on almost any device, from scientific workstations to notebooks or even smartphones. The other way utilizes a dedicated Python script running the CNN locally on a workstation. This latter case is suited for experiments with specific requirements, like high and stable framerate or online processing of pupil size in which on-the-fly pupil computer interaction is required. Valid open source and commercial alternatives exist, most of them are dedicated to gazing tracking and/or pupillometry. Commercial options are costly (tobii.com, sr-research.com, neuroptics.com), whereas open-source code instead requires programming knowledge and most of them are explicitly dedicated to one species (Privitera et al. 2020; Yiu et al. 2019). One of these papers (Privitera et al. 2020) assessed pupil dilation in mice through DeepLabCut (Mathis et al. 2018), a technique for 3D markerless pose estimation based on transfer learning. This approach, albeit powerful, is conceptually different, since it is trained on user-defined key points instead of using the entire pupil to perform semantic segmentation. The former technique is more suited to track and locate arbitrary objects on an image, the latter technique is focused on a more precise quantification of even small changes of the object area, since pixel-wise segmentation masks are refined iteratively using local and global context. The possible contribution of the web app technology resides in its portability: no software needs to be manually installed and configuration is minimal. Only a clear IR image of the subject's eye is required. The performances of the tool are dependent on the host computer but it runs at > 10 fps in most of the machines tested. This advantage is particularly useful for settings with limited resources and space or for educational purposes. Web browser-embedded pupillometry will also be crucial for human scientific research, and clinical and preventive medicine. It would also be a promising tool in the recently growing field of telemedicine given its minimal setup that can run on an average notebook or even

on a smartphone, it allows possible large-scale recruitment of subjects directly in their own homes. This greatly facilitates infants, psychiatric, and motor-impaired patients' compliance, particularly for longitudinal research designs. We also released an open-source database of eyes composed of more than 11.000 images in various settings: head-fixed mice (black pupil), head-fixed two-photon imaging mice (white pupil), and human eyes. This dataset will grow over time to introduce new species and new use cases to increase, update, and strengthen MEYE performances. The possible scenarios can be further expanded in the future, due to the dynamic nature of CNN. It can be updated from the source, providing instantaneous updates on each computer running an instance of the program. Our hope is to create a community that refines and consolidates pupillometric performances, to produce a tool that can be applied in different environments.

4 Methods

4.1 Dataset

For this study, we collected a dataset (Figure 4.1A) composed of 11897 grayscale images of humans (4285) and mouse (7612) eyes. The pictures' majority depict mouse eyes during head-fixation sessions (HF: 5061) in a dark environment using infrared (IR, 850 nm) light sources. In this environment, the pupil is darker than the rest of the image. We also collected mouse eyes (2P: 2551) during 2-photon Ca2+ imaging. In this particular condition, the pupil is inverted in color and tends to be brighter than the iris. Finally, we acquired images of human eyes in IR light (H: 4285) during virtual reality experiments (wearing a headset for virtual reality), using an endoscopic camera (www.misumi.com.tw/). The dataset contains 1596 eye blinks, 841 images in the mouse, and 755 photos in the human datasets. Five human raters segmented the pupil in all pictures (one per image), using custom labeling scripts implemented in Matlab or Python, by manual placement of an ellipse or polygon over the pupil area. Raters flagged blinks using the same code.

4.2 CNN architecture

The CNN model (Figure 4.1C) takes a grayscale 128x128 image as input and produces three outputs: a) a 128x128 probability map of each pixel belonging to the pupil, b) the probability the image contains an eye, and c) the probability the image depicts a blinking eye. We evaluated three architectures; two were based on DeepLabv3+ (L.-C. Chen et al. 2018), a family of image segmentation models that employ atrous convolutions and spatial pyramid pooling known to improve robustness to scale changes. The two models differ for the CNN backbone adopted, respectively a ResNet-50 (He et al. 2016) and MobileNet V3 (Howard et al. 2019) CNNs. The third evaluated model is a specialized variant of the U-Net architecture (Ronneberger et al. 2015), a widely used CNN in image segmentation tasks. The model has an encoder-decoder "hourglass" architecture; the encoder part comprises a sequence of convolutional layers with ReLU activation and 2x2 max pooling operation, each halving the spatial resolution of feature maps at every layer; this produces a sequence of feature maps of diminishing spatial dimensions that provides both spatially local information and global context for the subsequent steps. Starting from the last encoder output, the decoder part iteratively upsamples and fuses feature maps with corresponding encoder maps, using convolutional layers, to produce the output pixel map. All convolutional layers have 16 3x3 kernels and pad their input to obtain the same-shaped output. Convolutional layer upsampling and downsampling were by a factor of 2 (Figure 4.1C). In all the tested architectures, eye and blink probabilities are predicted by an additional branch that applies global average pooling and a two-output fully connected layer to the bottleneck feature map. The pixel probability map and eye/blink probabilities are

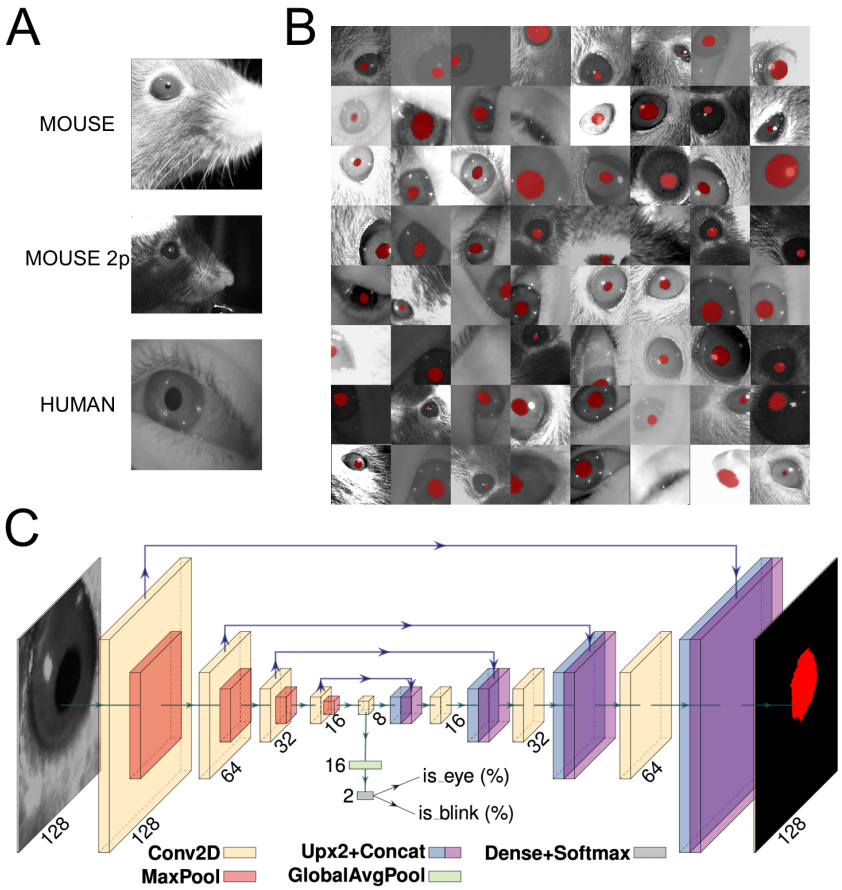

Figure 4.1: **Dataset, CNN architecture, and performances**. **(A)** examples of images taken from the dataset. The first image depicts a head-fixed mouse with dark pupils, and the second one is a head-fixed mouse with a bright pupil, during 2-photon microscope sessions. The last image is a human eye taken during experiments wearing virtual reality goggles. **(B)** 64 examples of data augmentation fed to CNN. The images are randomly rotated, cropped, flipped (horizontally or vertically), and changed in brightness/contrast/sharpness. **(C)** CNN architecture with an encoder-decoder "hourglass" shape. The encoder part comprises a sequence of convolutional layers. Starting from the last encoder output, the decoder part iteratively upsamples and fuses feature maps with the corresponding encoder's maps, to produce the output pixel map. The pixel probability map and eye/blink probabilities are computed by applying the sigmoid activation to the network outputs element-wise

computed by applying the sigmoid activation to the network outputs element-wise. Among the tested architectures, we chose to adopt the UNet variant in this work, as we observed it provided the best trade-off in terms of speed and segmentation quality (for further information see: https://github.com/fabiocarrara/meye/wiki/MEYE-Models).

4.3 Augmentation, training, and validation

We randomly split the dataset into training, validation, and test subsets following a 70/20/10% split. We performed strong data augmentation during the training phase by applying random rotation, random cropping, random horizontal and vertical flipping, and random brightness/contrast/sharpness changes; images were resized to 128x128 before feeding them to the

CNN (Figure 4.1B). For validation and test images, we used a 128x128 crop centered on the pupil. We computed the binary cross-entropy for all outputs (pixels and eye/blink logits) and took the sum as the loss function to minimize. The network was trained with the AdaBelief optimizer (Zhuang et al. 2020) for 750 epochs with a learning rate of 0.001. The best-performing snapshot on the validation set was selected and evaluated on the test set.

4.4 MEYE: web-browser tool

We built a web app for pupillometry on recorded or live-captured videos harnessing a CNN segmentation model as the core component. The trained models have been converted to a web-friendly format using TensorFlow.js, thus enabling predictions on the user machine using a web browser. This choice greatly facilitates the deployment and reduces set-up time, as a modern web browser is the only minimum requirement. Once loaded, an internet connection is not mandatory, as no data leaves the user's browser, and all the processing is performed on the user's machine. This implies that performance greatly depends on the user's hardware; if available, hardware (GPU) acceleration is exploited automatically by TensorFlow.js. In our tests, a modern laptop shipping an Intel(R) Core(TM) i7-9750H 2.60GHz CPU and an Intel(R) UHD Graphics 630 GPU can process up to 28 frames per second. The web app also offers additional features that facilitate the recording process, such as:

- Processing of pre-recorded videos or real-time video streams captured via webcam;
- ROI placement via user-friendly web UI (drag&drop) and automatic repositioning following tracked pupil center;
- Embedded tunable pre-processing (image contrast/brightness/gamma adjustment and color inversion) and post-processing (map thresholding and refinement via mathematical morphology);
- Support for registering trigger events;
- Live plotting of pupil area and blink probability;
- Data export in CSV format including pupil area, blink probability, eye position, and trigger channels.

4.5 Behavioral experiments on mice

4.5.1 Animal Handling

Mice were housed in a controlled environment at 22 °C with a standard 12-h light-dark cycle. During the light phase, a constant illumination below 40 lux from fluorescent lamps was maintained. Food (standard diet, 4RF25 GLP Certificate, Mucedola) and water were available ad libitum and changed weekly. Open-top cages (36.5x20.7x14cm; 26.7x20.7x14cm for up to 5 adult mice or 42.5x26.6x15.5cm for up to 8 adult mice) with wooden dust-free bedding were used. All the experiments were carried out following the directives of the European Community

Council and approved by the Italian Ministry of Health (1225/2020-PR). All necessary efforts were made to minimize both stress and the number of animals used. The subjects used in this work were three female C57BL/6J mice at 3 months of age for the auditory stimulation and five male 2-month-old mice for the VR experiment.

4.5.2 Surgery

The mouse was deeply anesthetized using isoflurane (3% induction, 1.5% maintenance). Then it was mounted on a stereotaxic frame through the use of ear bars. Prilocaine was used as a local anesthetic for the acoustic meatus. The eyes were treated with a dexamethasone-based ophthalmic ointment (Tobradex, Alcon Novartis) to prevent cataract formation and keep the cornea moist. Body temperature was maintained at 37 degrees using a heating pad monitored by a rectal probe. Respiration rate and response to toe pinch were checked periodically to maintain an optimal level of anesthesia. Subcutaneous injection of Lidocaine (2%) was performed before scalp removal. The Skull surface was carefully cleaned and dried, and a thin layer of cyanoacrylate was poured over the exposed skull to attach a custom-made head post that was composed of a 3D printed base equipped with a glued set screw (12 mm long, M4 thread, Thorlabs: SS4MS12). The implant was secured to the skull using cyanoacrylate and UV-curing dental cement (Fill Dent, Bludental). At the end of the surgical procedure, the mice recovered in a heated cage. After 1 hour, the mice were returned to their home cage. Paracetamol was used in the water as antalgic therapy for three days. We wait seven days before performing head-fixed pupillometry to provide sufficient time for the animal to recover.

4.5.3 Head fixation

In the awake mouse head-fixation experiments, we employed a modified version of the apparatus proposed by Silasi et al. (Silasi et al. 2016), equipped with a 3D printed circular treadmill (diameter: 18cm). A locking ball socket mount (TRB1/M) was secured to an aluminum breadboard (MB2020/M) using two optical posts (TR150/M-P5) and a right-angle clamp (RA90/M-P5). The circular treadmill was blocked between the base plate pillar rod and the optical post through a ball-bearing element (BU4041, BESYZY) to allow the disk to spinning with low effort. To couple the head-fixing thread on the mouse to the locking ball, an ER025 post was modified by re-tapping one end of it with M4 threads to fit the ball and socket mount. Velocity was detected using an optical mouse under the circular treadmill. Pupillometry was performed using a USB camera (oCam-5CRO-U, Withrobot) equipped with a 25 mm M12 lens connected to a Jetson AGX Xavier Developer Kit (NVIDIA) running a custom Python3 script (30fps). The Jetson hardware was connected with an Arduino UNO through a GPIO digital connection. The Arduino UNO managed the auditory stimuli through a speaker (W3-1364SA 3", Tang Band).

4.5.4 Behavioural procedures

Mice were handled for 5 minutes each day during the week preceding the experiments; then, they were introduced gradually to head-fixation for an increasing amount of time for five days.

During Days 1 and 2, we performed two sessions of 10 minutes of head-fixation, one in the morning and one in the afternoon. On Day 3, we performed one session of twenty minutes, Day 4 thirty minutes, and on Day 5 thirty-five minutes. Each recording started with 5 minutes of habituation. We exposed the animal to auditory stimuli during the last day. During each head-fixation session, a curved monitor (24 inches Samsung, CF390) was placed in front of the animal (at a distance of 13 cm) showing a uniform gray with a mean luminance of 8.5 cd/m2. The frequency of tone 1 was 3000Hz, and tone 2 was 4000Hz, both at 70dB, 20 seconds duration, and 120 seconds of interstimulus. Virtual reality was composed of a gamma linearized procedural virtual corridor with episodic visual stimulation written in C# and Unity. The virtual corridor was composed of sine-wave gratings at different orientations (wall at 0° and floor at 90°), and spatial frequencies (from 0.06 to 0.1 cycles/deg). The position of the animal in the virtual corridor was updated using an optical mouse connected to the circular treadmill. The episodic visual stimulus consisted of a square wave grating patch of 55° (in width and height) of visual space in the binocular portion of the visual field. The gratings parameters were: luminance 8.5 cd/m2, orientation 0°, contrast 90%, spatial frequency 0.1 cycles/deg, drifting at 0.5 cycle/s.

4.5.5 Data analysis

Data has been analyzed using Python 3. All tracks were loaded, and blink removal was applied using the blink detector embedded in MEYE. Blink epochs were filled using linear interpolation and median filtering (0.5 s). Spearman ρ rank-order correlation was performed using the function corr from the Python library pingouin (Vallat 2018). Z-score was performed for each trial using the formula $z = \frac{x - \overline{x_b}}{s_b}$, where $\overline{x}$ and s_b were respectively the average and the standard deviation of the baseline. To evaluate if Event-Related Transients (ERTs) amplitude was significantly different from baseline, two-way repeated-measures ANOVA was computed on each time sample using the pingouin function rm_anova. Post hoc analyses and multiple comparison P-values correction were carried out using the function pairwise_ttests from pingouin. For both pupil size and velocity, we compared each time sample after sensory stimulation with the average value of the baseline, adjusting the P-values using Benjamini/Hochberg FDR correction. For the behavioral state analysis, locomotion activity was identified using a threshold algorithm. We tagged as moving all the samples in which velocity was ¿=10% with respect to the maximal speed of the animal. Paired t-tests between behavioral states were performed using the function ttest from pingouin. Eyes Movements comparison was carried out normalizing (in the range between -1 and 1) data from both setups, upsampling MEYE data from 15 to 1000 fps using linear interpolation, and then calculating the Mean Absolute Error (MAE), performed using the Python function mean_absolute_error from the library sklearn.

4.6 Behavioral experiments on humans

4.6.1 PLR

Pupillometry has been performed using a MacBook Pro (Retina, 13-inch, Early 2015, Intel Core i5 Dual-core 2.7GHz, 8GB of RAM, Intel Iris Graphics 6100 1536 MB) running MEYE application on Firefox (84.0). The tool is able to compute online pupil size quantification,

plotting the instantaneous pupil area and saving the results on file. Furthermore, the tool accepts four independent manual push-button triggers (keys T or Y on the keyboard). This feature allowed us to annotate stimulation events. A USB IR webcam (Walfront5k3psmv97x, Walfront) equipped with a Varifocal 6-22mm M12 objective (149129, Sodial) was used to acquire images of the eye. The camera was equipped with 6 IR LEDs to illuminate the eye uniformly, optimizing contrast between the iris and the pupil. Photic stimulation was delivered using an Arduino Due (Arduino) microcontroller connected via USB to the notebook and programmed to emulate a keyboard. The Arduino emulates a keyboard (using the keyboard.h library) to send event triggers to MEYE in the form of keystroke events. The microcontroller drives a stripe of four LEDs (WS2813, WorldSemi) using the FastLED.h library, flashing bright white light for 500 ms with an interstimulus of 5 s (Figure 2.3A). The Subject sat in front of a monitor screen (24 inches Samsung, CF390) at a distance of 60 cm, with the head stabilized by a chin rest and instructed to maintain fixation on a small dot presented in the center of the screen for the whole duration of the recording (57 s). A total of 10 flash stimuli have been presented through the strip of LEDs mounted above the screen.

4.6.2 Oddball paradigm corecordings

To compare the performances shown by the CNN system with that of a state-of-the-art commercial software, we coregistered pupillometry using MEYE and an EyeLink 1000 system while 9 (3 males, 6 females, average age 28.78 years) participants executed an oddball paradigm. The experiment was conducted in a quiet, dark room. The participant sat in front of a monitor screen (88x50 cm) at a distance of 100 cm, with their head stabilized by a chin rest. The viewing was binocular. Stimuli were generated with the PsychoPhysics Toolbox routines (Brainard, 1997; Pelli, 1997) for MATLAB (MATLAB r2010a, The MathWorks) and presented on a gamma-calibrated PROPixx DLP LED projector (VPixx Technologies Inc., Saint-Bruno-de-Montarville, Canada) with a resolution of 1920x1080 pixels, and a refresh rate of 120 Hz. Pupil diameter was monitored at 1kHz with an EyeLink 1000 system (SR Research) with an infrared camera mounted below the screen and recording from the right eye. The participant was instructed to maintain fixation on a small dot (0.5°) presented in the center of the screen for the whole duration of the recording (300 s). In this study, the visual stimuli consisted in the appearance of a high probability stimulus (80% of times) defined as "Standard" and a lower probability stimulus (20% of times) defined as "Target". The Standard stimulus consisted of a 100% contrast-modulated annular grating (mean luminance 25 cd/m^2), horizontally orientated, spatial frequency of 0.5 cpd, with an inner and outer diameter of 1.5 and 5 deg, respectively. The edges of the annulus were smoothed by convolving the stimulus with a gaussian mask (sigma = 0.5 deg). The Target stimulus has the same parameters as the Standard stimulus except for the orientation that was 45 deg (see Figure 2.4A). The presentation duration of each trial, either the Standard (0 deg) or Target (45 deg) trial, was 200 ms with the intertrial interval between two consecutive trials was 2800 ms. The phase of both the Target and the Standard stimuli was randomized across trials. The participants were instructed to press a button for a Target stimulus and not to respond for a Standard stimulus. The Z-scored ERTs were computed as described for mice. The correlation was performed by taking the Targets' amplitude peaks for each subject using both EyeLink and

MEYE and then performing the Spearman ρ rank-order correlation between the two measures.

4.6.3 Eye movements corecordings

For eye-tracking recording we employed both the MEYE tool and EyeLink 1000 as described above. In the smooth pursuit condition a small dot (0.5 deg), moved on the screen horizontally, changing the direction every 20 degrees of the visual field with a constant velocity of 8 deg/s. In the Saccades condition, every 2.5 s the small dot changes abruptly position horizontally with a span of 20 degrees.

4.6.4 Offline video analysis

The MP4 videos were loaded into MEYE, the parameters were chosen by visually inspecting the quality of the pupillometry. Threshold values were 0.25, 0.15, 0.5, with morphology FALSE, TRUE, TRUE for 'human', 'mouse' and '2P-mouse' videos respectively. Once the video analysis was completed, the CSV file was loaded in Python. Blink removal and linear interpolation were applied, then the track was plotted using the Python library matplotlib.

4.6.5 Data Availability

The code and web app are freely available on Github: https://github.com/fabiocarrara/meye MEYE is available at: www.pupillometry.it MEYE wiki: https://github.com/fabiocarrara/meye/wiki The dataset is available on: https://doi.org/10.5281/zenodo.4488164

5 Behavioral Impulsivity is Associated with Pupillary Alterations and Hyperactivity in CDKL5 Mutant Mice

5.1 Summary

Cyclin-dependent kinase-like 5 (Cdkl5) deficiency disorder (CDD) is a severe neurodevelopmental condition caused by mutations in the X-linked Cdkl5 gene. CDD is characterized by early-onset seizures in the first month of life, intellectual disability, motor and social impairment. No effective treatment is currently available and medical management is only symptomatic and supportive. Recently, mouse models of Cdkl5 disorder have demonstrated that mice lacking Cdkl5 exhibit autism-like phenotypes, hyperactivity, and dysregulations of the arousal system, suggesting the possibility to use these features as translational biomarkers. In this study, we tested Cdkl5 male and female mutant mice in an appetitive operant conditioning chamber to assess cognitive and motor abilities, and performed pupillometry to assess the integrity of the arousal system. Then, we evaluated the performance of artificial intelligence models to classify the genotype of the animals from the behavioral and physiological phenotype. The behavioral results show that CDD mice display impulsivity, together with low levels of cognitive flexibility and perseverative behaviors. We assessed arousal levels by simultaneously recording pupil size and locomotor activity. Pupillometry reveals in CDD mice a smaller pupil size and an impaired response to unexpected stimuli associated with hyperlocomotion, demonstrating a global defect in arousal modulation. Finally, machine learning reveals that both behavioral and pupillometry parameters can be considered good predictors of CDD. Since early diagnosis is essential to evaluate treatment outcomes and pupillary measures can be performed easily, we proposed the monitoring of pupil size as a promising biomarker for CDD.

5.2 Introduction to the project

Mutations in cyclin-dependent kinase-like 5 (Cdkl5) cause Cdkl5 deficiency disorder (CDD, OMIM no. 300203). The disorder predominantly affects females heterozygous for mutations in Cdkl5, with an incidence of 1 per 42,000 live births (Symonds et al. 2019). Hemizygous male cases have also been reported with a much lower prevalence (Olson et al. 2019; Demarest et al. 2019). Mutations in the Cdkl5 gene are currently one of the most common genetic causes of epilepsy in children (Symonds et al. 2019). CDD has been genetically linked to multiple neurodevelopmental disorders, including Rett syndrome, early infantile epileptic encephalopathy, and autism spectrum disorder (ASD) (I.-T. J. Wang et al. 2012). However, today CDD is considered an autonomous etiopathological entity, with a clearly distinct genetic and clinical phenotype with respect to other similar infantile encephalopathies (Fehr et al. 2013). Cdkl5 encodes a serine/threonine

kinase whose catalytic domains share homology with members of the cyclin-dependent kinase family and mitogen-activated protein kinases (Moseley et al. 2012; Weaving et al. 2004; Fuchs et al. 2018). In mice, Cdkl5 is strongly upregulated postnatally and seems to be active both in the cytoplasm and nucleus (Rusconi et al. 2008). Cdkl5 was also found to be localized in postsynaptic structures, where it can regulate dendritic spine maturation and density, and regulate excitatory synaptic function (Ricciardi et al. 2012; Della Sala et al. 2016). Recently has been shown that temporal manipulation of endogenous Cdkl5 expression in adult mice can induce or rescue behavioral symptoms, demonstrating an indispensable role for Cdkl5 also in the adult brain: postdevelopmental loss of Cdkl5 disrupts many behavioral domains, hippocampal functional connectivity, and dendritic spine morphology. By contrast, restoration of Cdkl5 after the early stages of brain development using a conditional rescue mouse model, ameliorates CDD-related behavioral impairments and aberrant NMDA receptor signaling, suggesting the existence of a broad therapeutic time window for potential treatment (Terzic et al. 2021). However, the role of Cdkl5 in modulating neural substrates for cognitive and motor function is poorly understood and no effective treatment is currently available. Since 2012, multiple murine models of Cdkl5 disorder have been generated, all of them showing similar behavioral deficits, highlighting the reproducibility of CDD-related phenotypes in mice, and raising the possibility of preclinical testing of therapeutic strategies (I.-T. J. Wang et al. 2012; Amendola et al. 2014; Tang et al. 2019). Recent studies have demonstrated that mice lacking Cdkl5 exhibit impulsivity, and hyperlocomotion, resembling core symptoms of attention-deficit hyperactivity disorder (ADHD) (Jhang et al. 2017; Jhang et al. 2020; Adhikari et al. 2022). Deficits in attentional and executive functions in ADHD patients have been linked to dysregulations of arousal (Strauß et al. 2018; Geissler et al. 2014; Martella et al. 2020). The arousal system is a distributed network aimed to optimize the level of responsivity to sensory stimulation (Hebb 1955). The concept arises from classical electrophysiological studies relating to the different stages of sleep and wakefulness (Robbins 1997). Fluctuations in arousal are characterized by ultradian rhythmicity (Lavie 1989; Blum et al. 2014), they can also be elicited by external stimulation (Wainio-Theberge et al. 2021; Park et al. 2021). The stimulus-evoked changes in arousal are generally referred to as orienting responses (Bohlin 1976; Sokolov 1990). The orienting response is an automatic and immediate response to an unexpected stimulus or changes in the environment (Sokolov 1990; Sokolov 1963; Lynn 2013) with effects on different levels of body responses (i.e., motor system, autonomic nervous system, and central nervous system) (Sokolov 1963; Lynn 2013; Berti et al. 2017)including changes in pupil size and locomotion (C.-A. Wang et al. 2015). Automatic orienting response to unexpected changes in the environment is a prerequisite for adaptive behavior; it is perceived as a disruption of the current attentional focus to immediately respond to changes in the environment on a physiological, behavioral, and cognitive level (Montes-Lourido et al. 2021). The arousal system is under the direct control of the noradrenergic circuit (along with acetylcholine) that widely innervates brain regions to control cortical processing (Pfeffer et al. 2022; Stitt et al. 2018), hippocampal excitability (McGinley et al. 2015a), and cognitive functions (McGinley et al. 2015a; Storbeck et al. 2008; Barnard et al. 2011). Moreover, it controls many peripheral autonomous functions, like pupillary and cardiac levels, mediating complex behavioral outcomes, such as fight or flight response (Artoni

et al. 2020). Fluctuations in pupil size have been reported as a reliable index of arousal across species (Joshi et al. 2016; Pan et al. 2022; Bradley et al. 2008; C. R. Lee et al. 2016; Ganea et al. 2020; Gee et al. 2020; Mazziotti et al. 2021), including mice (Reimer et al. 2016) and humans (C.-A. Wang et al. 2018). Arousal alterations have also been documented in children with ASD and in a recent study revealed arousal alterations in MeCP2- and Cdkl5-deficient mouse models (Artoni et al. 2020). In order to evaluate psychomotor and cognitive abilities in Cdkl5 mice, we performed an appetitive conditioning task in Cdkl5 (P60) null mice ($Cdkl5^{-/y}$) and WT littermates control ($Cdkl5^{+/y}$), using a 3D printed and automated appetitive operant conditioning chamber (Mazziotti et al. 2020). Appetitive operant conditioning (F. N. Jones 1939) is a standard technique used in experimental psychology in which animals, including rodents (Francis et al. 2017; O'Leary et al. 2018), learn to perform an action to achieve a reward. Using this paradigm makes it possible to extract learning curves, accurately measure mental chronometry (e.g., reaction times), and track an animal's position to assess motor and spatial performances (Mazziotti et al. 2020). In addition, we performed pupillometry in Cdkl5 male and female mutant mice and their WT littermates to assess the integrity of the arousal system by simultaneous recording of pupil size and locomotor activity in basal conditions and in response to unexpected isoluminant stimuli presented in a virtual reality environment. The behavioral results indicated that CDD mice display an impulsive and hyperactive phenotype. Pupillometry showed decreased pupil size associated with hyperlocomotion and an impaired orienting response to virtual reality. Furthermore, we trained different machine learning models to recognize the genotype of the animals starting from behavioral and/or pupillometric data. This approach allows us to quantify the performances of the models to blindly classify subjects at a single animal level and evaluate analytically the quality of the biomarkers (Mazziotti et al. 2017b). These data reveal a global defect in arousal modulation in CDD mice and introduce metrics for quantitative, non-invasive, and translational biomarkers for neurodevelopmental disorders.

5.3 Declaration of author contributions

Here I summarize, for clarity, the details of my specific personal contribution to this project. All of the conceptual, experimental and analytical tasks are grouped according to the level of my involvement in three categories as follows:

- I was the only/main contributor
  - Conceptualization of the project
  - Designing and conducting pupillometry experiments
  - Figures layout and data visualizations
- I collaborated in the tasks
  - Designing and conducting behavioral experiments
  - Data Analysis
- Task performed by other people or institutions
  - Machine Learning for genotype prediction

6 Results

6.1 Abnormal behavior of male and female Cdkl5 mutant mice in an automated appetitive operant conditioning task

During the operant conditioning task, the animal used its position to trigger a new trial by remaining in a specific place (active area, Figure 6.1A) for a given amount of time (1.5 sec). The visual stimulus consists of two bright blue dots, appearing above each response button. The mouse needs to touch one of the two buttons to obtain the reward (Figure 6.1B). We found that Cdkl5$^{-/y}$ mice produced an increasingly higher number of trials than Cdkl5$^{+/y}$ mice, reaching a statistical difference on Day 3 (Figure 6.1C). Cdkl5$^{-/y}$ mice also showed reduced reaction times (Figure 6.1D) but no difference in intertrial intervals (time elapsing between the response and the activation of a novel trial, Figure 6.1E). Moreover, the tracking analysis revealed altered locomotor activity in Cdkl5$^{-/y}$ mice. In particular, during the task, Cdkl5$^{-/y}$ mice moved faster and covered a greater distance than Cdkl5$^{+/y}$ (Figure 6.2A-C). Most CDD patients are heterozygous females carrying missense, nonsense, splice, or frameshift Cdkl5 gene mutations or a genomic deletion (Bahi-Buisson et al. 2012). In females, the phenotypic spectrum of the disease spans from mild to severe forms, while boys carrying mutations in Cdkl5 have more severe epileptic encephalopathy than girls (Liang et al. 2019; Kluckova et al. 2021). Thus, we decided to test Cdkl5 heterozygous female mice (Cdkl5$^{+/-}$). Again, we found that Cdkl5$^{+/-}$ mice performed a higher number of trials than control littermates (Cdkl5$^{+/+}$) (Figure 6.1F). In particular, we found a statistical difference in the number of trials performed, already present on Day 1 and Day 2 (Figure 6.1F). Cdkl5$^{+/-}$ mice also showed reduced reaction times (Figure 6.1G) and intertrial intervals compared to Cdkl5$^{+/+}$ (Figure 6.1H). The tracking analysis revealed an enhanced locomotor activity in Cdkl5$^{+/-}$ mice, in terms of speed and distance traveled. (Figure 6.2D-F) Thus, Cdkl5$^{+/-}$ mice are also altered in this behavioral task.

6.2 Low level of cognitive flexibility, perseverative behavior, and hyperactivity in Cdkl5 null mice

To better investigate the hyperactive behavior observed in Cdkl5$^{-/y}$ mice, we introduced a modified version of the operant conditioning task: the delayed task (Figure 6.3A). This test version increased the time needed to activate a single trial from 1.5 sec to 4 sec, thus requiring a stronger inhibitory control. The delayed task revealed opposite results compared to the previous test: Cdkl5$^{-/y}$ mice performed a lower average number of trials than Cdkl5$^{+/y}$ littermates (Figure 6.3B-C). In particular, we found a difference between groups in the number of trials performed on the first and second day of the delayed task (Post day 1 and Post day 2). This difference disappears on the last day of the test when Cdkl5$^{-/y}$ mice reach the same performance

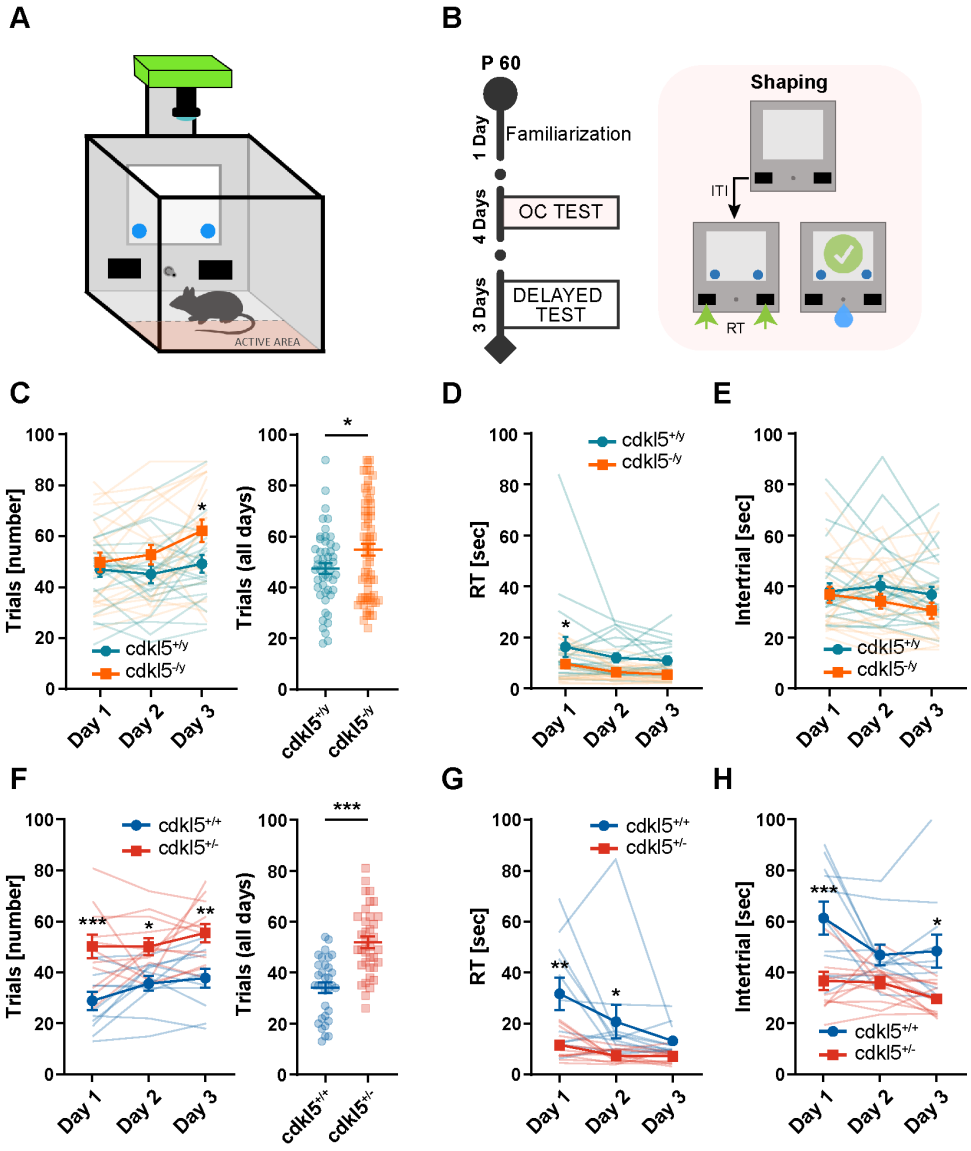

Figure 6.1: **Appetitive Operant Conditioning test results in Cdkl5 male and female mice**. **(A)** Schematic representation of the conditioning chamber. **(B)** Diagram showing the appetitive conditioning timeline and paradigm. **(C)** On the left, single day trials in male mice: two-way ANOVA, effect of time < 0.05, effect of genotype < 0.05; post hoc Sidak multiple comparisons at Day 3 < 0.05. On the right, cumulative number of trials performed in the three days of appetitive operant conditioning test: P-value < 0.05, Unpaired T-Test. **(D)** Reaction Time in male mice: two-way ANOVA, effect of time < 0.005, effect of genotype < 0.005; post hoc Sidak multiple comparisons at Day 1 < 0.05. **(E)** Intertrial intervals in male mice show no differences between genotypes. **(F)** On the left, single day trials in female mice: two-way ANOVA, effect of genotype < 0.001; post hoc Sidak multiple comparisons at Day 1 < 0.001, Day 2 < 0.05, Day 3 < 0.01. On the right, number of trials performed in the three days of shaping: P-value < 0.0001, Unpaired T-Test. **(G)** Reaction Time in female mice: two-way ANOVA, effect of time < 0.05, effect of genotype < 0.05; post hoc Sidak multiple comparisons at Day 1 < 0.01, Day 2 < 0.05. **(H)** Intertrial intervals in female mice: two-way ANOVA, effect of time < 0.05, effect of genotype < 0.01; post hoc Sidak multiple comparisons at Day 1 < 0.001, Day 3 < 0.05. n = 20 Cdkl5$^{+/y}$; n = 22 Cdkl5$^{-/y}$; n = 11 Cdkl5$^{+/+}$; n = 12 Cdkl5$^{+/-}$. *P-value < 0.05, **P-value < 0.01, ***P-value < 0.001. OC: operant Conditioning; RT: Reaction Time; ITI: Intertrial.

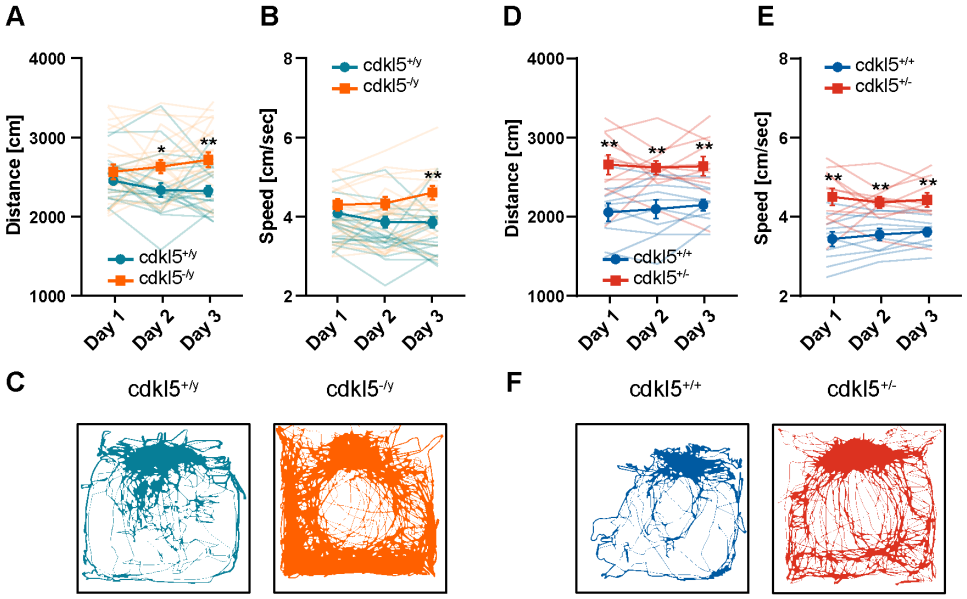

Figure 6.2: **Operant Conditioning locomotor activity in male and female mice**. **(A)** distance moved: two-way ANOVA, effect of genotype < 0.05; post hoc Sidak multiple comparisons at Day 2 < 0.05; post hoc Sidak multiple comparisons at Day 3 < 0.01. **(B)** speed: two-way ANOVA, effect of genotype < 0.05; post hoc Sidak multiple comparisons at Day 3 < 0.01. **(C)**tracking examples from a cdkl5 WT ($Cdkl5^{+/y}$) male mice and a cdkl5 null mice ($Cdkl5^{-/y}$). **(D)**distance moved: two-way ANOVA, effect of genotype < 0.01; post hoc Sidak multiple comparisons at Day 1, Day 2 and Day 3 < 0.01. **(E)** speed: two-way ANOVA, effect of genotype < 0.001; post hoc Sidak multiple comparisons at Day 1, Day 2 and Day 3 < 0.01. **(F)** tracking examples from a cdkl5 WT ($Cdkl5^{+/+}$) female mice and a cdkl5 heterozigous mice ($Cdkl5^{+/-}$). n = 20 $Cdkl5^{+/y}$; n = 22 $Cdkl5^{-/y}$; n = 10 $Cdkl5^{+/+}$; n = 11 $Cdkl5^{+/-}$; *p < 0.05, **p < 0.01.

as $Cdkl5^{+/y}$ mice (Figure 6.3B, Post day 3). We did not find differences in the reaction times, demonstrating that the reduction in the number of trials was not attributable to a lack of interest in the task (Figure 6.3D). However, we found a significant difference in the intertrial intervals. In particular, $Cdkl5^{-/y}$ mice showed longer intertrial intervals in the first two days of the delayed task (Figure 6.3E). The diminished number of trials and longer intertrial intervals were caused by the higher number of invalid trials performed by $Cdkl5^{-/y}$ with respect to $Cdkl5^{+/y}$ mice. These findings demonstrate lower cognitive flexibility of $Cdkl5^{-/y}$ mice, probably due to an impairment in inhibitory control. We also introduced a new parameter called perseveration index to determine whether the learning impairment observed in $Cdkl5^{-/y}$ mice was associated with perseverative and impulsive behaviors. In detail, the perseveration index counts every time the mouse follows the previous rule instead of the new one (e.g. waiting for 1.5 sec instead of 4 sec in the active area). We found a significantly higher perseveration index in $Cdkl5^{-/y}$ mice compared to $Cdkl5^{+/y}$ on Post day 1 and Post day 2 (Figure 6.3F). This suggests that for the first two days of the delayed task, $Cdkl5^{-/y}$ mice continued to adopt the old operant task rules instead of adapting to the new paradigm, demonstrating an impairment in cognitive flexibility accompanied by impulsive and perseverative behaviors.

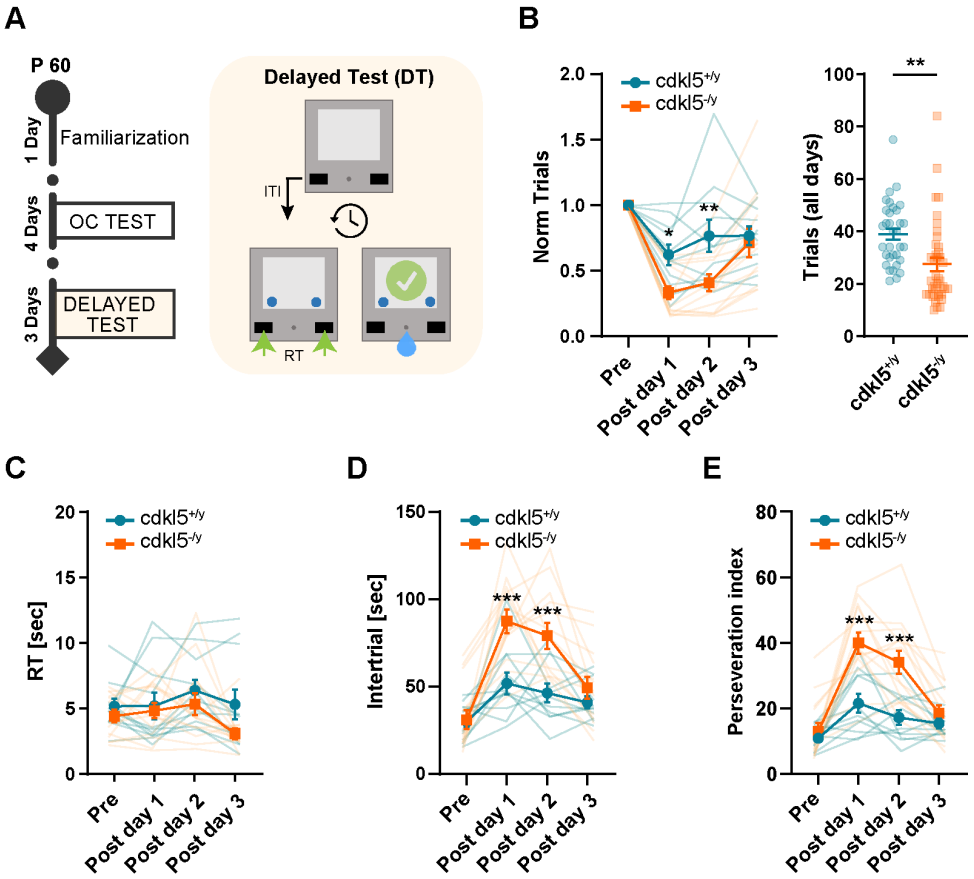

Figure 6.3: **Delayed task in Cdkl5 null mice**. **(A)** Diagram showing the appetitive conditioning timeline and the delayed task paradigm. **(B)** Number of trials normalized on the last day of the appetitive operant conditioning test (Pre): two-way ANOVA, interaction time x genotype < 0.01, post hoc Sidak multiple comparisons at Day 5 < 0.05 and Day 6 ¡ 0.01. **(C)** Number of trials performed in all the three day of delayed time: P-value < 0.01, Unpaired T-Test. **(D)** Reaction Times show no differences between genotypes. **(E)** Intertrial intervals: two-way ANOVA, interaction time x genotype < 0.01, post hoc Sidak multiple comparisons at Post day 1 < 0.001 and Post day 2 < 0.001. **(F)** Perseveration index: two-way ANOVA, interaction time x genotype < 0.001, post hoc Sidak multiple comparisons at Post day 1 < 0.0001 and Post day 2 $= 0.0001$. n = 11 Cdkl5$^{+/y}$; n = 13 Cdkl5$^{-/y}$. *P-value < 0.05, **P-value < 0.01, ***P-value < 0.001. OC: operant Conditioning; RT: Reaction Time; ITI: Intertrial.

6.3 Head-fixed male and female Cdkl5 mutant mice show an enhanced locomotor activity and a smaller pupil size

Pupil function abnormalities have been described in children with attention deficits (e.g. ADHD) and ASD (Boxhoorn et al. 2020; Wainstein et al. 2017). We performed pupillometry in P90 Cdkl5$^{-/y}$ mice and Cdkl5$^{+/y}$ littermates control (Figure 6.4A). During pupillometry, mice were head-fixed and free to run on a circular treadmill equipped with an optical sensor to assess locomotor activity (Figure 6.4B). Pupillometry was performed using the MEYE Deep Learning tool (Mazziotti et al. 2021). During pupillometry, the animal was exposed to the following stimuli: a mean luminance uniform gray screen, a virtual reality isoluminant stimulus composed of a virtual corridor moving coherently with the animal movement to elicit an orienting response, and a high luminance white screen to assess the pupillary light reflex (Figure 6.4B). The uniform

gray background was also presented before and after orienting response and pupillary light reflex assessment to allow the pupil to return to baseline (Figure 6.4B). We first investigated pupil dynamics and locomotion in the absence of stimulation during the exposure to the uniform gray field. We found that Cdkl5$^{-/y}$ mice exhibit enhanced locomotor activity (Figure 6.4C, D) also in the head-fixed condition. In particular, Cdkl5$^{-/y}$ mice showed more moving epochs and a higher velocity per epoch (Figure 6.4D) than controls. We also found that the duration of a single running event was significantly longer in Cdkl5$^{-/y}$ mice compared to Cdkl5$^{+/y}$ (Fig. 3 Figure 6.4D). These results confirm in Cdkl5$^{-/y}$ mice the hyperactive phenotype observed in the appetitive operant conditioning chamber, suggesting the presence of altered arousal levels. Pupillometric analysis revealed a constitutively smaller pupil size in Cdkl5$^{-/y}$ mice compared to controls (Figure 6.4E). However, the normalized pupil dilation present during running was unaffected (Figure 6.5). Locomotor activity and pupil size were also affected in Cdkl5$^{+/-}$ heterozygous female mice. In particular, locomotor activity was enhanced in Cdkl5$^{+/-}$ mice as compared to control female Cdkl5$^{+/+}$, both in terms of time spent running and velocity (Figure 6.4F, G). Moreover, as in male mutants, Cdkl5$^{+/-}$ mice displayed a significantly smaller pupil size during the running state and a strong trend (p=0.057) when resting (Figure 6.4H).

6.4 Cdkl5 null mice show altered orienting response but intact pupillary light response

Previous studies have demonstrated atypical visuospatial orienting response in children with attention-related deficits and ASD (Boxhoorn et al. 2020; Cohen et al. 1972; Harris et al. 1999). Thus, we investigated the orienting response induced by the virtual reality stimulus. Cdkl5$^{+/y}$ mice clearly showed an orienting response consisting of a substantial pupil dilation immediately after the stimulus onset. By contrast, Cdkl5$^{-/y}$ mice displayed a dramatically reduced and transient pupillary response (Figure 6.6A). Virtual reality also induced different locomotor responses. In particular, while virtual reality elicited an increase in motility of Cdkl5+/y mice, Cdkl5$^{-/y}$ mice did not show significant changes in running velocity (Figure 6.6B). Finally, we tested whether the pupillary light reflex, an autonomic reflex that constricts the pupil in response to an increase in luminance, was changed in Cdkl5 mutants. As shown in Figure 6.6C, we did not observe any significant differences in pupil constriction amplitude (maximal relative change in pupil area during constriction) or pupil re-dilation (maximal relative change in pupil area to recover the constriction, Figure 6.6D). These results reveal an unaltered pupillary light reflex, suggesting a central origin for the orienting response alterations observed. Taken together, these results demonstrate in Cdkl5$^{-/y}$ mice an altered physiological and behavioral response to an orienting visual stimulus.

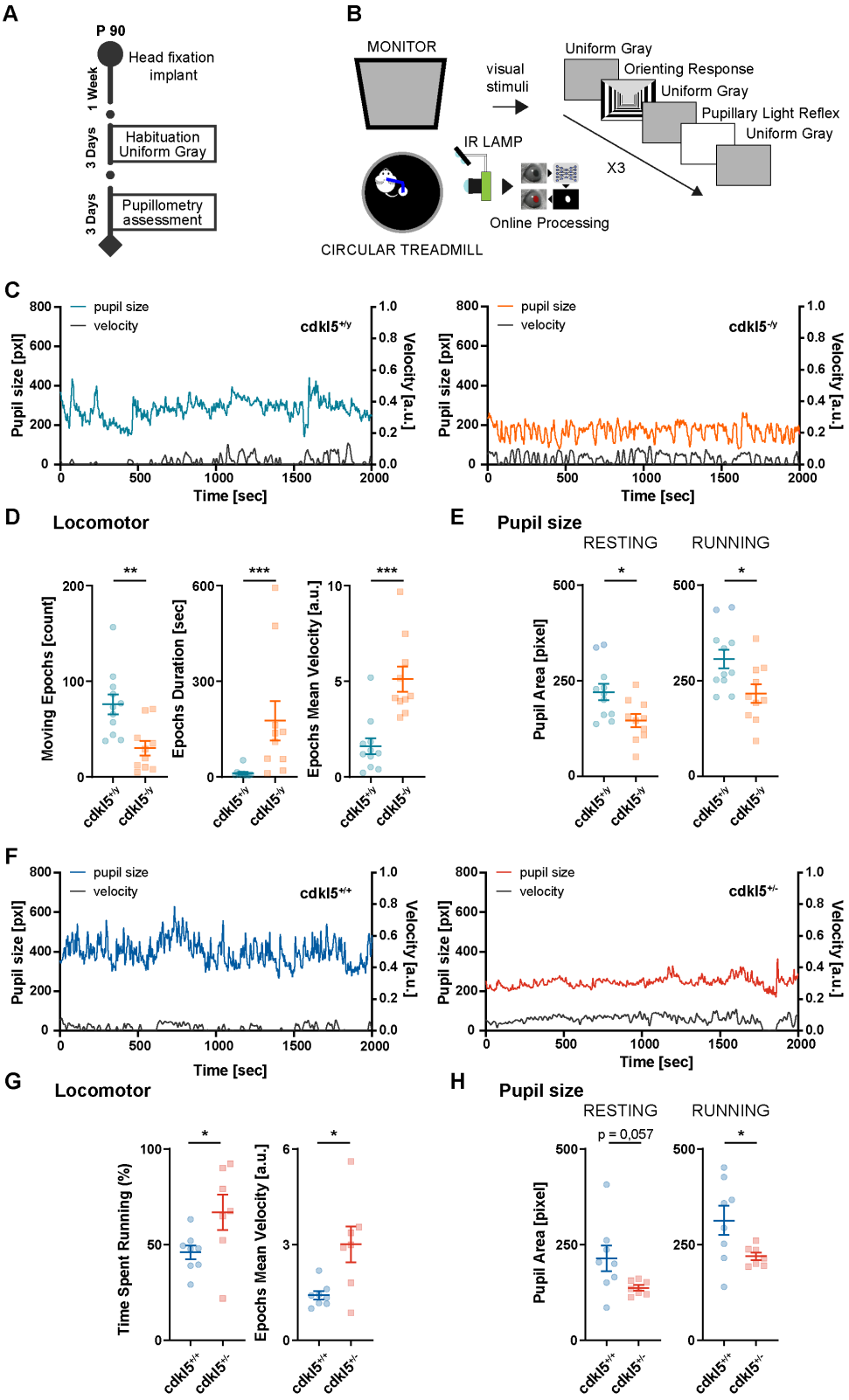

Figure 6.4: **Locomotor activity and pupil size reveal arousal alterations in Cdkl5 male and female mutant mice. (A)** Diagram showing the pupillometry timeline. *Continued on next page.*

Figure 6.4: **(B)** Schematic representation of the head-fixed pupillometry setup. The mouse was head-fixed to a custom made metal arm equipped with a 3D printed circular treadmill to monitor running behavior. In the meantime, we assessed: baseline pupil size (uniform gray screen), orienting response (to isoluminant virtual reality) and the pupillary light reflex (high luminance white screen). Each condition is repeated three times. We repeated the same protocol on three different days. **(C)** Pupil diameter trace from a WT male mouse ($Cdkl5^{-/y}$) and a Cdkl5 null male mouse ($Cdkl5^{+/y}$). **(D)** Cdkl5 null mice showed alterations in locomotor activity compared to WT: a decreased number of moving epochs (defined as a period of continuous movement): P-value < 0.01, Unpaired T-Test; an increase in the average duration of moving epoch: P-value < 0.05, Unpaired T-Test; and an increase in epochs mean velocity: P-value < 0.001, Unpaired T-Test. **(E)** $Cdkl5^{-/y}$ showed a constitutively smaller pupil size compared to $Cdkl5^{+/y}$ both during resting and running (resting, P-value < 0.05; running, P-value < 0.05; Unpaired T-Test). **(F)** Pupil diameter trace from a WT female mouse ($Cdkl5^{+/+}$) and a Cdkl5 heterozygous female mouse ($Cdkl5^{+/-}$). **(G)** $Cdkl5^{+/-}$ mice showed an enhanced locomotor activity compared to $Cdkl5^{+/+}$, in terms of percentage of time spent running, P-value < 0.05, Unpaired T-Test and velocity, P-value < 0.05, Unpaired T-Test. **(H)** $Cdkl5^{+/-}$ mice showed a baseline smaller pupil size compared to $Cdkl5^{+/+}$ during running, P-value < 0.05, Unpaired T-Test, and a strong trend in resting, P-value $= 0.057$, Unpaired T-Test. n $= 11$ $Cdkl5^{+/y}$, n $= 10$ $Cdkl5^{-/y}$; n $= 8$ $Cdkl5^{+/+}$, n $= 7$ $Cdkl5^{+/-}$. *P-value < 0.05, **P-value < 0.01, ***P-value < 0.001.

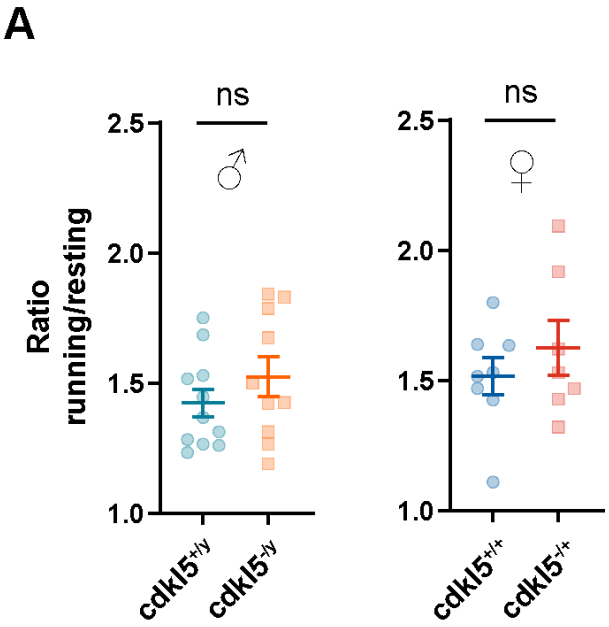

Figure 6.5: **Unaltered pupil size ratio between running and resting**. **(A)** $Cdkl5^{-/y}$ male mice and $Cdkl5^{-/+}$ heterozygous female mice show an invariant pupil dilation between resting and running compaired to their respectively controls (male: P-value $= 0.28$, Unpaired T-Test; female: P-value $= 0.39$, Unpaired T-Test). n $= 11$ $Cdkl5^{+/y}$, n $= 10$ $Cdkl5^{-/y}$; n $= 8$ $Cdkl5^{+/+}$, n $= 7$ $Cdkl5^{+/-}$. ns, non significat.

6.5 Behavioral appetitive conditioning parameters and head-fixed pupillometric and behavioral responses are robust predictors of Cdkl5 null mice alterations

To test whether the behavioral and pupillary alterations observed in Cdkl5 null mice can be used to classify single animals, we employed machine learning algorithms to build models capable of predicting mouse genotype from the behavioral and pupillary alterations that we measured. We found that by training the models only with the behavioral parameters collected during the

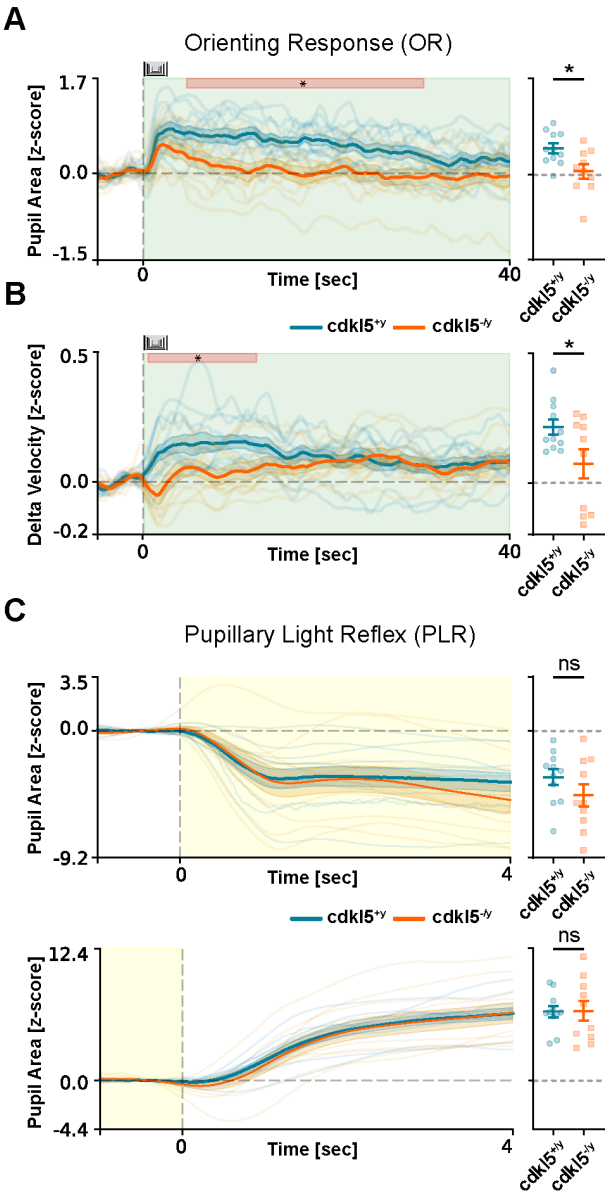

Figure 6.6: **Pupillary orienting response and pupillary light reflex assessment**. **(A)** On the left, the average fluctuation of pupil size for all the stimulus repetitions. On the right the average pupil size. During the presentation of the orienting stimulus, Cdkl5$^{-/y}$ mice showed a reduced pupillary dilation compared to Cdkl5$^{+/y}$ (P-value < 0.05, Unpaired T-Test); the shaded area represents the presentation of the VR stimulus. **(B)** On the left, the average running velocity for all the stimulus repetitions. On the right the average velocity. Cdkl5y$^{-/y}$ mice showed a different behavioral response compared to Cdkl5$^{+/y}$ (P-value < 0.05, Unpaired T-Test), the shaded area represents the presentation of the VR stimulus. **(C,D)** PLR response reveals no significant differences in both pupil constriction (top) and pupil re-dilation (bottom) between Cdkl5$^{-/y}$ mice and Cdkl5$^{+/y}$. On the left, single animal traces and average fluctuation (thick line) of pupil size. Shaded area represents the presentation of the high luminance stimulus. Vertical dashed lines represent the onset of the visual stimulus. On the right the average pupil size during pupil constriction and pupil re-dilation. n = 11 Cdkl5$^{+/y}$, n = 10 Cdkl5$^{-/y}$. *P-value < 0.05, ns = not significant.

appetitive operant conditioning task, almost all the models showed a remarkable discriminative capability between mutated and WT mice. In particular, depending on the model adopted, single mouse accuracy ranged between 77 and 83% and sensitivity between 75 and 87% (Table 6.1).

The same machine learning models were employed to test the predictive power of the alterations found in Cdkl5 mutant mice during pupillometry. Interestingly, we found that the pupillary and behavioral responses collected during the pupillometric assessments were good genotype predictors, with accuracy between 77 and 83% and sensitivity between 79 and 83% (Table 6.2). Finally, when we combined the models of the appetitive operant conditioning parameters with the parameters acquired during pupillometry, we found that the prediction power remarkably increased, reaching an accuracy between 77 and 91% and sensitivity between 73 and 91% (Table 6.3).

Table 6.1: Genotype classification of machine learning models using operant conditioning parameters

Model	Accuracy (Mean %)	Specificity (Mean %)	Sensitivity (Mean %)	Permutation Scores (%)	p-value	Significance
SVC	82.8	88.4	78.6	52.5	< 0.01	**
MLP Classifier	82.5	80.0	86.8	53.1	< 0.01	**
Gaussian Process Classifier	81.9	85.2	83.2	52.8	< 0.01	**
Decision Tree Classifier	81.3	84.3	81.0	51.0	< 0.01	**
AdaBoost Classifier	81.2	83.9	83.0	51.6	0.02	*
Logistic Regression	76.9	80.3	75.25	53.3	< 0.01	**
K Neighbors Classifier	74.2	84.8	66.3	52.9	0.12	ns
Dummy Classifier	50.4	51.2	48.4	50.1	0.47	ns

Abbreviations: OC, Operant Conditioning; ns, not significant.

Table 6.2: Genotype classification of machine learning models using head-fixed condition parameters

Model	Accuracy (Mean %)	Specificity (Mean %)	Sensitivity (Mean %)	Permutation Scores (%)	p-value	Significance
Logistic Regression	83.1	86.1	82.5	52.3	0.02	*
MLP Classifier	81.7	82.9	83.1	51.2	0.02	*
SVC	81.0	82.2	80.9	49.9	<0.01	**
Ada Boost Classifier	80.1	87.7	74.3	50.0	0.02	*
Decision Tree Classifier	79.7	85.7	73.1	50.3	<0.01	**
Gaussian Process Classifier	77.1	79.4	79.7	50.4	0.02	*
K Neighbors Classifier	73.7	74.8	74.7	49.2	0.11	ns
Dummy Classifier	48.8	47.3	49.9	50.6	0.18	ns

Abbreviations: OR, Orienting Response; ns, not significant.

Table 6.3: Genotype classification of machine learning models using operant conditioning and head-fixed parameters

Model	Accuracy (Mean %)	Specificity (Mean %)	Sensitivity (Mean %)	Permutation Scores (%)	p-value	Significance
MLP Classifier	91.4	92.6	91.7	51.1	0.02	*
Logistic Regression	88.8	89.6	88.3	50.8	0.04	*
SVC	87.7	92.9	84.4	50.6	< 0.01	**
Gaussian Process Classifier	86.6	93.6	81.0	50.4	< 0.01	**
K Neighbors Classifier	82.4	94.5	70.5	51.2	< 0.01	**
Decision Tree Classifier	78.8	86.1	72.6	50.8	< 0.01	**
Ada Boost Classifier	77.2	82.8	73.7	51.2	< 0.01	**
Dummy Classifier	51.5	50.8	52.5	49.2	0.62	ns

Abbreviations: OC, Operant Conditioning; OR, Orienting Response; ns, not significant.

7 Discussion

This study reports alterations in behavioral and physiological parameters of male Cdkl5 deficient and female heterozygous mice capable of classifying CDD subjects with high accuracy and sensitivity. Behavioral impairment was assessed in an appetitive operant conditioning task using a fully automated and standardized appetitive operant conditioning chamber (Mazziotti et al. 2020). In agreement with previous studies, (Jhang et al. 2017; Jhang et al. 2020; Adhikari et al. 2022), the appetitive operant conditioning task revealed hyperactive and impulsive behavior in both male and female Cdkl5 mutant mice. Intriguingly, differences in the strategies employed by mutant female and male mice appeared. Indeed, female mutants showed a difference already during the first day of testing. Although this difference could be further explored, it could be related to the sex influence on the strategies used during reinforcement learning displayed by mice. Indeed, previous studies showed that WT female mice had faster task acquisition than males. Thus, a deficit present in CDKL5 deficient mice could emerge at earlier time points than in males (C. S. Chen et al. 2021). We also demonstrated lower levels of cognitive flexibility, linked to an impairment in inhibitory control in Cdkl5 null mice. Indeed, while mutant mice could successfully perform more trials than controls if they had to wait only for a short time, they persevered with the previous strategy if the waiting time was prolonged, resulting in less successful trials than controls. This deficit is transient, returning to WT levels in three days and suggesting the presence of slower residual flexibility in Cdkl5 null mice. Inhibitory control, such as cognitive flexibility, is an executive function mediated by the prefrontal cortex (Narayanan et al. 2017), that implies being able to control impulses and old habits of thought or action (e.g. conditioned responses) (A. Diamond 2013). Impairments in executive abilities such as cognitive flexibility and inhibitory control have been identified in individuals with ASD (L. M. Schmitt et al. 2018). In particular, deficits in inhibitory control were associated with restricted and repetitive behaviors (St John et al. 2016). Intriguingly, symptoms of inattention and hyperactivity, typical features of ADHD, have been frequently documented in children with ASD (Leitner 2014) and could also be present in CDD patients, although the Cdkl5 gene has not been linked to ADHD in a genome-wide association study (Demontis et al. 2019). Previous studies showed that impulsivity and hyperlocomotion of Cdkl5 null mice could be corrected by methylphenidate, an inhibitor of the dopamine transporter clinically effective in improving ADHD symptoms, suggesting a role for dopaminergic impairment in mediating impulsivity deficits (Jhang et al. 2017; Jhang et al. 2020).

7.0.1 Arousal impairment in Cdkl5 null and heterozygous mice

Our study shows that the presence of hyperactivity is also associated with impairment in processes controlling general arousal in Cdkl5 mice assessed by measuring pupil size regulation and locomotor behavior. We found that Cdkl5 mutants stay longer than wild-type mice in

a high arousal state characterized by a dilated pupil and running. Absolute values of pupil size were always significantly smaller than controls in both male null and female heterozygous Cdkl5 mutant mice, although relative pupillary dilation during running or pupillary response to illumination change was unaffected. Constitutive smaller pupil size is reported to be linked with working memory and cognitive abilities and could be related to altered activity of the locus coeruleus-noradrenergic system (Kucewicz et al. 2018; Tsukahara et al. 2021; Gary Aston-Jones et al. 2005). Our study also revealed alterations in pupillary response to unexpected visual stimuli, a component of the orienting response commonly used also for human assessment (C.-A. Wang et al. 2015). Indeed, we found that wild-type mice exhibited a considerable and sustained pupil dilation in response to unexpected stimuli while mutants showed a smaller and transient dilation. The presentation of the unexpected stimulus also led to an increased running in wild-type mice but not in mutant mice. Previous studies showed that cortical processing of visual stimuli is altered in mice carrying mutations of the CDKL5 gene (Mazziotti et al. 2017b). This comprises aberrant visual cortical responses, and moderately reduced contrast sensitivity and visual acuity. Aware of this limitation, we designed the virtual reality environment, adopted as an orienting stimulus, with a spatial frequency content (0.06-0.1 cyc/deg) and contrast (90%), well within the visual perceptual thresholds of mutant mice. However, arousal alterations per se could affect perception since interaction between arousal (and behavioral state) and visual (in general sensory) perception has been clearly revealed by studies on the visual primary areas both in mice (Neske et al. 2019; Shimaoka et al. 2018) and in humans (Woods et al. 2013; T.-H. Lee et al. 2014). Further studies on the interaction between arousal and visual perception in CDKL5 mutant mice could elucidate the presence of possible bidirectional effects. Overall, these data are consistent with a scenario in which Cdkl5 mutants are most of the time in a high arousal state that is not further increased by novel stimuli. Notably, the pupillary light reflex analysis did not show alterations, demonstrating that the observed pupillary alterations are attributable to central dysfunctions rather than iris muscle or autonomic control abnormalities. The central origin of these deficits is in line with a recent study by Artoni et al. revealing broadly distributed pupil sizes as a signature shared by mouse models of idiopathic or monogenic ASD, comprising CDD (Artoni et al. 2020). In particular, in this study, the pupillary deficit of MeCP2 deficient mice could be rescued by the selective expression of MeCP2 in cholinergic circuits. The combination of behavioral inflexibility and arousal deficits could arise from alterations in the multistage neural pathways between the prefrontal cortex and subcortical nuclei, such as the striatum and the subthalamic nucleus that have been proposed to support inhibitory control and behavioral states through direct and indirect routes (Rae et al. 2015; Zhang et al. 2014). Cdkl5 mRNA is expressed in cholinergic nuclei and superior colliculus (mousebrain.org), two structures implicated in central pupillary control and orienting response (Nieuwenhuis et al. 2011; C.-A. Wang et al. 2015). However, an in-depth investigation is needed to clarify this point.

7.0.2 Machine learning reveals a robust biomarker of CDD

Our machine learning models revealed that behavioral impulsivity and orienting response assessed by pupillometry are good predictors of CDD, with an enhanced power when evaluated together. Pupillometry is a non-invasive, quantitative, and fully translational tool already used in clinical

practice that requires minimal collaboration by the subject, and it has been used even in newborns and preterm infants at postpartum age of 1 day (Cocker et al. 2005). Recently developed methods are opening the possibility to perform these measurements in a clinical and a domestic environment (Mazziotti et al. 2021). Since early diagnosis is essential to evaluate treatment outcomes and pupillary measures can be performed quickly, also in preverbal subjects, we propose the monitoring of resting-state and orienting response pupillometry as a promising and practical biomarker for CDD. The presence of arousal impairments in different neuropsychiatric disorders raises the possibility that pupillometry could be used also in ASD (Vries et al. 2021) and ADHD (Sekaninova et al. 2019) or in psychiatric conditions involving arousal alterations such as bipolar disorder.

8 Methods

8.1 Animal handling

Animals were maintained in rooms at 22°C with a standard 12-h light-dark cycle. During the light phase, a constant illumination below 40 lux from fluorescent lamps was maintained. Food (standard diet, 4RF25 GLP Certificate, Mucedola) and water were available ad libitum and changed weekly. Open-top cages with wooden dust-free bedding were used. All the experiments were carried out according to the directives of the European Community Council (2011/63/EU) and approved by the Italian Ministry of Health. All necessary efforts were made to minimize both stress and the number of animals used. The mice used in this work derive from the Cdkl5 null strain in C57BL/6N background developed in (Amendola et al. 2014), and backcrossed in C57BL/6J for seven generations. Male WT mice were bred with female heterozygous to obtain mutant and WT littermates. Weaning was performed on postnatal day (P)21–23. Genotyping (P10–12) was performed on tail tissue as described in (Amendola et al. 2014). We tested mice from P60 to P120. Colony founders were selected for the absence of the rd8 retinal degeneration allele spontaneously present in C57BL/6N mice (Mattapallil et al. 2012). Data analysis was performed by experimenters blind to the genotype.

8.2 The Appetitive Operant Conditioning protocol

To perform the appetitive conditioning task we used a custom-made appetitive operant conditioning chamber, as described in Mazziotti et al. 2020 (Mazziotti et al. 2020). Before starting the experiments, mice were handled for one week 5 minutes per day. During appetitive operant conditioning protocol, mice were water restricted (all mice maintained a body weight above 85% of their baseline). We performed the first day of familiarization, by placing each animal in the appetitive operant conditioning box for three sessions of 10 min, spaced by at least 2h between each other. During this phase, a liquid reward (1% saccharin), coupled with the reward tone (3300 Hz), is provided manually whenever the mouse is in the active area (located on the side opposite to the interface wall), in this way the animal learns where to find the reward and associate it with the tone. The day after the familiarization we start the OC task (3 sessions per day, duration: 4 days). In the OC phase a visual stimulus was introduced, consisting of two bright blue dots (luminance: 0.9 cd/m^2, wavelength: 465–475 nm, diameter: 5 mm) that appear above the two buttons after waiting for 1.5 sec in the activation area. Mice must touch one of the two buttons to obtain the liquid reward. We quantify the number of trials per session, the reaction time (the time between the activation of the trial and the button touch), the intertrial interval (the time elapsed between the response and the activation of a new trial), the speed and distance traveled. The second group of mice, after the appetitive operant conditioning task, was introduced to the delayed task (duration 3 days). In this new version of the test, the time

needed to activate a new trial was extended from 1.5 sec to 4 sec. In order to evaluate the ability to inhibit a learned automatic response, we also introduced the perseveration index using a custom-made Matlab software processing the mouse-tracking data. To analyze mouse-tracking data the arena is virtually divided into 256 (16 x 16) bins and raw exploration is z-scored to obtain relative exploration measures. In particular, a perseveration was counted every time the mouse exited the active zone before the 4 sec limit.

8.3 Surgery

Mice were deeply anesthetized using isoflurane (3% induction, 1.5% maintenance), placed on a stereotaxic frame, and head fixed using ear bars. Prilocaine was used as a local anesthetic for the acoustic meatus. Body temperature was maintained at 37 degrees using a heating pad, monitored by a rectal probe. The eyes were treated with a dexamethasone-based ophthalmic ointment (Tobradex, Alcon Novartis) to prevent cataract formation and keep the cornea moist. Respiration rate and response to toe pinch were checked periodically to maintain an optimal level of anesthesia. Subcutaneous injection of Lidocaine (2%) was performed prior to scalp removal. The Skull surface was carefully cleaned and dried, and a thin layer of cyanoacrylate was poured over the exposed skull to attach a custom-made head post that was composed of a 3D printed base equipped with a glued set screw (12 mm long, M4 thread, Thorlabs: SS4MS12). The implant was secured to the skull using cyanoacrylate and UV curing dental cement (Fill Dent, Bludental). At the end of the surgical procedure, the mice recovered in a heated cage. After 1 hour, the mice were returned to their home cage. Paracetamol was used in the water as antalgic therapy for three days. We waited for seven days before performing head-fixed pupillometry to provide sufficient time for the animals to recover.

8.4 Pupillometry

During pupillometry, mice were head-fixed and free to run on a circular treadmill. We employed a modified version of the apparatus proposed by Silasi et al. (Silasi et al. 2016), equipped with a 3D printed circular treadmill (diameter: 18cm). Velocity was detected using an optical mouse below the circular treadmill. To record the pupil, we used a USB camera (oCam-5CRO-U, Withrobot Lens: M12 25mm) connected to a Jetson AGX Xavier Developer Kit (NVIDIA) running a custom Python3 script (30fps). Real-time pupillometry was performed using MEYE (Mazziotti et al. 2021), a convolutional neural network that performs online pupillometry in mice and humans (Mazziotti et al. 2021). Before the experiments, mice were handled for one week 5 minutes each day; then, they were introduced gradually to head-fixation for an increasing amount of time for three days (habituation). During days 1 and 2, we performed two sessions of 10 minutes of head-fixation, one in the morning and one in the afternoon. On Day 3, we performed one session of twenty minutes. During each head-fixation session, a curved monitor (24 inches Samsung, CF390) was placed in front of the animal (at a distance of 13 cm), showing a uniform gray with a mean luminance of 8.5 cd/m2. After the habituation phase, we performed the pupillary assessments. The assessment contains different epochs: 1) Uniform gray screen with a

mean luminance (Duration: 225 sec, mean luminance: 8.5 cd/m2). To allow the pupil to return to baseline, a uniform gray screen is also presented for 60 seconds between each stimulation. 2) VR coherent with the animal movement eliciting an orienting response (180 sec). Composed of a luminance linearized procedural virtual corridor written in C# and running in Unity. The virtual corridor was composed of sine-wave gratings at different orientations (walls at 0° and floor at 90°) and spatial frequencies (from 0.06 to 0.1 cycles/deg), with a mean luminance of 8.5 cd/m2. The animal position in the virtual corridor was updated using an optical mouse connected to the circular treadmill. 3) PLR (15 sec white screen. Luminance: 30 cd/m2). Each epoch is presented three times for a total duration of 30 minutes. For the pupillary assessment of female mice, we evaluated baseline pupil size and locomotion during the presentation of a uniform gray screen with a mean luminance of 8.5 cd/m2.

8.5 Machine Learning

Machine learning models were fitted and evaluated using Python and Scikit-Learn. All adopted models are binary classifiers predicting the genotype from numeric behavioral and physiological features. We considered as behavioral parameters, the number of trials per session, the reaction time and the intertrial interval during the appetitive operant conditioning test and delayed task; as physiological features, we considered the average pupil size in resting and in running, the running speed, the running duration, and the pupillary ratio between resting and running in the different visual presentations. Input features are standardized before training. The specific models we adopt, together with the hyperparameter we tuned, are the following. The default Scikit-Learn parameters were used, if otherwise not specified.

Logistic Regression with L2 regularization (Bishop 2006); regularization strength is searched in logarithmic scale in [10-4, 105]. Support Vector Machine Classifier (SVC, (Platt et al. 1999)); we test linear and Gaussian kernels; the regularization parameter and the kernel scaling coefficient (only for Gaussian kernels) are searched in logarithmic scale respectively in [10-4, 105] and [2-4, 25]. Gaussian Process Classifier (Rasmussen et al. 2005) with unitary RBF kernel. Decision Tree (Hastie et al. 2013) with maximum depth searched in [1, 6]. AdaBoost Classifier (Freund et al. 1997) with a 1-level-deep decision tree as a base estimator. K-Nearest Neighbors Classifier with uniform neighbors weighting; the best number of neighbors k is searched in [1,3]. Multi-layer Perceptron (MLP) Classifier (Hinton 1989) with one 100-neuron hidden layer and ReLU activation; the network is trained with the Adam optimizer for 1000 iterations; the learning rate and L2 regularization strength parameters are grid-searched respectively in [0.001, 0.01, 0.1] and [0.0001, 0.01, 1, 10].

For each model and each configuration of hyperparameters, the mean and standard deviation of accuracy, specificity, and sensitivity are computed using 100 bootstrapped data splits; in addition, a permutation test with 100 permutations is performed using the 5-fold accuracy as a score. For brevity, only the best-performing configuration of hyperparameters is reported for each model. As a baseline, we also report the performance of the random classifier (Dummy Classifier).

8.6 Data analysis and statistics

Data analysis was performed using Python (Pupillometry and locomotion activity) and Matlab (Appetitive operant conditioning). Resting and running epochs are identified using an automated algorithm written in Python. The beginning of a moving epoch is defined as a period of at least 2 seconds in which velocity is higher than 1% with respect to the peak velocity of the subject. The epoch ends when velocity is below 1% for at least two seconds. The statistical analysis was performed using Python custom scripts and GraphPad Prism 7.

9 Selective Disruption of Perineuronal Nets in Mice Lacking Crtl1 is Sufficient to Make Fear Memories Susceptible to Erasure

9.1 Summary

The ability to store, retrieve, and extinguish memories of adverse experiences is an essential skill for animals' survival. The cellular and molecular factors that underlie such processes are only partially known. Using chondroitinase ABC treatment targeting chondroitin sulfate proteoglycans (CSPGs), previous studies showed that the maturation of the extracellular matrix makes fear memory resistant to deletion. Mice lacking the cartilage link protein Crtl1 (Crtl1-KO mice) display normal CSPG levels but impaired CSPG condensation in perineuronal nets (PNNs). Thus, we asked whether the presence of PNNs in the adult brain is responsible for the appearance of persistent fear memories by investigating fear extinction in Crtl1-KO mice. We found that mutant mice displayed fear memory erasure after an extinction protocol as revealed by analysis of freezing and pupil dynamics. Fear memory erasure did not depend on passive loss of retention; moreover, we demonstrated that, after extinction training, conditioned Crtl1-KO mice display no neural activation in the amygdala (Zif268 staining) in comparison to control animals. Taken together, our findings suggest that the aggregation of CSPGs into PNNs regulates the boundaries of the critical period for fear extinction.

9.2 Introduction to the project

The ability to extinguish fear memories when threats are no longer present is critical for adaptive behavior. During fear conditioning, the repeated pairing of an initially neutral stimulus (conditioned stimulus; CS) with an aversive stimulus (unconditioned stimulus; US) induces a strong and persistent fear memory (J E LeDoux 2000) that can be inhibited by repeated exposure to the CS in the absence of the US, a process called fear extinction (An et al. 2017). There is compelling behavioral evidence that extinction training does not erase or reverse the original CS-US association but rather leads to the formation of a new inhibitory memory that competes with the initial fear memory for the control of behavior (Myers et al. 2007; Bouton 2004). Fear memory extinction in adult animals is not permanent but decays with time, a process known as spontaneous fear recovery (Gregory J Quirk et al. 2008). Moreover, conditioned fear responses can be restored by presenting the US alone in the context in which extinction training occurred (reinstatement) (Bouton 2004; Gregory J Quirk et al. 2008; Vouimba et al. 2011) or may re-emerge following a shift in context (renewal) (Gogolla et al. 2009; Baldi et al. 2015). The extinction of conditioned fear memories in adults relies on a network of structures, such as the basolateral amygdala (BLA), the lateral amygdala (LA), and the ventromedial prefrontal

cortex (vmPFC) (Merz et al. 2018; Milad et al. 2002; Herry et al. 2008; Amano et al. 2010). Previous studies have provided numerous lines of evidence showing that extinction training of adult animals produces a new memory that inhibits the original fear memory stored in the lateral amygdala (LA) (Joseph E LeDoux 2014; Stephen Maren et al. 2004). In contrast, extinction seems to produce a permanent erasure of fear memory in juvenile animals, which do not exhibit reinstatement or context-dependent renewal of conditioned fear responses following an extinction protocol (Gregory J Quirk et al. 2010; Kim et al. 2007; Kim et al. 2009). The transition from a fear memory that can be erased in juvenile mice to a persistent fear memory in the adult has been suggested to rely on the maturation of the circuits involved in conditioned fear extinction (Gogolla et al. 2009). For example, removal of chondroitin sulfate proteoglycans (CSPGs) from the amygdala extracellular matrix (ECM) by enzymatic digestion allowed juvenile-like erasure of conditioned fear memories in adult animals (Gogolla et al. 2009). CSPGs are diffusely present in the ECM of the adult brain (Mouw et al. 2014) and condense around some cells forming perineuronal nets (PNNs) (Brückner et al. 2000). This process is triggered by neuronal production of the cartilage link protein Crtl1 (also known as HAPLN1), which is upregulated during development (Carulli et al. 2010; Carulli et al. 2007). The developmental condensation of CSPGs in PNNs of the visual cortex, rather than their sheer presence, plays a crucial role in protecting adult visual cortical circuits from being modified by experience (Carulli et al. 2010). However, it is unknown whether the condensation of CSPGs in PNNs, taking place during development, is also involved in the transition from a conditioned fear memory that can be erased by extinction to a fear memory that is no more susceptible to erasure. Also unknown is the mechanism through which PNNs make adult amygdala circuits resilient to extinction effects, protecting fear memories from erasure.

Here, we exploited mice lacking the Crtl1 protein (Crtl1-KO) which have attenuated PNNs but unchanged overall levels of CSPGs (Carulli et al. 2010), to investigate whether preventing the aggregation of CSPGs into PNNs is sufficient to induce fear memory susceptible to erasure, and assessing the associated pattern of activation. In particular, we assessed fear responses through freezing and pupil size, two well-established behavioral and physiological markers of fear memories. Freezing is a defensive response commonly used to evaluate associative fear memory in rodents, while pupil dilation has been widely used to objectively assess fear learning in humans (Leuchs et al. 2019; Leuchs et al. 2017; Korn et al. 2017) and provides valuable information about the role of arousal in modulating fear circuits (Bradley et al. 2008). We found that Crtl1-KO animals retain the juvenile feature of erasing a specific conditioned fear memory following a protocol of extinction. In particular, Crtl1-KO mice exhibited a stronger reduction in both pupillary and freezing response to the CS with respect to Crtl1-WT mice. This persistent reduction of fear in Crtl1-KO mice did not depend on passive loss of memory, since fear memories assessed 9 days after learning without intervening extinction protocol is comparable in Crtl1-KO and Crtl1 wild-type mice (Crtl1-WT). To assess the mechanisms through which PNN disruption leads to permanent erasure of a fear memory, we analyzed neuronal activation in the amygdala and in the infralimbic cortex (IL) at the end of the extinction protocol via immunostaining for Zif268. We found that following extinction, there was no neural activation in the amygdala of conditioned Crtl1-KO mice in response to CS, in accordance with the erasure of the conditioned

fear memory. On the contrary, Crtl1-WT mice showed a clear activation of these regions.

9.3 Declaration of author contributions

Here I summarize, for clarity, the details of my specific personal contribution to this project. All of the conceptual, experimental, and analytical tasks are grouped according to the level of my involvement in three categories as follows:

- I was the only/main contributor
  - Conceptualization of the project
  - Designing and conducting pupillometry experiments
  - Figures layout and data visualizations
  - Data Analysis
- I collaborated in the tasks
  - Behavioral experiments
  - Immunohistochemistry

10 Results

10.1 Lack of Crtl-1 accelerates extinction of fear memories in adult Crtl1-KO mice

To investigate whether the condensation of CSPGs in PNNs is crucial in the transition from a conditioned fear memory that can be erased by extinction to a conditioned fear memory that is not erasable, we performed a classical auditory cued fear conditioning and extinction protocol in Crtl1-KO mice and their WT littermates (Figure 10.1A). Crtl1-KO mice exhibit a marked decrease in the number of PNNs in the amygdala and IL cortex (Figure 10.2), key regions for the extinction of adult conditioned fear memories. During the habituation, mice freely explored the chamber (day 0, context A) showing low levels of freezing (below 4%), consistently with normal habituation to the context, with no difference between genotypes (Figure 10.1B). We also found comparable freezing levels between conditioned Crtl1-KO and Crtl1-WT mice during the learning phase of the test (day 1, Figure 10.1C). However, we found that Crtl1-KO mice exhibited a significantly accelerated pattern of freezing reduction with respect to Crtl1-WT mice (Figure 10.1D) during the first day of extinction (early extinction, day 2). In particular, freezing levels in Crtl1-KO become significantly lower than in Crtl1-WT mice as early as the third block of 2 conditioned stimuli (CS), reaching significantly lower levels of freezing with respect to the beginning of CS presentations (Figure 10.1D) at the end of the first day of extinction. During the second day of the extinction protocol (late extinction, day 3), Crtl1-KO mice maintained the low freezing levels achieved during the first day of extinction (Figure 10.1E), while Crtl1-WT mice began to decrease freezing, reaching levels comparable to Crtl1-KO mice from the fifth block of 2 CS (Figure 10.1E). These results demonstrate that CSPG condensation in PNNs due to cartilage link protein Crtl1 has an important role in promoting accelerated fear memory extinction but not in learning.

10.2 Pupillometry as a physiological readout of fear extinction in Crtl1-KO mice

Due to its sensitivity to arousal (Bradley et al. 2008; Bradshaw 1967; Nassar et al. 2012), the pupil responds with dilation to salient or threatening stimuli. For this reason, pupil dilations have gained interest as a measure of the conditioned response (Leuchs et al. 2019). We used pupillometry as a physiological readout of fear learning and extinction in Crtl1-KO mice and their WT littermates. We designed a virtual cued fear conditioning protocol, using a visual cue as CS, paired with a tail shock (US). During fear conditioning, mice were head-fixed and free to run on a circular treadmill. An infrared webcam was used to record the pupil and the MEYE Deep Learning tool was employed to perform pupillometry (Mazziotti et al. 2021)

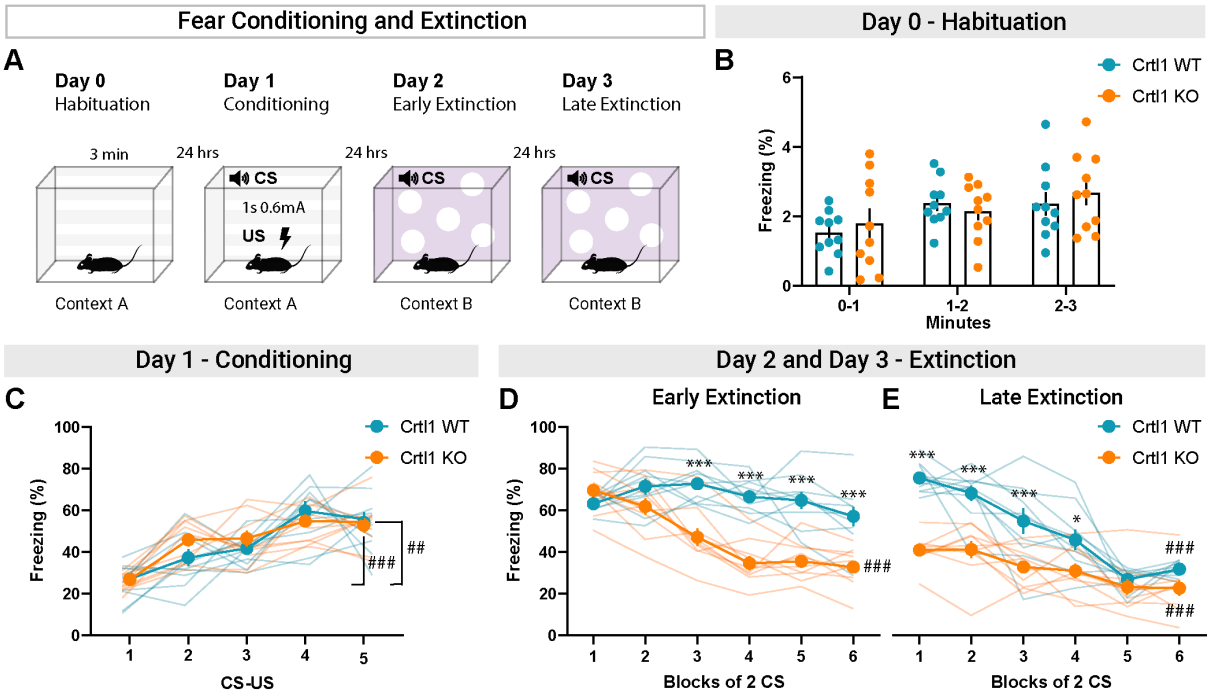

Figure 10.1: **Fear extinction in Crtl1-KO mice**. **(A)** Diagram showing the fear conditioning and extinction paradigm. **(B)** Habituation in Crtl1-KO and Crtl1-WT mice show low freezing levels and no differences between genotypes during 3-min exposition to the conditioned context **(C)** Freezing levels in Crtl1-KO and Crtl1-WT mice during conditioning. Both genotypes exhibit a comparable pattern of freezing increase, coherent with a normal pattern of fear learning and no deficits of fear acquisition (two-way RM ANOVA: genotype $p = 0.523$, CS-US $p < 0.001$, interaction genotype x CS-US $p = 0.346$; post hoc Sidak multiple comparisons, CS-US within Crtl1-WT: 1 vs. 5 $p < 0.01$; CS-US within Crtl1-KO: 1 vs. 5 $p < 0.001$). **(D)** During early extinction, Crtl1-KO mice but not Crtl1-WT mice exhibited a significantly accelerated pattern of freezing reduction, as early as third block of 2 CS (two-way RM ANOVA: genotype $p < 0.001$; blocks of 2 CS $p < 0.001$; interaction genotype x blocks of 2 CS $p < 0.001$; post hoc Sidak multiple comparisons, genotype within blocks of 2 CS, 1: $p = 0.721$, 2: $p = 0.251$, 3: $p < 0.001$, 4: $p < 0.001$, 5: $p < 0.001$, 6: $p < 0.001$), and significantly reduced their freezing levels at the end of the extinction protocol (post hoc Sidak multiple comparisons, Crtl1-WT 1 vs. 6: $p = 0.836$; Crtl1-KO 1 vs. 6: $p < 0.001$). **(E)** During late extinction, Crtl1-KO mice kept showing significantly lower freezing from first to fourth block of 2 CS (two-way RM ANOVA: genotype $p < 0.001$, blocks of 2 CS $p < 0.001$, interaction genotype x blocks of 2 CS $p < 0.001$; post hoc Sidak multiple comparisons, genotype within blocks of 2 CS, 1: $p < 0.001$; 2: $p < 0.001$; 3: $p < 0.001$; 4: $p < 0.05$; 5: $p = 0.980$; 6: $p = 0.369$) and significantly reduced their freezing levels (post hoc Sidak multiple comparisons, Crtl1-KO 1 vs. 6: $p < 0.001$). From the fifth block of 2 CS, Crtl1-WT mice reached freezing levels comparable to Crtl1-KO and significantly reduced their freezing levels (post hoc Sidak multiple comparisons, Crtl1-WT 1 vs. 6: $p < 0.001$). $n = 10$ Crtl1-KO, $n = 10$ Crtl1-WT. *P-value between genotypes, #P-value between CS. CS = conditioned stimulus; US = unconditioned stimulus

(Figure 10.3A). To assess the efficacy of our virtual fear conditioning protocol, first, we tested C57BL6/J wild-type mice receiving the CS alone (sham) or the CS paired with the US (shock) (Figure 10.4A, B). As shown in Figure 10.4, we observed stronger pupil dilations in response to CS in shocked mice compared to sham mice the day after conditioning (recall, Figure 10.4C, D) validating the use of pupil size measurement to reveal learned fear. Then, we evaluated fear learning in Crtl1-KO and Crtl1-WT mice (Fig. 2) in a cohort of mice different from the one used for freezing assessment. As assessed with freezing levels, we observed comparable pupillary

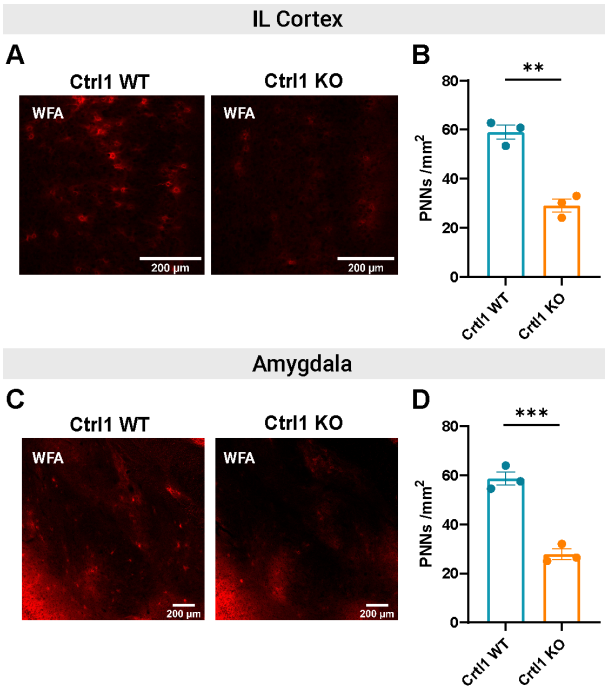

Figure 10.2: **PNNs number in the Infralimbic cortex (IL) and amygdala of Crtl1-KO and WT mice**. **(A)** Representative images of WFA staining in the IL cortex of Crtl1-KO and WT mice. **(B)** Number of PNNs in the IL cortex. Crtl1-KO mice present a lower number of aggregated PNNs compared to Crtl1-WT mice (Unpaired T-test $p < 0.01$). **(C)** Representative images of WFA staining in the amygdala of Crtl1-KO and WT mice. **(D)** Number of PNNs in the IL cortex. Crtl1-KO mice present a lower number of aggregated PNNs compared to Crtl1-WT mice (Unpaired T-test $p < 0.001$). n = 3 Crtl1-KO, n = 3 Crtl1-WT.

response between genotypes to the CS after learning (Figure 10.3B-D). Interestingly, we found that Crtl1-KO mice exhibited a stronger reduction in the pupillary response to CS with respect to Crtl1-WT mice during the first day of extinction (early extinction) (Figure 10.3E, F). Pupillary responses in Crtl1-KO become significantly lower than in Crtl1-WT mice as early as the second block of 5 CS (Figure 10.3F). During the second day of the extinction protocol (late extinction), Crtl1-KO mice still showed significantly lower pupillary responses compared to Crtl1-WT mice (Figure 10.3G). Crtl1-WT mice reached pupillary responses comparable to Crtl1-KO mice from the second block of 5 CS of late extinction (Figure 10.3H). To exclude possible defects in the pupillary light response present in mutant mice, we evaluated the pupillary light reflex (PLR). The results revealed in Crtl1-KO mice an unaltered PLR during both constriction and pupil re-dilation (Figure 10.5). Thus, we observed a faster extinction of fear memories in Crtl1-KO mice also using a physiological measure.

10.3 Abnormal Spontaneous Recovery and Fear Renewal in adult Crtl1-KO mice

Seven days after late extinction (day 10), we assessed spontaneous recovery and fear renewal (Figure 10.6A). The results clearly showed that Crtl1-KO mice still displayed attenuation of fear response caused by the extinction protocol while Crtl1-WT mice exhibited a higher fear response

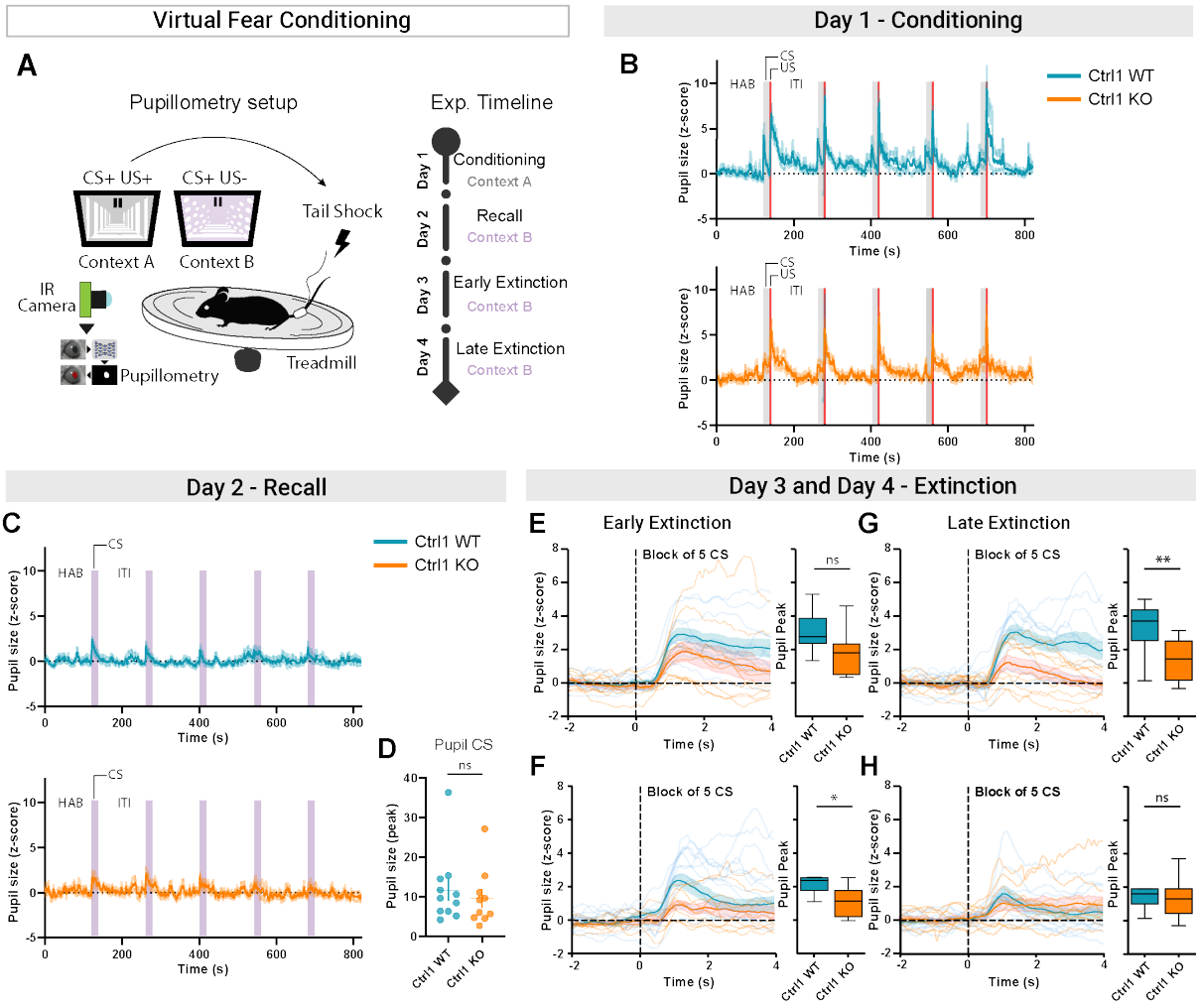

Figure 10.3: **Pupillometry assessment of fear extinction in Crtl1-KO mice**. **(A)** Diagram showing the pupillometry setup and the virtual fear conditioning timeline. **(B)** Average of the pupillary responses of Crtl1-WT (top) and Crtl1-KO (bottom) mice during the virtual fear conditioning. The gray area represents the presentation of the CS stimulus and the red area the presentation of the US stimulus. **(C)** Average of the pupillary responses of Crtl1-WT (top) and Crtl1-KO (bottom) mice during the virtual fear recall. The purple area represents the presentation of the CS stimulus. **(D)** During fear recall, we observed comparable pupillary responses between genotypes to the CS stimulus (unpaired T-test $p = 0.566$). **(E)** On the left, the average fluctuation of pupil size for the first block of 5 CS during early extinction. On the right, the pupil peaks during the presentation of the first 5 CS. We found no differences between genotypes (unpaired T-test $p = 0.208$). **(F)** On the left, the average fluctuation of pupil size for the second block of 5 CS during early extinction. On the right, the pupil peaks during the presentation of the second block of 5 CS. We found a lower pupillary response in Crtl1-KO mice compared to Crtl1-WT mice (unpaired T-test $p < 0.05$). **(G)** On the left, the average fluctuation of pupil size for the first block of 5 CS during late extinction. On the right, the pupil peaks during the presentation of the first 5 CS. We still found a lower pupillary response in Crtl1-KO mice compared to Crtl1-WT mice (unpaired T-test $p < 0.01$). **(H)** On the left, the average fluctuation of pupil size for the second block of 5 CS during late extinction. On the right, the pupil peaks during the presentation of the second 5 CS. We found no differences between genotypes (unpaired T-test $p = 0.527$). $n = 10$ Crtl1-KO, $n = 11$ Crtl1-WT. CS = conditioned stimulus; US = unconditioned stimulus; HAB = habituation; ITI = inter-trial; ns = not significant

retrieval, both for spontaneous recovery (Figure 10.6B) and for fear renewal (Figure 10.6D).

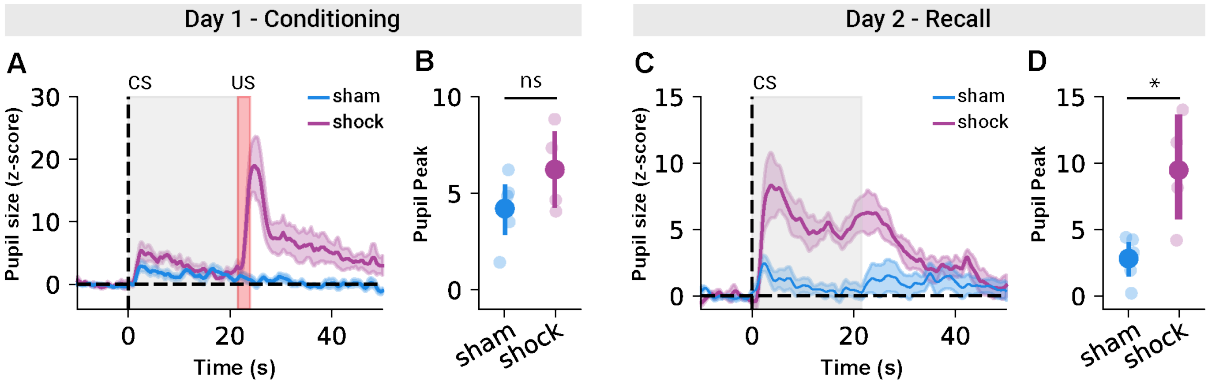

Figure 10.4: **Pupillary responses during the virtual fear conditioning in shock and sham wild-type mice**. **(A)** Average fluctuation of pupil size during the presentation of 5 CS (total CS duration 20 s) co-terminating (shock animals) or not (sham animals) with a US (2 s tail shock, 0.6 mA.). Gray shaded area represents the presentation of the CS and vertical dashed lines represent the onset of the CS. The red shaded area represents the presentation of the US. **(B)** Pupil peaks during the presentation of the 5 CS. We found no significant differences between groups but a trend in the pupillary response to CS in shock mice (Unpaired T-test $p = 0.352$). Gray shaded area represents the presentation of the CS and vertical dashed lines represent the onset of the CS. **(C)** Average fluctuation of pupil size during the presentation of 5 CS the day after conditioning (Recall) in shock and sham mice. **(D)** Pupil peaks during the presentation of the 5 CS. We found a significant difference between groups. In particular shock mice showed a higher pupillary response to CS compared to sham mice (Unpaired T-test $p < 0.05$). $n = 6$ sham, $n = 4$ shock. CS = Conditioned Stimulus; US = Unconditioned Stimulus; ns = not significant.

Moreover, the lower freezing level of Crtl1-KO mice remained evident throughout the repetition of CS, both for spontaneous recovery and for fear renewal protocols. Interestingly, we also found that both Crtl1-KO and Crtl1-WT mice showed the same freezing levels when placed in the unconditioned context (context B, spontaneous recovery) (Figure 10.6C), while Crtl1-WT mice showed a higher context-dependent freezing behavior compared to Crtl1-KO mice when placed in the conditioned context (fear renewal, context A) (Figure 10.6E).

Assessment of spontaneous recovery and fear renewal 42 days after the end of the late extinction (day 45, Figure 10.6A) showed that Crtl1-KO mice still displayed lower fear response caused by the extinction protocol compared to Crtl1-WT (Figure 10.6F and Figure 10.6H). The lower freezing level of Crtl1-KO mice with respect to Crtl1-WT mice during spontaneous recovery remained evident throughout the repetition of CS (Figure 10.6F). When the fear renewal protocol was employed, we found that Crtl1-KO mice showed significantly lower freezing during the 1 and 2 CS with respect to Crtl1-WT mice, while, during the 3 and 4 CS, Crtl1-WT mice reached freezing levels comparable to Crtl1-KO mice (Figure 10.6H). Again we found that both genotypes showed comparable freezing levels in the unconditioned context (context B, spontaneous recovery) (Figure 10.6G), while Crtl1-WT mice showed a higher context-dependent freezing behavior compared to Crtl1-KO mice when placed in the conditioned context (fear renewal, context A) (Figure 10.6I).

Taken together, these results suggest that PNN disruption in Crtl1-KO mice is sufficient to determine a juvenile-like fear extinction: Crtl1-KO mice show a persistent reduction of fear both in spontaneous recovery and in context-dependent renewal, 7 and 42 days after extinction; Crtl1-WT mice show, instead, the lack of long-term effects of extinction typical of adults.

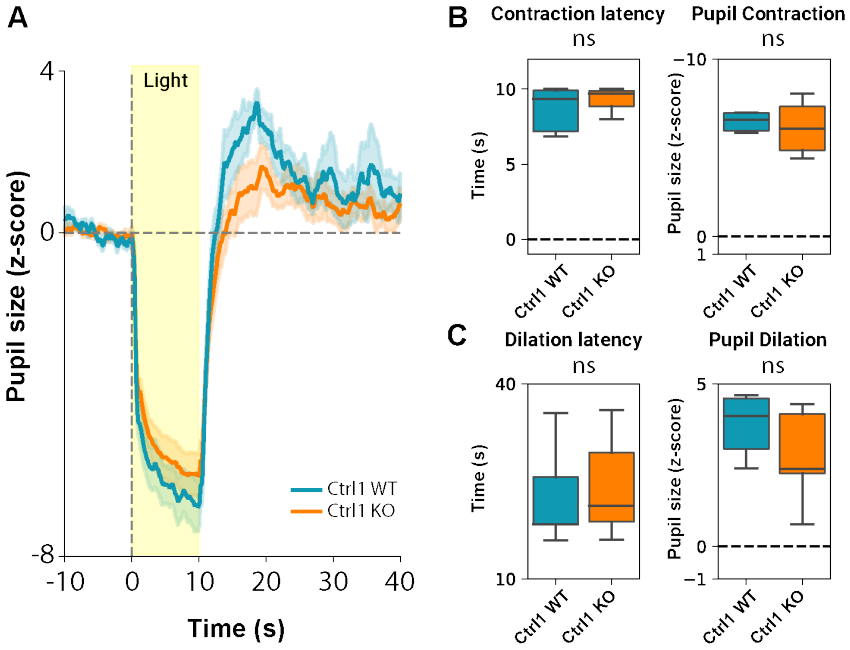

Figure 10.5: **Pupillary Light Reflex in Ctrl1-WT and Ctrl1-KO mice**. **(A)** Average fluctuation of pupil size during the presentation of the light flashes in Ctrl1-WT and Ctrl1-KO mice. The shaded area represents the presentation of the high-luminance stimulus. Vertical dashed lines represent the onset of the visual stimulus. **(B)** On the left, the average contraction latency during the presentation of the light flashes. On the right, is the average pupil size during contraction. For both the measures we found no significant differences between genotypes (contraction latency: Unpaired T-test p = 0.404, pupil contraction: Unpaired T-test p = 0.359). **(C)** On the left, the average re-dilation latency at the end of the light flashes. On the right, is the average pupil size during re-dilation. For both the measures we found no significant differences between genotypes (contraction latency: Unpaired T-test p = 0.759, pupil contraction: Unpaired T-test p = 0.177). n = 10 Crtl1-KO, n = 11 Crtl1-WT. ns = not significant.

10.4 Reduction of fear in Crtl1-KO mice did not depend on passive loss of memory

To ensure that the reduction in fear memory observed in Crtl1-KO mice after extinction was not due to a weakened consolidation and retention of the memory, we conducted a fear memory extinction test 9 days after fear conditioning (Figure 10.7A). We found that freezing levels in the 1 and 2 blocks of 2 CS did not differ between Crtl1-WT and Crtl1-KO mice (Figure 10.7B). This result confirms that Crtl1-KO mice do not show deficits in fear memory consolidation and retention. Moreover, we observed a faster decrease in fear response in Crtl1-KO mice compared to Crtl1-WT mice (Figure 10.7B). Also in this case, Crtl1-KO, but not Crtl1-WT mice, significantly reduced their freezing levels at the end of the early extinction protocol (Figure 10.7B). These results suggest that the higher efficacy of the extinction protocol in Crtl1-KO mice is present for both recent and older memories.

10.5 Fear extinction in adult Crtl1-KO mice is accompanied by a complete loss of amygdala activation in response to the CS

To assess neuronal activation in the amygdala and IL cortex of Crtl1-KO mice, we performed immunostaining for Zif268. Zif268 is an immediate early gene known to be implicated in neuronal plasticity and memory formation (Veyrac et al. 2014). We focused the analysis on the early extinction stage, corresponding to the maximal difference between Crtl1-KO and Crtl1-WT mice. To isolate the specific effect of associative learning on amygdala and IL activation from the effect of exposure to the CS and to the US, we compared conditioned mice to animals that received tone and electrical stimulation in an unpaired pattern (pseudo-conditioned mice) (Sacchetti et al. 2004) (Figure 10.8A).

The behavioral results show that both conditioned and pseudo-conditioned Crtl1-KO and Crtl1-WT mice showed a comparable response to the US, reaching a freezing level around 60% at the end of conditioning (Figure 10.8C). However, conditioned mice developed a strong response to the CS (Figure 10.8D). The results confirmed the enhanced extinction of Crtl1-KO mice by revealing a faster reduction of fear response in Crtl1-KO compared to Crtl1-WT mice (Figure 10.8D). As expected, pseudo-conditioned mice showed significantly lower levels of freezing with respect to conditioned mice, and did not show any significant reduction of freezing levels with extinction (Figure 10.8D). Therefore, this group of animals could be used to test Zif268 activation.

It has been shown that neurons in the lateral amygdala (LA) maintain high levels of response to CS even after extinction protocols (Repa et al. 2001). However, we found that there was no significant neuronal activation in the LA of conditioned Crtl1-KO mice after extinction, while neuronal activation was clearly present in conditioned Crtl1-WT mice compared to pseudo-conditioned Crtl1-WT mice (Figure 10.8E). Density for Zif268+ cells in the main output nucleus of the amygdala, the medial part of the central amygdala (CeM), resulted significantly higher in conditioned Crtl1-WT mice than in pseudo-conditioned Crtl1-WT mice, showing significant neuronal activation in CeM (Figure 10.8E). In conditioned Crtl1-KO mice, there was no significant difference in Zif268+ cell density with respect to Crtl1-KO pseudo-conditioned mice, showing absence of neuronal activation in CeM (Figure 10.8E), in accordance with behavioral results of very low fear response at the end of early extinction (Fig. 5D). Neuronal activation in conditioned Crtl1-KO mice was significantly lower than in conditioned Crtl1-WT mice, while no difference in neuronal activation was found between the two pseudo-conditioned groups (Figure 10.8E). We also found that density for Zif268+ cells in the lateral part of the central amygdala (CeL) resulted significantly higher in both conditioned Crtl1-WT and Crtl1-KO mice than in pseudo-conditioned mice, showing significant neuronal activation in CeL after extinction (Figure 10.8E). Thus, the lack of CeM activation in Crtl1-KO mice seems to be due to lack of LA activation (Figure 10.8E-F).

BLA is a crucial part of the intra-amygdala circuitry, providing a major point of control in the transmission of information between LA and CeM, and in particular is an important site of modulation of LA-CeM transmission during extinction (Herry et al. 2008; Bocchio et al. 2017; Critchley et al. 2002). The density of Zif268+ cells in the BLA showed the same pattern

found in CeM, with only conditioned Crtl1-WT mice showing significant neuronal activation in response to CS (Figure 10.8G). Thus, the absence of neuronal activation in Crtl1-KO mice is already present in BLA, one of the main inputs to CeM (Figure 10.8G-H). We also assessed neuronal activation in IL during early extinction as it seems to play a relevant role in reducing fear response during extinction protocols (Do-Monte et al. 2015; Milad et al. 2002). We found that both conditioned Crtl1-WT and Crtl1-KO mice showed significant IL activation at the end of early extinction although there was a strong trend for lower IL activation in KO with respect to WT mice (Figure 10.8G-H). Intriguingly, Zif268 induction in conditioned Crtl1-WT mice was observed also restricting Zif268 analysis to cells positive for WFA (Figure 10.9).

To analyze neuronal activation in Crtl1-KO and WT immediately after memory recall, we performed immunostaining for Zif268 in a different group of conditioned Crtl1-KO and WT mice perfused immediately after presenting one block of two CS (Figure 10.10A). We found that Zif268 + cells were higher in LA, BLA, CeM, CeL, and IL of Crtl1-KO than in WT mice (Figure 10.8B-E). This result is in line with the behavioral data shown in Figure 10.1D, Figure 10.7B, and Figure 10.8D, in which we found that Ctrl1-KO mice showed a consistent trend for higher freezing levels in response to the first block of two CS presented during early extinction. Thus, both behavioral and molecular data suggest in Crtl1-KO mice a more flexible circuit compared to WT, characterized by not only stronger memory recall but also faster and more persistent fear extinction (Figure 10.8D-H).

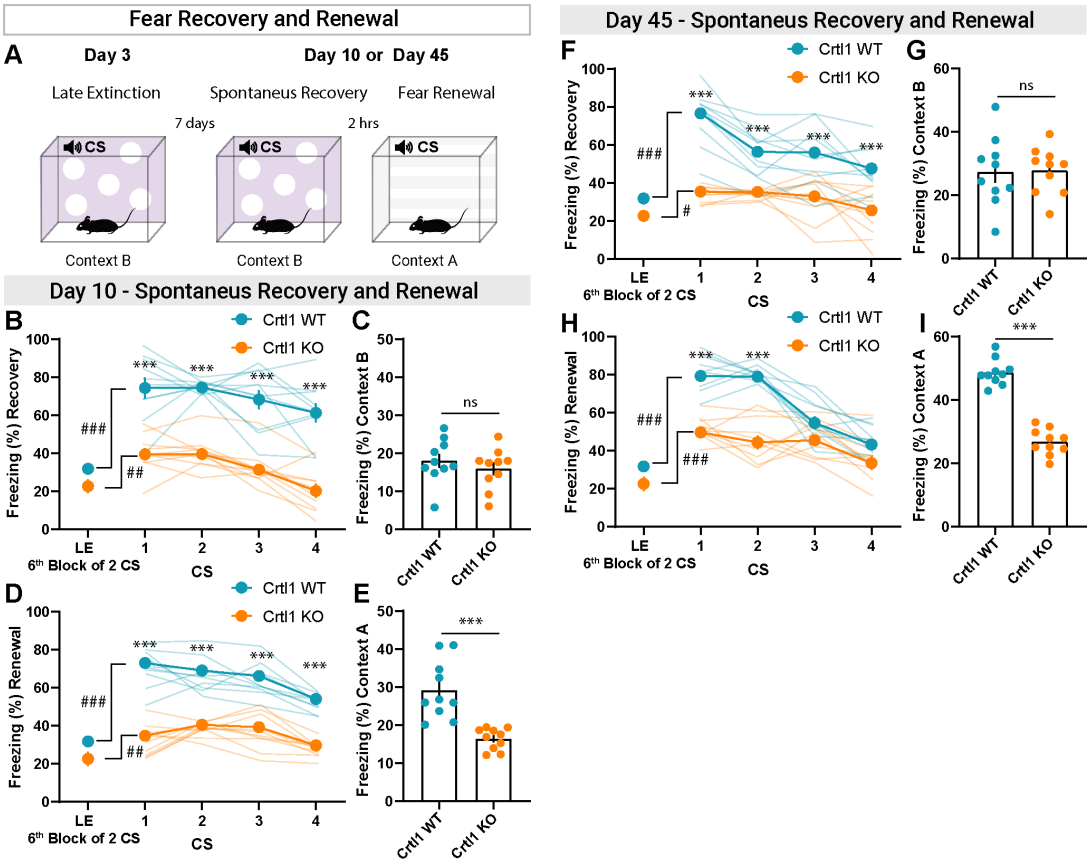

Figure 10.6: **Spontaneous recovery and fear renewal in Crtl1-KO mice.**. **(A)** Diagram showing the spontaneous recovery and fear renewal paradigm. **(B)** Spontaneous recovery 7 days after extinction (day 10). Crtl1-KO mice kept showing significantly lower freezing during all four CS presentations with respect to Crtl1-WT mice (two-way RM ANOVA, interaction genotype x CS $p < 0.001$, genotype $p < 0.001$, CS $p < 0.001$; post hoc Sidak multiple comparisons, genotype within CS, 1: $p < 0.001$, 2: $p < 0.001$, 3: $p < 0.001$, 4: $p < 0.001$). **(C)** Crtl1-KO and Crtl1-WT mice showed the same freezing levels when placed in the unconditioned context B, 7 days after extinction (day 10) (unpaired T-test, $p = 0.408$). **(D)** Fear renewal 7 days after extinction (day 10). Crtl1-KO mice kept showing significantly lower freezing during all four CS presentations with respect to Crtl1-WT mice (two-way RM ANOVA, interaction genotype x CS $p < 0.001$, genotype $p < 0.001$, CS $p < 0.001$; post hoc Sidak multiple comparisons, genotype within CS, 1: $p < 0.001$, 2: $p < 0.001$, 3: $p < 0.001$, 4: $p < 0.001$). **(E)** Crtl1-WT mice showed a higher context-dependent freezing behavior compared to Crtl1-KO mice when placed in the conditioned context A, 7 days after extinction (day 10) (unpaired T-test, $p < 0.001$). **(F)** Spontaneous recovery 42 days after extinction (day 45). Crtl1-KO mice kept showing significantly lower freezing during all four CS presentations with respect to Crtl1-WT mice (two-way RM ANOVA, interaction genotype x CS $p < 0.001$, genotype $p < 0.001$, CS $p < 0.001$; post hoc Sidak multiple comparisons, genotype within CS, 1: $p < 0.001$, 2: $p < 0.001$, 3: $p < 0.001$, 4: $p < 0.001$). **(G)** Crtl1-KO and Crtl1-WT mice showed the same freezing levels when placed in the unconditioned context B, 42 days after extinction (day 45) (unpaired T-test, $p = 0.928$). **(H)** Fear renewal 42 days after extinction (day 45). Crtl1-KO mice kept showing significantly lower freezing during the first two CS presentations with respect to Crtl1-WT mice (two-way RM ANOVA, interaction genotype x CS $p < 0.001$, genotype $p < 0.001$, CS $p < 0.001$; post hoc Sidak multiple comparisons, genotype within CS, 1: $p < 0.001$, 2: $p < 0.001$, 3: $p = 0.127$, 4: $p = 0.092$). **(I)** Crtl1-WT mice showed a higher context-dependent freezing behavior compared to Crtl1-KO mice when placed in the conditioned context A, 42 days after extinction (day 45) (unpaired T-test, $p < 0.001$). n = 10 Crtl1-KO, n = 10 Crtl1-WT. *P-value between genotypes, #P-value between CS. CS = conditioned stimulus; ns = not significant; LE = late extinction

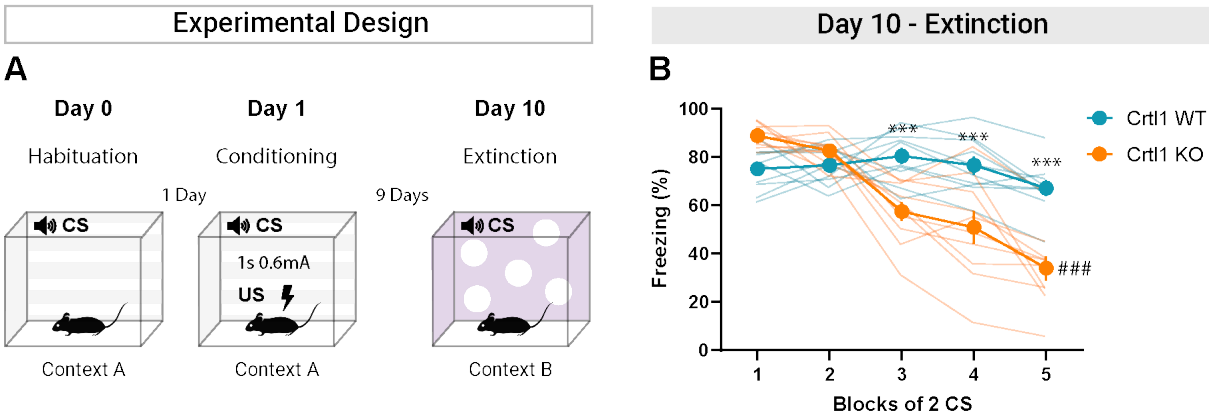

Figure 10.7: **Freezing levels in conditioned Crtl1-KO and Crtl1-WT mice during early extinction starting 9 days after fear conditioning.**. **(A)** Diagram showing the fear conditioning and extinction paradigm. **(B)** Even if the extinction procedure started 9 days after fear learning, Crtl1-KO mice, but not Crtl1-WT mice, exhibited a significantly accelerated pattern of freezing reduction, as early as third block of 2 CS (two-way RM ANOVA: genotype, $p < 0.01$; blocks of 2 CS: $p < 0.001$; interaction genotype x blocks of 2 CS: $p < 0.001$; post hoc Sidak multiple comparisons, genotype within blocks of 2 CS, 1: $p = 0.059$, 2: $p = 0.794$, 3: $p < 0.001$, 4: $p < 0.001$, 5: $p < 0.001$), and significantly reduced their freezing levels during early extinction (post hoc Sidak multiple comparisons, blocks of 2 CS Crtl1-WT, 1 vs. 5: 0.520, Crtl1-KO, 1 vs. 5: $p < 0.001$). n = 10 Crtl1-KO, n = 10 Crtl1-WT. *P-value between genotypes, #P-value between CS. CS = conditioned stimulus; US = unconditioned stimulus

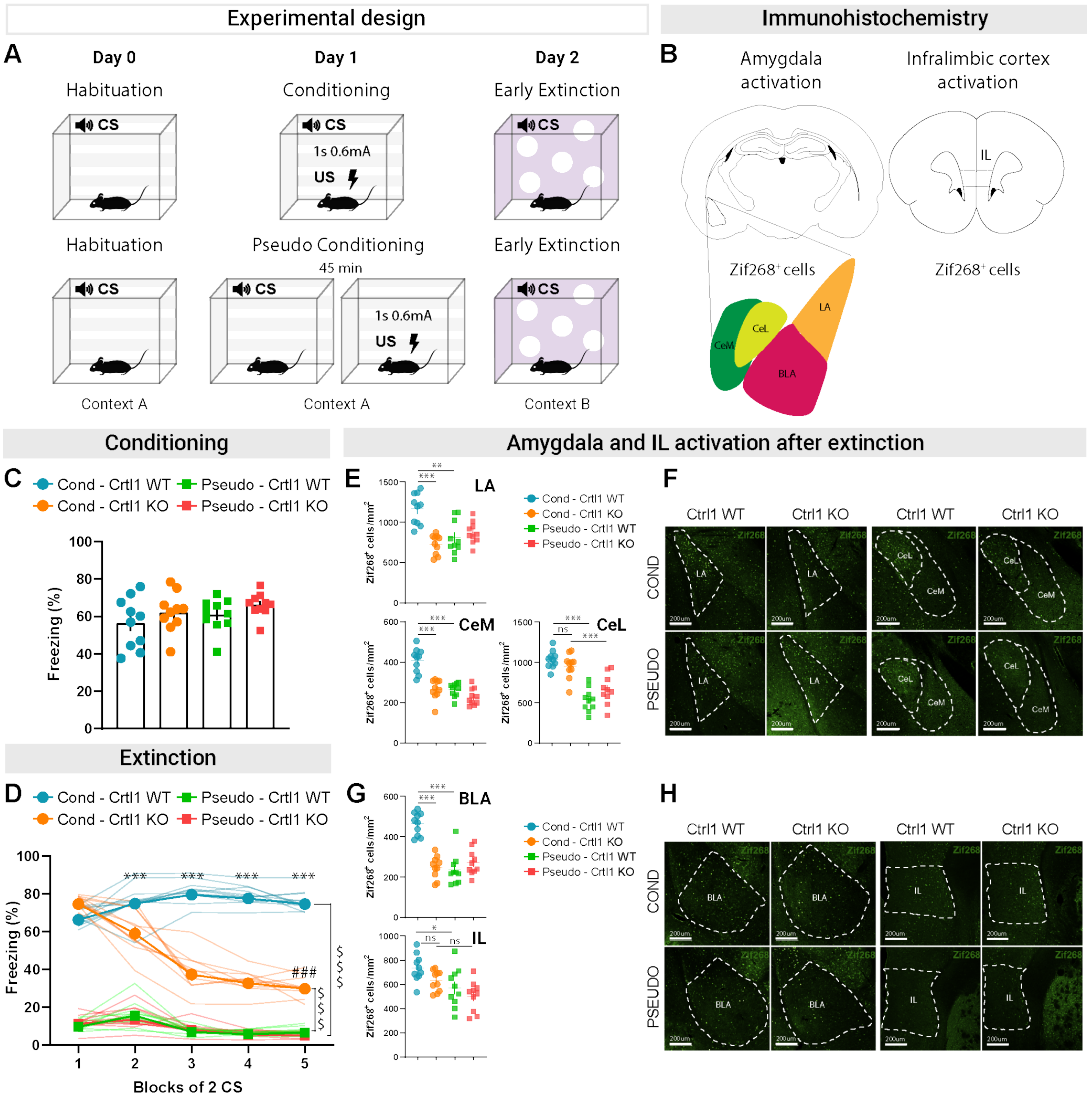

Figure 10.8: **Amygdala and IL cortex activation after extinction in Crtl1-KO mice**. **(A)** Diagram showing the experimental design. **(B)** Representative diagram of the areas considered for the Zif268 immunohistochemistry: BLA, basolateral amygdala; LA, lateral amigdala; CeM, medial part of the central amygdala; CeL, lateral part of the central amygdala; IL, infralimbic cortex. **(C)** Freezing levels in conditioned and pseudo-conditioned Crtl1-KO and Crtl1-WT mice at the end of the conditioning protocol. After 5 presentations of US, pseudo-conditioned Crtl1-KO and Crtl1-WT mice reached freezing levels comparable to conditioned mice (one-way ANOVA, $p = 0.216$). **(D)** Freezing levels in conditioned and pseudo-conditioned mice during the early extinction. Cond-Crtl1-KO mice exhibited a significantly accelerated pattern of freezing reduction (three-way ANOVA, genotype x condition x blocks of 2 CS $p < 0.001$. Genotype $p < 0.001$, condition: $p < 0.001$, blocks of 2 CS $p < 0.001$; genotype x condition $p < 0.001$, genotype x blocks of 2 CS: $p < 0.001$, condition x block of 2 CS, $p < 0.001$; post hoc Sidak multiple comparisons, the difference between Cond-Crtl1-KO and Cond-Crtl1-WT, CS-1: $p = 0.218$, CS-2: $p < 0.001$, CS-3: $p < 0.001$, CS-4: $p < 0.001$, CS-5: $p < 0.001$) and significantly reduced their freezing levels during early extinction (post hoc Sidak multiple comparisons, difference between freezing levels for the 1 and 5 blocks of 2 CS Crtl1-WT, $p = 0.200$; Crtl1-KO, $p < 0.001$). Pseudo-Crtl1-WT and pseudo-Crtl1-KO mice did not show any significant difference of freezing levels between genotypes but significantly lower freezing levels during all five blocks of 2 CS with respect to conditioned mice (post hoc Sidak multiple comparisons, condition within blocks of 2 CS, Cond-Crtl1-WT, 1 to 5: $p < 0.001$; Cond-Crtl1-KO, 1 to 5: $p < 0.001$). *Continued on next page.*

Figure 10.8: **(E)** Analysis of Zif268-positive cells in the LA (top), CeM (bottom left), and CeL (bottom right) of conditioned and pseudo-conditioned mice. Cond-Crtl1-KO mice showed significantly reduced levels of LA and CeM activation with respect to Cond-Crtl1-WT mice (LA, two-way ANOVA: genotype $p < 0.01$; condition $p = 0.051$; interaction genotype x condition $p < 0.001$. Post hoc Sidak multiple comparisons: Cond-Crtl1-WT vs. Cond-Crtl1-KO $p < 0.001$, Cond-Crtl1-WT vs. pseudo-Crtl1-KO $p < 0.01$) (CeM, two-way ANOVA: genotype $p < 0.001$; condition $p < 0.001$; interaction genotype x condition $p < 0.001$. Post hoc Sidak multiple comparisons: Cond-Crtl1-WT vs. Cond-Crtl1-KO $p < 0.001$, Cond-Crtl1-WT vs. pseudo-Crtl1-KO $p < 0.001$) and indistinguishable from those shown by pseudo-Crtl1-WT and pseudo-Crtl1-KO mice (LA, post hoc Sidak multiple comparisons: Cond-Crtl1-KO vs. pseudo-Crtl1-WT $p = 0.858$, Cond-Crtl1-KO vs. pseudo-Crtl1-KO $p = 0.349$) (CeM, post hoc Sidak multiple comparisons: Cond-Crtl1-KO vs. pseudo-Crtl1-WT $p > 0.99$, Cond-Crtl1-KO vs. pseudo-Crtl1-KO $p = 0.430$). Conditioned mice showed higher levels of CeL activation compared to pseudo-conditioned mice (two-way ANOVA: genotype $p = 0.630$; condition $p < 0.001$; interaction genotype x condition $p < 0.05$. Post hoc Sidak multiple comparisons: condition within WT mice $p < 0.001$, condition within KO mice $p < 0.001$). **(F)** Representative images of Zif268-positive cells in LA, CeM, and CeL of conditioned and pseudo-conditioned Crtl1-WT and Crtl1-KO mice after the fifth block of 2 CS during early extinction. Scale bar, 200 µm. **(G)** Analysis of Zif268-positive cells in the BLA (top) and IL (bottom) of conditioned and pseudo-conditioned Crtl1-WT and Crtl1-KO mice. Cond-Crtl1-KO mice showed significantly reduced levels of BLA activation with respect to Cond-Crtl1-WT mice (two-way ANOVA: genotype, $p < 0.001$; condition, $p < 0.001$; interaction genotype x condition, $p < 0.001$. Post hoc Sidak multiple comparisons: Cond-Crtl1-WT vs. Cond-Crtl1-KO $p < 0.001$, Cond-Crtl1-WT vs. pseudo-Crtl1-KO $p < 0.001$) and indistinguishable from those shown by pseudo-Crtl1-WT and pseudo-Crtl1-KO mice (post hoc Sidak multiple comparisons: Cond-Crtl1-KO vs. pseudo-Crtl1-WT $p = 0.997$, Cond-Crtl1-KO vs. pseudo-Crtl1-KO $p = 0.965$). Cond-Crtl1-KO mice showed comparable levels of IL activation such as that shown by Cond-Crtl1-WT mice (two-way ANOVA: genotype $p < 0.05$; condition $p < 0.001$; interaction genotype x condition $p = 0.634$. Post hoc Sidak multiple comparisons: genotype within conditioned mice $p = 0.124$, genotype within pseudo-conditioned mice $p = 0.401$), while pseudo-Crtl1-WT but not pseudo-Crtl1-KO mice showed reduced Zif268-positive cell density with respect to conditioned mice (post hoc Sidak multiple comparisons: condition within WT, $p < 0.05$; condition within KO, $p = 0.058$). **(H)** Representative images of Zif268-positive cells in BLA and IL of conditioned and pseudo-conditioned Crtl1-WT and Crtl1-KO mice after the fifth block of 2 CS during early extinction. Scale bar, 200 µm. n = 10 in each group. *P-value between genotypes, #P-value between CS, $P-value between conditions. CS = conditioned stimulus; US = unconditioned stimulus.

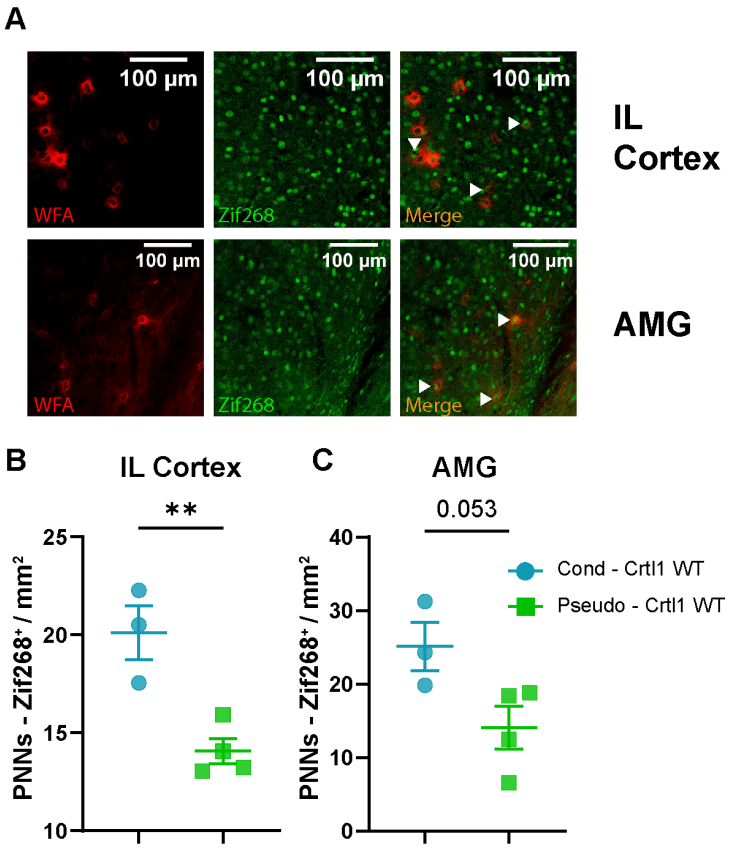

Figure 10.9: **Colocalization between PNNs and Zif268 in the infralimbic cortex and amygdala of conditioned and pseudo-conditioned Crtl-WT mice.**. **(A)** Double-immunofluorescence staining showing colocalization between WFA (red) and Zif268 (green) in the infralimbic cortex (IL) and amygdala (AMG) of conditioned and pseudo-conditioned Crtl1-WT mice after early extinction. **(B)** The number of PNNs surrounding a Zif268+ cell in the IL cortex is significantly higher in conditioned Crtl-WT mice compared to pseudo-conditioned Crtl-WT (Unpaired T-test, p= 0.0074). **(C)** The number of PNNs surrounding a Zif268+ cell in the amygdala of conditioned Crtl-WT mice is higher, albeit non-statistical significant, compared to pseudo-conditioned Crtl-WT (Unpaired T-test, p= 0.053). n = 3 Cond-Crtl WT , n = 4 Pseudo-Crtl WT. Scale bar, 100 µm.

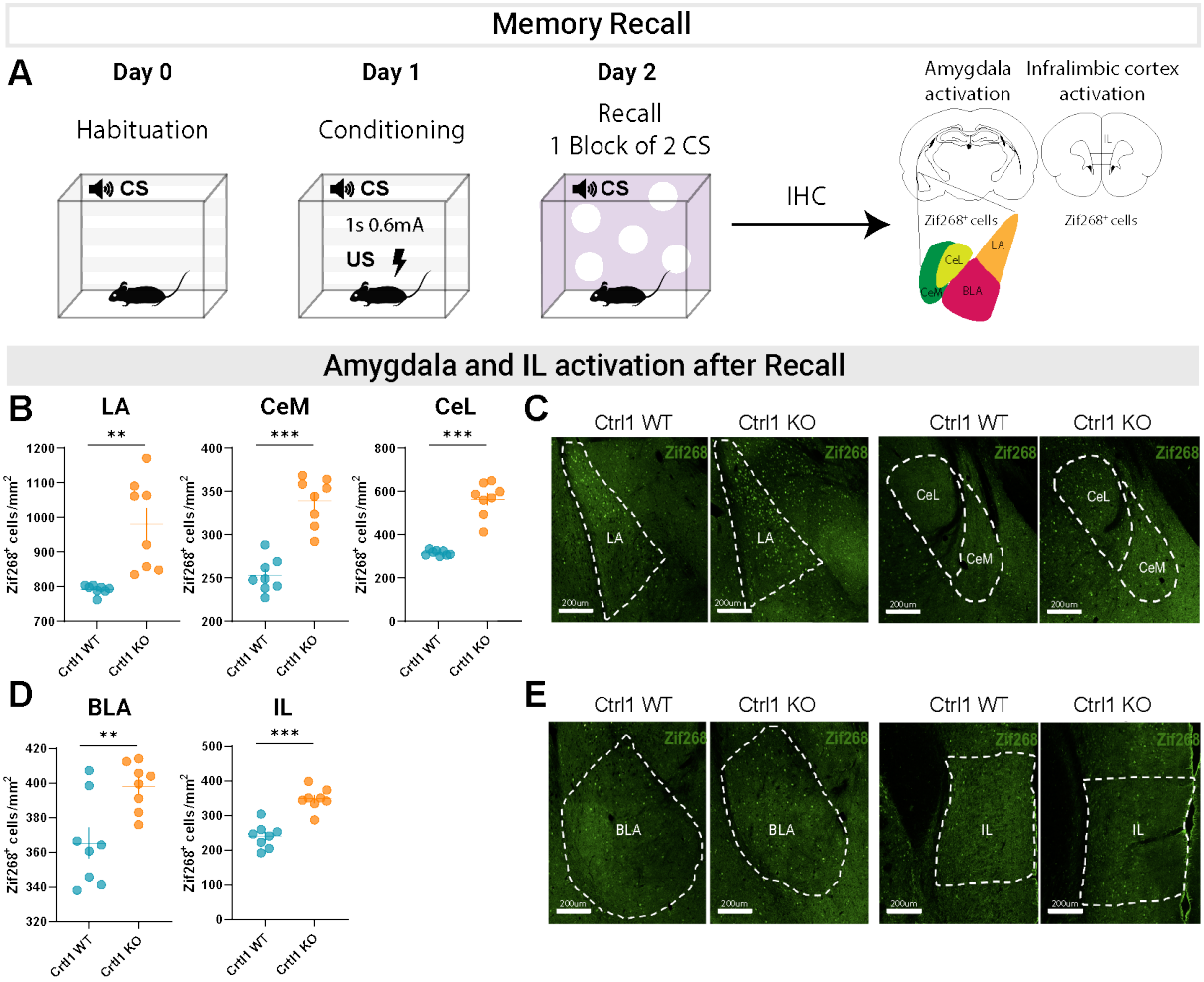

Figure 10.10: **Amygdala and IL activation after memory recall in Crtl1-KO mice**. **(A)** Diagram showing the experimental design **(B)** Analysis of Zif268+ cells in the LA, CeM, and CeL of Crtl1-WT and Crtl1-KO mice. Crtl1-KO mice showed significantly higher levels of LA, CeM, and CeL activation with respect to Crtl1-WT mice (unpaired T-test, LA: $p = 0.001$, CeM: $p < 0.0001$, CeL: $p < 0.0001$). **(C)** Representative images of Zif268+ cells in LA, CeM, and CeL of Crtl1-WT and Crtl1-KO mice after memory recall. Scale bar, 200 µm. **(D)** Analysis of Zif268+ cells in the BLA and IL of Crtl1-WT and Crtl1-KO mice. Crtl1-KO mice showed significantly higher levels of BLA and IL activation with respect to Crtl1-WT mice (unpaired T-test, BLA: $p = 0.006$, IL: $p < 0.0001$). **(E)** Representative images of Zif268+ cells in BLA and IL of Crtl1-WT and Crtl1-KO mice after memory recall. Scale bar, 200 µm. $n = 8$ Crtl1-KO, $n = 8$ Crtl1-WT. CS = conditioned stimulus; US = unconditioned stimulus

11 Discussion

Our results show that the removal of the Crtl1 protein that selectively disrupts the aggregation of CSPGs in PNNs is sufficient to promote an accelerated and persistent fear memory erasure after the administration of an extinction protocol. Indeed, during early extinction, Crtl1-KO mice showed reduced freezing levels as soon as the 3rd block of 2 CS while Crtl1-WT mice started showing freezing reduction at the end of the second day of extinction. These results were confirmed also by testing mutant and WT mice in a virtual fear conditioning protocol and using pupil dynamics as a physiological readout of fear learning and extinction. In humans, fear conditioning is often probed by measuring autonomic responses (Critchley et al. 2002), such as skin conductance responses or startle responses (A O Hamm et al. 1993; Leuchs et al. 2019). In recent years, these physiological measures have been complemented by pupil dilations (Leuchs et al. 2019; Leuchs et al. 2017; Korn et al. 2017). Pupillometry offers a promising, complementary method for the quantification of the conditioned response. Indeed, pupil size assessment is not aversive, and it can be easily combined with other measurements and provides information about the activity of the autonomic nervous system (Bradley et al. 2008) and locus coeruleus noradrenergic system (Reimer et al. 2016), which plays an important role in modulating fear responses and extinction (Giustino et al. 2018). Coherent with the behavioral results, we found in Crtl1-KO mice an accelerated reduction in the pupillary response to CS with respect to Crtl1-WT mice as soon as the first day of extinction.

We have also demonstrated that the condensation of CSPGs in PNNs triggered by neuronal production of the Crtl1 protein is needed for the transition from a conditioned fear memory that can be erased by extinction to a conditioned fear memory which is not. In order to assess if the observed acceleration in fear extinction translates in lower fear response at later stages, we tested freezing levels of Crtl1-KO and Crtl1-WT mice in the extinction context (spontaneous recovery) and in the training context (fear renewal) 7 and 42 days after late extinction. Interestingly, for both time points, we found a reduced spontaneous recovery and fear renewal in Crtl1-KO mice with respect to Crtl1-WT. Since early and late extinction were performed immediately after learning, the observed accelerated fear extinction pattern and the reduced freezing shown during spontaneous recovery and fear renewal may be the effect of an impairment in memory consolidation and a manifestation of oblivion. To rule out this possibility, we tested another group of Crtl1-KO and Crtl1-WT mice with a delay of 9 days between the end of the learning phase and the beginning of early extinction. We found that Crtl1-KO mice recapitulated the previous results, revealing that mutant mice do not show an impairment in memory consolidation and retrieval with respect to Crtl1-WT mice.

Our behavioral and physiological data are in accordance with the results of Gogolla et al. 2009, in which the injection of the chondroitinase ABC enzyme in the BLA is able to induce the acquired fear memories susceptible to erasure. In adult animals, the organization of CSPGs in PNNs is a key event in the control of central nervous system plasticity and in the closure of

critical periods in many brain regions (Gogolla et al. 2009; Pizzorusso et al. 2002; Nowicka et al. 2009). In the visual cortex, it has been shown that the developmental condensation of CSPGs in PNNs, rather than their sheer presence, play a crucial role in protecting adult visual cortical circuits from being modified by experience. The response of visual cortical circuits to monocular deprivation, which can be reinstated in the adult visual cortex by enzymatic removal of CSPGs (Pizzorusso et al. 2002), is also present in mice lacking Crtl1, which have attenuated PNNs but unchanged overall levels of CSPGs (Carulli et al. 2010). Overall, our data suggest the possibility that common general mechanisms of critical period closure exist in different brain circuits.

The exact mechanism of action of PNNs in plasticity is only partially known (Fawcett et al. 2019). Recently, superresolution microscopy provided a detailed description of the tight relationship between the PNN and the synaptic microstructure (Sigal et al. 2019). It would be of great interest to analyze if these high-resolution features are affected by Crtl1 mutation and if they correlate with memory changes.

The extinction of conditioned fear memories in adults relies on a network of structures, such as the amygdala, the vmPFC, and the hippocampus (Duvarci et al. 2014; Merz et al. 2018). In particular, when the CS is present, the LA excite glutamatergic neurons in the BLA and GABAergic neurons in the lateral and medial intercalated cells (ITCs) (Ehrlich et al. 2009) which separates the BLA from the central nucleus (CeA) (McDonald 1982; Nitecka et al. 1987). LA and BLA project dense glutamatergic synapses onto CeA, with the LA projecting only to its lateral sector (CeL) (H. Li et al. 2013), and the BLA projecting to both the lateral and the medial (CeM) sectors (Krettek et al. 1978; Pitkänen et al. 1995; Savander et al. 1995). In addition, convergent evidence suggests that the vmPFC, and in particular the IL (Sotres-Bayon et al. 2010), is necessary for the retention and recall of extinction (G J Quirk et al. 2000; Hugues et al. 2006; Burgos-Robles et al. 2007; Laurent et al. 2009). To elucidate the functional activation of amygdala and IL cortex in Crtl1-KO mice, we replicated our previous extinction experiment trying to isolate the effect of the association between the CS and the US. We compared the neuronal activation of a group of conditioned Crtl1-KO and Crtl1-WT mice with a group of pseudo-conditioned Crtl1-KO and Crtl1-WT mice, in which the CS and US were unpaired. In particular, we performed immunohistochemistry for the immediate early gene Zif268 after early extinction. Zif268 is a member of the zinc finger transcription factor family. It regulates the expression of various late-response genes involved in different neuronal processes, including synaptic plasticity (Veyrac et al. 2014). The role of Zif268 and other immediate early genes, such as c-fos and Arc, in learning and memory has been well described (Gallo et al. 2018). Zif268 expression is known to increase shortly after fear conditioning (Ressler et al. 2002), suggesting its importance in fear memory formation (Malkani et al. 2000). Studies in mutant mice have also shown that overexpression of Zif268 enhanced resistance to extinction of aversive memories (Baumgärtel et al. 2008), while failure to induce Zif268 allowed spontaneous recovery (Baumgärtel et al. 2008; Herry et al. 2004). Here we provide further evidence of Zif268's role as a marker of activity and plasticity changes in the amygdala and IL cortex after fear extinction. Indeed, the density of Zif268+ cells revealed a significant reduction in BLA, LA, and CeM activation of Crtl1-KO mice with respect to Crtl1-WT mice. Notably, Crtl1-KO mice activation was not significantly different from pseudo-conditioned mice. The reduced activation of CeM, as the

output of the amygdala, is in line with the reduced behavioral freezing shown by Crtl1-KO mice. Remarkably, the reduced activation of LA is coherent with the possibility that the behavioral reduction of freezing shown in Crtl1-KO mice may be implemented as early as in LA. Regarding IL, we did not find significant differences between Crtl1-KO and Crtl1-WT mice; however, Zif268+ cell density of Crtl1-KO mice showed a reduced variability and the levels are at the significance threshold. Since it has been shown that optogenetic activation of IL for 30 s is able to accelerate and reduce freezing levels (Do-Monte et al. 2015), it could be hypothesized that in Crtl1-KO mice IL may be precociously (as soon as the first block of 2 CS) and increasingly recruited, with respect to Crtl1-WT mice, contributing to the accelerated reduction of fear. During the fifth block of 2 CS, IL activation would be decreased (or comparable to the Crtl1-WT mice), since fear reduction has already been achieved. We also evaluated the activation of amygdala and IL neurons in Crtl1-KO and WT mice immediately after conditioning (memory recall). Our results revealed a higher number of Zif268+ neurons in Crtl1-KO mice compared to WT mice in both the amygdala nuclei and IL cortex. This observation aligns with previous research demonstrating enhanced memory following degradation of PNNs (Morellini et al. 2010; Romberg et al. 2013). It is plausible that the more flexible circuits present in Crtl1-KO mice not only lead to stronger fear conditioning but also facilitate faster and longer-lasting extinction.

Taken together, our behavioral and molecular findings suggest that the aggregation of CSPGs into PNNs is a key factor in regulating the boundaries of the critical period for fear memories. Moreover, we suggest a possible activation pathway responsible for the accelerated reduced behavioral freezing shown by Crtl1-KO mice after extinction. We also propose pupillometry as a complementary physiological readout of fear learning, which can be easily coupled with other physiological measures that require head-fixation procedures.

12 Methods

12.1 Animals

For this study, we used adult mice (P75-P120) lacking the Crtl1/Hapln1 gene in the CNS, but not cartilage, which leads to attenuated PNNs in the adult brain (Crlt1-KO) (Czipri et al. 2003) and their wild-type littermates control (Crtl1-WT) mice. In our experiments, both male and female mice were utilized as study subjects. To control for the potential influence of sex on our results, we conducted a thorough evaluation of any sex-specific effects across all experiments. Our findings indicated that there were no significant differences observed that could be attributed solely to sex (data not shown). Because the Crtl1 product is essential for cartilage, Crtl1 was disrupted globally ($Crtl1^{-/-}$) and then reintroduced under the control of the type II collagen-cartilage-specific promoter by crossbreeding with a second transgenic mouse line (Crtl1-Tg), as better described in Czipri et al. 2003. The resulting $Crtl1^{-/-}$/Crtl1-$Tg^{+/+}$ mice were on a BALB/C background; thus, for this study, they were backcrossed into a C57BL/6 J background for seven generations as described in Carulli et al. 2010. Animals' genotypes were identified through PCR on tail tissue (P10-P12), with primers for wild-type Crtl1, disrupted Crtl1, and Crtl1 transgene expressed in cartilage (Carulli et al. 2010). Mice were housed in groups, from two to five animals per cage (60 cm x 40 cm x 20 cm), and maintained in rooms at 22 °C with a standard 12-h light–dark cycle. Food (standard diet, 4RF25 GLP Certificate, Mucedola) and water were available ad libitum and changed weekly. Open-top cages with wooden dust-free bedding were used. All the experiments were carried out according to the directives of the European Community Council (2011/63/EU) and approved by the Italian Ministry of Health. All necessary efforts were made to minimize both stress and the number of animals used. One week before the start of behavioral experiments, all mice were handled daily by the experimenter for 5 min using an open hand approach to minimize anxiety and stress response induced by experimenter manipulation (Hurst et al. 2010).

12.2 Fear conditioning

Mice were subjected to an auditory fear conditioning and extinction procedure using a custom-made PVC fear conditioning setup (50 cm x 15 cm x 21 cm). During the test days, the mice were transported in their home cages to a room adjacent to the testing room and left for 2 h before behavioral testing. We used two different contexts: In context A, the walls and the floor were completely black; in context B, the walls had white vertical plastic strips 2.5 cm long, 0.5 cm wide, and 18 cm deep, interposed every 2.5 cm, and white floor. Both chambers were covered with transparent plexiglass lids with a loudspeaker in its center point. The shock grid on the floor was made of stainless steel. Only the grid of context A was electrified by a shock generator (World Precision Instruments, Sarasota, FL) guided by an automated program for CS and US

parameter control and footshock delivery. Mice behavior was recorded by a camera controlled by the EthoVision XT 8 software (Noldus Information Technology, The Netherlands). The two chambers were cleaned with 70% ethanol before and after each animal. After each session, mice were housed separately until the end of the test to avoid possible observational fear learning.

12.3 Conditioning and extinctions

During the habituation day (day 0), mice were placed in context A for 3 min. On day 1 (conditioning), mice were placed again in the context A and conditioned using 5 pairings of the CS (total CS duration 10 s, 7.5 kHz, 80 dB) co-terminating with a US (1 s footshock, 0.6 mA, inter-trial interval: 20 s). On day 2 (early extinction) and day 3 (late extinction), conditioned mice were subjected to the extinction training in context B during which they received 12 unreinforced presentations of the CS on each day. We also tested fear spontaneous recovery and context-dependent fear renewal 7 and 42 days after late extinction using 4 unreinforced presentations of the CS in context B and A respectively. Fear memory retention was tested by submitting an additional group of mice to extinction training 9 days after conditioning, during which they received 10 unreinforced presentations of the CS.

12.4 Amygdala and Infralimbic cortex activation after Early Extinction

To assess amygdala and IL activation, after early extinction, a separate group of conditioned Crtl1-KO and Crtl1-WT mice was used. Mice were subjected to the early extinction protocol during which they received 10 unreinforced presentations of the CS. At the end of the extinction training, mice were sacrificed for immunohistochemistry analysis. To isolate the specific effect of associative learning on amygdala and IL activation, we used pseudo-conditioned mice. For pseudoconditioning, on the day of conditioning, mice received the same number of CS as conditioned mice, administered at 1 s interstimulus intervals in context A, without US. Then, mice were placed back in their home cage. After 45 min, the animals were placed again in the context A where they immediately received 5 US at 1 s intervals (1 s footshock, 0.6 mA). This procedure has been designed to make it difficult for animals to associate the US with the CS and the context [30]. On day 2, pseudo-conditioned mice were subjected to the same early extinction protocol of conditioned mice and were then sacrificed for immunohistochemistry.

12.5 Analysis of freezing behavior

Recorded videos were manually scored for freezing behavior by two separate experimenters blind to genotype and experimental conditions. Mice were considered to be freezing if no movement was detected for 2 s (defined as the complete absence of movement except for respiratory movements). For all fear conditioning and extinction paradigms, cue evoked freezing behavior was analyzed by calculating the percentage time an animal spent freezing during a given CS presentation, and averages were calculated by pooling freezing across 2 CS presentations if not indicated otherwise.

12.6 Virtual Fear conditioning

During the virtual fear conditioning mice were head-fixed. We employed a custom made apparatus equipped with a 3D printed circular treadmill (diameter: 18 cm) as described in Mazziotti et al. 2021. During each head-fixation session, a curved monitor (24 inches Samsung, CF390) was placed in front of the animal (at a distance of 13 cm). We designed two different virtual environments composed of a γ -linearized procedural virtual corridors written in C# and Unity. The two environments presented sine-wave gratings (context A) or plaid-wave gratings (context B) at different orientations (wall at 0° ; floor at 90°), and spatial frequencies (from 0.06 to 0.1 cycles/°). The apparatus was cleaned before and after each animal with 70% ethanol or 1% acetic acid for context A and context B respectively, since the mice may associate the smell with the context. The position of the animal in the virtual corridor was updated using an optical computer mouse, positioned below the circular treadmill, that interfaced with the virtual environment software. As a CS we used a visual stimulus consisting of a square wave grating patch of 55° (in width and height) of visual space in the binocular portion of the visual field. The grating parameters were as follows: luminance, 8.5 cd/m^2; orientation, 0° ; contrast, 90%; spatial frequency, 0.1 cycles/° ; drifting, 0.5 cycle/s. A custom made electrode connected to a shock generator (World Precision Instruments, Sarasota, FL) and controlled by the virtual environment software was positioned on the mouse tail for tail shock delivery (US). For fear conditioning in the virtual environment mice were introduced gradually to head-fixation and to the tail electrode for five days (habituation). During the habituation, we performed two sessions of head-fixation in which mice were exposed to the two contexts. Each session consisted of two minutes of a uniform gray (luminance, 8.5 cd/m^2), to assess the pupil diameter in baseline, and 10 minutes of the isoluminant virtual environment. After habituation, mice underwent a 4-day fear conditioning training and extinction protocol. On day 1, a group of mice were exposed to context A and a second group to context B and conditioned using 5 pairings of the CS (total CS duration 20 s) co-terminating with a US (2 s tail shock, 0.6 mA, inter-trial interval: 120 s). Fear memory was tested on day 2 in a recall session, presenting 5 unreinforced presentations of the CS in the context opposite of the conditioning one. On day 3 (Early Extinction) and day 4 (Late Extinction), conditioned mice were subjected to the extinction training again in the context opposite of the conditioning one during which they received on each day 10 unreinforced presentations of the CS. To test the efficacy of the virtual fear conditioning protocol, we compared the responses of a group of conditioned C57BL/6J WT mice (shock) with a group of mice that underwent the same conditioning protocol without receiving the tail shock (sham). After each session mice were housed separately until the end of the test to avoid possible observational fear learning.

12.7 Surgery

Mice were deeply anesthetized using isoflurane (3% induction, 1.5% maintenance), placed on a stereotaxic frame and head fixed using ear bars. Prilocaine was used as a local anesthetic for the acoustic meatus. Body temperature was maintained at 37 degrees using a heating pad, monitored by a rectal probe. The eyes were treated with a dexamethasone-based ophthalmic

ointment (Tobradex, Alcon Novartis) to prevent cataract formation and keep the cornea moist. Respiration rate and response to toe pinch were checked periodically to maintain an optimal level of anesthesia. A subcutaneous injection of Lidocaine (2%) was performed prior to scalp removal. The Skull surface was carefully cleaned and dried, and a thin layer of cyanoacrylate was poured over the exposed skull to attach a custom-made head post that was composed of a 3D printed base equipped with a glued set screw (12 mm long, M4 thread, Thorlabs: SS4MS12). The implant was secured to the skull using cyanoacrylate and UV curing dental cement (Fill Dent, Bludental). At the end of the surgical procedure, the mice recovered in a heated cage. After 1 hour, mice were returned to their home cage. Paracetamol was used in the water as antalgic therapy for three days. We waited for seven days before performing head-fixed pupillometry to provide sufficient time for the animals to recover.

12.8 Pupillometry

During the virtual fear conditioning paradigm, we analyzed pupil diameter as a physiological readout of fear response. To record the pupil, we used a USB camera (oCam-5CRO-U, Withrobot Lens: M12 25mm) connected to a Jetson AGX Xavier Developer Kit (NVIDIA) running a custom Python3 script (30fps). Real-time pupillometry was performed using MEYE, a convolutional neural network that performs online pupillometry in mice and humans. Pupillometry data has been analyzed using Python 3. All tracks were loaded, and blink removal was applied using the blink detector embedded in MEYE. Blink epochs were filled using linear interpolation and median filtering (0.5 s). The z-score was obtained for each trial using the formula $z = \frac{x-\overline{x_b}}{s_b}$, where $\overline{x}$ and s_b were respectively the average and the SD of the baseline.

12.9 Pupillary Light Reflex

For the evaluation of the PLR, we presented 10 s of a white screen (Luminance: $30m^2$) repeated ten times, interspersed with 50 s of a uniform gray (luminance, 8.5 cd/m^2). Each session started with two minutes of a uniform gray (luminance, 8.5 cd/m^2) for pupil adaptation. We evaluated the pupil constriction latency (the time needed to reach the minimal pupil size during pupil constriction), the pupil constriction amplitude (maximal relative change in pupil area during constriction), the pupil re-dilation latency (the time needed to reach the maximal pupil size during pupil re-dilation) and the pupil re-dilation amplitude (maximal relative change in pupil area to recover the constriction).

12.10 Surgery

Mice were deeply anesthetized using isoflurane (3% induction, 1.5% maintenance), placed on a stereotaxic frame and head-fixed using ear bars. Prilocaine was used as a local anesthetic for the acoustic meatus. Body temperature was maintained at 37° using a heating pad, monitored by a rectal probe. The eyes were treated with a dexamethasone-based ophthalmic ointment (Tobradex, Alcon Novartis) to prevent cataract formation and keep the cornea moist. Respiration rate

and response to toe pinch were checked periodically to maintain an optimal level of anesthesia. A subcutaneous injection of Lidocaine (2%) was performed prior to scalp removal. The skull surface was carefully cleaned and dried, and a thin layer of cyanoacrylate was poured over the exposed skull to attach a custom-made head post that was composed of a 3D printed base equipped with a glued set screw (12 mm long, M4 thread, Thorlabs: SS4MS12). The implant was secured to the skull using cyanoacrylate and UV curing dental cement (Fill Dent, Bludental). At the end of the surgical procedure, the mice recovered in a heated cage. After 1 h, mice were returned to their home cage. Paracetamol was used in the water as antalgic therapy for 3 days. We waited for 7 days before performing head-fixed pupillometry to provide sufficient time for the animals to recover.

12.11 Immunohistochemistry

For immunofluorescence labeling, following the early extinction protocol, conditioned and pseudo-conditioned mice were transcardially perfused with 4% paraformaldehyde in phosphate buffer 1 h after behavioral testing, when Zif268 peaks in its expression (Lonergan et al. 2010). Brains were removed and post-fixed for 24 h at 4 ° C in 4% paraformaldehyde and then cryoprotected for 72 h at 4 ° C in 20% sucrose and 0.05% sodium azide in PBS, pH 7.4. Brains were then snap-frozen in 2-methylbutane and cryosectioned in OCT using a cryostat (Leica Biosystems, CM 3050S) to obtain 40-µm-thick sections collected in PBS. Free-floating sections were incubated for 2 h at room temperature (RT) in a blocking solution composed of 10% bovine serum albumin (BSA), 0.5% Triton X-100, in PBS. For Zif268 staining, sections were incubated overnight at 4 ° C in a solution composed of 10% BSA, 0.3% Triton X-100, and 1:500 rabbit polyclonal anti-Zif268 primary antibody (SantaCruz), in PBS. Sections were then washed for 3 times, 10 min each time. Primary antibody was revealed by incubating sections for 2 h at RT in a solution composed of 1% BSA, 0.1% Triton X-100, and 1:400 goat anti-rabbit AlexaFluor 488 secondary antibody (Invitrogen), in PBS. Sections were then washed for 3 times, 10 min each time and mounted on glass slides and covered with VectaShield mounting medium (Vector). For the quantification of PNNs, mice were transcardially perfused and the 40-µm coronal sections were cut on a freezing microtome (Leica). Slices were incubated for 2 h RT in a blocking solution composed of 3% BSA in PBS. Then, slices were incubated overnight at 4 ° C with a solution containing biotinylated Wisteria floribunda Lectin (WFA, B-1355–2, Vector Laboratories, 1:200) and 3% BSA in PBS. On the following day, sections were washed for 3 times in PBS (10 min each) and incubated with a solution of red fluorescent streptavidin (Streptavidin, Alexa Fluor™ 555 conjugate, S21381, Thermo Fisher, 1:400) and 3% BSA in PBS for 2 h at RT, and washed again 3 times in PBS and subsequently mounted on glass slides and covered with VectaShield mounting medium. Sections were acquired at 16X using a confocal laser scanning microscope (Leica Biosystems, BM 6000) and digitized with Leica confocal software. From 3 to 5 sections were acquired for each amygdala nucleus and IL for each animal. Zif268-positive cells and PNNs were manually counted using the MetaMorph software and ImageJ software by two separate experimenters blind to genotype and experimental conditions.

12.12 Statistical analysis

All statistical analyses were performed using GraphPad Prism 7 and Python custom scripts (Pupillometry). Parametric t-test, analysis of variance (ANOVA) and repeated measure-ANOVA (RM-ANOVA) were used. ANOVA was followed by appropriate post-hoc tests. Significance was set at $P < 0.05$ for all tests. Error bars represent s.e.m. in all figures.

Conclusions and future perspectives

The first part of this thesis explored pupillometry as a physiological measure of brain functions in both physiological and pathological conditions. The primary focus was to develop a versatile deep-learning pupillometry tool, the MEYE web app, for investigating pupil dynamics in human and murine subjects. This endeavor was motivated by the financial constraints of the existing commercial tools, while open-source alternatives often demand programming expertise and are species-specific (Yiu et al. 2019; Privitera et al. 2020). Our core objective was to devise a cost-effective and user-friendly tool capable of performing pupillometry across diverse species. The non-invasive nature of pupillometry renders it suitable for human studies. Nevertheless, the possibility of conducting analogous experiments in animal models, ranging from mice to humans, increases the translatability of experimental protocols and findings (Aleman et al. 2004; Rorick-Kehn et al. 2014; Artoni et al. 2020). In addition, in two-photon calcium imaging studies in mice, monitoring the pupil is crucial for assessing the impact of arousal on the measured outcomes. In recent years, the impact of deep learning on machine learning, particularly in neuroscience applications, has been profound. Numerous scientific publications annually showcase the efficacy of deep neural networks in biomedical data analysis (Tshimanga et al. 2023). In this context, MEYE positions itself as a deep learning tool designed to be reproducible by scientists with non-technical backgrounds in both clinical and preclinical settings. Unlike many deep learning algorithms that necessitate a training phase on dedicated datasets (Yiu et al. 2019; Privitera et al. 2020), MEYE stands out by offering a pre-trained model embedded into a web app that facilitates usage on a wide array of devices, from scientific workstations to notebooks and smartphones. The web browser solution simplifies the process for users, who only need a web browser and an infrared camera. A dedicated Python script also enables the local execution of the model on a workstation, while a Matlab script has been recently implemented enhancing usability for Matlab users. These solutions are advantageous for experiments with specific requirements, such as high and stable frame rate or real-time processing of pupil size necessitating on-the-fly pupil-computer interaction. The project workflow, scripts, and data set are open-source and available on GitHub and Zenodo respectively, along with the wiki documentation. After the release of MEYE, an integrated cross-platform pupillometry software called PupilEXT has been developed to run on macOS, Windows, and Linux (Zandi et al. 2021). PupilEXT, equipped with a user-friendly graphical interface, has been designed with the specific needs of professional pupil behavior research while adhering to an open-source philosophy (Zandi et al. 2021). While PupilEXT relies on computer vision, MEYE incorporates deep learning approaches for pupil detection, aligning with the goal of versatility and generalization across species without retraining on specific datasets. Indeed, despite being trained with human and mouse eye images, MEYE has demonstrated the capability to detect pupils in various species. The MEYE web app also emerges as an attractive tool in the telemedicine field. Recently, Ney and colleagues (Ney et al. 2023) announced the development of an application that will

allow online pupillometry measurement. To achieve this, they converted MEYE into a JsPsych tool (Leeuw 2015), called Js-mEye so that it can be used by researchers to collect real-time pupillometric data directly from participants' webcams. They affirm that Js-mEye can be installed entirely automatically by the participant involved in online studies with minimum manual calibration. The intersection of smartphones and pupillometry has garnered considerable interest due to these devices' widespread availability and convenience. A recent study has introduced and validated smartphone-based infrared pupillography, employing two synchronized mini-infrared camera modules with a compatible smartphone (Solyman et al. 2022). A second study has proposed a deep learning approach for pupil segmentation with the specific purpose of building a smartphone-based pupillometer (Phatak et al. 2023). Considering the significant advantages of conducting large-scale recruitment of subjects directly in their homes, future considerations should explore the integration of the MEYE tool into a smartphone app.

Pupillometry holds promise as a biomarker and a means to monitor the progression of pathology and treatment outcomes. Specifically, pupillary alterations have been linked to Alzheimer's (Frost et al. 2017; Chougule et al. 2019; Sparks et al. 2023), Parkinson's disease (Micieli et al. 1991; You et al. 2021), and neurodevelopmental disorders (Nyström et al. 2018; Blaser et al. 2014; Burley et al. 2020; Artoni et al. 2020; Iadanza et al. 2020). The possibility to conduct longitudinal assessments by using automated measurements through deep learning techniques, opens to the broad use of pupillometry as a diagnostic tool in pre-symptomatic stages. In this perspective, the second study discussed in this thesis focuses on the exploration of pupillary alterations in a mouse model of Cdkl5 deficiency disorder. The findings indicate hyperactive and impulsive behavior in both male and female Cdkl5 mutant mice, indicative of the presence of arousal deficits. Additionally, Cdkl5 null mice exhibit reduced cognitive flexibility and impaired inhibitory control. A recent study confirmed the presence of these alterations in Cdkl5 null mice and demonstrated that long-term voluntary running as physical exercise improved hyperlocomotion, impulsivity, and memory performance (Mottolese et al. 2023). Our measurement of pupil responses and locomotor behavior confirmed that Cdkl5 mutant mice stay in a heightened arousal state for an extended duration compared to wild-type mice. Despite consistently smaller absolute pupil sizes than controls, mutant mice showed unaffected responses to illumination changes, suggesting the presence of central neuromodulatory alterations. Previous research has demonstrated the involvement of the cholinergic and dopaminergic systems in CDD (Jhang et al. 2020; Jhang et al. 2017; Artoni et al. 2020). Cdkl5 null mice show altered cholinergic tone (Artoni et al. 2020) and increased levels of extracellular dopamine (Jhang et al. 2020). A recent study, employing phosphoproteomics, identified reduced phosphorylation of a voltage-gated Ca2+ channel (i.e. Cav2.3) in CDKL5 null mice, resulting in a hyperactive channel with slower inactivation. They also found that loss of Cav2.3 phosphorylation leads to enhanced cholinergic stimulation, resulting in increased neuronal excitability, suggesting the contribution of cholinergic alterations in the severity of the disease (Sampedro-Castañeda et al. 2023). The established link between neuromodulatory systems and the regulation of pupil size (Larsen et al. 2018; Viglione et al. 2023) supports the employment of pupillary responses as a valid biomarker for the disorder. The impact of the noradrenergic system on CDD remains unexplored, representing a critical area for further investigation. Moreover, future experiments

are needed to explore the presence of pupillary alterations in juvenile mice, to assess the potential correlation with the severity of symptoms in adulthood. Our study is also notable for including female mice, a population less explored in existing literature, despite the disorder being more prevalent in girls. Due to the non-invasive nature of pupillometry, there is optimism that future investigations will focus on exploring pupillary responses in patients.

Beyond being a sensitive measure in clinical diagnosis, the measurement and analysis of pupillary responses provide valuable insights into cognitive and emotional processes, neurological functioning, and autonomic nervous system activity (Mathôt 2018). In fear conditioning, changes in pupil size have been associated with fear-inducing stimuli, providing robust markers of learning processes (Borrego et al. 1986; Finke et al. 2021). The assessment of pupil size changes during fear conditioning offers distinct advantages compared to other psychophysiological measures: pupillometry provides a continuous and precise measurement with superior temporal resolution in contrast to skin conductance responses, which typically exhibit a one-second delay between stimulus onset and response (Boucsein 2012). The measurement of pupil diameter does not necessitate the employment of electrodes or expensive equipment. Notably, pupil responses during fear acquisition do not habituate (Leuchs et al. 2019), and conditioned fear emerges more rapidly in pupil diameter than in other measures (Finke et al. 2021). In mice, traditional behavioral responses like freezing remain the primary method in fear conditioning studies. However, exploring pupillometry as a tool for investigating fear learning in rodents presents a promising avenue. Conventional behavioral measurements, especially the classical definition of freezing, can be challenging in head-fixed animals. Conversely, pupillometry appears as a valid alternative compared to other solutions (Ross et al. 2018; Wood et al. 2022; Ahmed et al. 2020; Lovett-Barron et al. 2014; Rajasethupathy et al. 2015; Kaifosh et al. 2013). Furthermore, studies have shown that the LC-NE system dynamically regulates fear memories and extinction circuitry (Bierwirth et al. 2022; Giustino et al. 2018). Nevertheless, exploring the noradrenergic system's role in fear extinction is less extensive in humans than in rodents (Bierwirth et al. 2022). Pupillometry, as a non-invasive way to measure the LC-NE system activity, holds great promise in human studies. Despite potential advantages, the adoption of pupillometry in fear conditioning research faces challenges. These include variability in reported results due to experimental design differences and susceptibility to physiological artifacts (Ney et al. 2023). Nonetheless, emerging quantification techniques and the potential for cost-effective alternatives, like MEYE, may contribute to standardizing pupillometry use in fear conditioning research. The last work presented in the first part of the thesis proposed pupillometry as a valid complementary method for quantifying fear-conditioned responses in mice. In particular, we investigated whether the presence of PNNs in the adult brain is responsible for the appearance of persistent fear memories, by exploited mice lacking the cartilage link protein Crtl1. These mice display normal CSPG levels but impaired CSPG condensation in PNNs. While various roles have been suggested, a key general function of PNNs is to tightly control the plasticity and stability of neuronal circuits (Fawcett et al. 2019; Nabel et al. 2013). The study shows that, in adult Crtl1-KO mice a fear extinction protocol can erase fear memory, a feature observed in juvenile mice. Moreover, after extinction training, conditioned Crtl1-KO mice displayed no neural activation in the amygdala compared to control animals. Fear responses were evaluated by observing freezing behavior

and pupil dynamics, and both measures revealed the same result. Additionally, the study has introduced and validated a virtual fear conditioning protocol that enables the examination of fear learning in head-fixed mice. A whole brain investigation has recently indicated that PNNs are negatively correlated with genes involved in synaptic plasticity, including postsynaptic density organization, regulation of synapse structure, and learning and memory (Lupori et al. 2023). Our behavioral and physiological results suggest that heightened plasticity is not inherently beneficial since its reduction during development is essential for circuit maturation. The proper closure of the critical period is crucial to promote the transition from a fear memory that can be erased in juvenile mice to a persistent fear memory in adults. Considering the pupillometry results, it becomes intriguing to investigate the role of PNNs in the maturation of the arousal-noradrenergic system, and its involvement in fear memory formation and extinction.

In conclusion, pupillometry emerges as an invaluable tool in clinical diagnosis, offering non-invasive and translational measures, and temporally precise insights into fear responses, cognitive states, and neural processes. Its application in neuroscience shows the promise to significantly advance our understanding of brain functions and complex behaviors.

Part II

Molecular and epigenetic mechanisms of fear memory stability

13 Bidirectional Impact of miR-29a Modulation on Memory Stability in the Adult Brain

13.1 Summary

The establishment and maintenance of enduring memories are complex processes driven by intricate modifications within neuronal circuits. These modifications rely on gene transcription activation and protein synthesis, critical for neuronal plasticity and memory. MicroRNAs (miRNAs), small non-coding RNA molecules, are recognized as regulators of gene expression through the modulation of target mRNA sequences. The miR-29 family plays a significant role in epigenetic regulation. With age, miR-29 levels increase in various tissues, including the nervous system, leading to the downregulation of genes associated with extracellular matrix and transcription regulation. A global miRNA association study identified miR-29a as significantly associated with cognitive trajectory, with higher miR-29a levels correlating with accelerated cognitive decline. However, the precise mechanisms through which miR-29a influences memory performance in the adult brain remain elusive. In this study, we manipulated miR-29a levels within the dorsal hippocampus of adult mice using LNA antagomir or a synthetic miR-29a mimic. Inhibition of miR-29a led to a significant increase in *Dnmt3a* levels and improved trace fear memory stability, while miR-29a enhancement had the opposite effect. Bidirectional control of miR-29a also impacted contextual memories, suggesting its pivotal role in the persistence of hippocampal memories, potentially through epigenetic modifications. To elucidate the underlying molecular mechanisms, we conducted reduced representation bisulfite sequencing (RRBS) on hippocampal tissue following LNA antagomir treatment. We found increased CpG methylation in promoter and exon regions, particularly associated with CpG islands. Gene Ontology analysis indicated that up-regulated CpGs were linked to gene expression and regulation processes, enriched in functions implicated in hippocampal-dependent learning and memory. In conclusion, our findings provide compelling evidence supporting the role of miR-29a in orchestrating the cellular changes associated with the establishment and stability of fear memories, while also exploring the underlying epigenetic mechanisms.

13.2 Introduction to the project

The formation and maintenance of long-lasting memory rely on intricate modifications within neuronal circuits, involving regulations in the expression of growth factors, ion channels, receptors, and structural proteins. These changes are underpinned by gene transcription activation and protein synthesis, processes established as crucial for neuronal plasticity and memory (Alberini et al. 2014; Benito et al. 2015). MicroRNAs (miRNAs) are small non-coding RNA molecules

that modulate gene expression through the binding of complementary sequences in target mRNAs (Bartel 2018). This results in the repression of translation and the destabilization of the transcript. The process of miRNAs biogenesis, characterized by their rapid turnover and versatile mechanisms of action, renders them well-suited candidates for orchestrating the dynamic and reversible control of gene expression necessary for the establishment and maintenance of memory (Rajman et al. 2017; Lippi et al. 2016). The miR-29 family (comprehending miR-29a, miR-29b, and miR-29c) has demonstrated a notable role in the realm of epigenetic regulation. Specifically, it has been observed that the miR-29 plays a significant part in modulating DNA methylation pathways (Fabbri et al. 2007; Amodio et al. 2015). This modulation occurs both through direct interactions, where the miR-29 family targets DNA methyltransferases (Dnmts), and through indirect mechanisms by influencing factors responsible for the transcriptional regulation of Dnmts (Fabbri et al. 2007; Benetti et al. 2008). Rapid and dynamic changes in DNA methylation have been observed in response to neuronal activity (Gu et al. 2011), and studies have demonstrated that DNA methylation writers are necessary for learning and memory stability (Miller et al. 2010; Miller et al. 2007; Lubin et al. 2008). Pharmacological and genetic approaches aimed at reducing DNA methylation levels have demonstrated disruptions in mechanisms related to plasticity, such as long-term potentiation (LTP), and cognitive functions (Levenson et al. 2006; Maddox et al. 2014). Notably, the administration of RG108, a nonnucleoside inhibitor of Dnmts (Brueckner et al. 2005), into the CA1 hippocampal region before contextual fear conditioning training, impairs the formation of long-term memory while leaving short-term memory unaffected (Lubin et al. 2008). With age, the levels of miR-29 increase in many tissues, including the nervous system (Mazziotti et al. 2017a). In the visual cortex, the increase of miR-29a specifically, has been correlated with a significant downregulation in categories related to extracellular matrix and transcription regulation (Napoli et al. 2020). In particular, *Dnmt3a* was found to be strongly downregulated in the visual cortex with age, and negatively correlated with miR-29a levels (Napoli et al. 2020). With age, increasing levels of miR-29 a have been associated with reduced plasticity and closure of the critical period in the visual cortex (Napoli et al. 2020). Moreover, within the brain-expressed miRNAs, miR-29a emerges as notably synaptically enriched, suggesting the involvement of miR-29a in the regulatory network underpinning synaptic plasticity and the formation of memories (Lugli et al. 2008; W. Wang et al. 2012). However, the precise mechanisms through which miR-29a influences memory performance during development and in the adult brain remain elusive. To investigate the regulatory influence of miR-29a on memory, we employed an experimental approach involving the manipulation of miR-29a levels within the dorsal hippocampus of mice. To achieve targeted inhibition of miR-29a, we utilized LNA antagomirs administered to the hippocampus of adult mice and we observed a significant increase in the levels of *Dnmt3a*. We found that miR-29a inhibition was instrumental in improving trace fear memory stability. Conversely, enhancing miR-29a levels, with a synthetic miR-29a mimic, resulted in an opposite effect on memory retention. The miR-29a bidirectional control on memory performances was also evident for contextual memories. These observations highlight the involvement of miR-29a in influencing the persistence of hippocampal memories, possibly by its ability to change the epigenetic landscape. Furthermore, to gain insights into the underlying molecular mechanisms involved, we conducted a reduced representation bisulfite

sequencing (RRBS) on the hippocampal tissue of mice subjected to LNA antagomir treatment. This analysis enabled us to explore the DNA methylation pattern associated with the behavioral response. Consistent with the observed increase in *Dnmt3a* levels after miR-29a inhibition, we found an increase in CpG methylation, enriched in promoter and exon regions and associated with CpG islands. Gene Ontology analysis revealed that up-regulated CpGs were associated with processes related to gene expression and regulation and were enriched in functions implicated in hippocampal-dependent learning and memory. Overall, our findings provide compelling evidence supporting the role of miR-29a in orchestrating the cellular changes associated with the maintenance of fear memories.

13.3 Declaration of author contributions

Here I summarize, for clarity, the details of my specific personal contribution to this project. All of the conceptual, experimental, and analytical tasks are grouped according to the level of my involvement in three categories as follows:

- I was the only/main contributor
  - Conceptualization of the project
  - Experimental design
  - Intracranial Injections
  - Real-Time PCR
  - Conducting behavioral experiments
  - Data analysis
  - Data Visualization
- Task performed by other people or institutions
  - Reduced representation bisulfite sequencing (RRBS)
  - RRBS data analysis

14 Results

14.1 Age-Dependent increase of miR-29a levels correlates with Dnmt3a reduction in the dorsal hippocampus

To investigate the temporal expression pattern of miR-29a in the dorsal hippocampus, we conducted a quantitative PCR (qPCR) analysis at different time points. Our results revealed a significant and remarkable 10-fold increase in miR-29a levels after postnatal day 10 (P10), reaching a plateau around P60 (Figure 14.1A). Interestingly, this specific temporal window aligns with critical periods characterized by heightened plasticity in various brain regions, accompanied by an increased sensitivity of chromatin configuration to environmental stimuli (Reh et al. 2020). In a previous study, a comparable expression pattern was reported for the visual cortex, wherein the age-related elevation of miR-29a levels was associated with a significant decrease in ocular dominance plasticity and the expression of extracellular matrix factors (Napoli et al. 2020). Simultaneously, we examined the age-related modulation of *Dnmt3a*, a well-validated target of miR-29 (Fabbri et al. 2007; Morita et al. 2013; Kuc et al. 2017). With increasing age, *Dnmt3a* expression showed a significant downregulation (Figure 14.1B), displaying a strong negative correlation with miR-29a levels (Figure 14.1C). Given the reported age-related decline in *Dnmt3a* levels, which has been proposed as a potential mechanism contributing to age-related cognitive impairments (Ana M M Oliveira et al. 2012), we decided to explore the involvement of miR-29a in modulating fear memories. To evaluate whether and how the reduction in miR-29a expression affects fear memory formation and extinction, we injected a locked nucleic acids (LNA) oligonucleotide, whose sequence is complementary to miR-29a (anti-miR29a), or scrambled oligonucleotide (scr) in the dorsal hippocampus of adult (P90) mice, and then we tested hippocampal memories through a trace fear conditioning protocol (TFC) (Figure 14.1D). LNA oligonucleotides demonstrate a stable and specific binding affinity to their complementary miRNA, effectively blocking its activity, and exhibit remarkable resistance to enzymatic degradation. These attributes render LNAs highly tolerable and validated, as evidenced by their approval for clinical use in human subjects (Braasch et al. 2001; Khvorova et al. 2017; C. I. E. Smith et al. 2019). As expected, the qPCR revealed that anti-miR29a treatment caused a decrease in miR-29a (Figure 14.1E) and an increase in the *Dnmt3a* (Figure 14.1F). We also found a strong negative correlation between *Dnmt3a* and miR-29a levels after LNA or scr injection (Figure 14.2A). We conducted quantification of *Dnmt3a* levels also in the ventral hippocampus. The results revealed no significant difference in *Dnmt3a* expression (Figure 14.2B), confirming the specificity of the injection effects within the dorsal hippocampus.

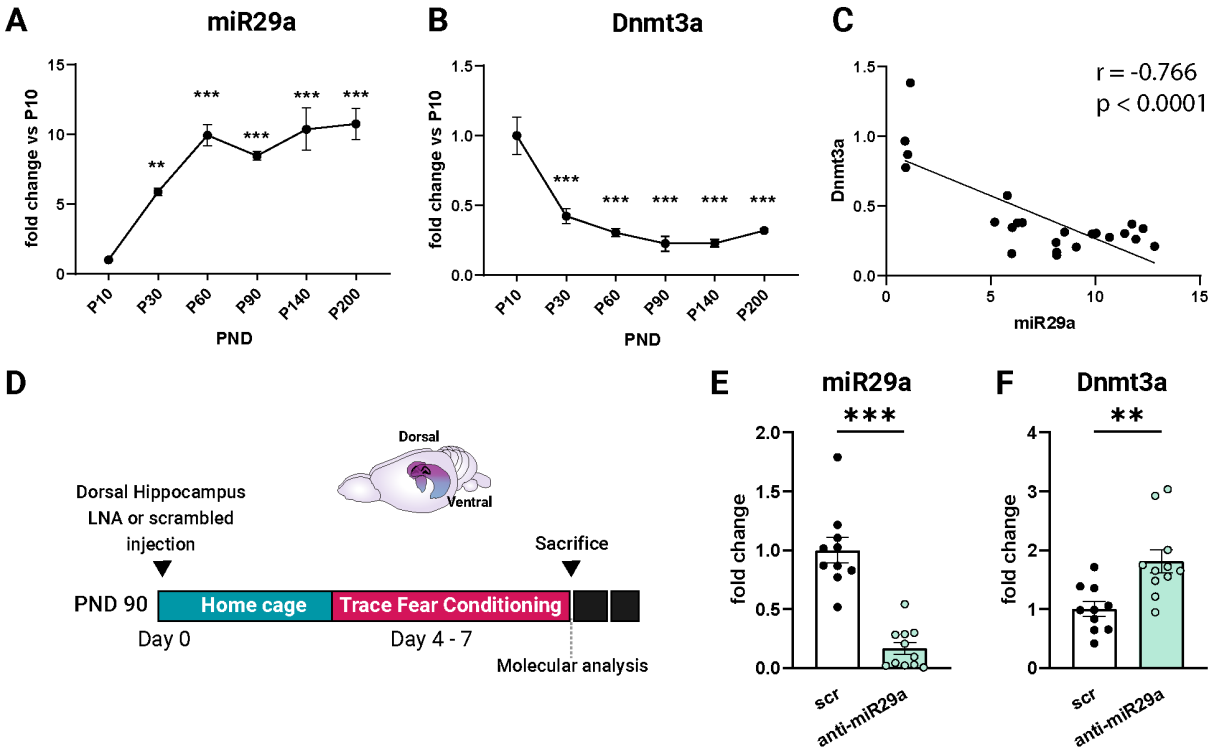

Figure 14.1: **Correlation between age-dependent miR-29a increase and *Dnmt3a*.** **(A)** Dorsal hippocampus miR-29a expression level (normalized to P10) at different ages (One-way ANOVA, $P < 0.0001$; Tukey's multiple comparison vs P10: $^{**}P < 0.01$, $^{***}P < 0.001$, n = 3/4 mice for each age). **(B)** Dorsal hippocampus *Dnmt3a* expression level (normalized to P10) at different ages (One-way ANOVA, $P < 0.0001$; Sidak's multiple comparison vs P10: $^{***}P < 0.001$; n = 3/4 mice for each age). **(C)** Animal by animal correlation between normalized miR-29a and *Dnmt3a* levels in the dorsal hippocampus at different ages (Pearson's correlation). **(D)** Experimental design for LNA-anti-miR29a treatment in the dorsal hippocampus. **(E)** Effects of LNA-anti-miR29a treatment on miR-29a expression. Fold change values normalized to scr treated animals (scr: N = 10, anti-miR29a N = 11; Unpaired t-test: $p < 0.001$). **(F)** Effects of LNA-anti-miR29a treatment on *Dnmt3a* expression. Fold change values normalized to scr treated animals (scr: N = 10, anti-miR29a N = 11; Unpaired t-test: $p < 0.01$). PND = Postnatal Day.

14.2 MiR-29a downregulation promotes memory stability during fear extinction

Three days after injection, we conditioned animals using a TFC protocol. During TFC the neutral conditioned stimulus (CS, Tone) and the aversive unconditioned stimulus (US, Shock) are separated in time by a trace interval (Trace). The absence of contiguity between the tone and the shock critically involves the hippocampus and this protocol can be used to evaluate hippocampal-dependent learning and memory (Bangasser et al., 2006) (Figure 14.3A). We observed that the treatment did not affect learning, since both anti-miR29a and scr treated mice showed similar fear acquisition (Figure 14.3B and Figure S.1A-C). When testing freezing responses 24 h after training, the two groups still did not differ in the percentage of time freezing (Figure 14.3C). However, on the first day of the extinction protocol (Early Extinction) we observed that anti-miR29a treated mice showed a higher fear retention, as compared to the control group (Figure 14.3D). This observation suggests that miR-29a developmental downregulation is involved in the strength

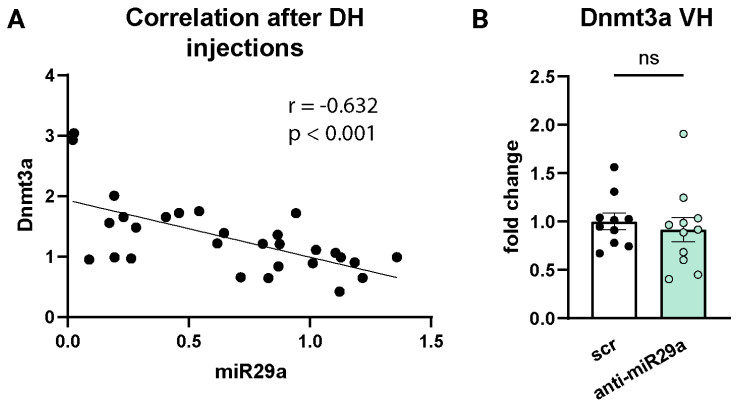

Figure 14.2: **anti-miR29a injection specificity**. (A) Correlation between *Dnmt3a* and miR-29a levels after the LNA injection. (B) LNA injection in the dorsal hippocampus did not affect the expression of *Dnmt3a* in the ventral hippocampus confirming the specificity of the injection site within the dorsal hippocampus (Unpaired t-test: p = 0.59). scr: N = 10, anti-miR29a N = 11. DH = Dorsal Hippocampus; VH = Ventral Hippocampus.

and persistence of memory, but is not required for memory formation. We also assessed freezing behavior induced by exposure to the conditioned context (Figure 14.3A). Remarkably, mice subjected to anti-miR29a treatment exhibited a pronounced enhancement in their response to the contextual cues compared with the scr control group (Figure 14.3F). Despite a general amplification in fear response, anti-miR29a treated mice exhibited a typical extinction profile. Following the second extinction session (Late Extinction), both anti-miR29a and scr treated mice demonstrated significantly reduced freezing responses (Figure 14.3E-G). Overall these results provide an opportunity to explore the influence of miR-29a in modulating the persistence of fear memories, potentially through its ability to coordinate DNA methylation patterns.

14.3 MiR-29a inhibition alters DNA methylation patterns and influences memory-associated pathways

We employed reduced representation bisulfite sequencing (RRBS) to investigate changes in DNA methylation patterns induced by anti-miR29a treatment in comparison to scr treated hippocampal samples. RRBS allows for a cost-effective exploration of methylation alterations in a CpG-enriched subset of the genome, primarily focusing on promoters (Meissner et al. 2005; Gu et al. 2011). We analyzed differential methylation of the sequenced CpGs and selected differentially-methylated CpGs (DMCs) with a difference greater than 10% in absolute value. Our analysis identified 2,279 DMCs, with a notable prevalence of hypermethylation (1,452 CpGs) over hypomethylation (827 CpGs, p < 10-16, Fisher's exact test, (Figure 14.4A). These DMCs exhibited an even distribution across chromosomes and were enriched in promoter and exon regions, as well as within CpG islands (Figure 14.4B). Interestingly, the observed increase in CpG methylation level after miR-29a inhibition is consistent with the measured increased expression of *Dnmt3a*. To identify biological functions that may be influenced by increased *Dnmt3a* we performed a Gene Ontology (GO) term overrepresentation analysis on all DMCs identified as up-regulated. Analyzing the DMCs that fall within promoters, we found that

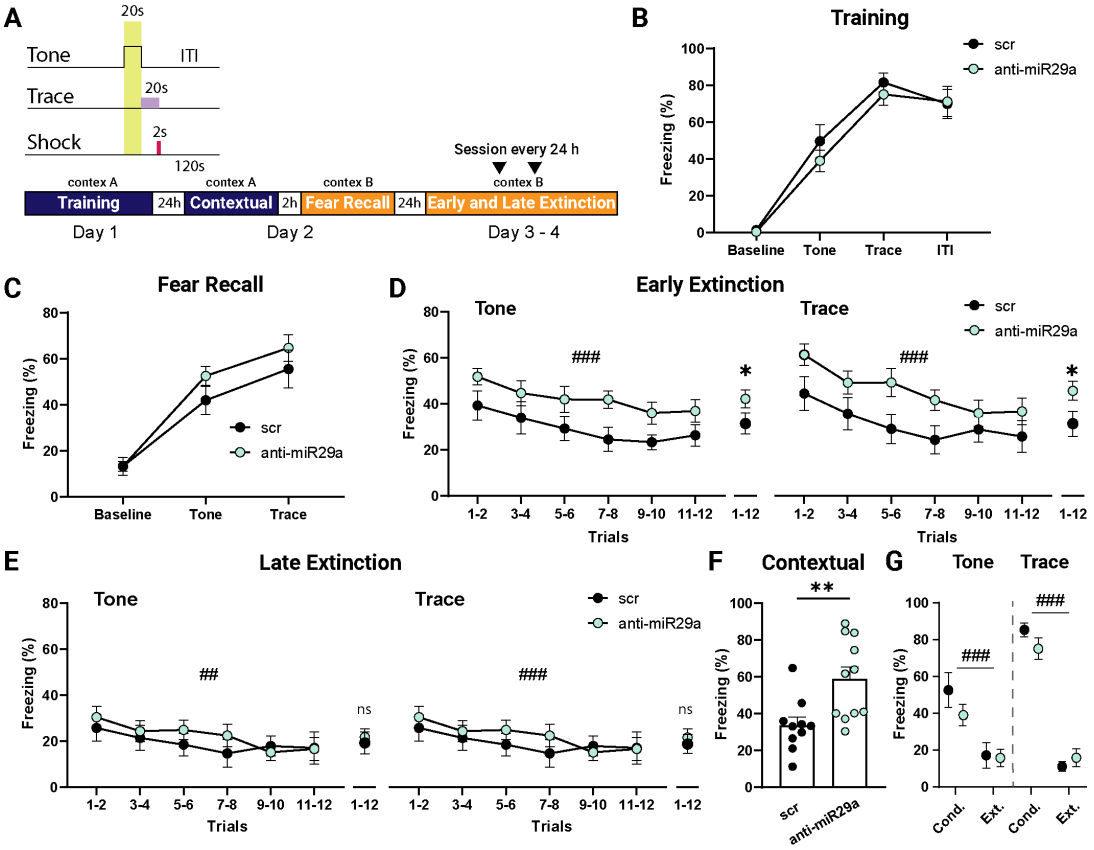

Figure 14.3: **Reducing hippocampal miR-29a expression promotes memory stability**. **(A)** Diagram showing the TFC paradigm and timeline. **(B)** Percentage of freezing during the different TCF training intervals. anti-miR29a and scr treated animals did not differ in the acquisition of fear memory (Baseline vs tone, trace or intertrial interval (ITI) last trial; Two-way ANOVA, test interval × treatment interaction $F(3, 76) = 0.39$, $p = 0.76$; main effect of test interval $F(3, 76) = 64.33$, $p < 0.0001$; main effect of treatment, $F(1, 76) = 0.93$, $p = 0.34$). **(C)** Twenty-four hours after training we tested animals in a novel environment. The test was identical to the training except that no shocks were presented (Fear recall). Treatment differences were not observed at baseline and during the last two-tone and trace trials (Two-way ANOVA, test interval × treatment interaction $F(2, 57) = 0.59$, $p = 0.56$; main effect of test interval $F(2, 57) = 41.74$, $p < 0.0001$; main effect of treatment, $F(1, 57) = 2.33$, $p = 0.13$). **(D)** Percentage of freezing during Early extinction. anti-miR29a mice showed a higher fear retention compared to the control group during both tone (Two-way RM ANOVA, main effect of treatment $F(1, 19) = 4.78$, $p < 0.05$; main effect of trials $F(2.98, 56.58) = 6.69$, $p < 0.0001$; trials × treatment interaction $F(5, 95) = 0.29$, $p = 0.92$) and trace intervals (Two-way RM ANOVA, main effect of treatment $F(1, 19) = 4.47$, $p < 0.05$; main effect of trials $F(3.26, 62.02) = 9.36$, $p < 0.0001$; trials × treatment interaction $F(5, 95) = 0.77$, $p = 0.57$). *Continued on next page.*

most of the enriched biological processes relate to the regulation of gene expression via miRNA, splicing, and RNA metabolism and via CpG island methylation (Figure 14.4C). This suggests miR-29a inhibition, via increased methylation through *Dnmt3a*, has a positive effect on gene expression by inhibiting repressive processes. Analyzing the DMCs that fall within the gene body, enrichment was found for extracellular matrix, protein tyrosine kinase activity, and notch activity, all mechanisms implicated in hippocampal-dependent learning and memory (Figure 14.4D). In particular, tyrosine kinase receptor B (TrkB) is known to play a role in the acquisition and consolidation of fear memory (Rattiner et al. 2004). With our methylation data, we confirmed the

Figure 14.3: **(E)** During the Late extinction, anti-miR29a treated mice showed no significant differences in the percentage of freezing compared with controls (Tone: Two-way RM ANOVA, main effect of treatment $F(1, 18) = 0.19$, $p = 0.66$; main effect of trials $F(2.56, 46.16) = 4.81$, $p < 0.01$; trials × treatment interaction $F(5, 90) = 0.87$, $p = 0.50$; Trace: Two-way RM ANOVA, main effect of treatment $F(1, 18) = 0.24$, $p = 0.63$; main effect of trials $F(3.95, 71.15) = 6.26$, $p < 0.001$; trials × treatment interaction $F(5, 90) = 2.12$, $p = 0.07$). **(F)** Downregulation of miR-29a in the dorsal hippocampus enhanced contextual memory recall (Unpaired t-test: $p < 0.01$, scr: N = 10, anti-miR29a N = 11). **(G)** Both anti-miR29a and scr treated mice significantly reduced their freezing response at the end of the extinction protocol (Cond. trial-5 vs Late est. trial-12, Tone: Two-way RM ANOVA, main effect of treatment $F(1, 18) = 1.32$, $p = 0.26$; main effect of trials $F(1, 18) = 18.02$, $p < 0.001$; trials × treatment interaction $F(1, 18) = 0.78$, $p = 0.39$; Trace: Two-way RM ANOVA: main effect of treatment $F(1, 18) = 0.46$, $p = 0.50$; main effect of trials $F(1, 18) = 156.3$, $p < 0.001$; trials × treatment interaction $F(1, 18) = 1.99$, $p = 0.17$). scr: N = 10, anti-miR29a N = 11; *indicates the main effect of treatment, #indicates the main effect of trials.

increase in methylation levels for TrkB following inhibition of miR-29a, providing further evidence for the involvement of this microRNA in fear memory persistence pathway via modulation of *Dnmt3a* (Figure 14.4E). Notch pathway genes also appear to be characterized by increased methylation (Figure 14.4D): it has previously been shown that a decrease in Notch signaling, through miRNA regulation, is important for fear memory consolidation (Dias et al. 2014). Overall, these findings confirm the central role of miR29 in orchestrating epigenetic mechanisms involved in memory persistence.

14.4 Elevated miR-29a levels in the hippocampus of adult mice result in impaired memory retention

To better investigate the role of miR-29a in memory retention, we conducted a second group of experiments by enhancing the levels of miR-29a in the dorsal hippocampus of adult mice. Before fear conditioning, we injected animals with a synthetic miR-29a mimic (mim29a) and then we tested fear responses using the same TFC protocol employed in the LNA experiments (Figure 14.5A). The administered treatment resulted in an upregulation of miR-29a expression and a concurrent downregulation of *Dnmt3a* levels in the dorsal(Figure 14.5B-C) but not in the ventral hippocampus (Figure 14.6). Our findings demonstrate that increasing miR-29a levels affect the trace's stability but not the CS response. Contrary to what we observed after the LNA treatment, during the extinction protocol (Early Extinction) mim29a mice showed an impaired trace fear retention compared to the control group (Figure 14.5E). A trend toward a reduced response to the trace interval was also evident during both the training and recall phases (Figure 14.5D, Figure S.3A-C). The bidirectional impact of miR-29a on memory strength during the extinction was also evident for contextual memories. In particular, mice receiving miR-29a mimics displayed a clear deficit in the recall of contextual fear memories (Figure 14.5G) compared to controls. Again we observed in mim29a treated mice a typical extinction profile. Following the second extinction session (Late Extinction), both mim29a and scr treated mice demonstrated significantly reduced freezing responses (Figure 14.5F-H). To further support the role of miR-29a on hippocampal fear memory stability we found a negative correlation between miR-29a levels and the percentage of freezing during early extinction and contextual fear recall. We also found a positive correlation between *Dnmt3a* levels and the percentage of freezing during the first

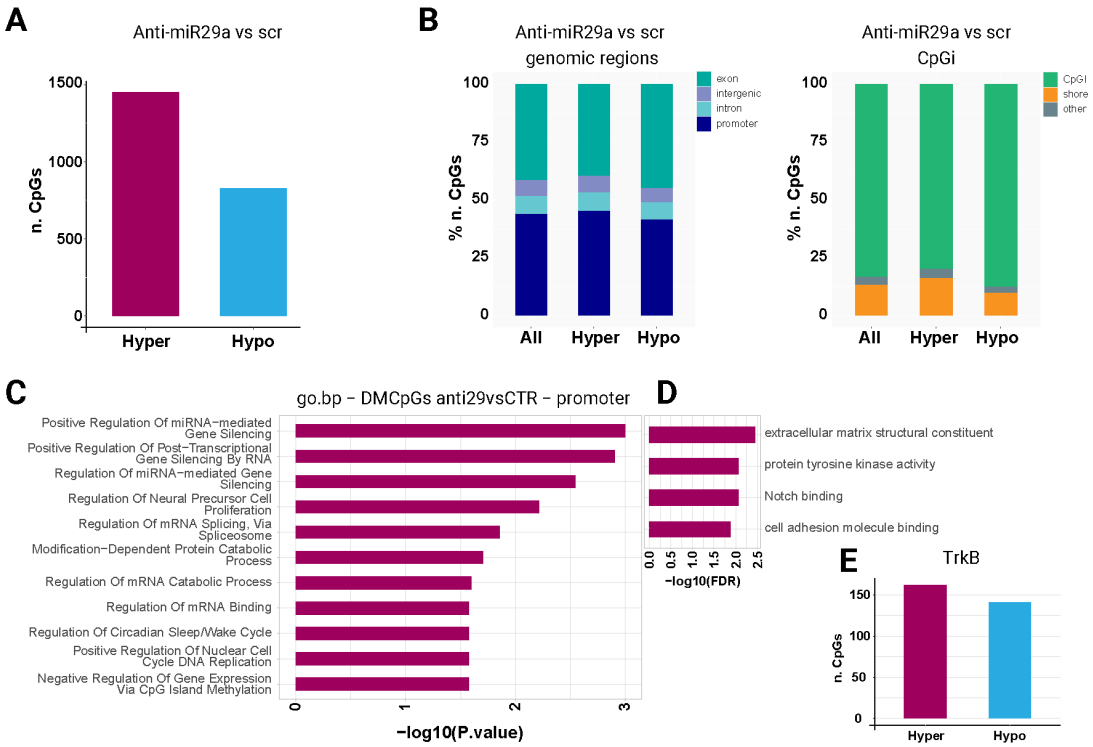

Figure 14.4: **DNA methylation changes in the dorsal hippocampus after miR-29a down-regulation**. **(A)** The number of hyper- and hypo- methylated CpGs. We found 2,279 differentially-methylated CpGs (DMCs), with a prevalence of hypermethylation over hypomethylation (1,452 CpGs vs 827 CpGs, p < 10-16, Fisher's exact test) between anti29a and scr hippocampal treated samples. **(B)** DMCs distribution across chromosomes. DMCs exhibited an even distribution across chromosomes and were enriched in CpG island (CpGi). **(C-D)** GO term overrepresentation analysis on all the up-regulated DMCs **(C)** falling within promoters and **(D)** within the gene body. **(E)** Number of CpGs hyper- and hypo- methylated in TrkB. N=7 for each treatment.

presentation of the trace interval during early extinction. Overall, these observations support the hypothesis that elevated miR-29a levels and reduced *Dnmt3a* expression contribute to impaired hippocampal fear memories To corroborate the involvement of miR-29a in the maintenance of hippocampal fear memory stability, a discernible inverse correlation was identified between miR-29a expression levels and the percentage of freezing behavior exhibited during early extinction and contextual fear recall (Figure 14.7A-B, D, Figure 14.8A-B). Concurrently, a positive correlation was established between the expression levels of *Dnmt3a* and the percentage of freezing behavior manifested during the initial presentation of the trace interval in the early extinction Figure 14.7C. Overall, these findings support the hypothesis that heightened miR-29a levels and diminished expression of *Dnmt3a* contribute to the compromised stability of hippocampal fear memories (Ana M M Oliveira et al. 2012; Wingo et al. 2022; Mei et al. 2023).

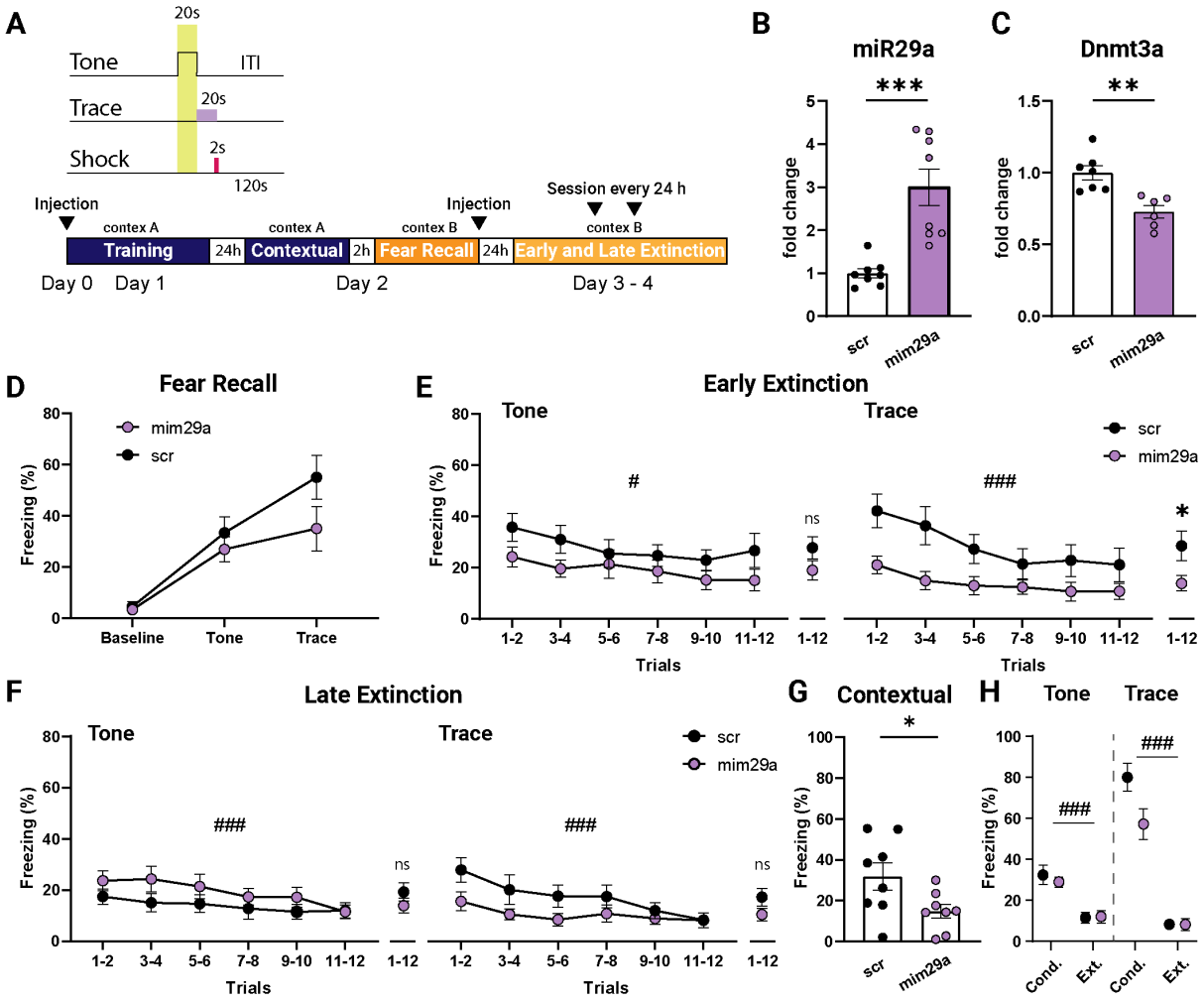

Figure 14.5: **Hippocampal miR-29a upregulation impaired memory retention**. **(A)** Diagram showing the TFC paradigm and timeline. To guarantee elevated miR-29a levels during all the sessions of the TFC test, mice were injected 24 hours before the start of the behavioral tests and again 24 hours before the start of the extinction protocol. **(B-C)** Effects of miR-29a mimic treatment on **(B)** miR-29a expression levels (fold change values normalized to scr treated animals; scr: N=8, mim29a N=8; Unpaired t-test: $p < 0.001$) and **(C)** *Dnmt3a* expression levels (fold change values normalized to scr treated animals; scr: N = 7, mim29a N = 6; Unpaired t-test: $p < 0.01$). **(D)** Treatment differences were not observed at baseline and during last two-tone and trace trials of the TFC fear recall session (Two-way ANOVA, test interval × treatment interaction $F(1, 42) = 3.52$, $p = 0.07$; main effect of test interval $F(2, 42) = 23.89$, $p < 0.0001$; main effect of treatment, $F(2, 42) = 1.30$, $p = 0.28$). *Continued on next page.*

Figure 14.5: **(E)** Percentage of freezing during Early extinction. Mim29a treated mice showed lower fear retention compared to the control group during the trace (Two-way RM ANOVA, main effect of treatment $F(1, 19) = 4.475$, $p < 0.05$; main effect of trials $F(3.26, 62.02) = 9.365$, $p < 0.0001$; trials × treatment interaction $F(5, 95) = 0.77$, $p = 0.57$) but not during the tone interval (Two-way RM ANOVA, main effect of treatment $F(1, 14) = 2.30$, $p = 0.15$; main effect of trials $F(3.21, 44.97) = 3.80$, $p < 0.05$; trials × treatment interaction $F(5, 70) = 0.65$, $p = 0.66$). **(F)** During the Late extinction, mim29a treated mice showed no significant differences in the percentage of freezing compared with controls (Tone: Two-way RM ANOVA, main effect of treatment $F(1, 14) = 1.33$, $p = 0.27$; main effect of trials $F(3.63, 50.83) = 6.41$, $p < 0.001$; trials × treatment interaction $F(5, 70) = 1.46$, $p = 0.21$; Trace: Two-way RM ANOVA, main effect of treatment $F(1,14)) = 2.54$, $p = 0.13$; main effect of trials $F(3.35, 46.88) = 9.09$, $p < 0.0001$; trials × treatment interaction $F(5, 70) = 2.14$, $p = 0.07$). **(G)** MiR-29a levels increase resulted in impaired contextual memory recall (Unpaired t-test: $p < 0.05$, scr: N = 8, miR-29a mimic N = 8). **(H)** Both mim29a and scr treated mice significantly reduced their freezing response at the end of the extinction protocol (Cond. trial-5 vs Late Ext. trial-12, Tone: Two-way RM ANOVA, main effect of treatment $F(1, 14) = 0.18$, $p = 0.68$; main effect of trials $F(1, 14) = 34.27$, $p < 0.001$; trials × treatment interaction $F(1, 14) = 0.36$, $p = 0.55$; Trace: Two-way RM ANOVA: main effect of treatment $F(1, 14) = 4.62$, $p < 0.05$; main effect of trials $F(1, 14) = 125.5$, $p < 0.001$; trials × treatment interaction $F(1, 14) = 4.44$, $p = 0.054$). scr: N = 8, mim29a N = 8; *indicates the main effect of treatment, #indicates the main effect of trials.

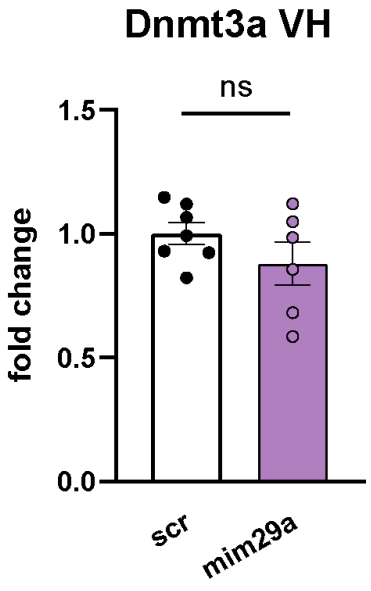

Figure 14.6: **Quantification of *Dnmt3a* levels in the ventral hippocampus of mim29a and scr treated mice**. (A) mimic 29a injection in the dorsal hippocampus did not affect the expression of *Dnmt3a* in the ventral hippocampus confirming the specificity of the injection site within the dorsal hippocampus (Unpaired t-test: $p = 0.22$). scr: N = 7, mim29a N = 6. DH = Dorsal Hippocampus; VH = Ventral Hippocampus.

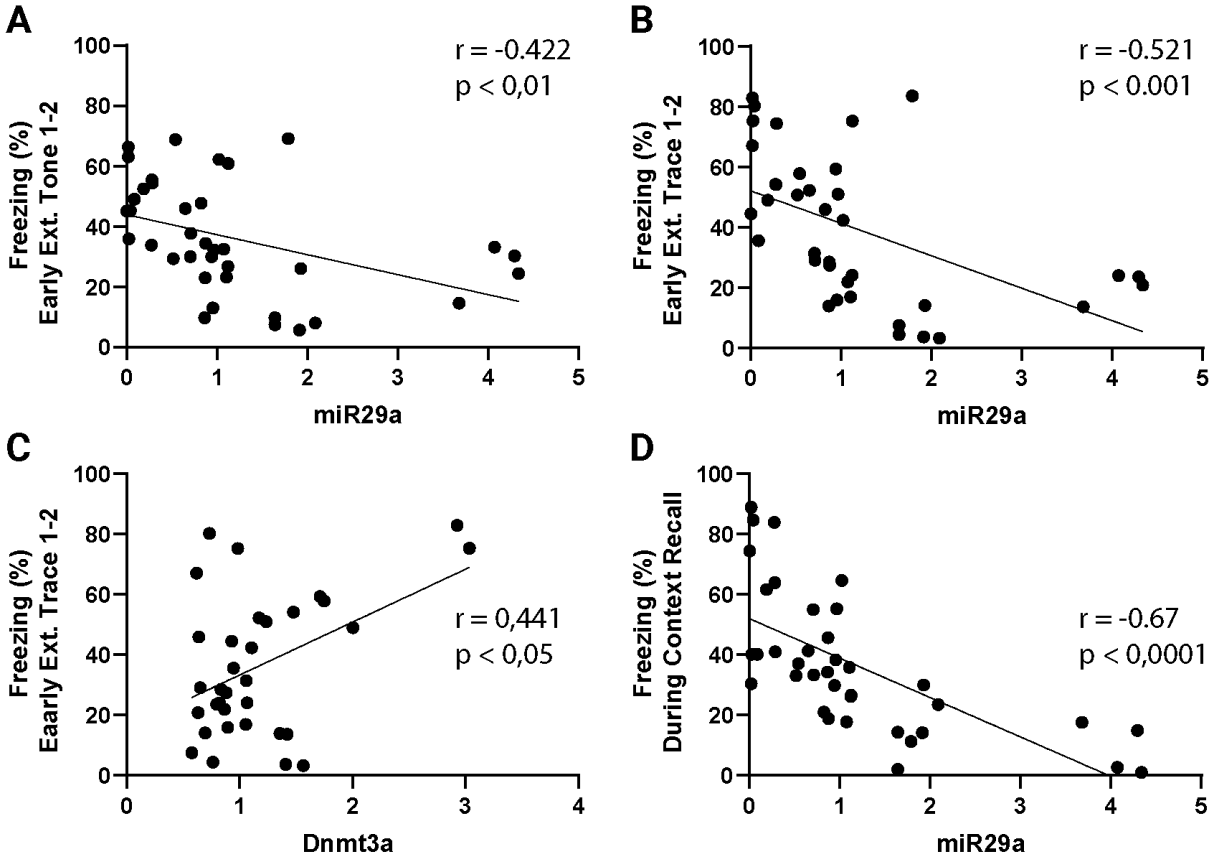

Figure 14.7: **Behavioral correlation with miR-29a and *Dnmt3a* levels post LNA and mimic injection**. (A) During early extinction miR-29a levels negatively correlate with freezing responses at the first two CS (Tone) and (B) trace presentations (Pearson's correlation). (C) During early extinction *Dnmt3a* levels positively correlate with freezing responses at the first two trace presentations (Pearson's correlation). (D) MiR-29a levels negatively correlate with freezing responses during contextual fear recall (Pearson's correlation).

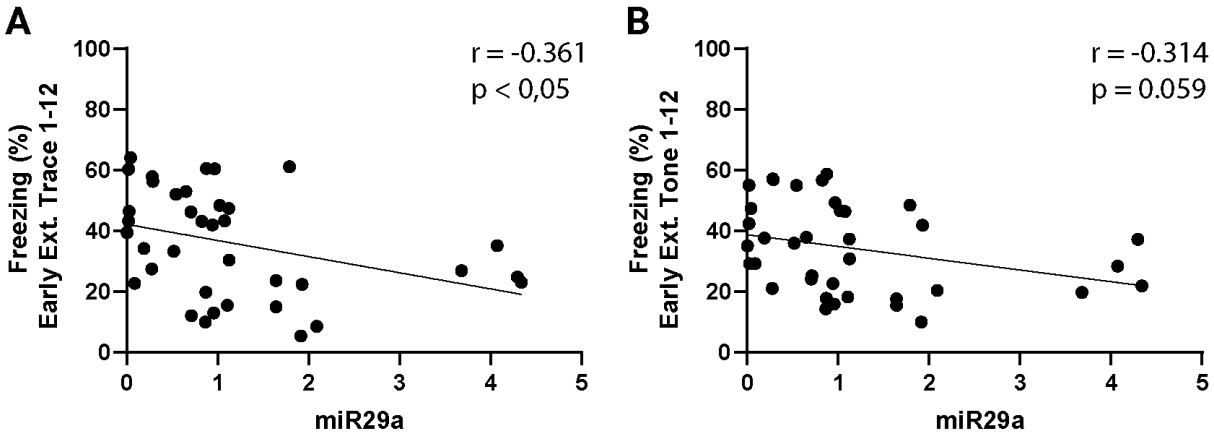

Figure 14.8: **Correlation between miR-29a levels and fear responses during early extinction post LNA and mimic injection**. (A) During early extinction miR-29 levels negatively correlate with freezing responses to trace (B) but not to CS presentations (Pearson's correlation).

15 Discussion

MiR-29 family regulation is characterized by a striking degree of conservation. Previous studies have demonstrated that miR-29a exhibits an age-associated upregulation across diverse species and tissues (Somel et al. 2010; Baumgart et al. 2012; Inukai et al. 2012; Ugalde et al. 2011). Furthermore, miR-29a plays a pivotal role in governing age-dependent processes such as neuronal maturation and iron accumulation within the brain (Ripa et al. 2017; Kole et al. 2011). In the visual cortex, miR-29a experiences the most significant upregulation during the visual critical period (Mazziotti et al. 2017a; Napoli et al. 2020). In addition, more than half of miR-29-predicted targets are downregulated with age, including key regulators of plasticity (Napoli et al. 2020). Our data confirmed this age-dependent upregulation of endogenous miR-29a expression in the dorsal hippocampus of wild-type mice, revealing a remarkable tenfold increase between P10 and P60. A previous study conducted in humans identified miRNAs linked to cognitive trajectories through a comprehensive global miRNA association study using postmortem brain samples (Wingo et al. 2022). Notably, among these miRNAs, miR-29a emerged as the second miRNA most significantly associated with cognitive decline (Wingo et al. 2022). To investigate the role of miR-29a function in influencing memory performances we bidirectionally modulate the levels of miR-29a in the dorsal hippocampus of adult mice. We found that the downregulation of miR-29a promotes hippocampal-dependent memory strength, while miR-29a upregulation impaired memory performances as observed during age cognitive decline. Furthermore, our investigation revealed a negative correlation between miR-29a levels and the percentage of freezing observed during early extinction and contextual fear recall. Conversely, levels of *Dnmt3a* exhibited a positive correlation with the percentage of freezing exhibited in the initial stages of trace extinction. This finding lends support to the specific regulatory role of miR-29a in memory persistence. Recent work shows that miR-29a downregulation in the hippocampus of 5XFAD mice results in a melioration of memory performances, reduction of beta-amyloid deposition, and lower microglia and astrocytes activation (Mei et al. 2023). This effect of miR-29a downregulation in memory maintenance is coherent with its role as a master regulator of age-related molecular mechanisms. With age, increasing levels of miR-29 a have been associated with reduced plasticity and closure of the critical period in the visual cortex (Napoli et al. 2020). Inhibition of miR-29a can reactivate ocular dominance plasticity in adult mice and upregulate genes associated with the extracellular matrix and epigenetic remodeling (Napoli et al. 2020). Epigenetic mechanisms have been increasingly recognized as important regulators of cognitive functions through the modulation of transcriptional responses (Barrett et al. 2008; Ana M M Oliveira 2016). Since we found a strong negative correlation between miR-29a and *Dnmt3a* levels, we decided to explore the profile of methylation of anti-miR29a treated mice to identify the effect of reduced miR-29a expression on the epigenetic landscape. DNA methylation is an essential epigenetic mechanism for various cellular processes and has emerged as a crucial regulator of memory consolidation (J. J. Day et al. 2010; Ferry et al. 2017). Contrary to what is observed for miR-29a

levels, with age the degree of DNA methylation decreases in many tissues, including the nervous system (K. Day et al. 2013; Jung et al. 2015). In particular, aging has been associated with a reduction in the expression of the DNA methyltransferase *Dnmt3a2* in the hippocampus, and restoring *Dnmt3a2* levels has been shown to rescue cognitive functions affected by aging (Ana M M Oliveira et al. 2012). It has also been reported that hippocampal *Dnmt3a2* levels determine cognitive abilities in both young adult and aged mice (A M M Oliveira et al. 2016). Furthermore, DNA methylation induced selectively within neuronal ensembles has been proposed as a mechanism for stabilizing engrams during consolidation, supporting successful memory retrieval (Gulmez Karaca et al. 2020). After miR-29a inhibition, we found an increase in CpG methylation level, consistent with the measured increased expression of *Dnmt3a*. Moreover, the GO analysis conducted on all the up-regulated DMCs, revealed for the DMCs that fall in promoters, an enrichment in biological processes related to regulation of gene expression. This suggests that miR-29a inhibition has a positive effect on gene expression by inhibiting repressive processes via increased methylation. For the DMCs that fall within the gene body, enrichment was found for mechanisms implicated in hippocampal-dependent learning and memory such as the Notch and TrkB. The Notch pathway stands as one of the most highly conserved signaling cascades governing cellular communication, cell fate determination, and morphogenetic processes, exerting its influence from early development onwards (Artavanis-Tsakonas et al. 1999; Guruharsha et al. 2012). Multiple investigations have demonstrated the fundamental role of Notch signaling in neurophysiological phenomena, including learning and memory, across various species, including mammals (Alberi et al. 2013). Moreover, research has unveiled compromised Notch signaling within the brains of Alzheimer's disease patients, implying a potential causal link between alterations in Notch function and memory impairment (Brai et al. 2016). Recent experimental evidence substantiates BDNF's involvement in memory functions (Yamada et al. 2022), where both memory acquisition and consolidation correlate with elevated BDNF mRNA expression (Tyler et al. 2002) and the activation of its receptor, TrkB (Minichiello et al. 1999). Genetic or pharmacological depletion of BDNF or TrkB has been shown to impair learning and memory (Mu et al. 1999; Alonso et al. 2002). Although our data showed hypermethylation of these pathways, it is noteworthy that, in contrast to the typical association between promoter methylation and gene repression, gene body methylation is positively correlated with gene expression (P A Jones 1999; Peter A Jones 2012). Overall, our results shed light on the intricate interplay between miR-29a and plasticity-related epigenetic mechanisms, specifically within the context of memory persistence. Further exploration of these molecular pathways holds great promise for advancing our understanding of memory consolidation and the development of potential therapeutic strategies for memory-related disorders. We are currently conducting transcriptomic and proteomic profiling to identify putative causal genes or sets of genes influenced by reduced miR-29a expression possibly responsible for the behavioral responses. Moreover, in light of the promising findings in our current study, it merits consideration to contemplate future experiments that delve into a more extensive exploration of the relationship between memory persistence and miR-29a levels during development. Specifically, performing behavioral analyses at various ages characterized by distinct miR-29a levels could offer valuable insights into the dynamics of this correlation across different developmental stages.

16 Methods

16.1 Animals

Mice used in all the experiments were of the C57BL/6J strain. Animals were maintained at 22°C under a 12-h light–dark cycle (average illumination levels of 1.2 cd/m2) and housed in standard cages according to current regulations about animal welfare. Food (4RF25 GLP Certificate, Mucedola) and water were available ad libitum. All experiments were carried out following the European Directive of 22 September 2010 (EU/63/2010) and were approved by the Italian Ministry of Health. All tissue explants were performed at the same time of the day (10–12 am).

16.2 Stereotaxic surgery

Mice were anesthetized and fixed on stereotaxic support through the use of metal bars in the ears. The skin was removed, and perforations were produced in the skull using a surgical drill. We injected an LNA oligonucleotide, whose sequence is complementary to miR-29a (miR-29a-3p miRCURY LNA, QIAGEN, Cat. No: 339121, 50µM) and a synthetic miR-29a mimic (mirVanaTM miRNA miR-29a-3p Mimic, ThermoFisher, Cat. No: 4464066, 100µM), or scrambled sequences as control. Injection in the dorsal hippocampus was done using the following stereotaxic coordinates: –2 mm anteroposterior, ±1.5 mm mediolateral, –1.5, –1.7 mm dorsoventral from bregma. A total of 2 µl of solution per hemisphere was injected, 1µl for each coordinate. The injection needle was left in place for an additional 60 s to allow the fluid to diffuse. The skin was subsequently sutured, and a physiological solution was injected subcutaneously to prevent dehydration. Paracetamol was administered in water ad libitum for two days. Due to the inherent stability of LNA oligonucleotides, a singular injection was administered to mice before the beginning of the behavioral test. In contrast, the miR-29a mimic exhibited faster degradation within a specific three-day timeframe (data not shown). To maintain the levels of miR-29a consistently elevated during all the sessions of the behavioral test, mice received injections every two days.

16.3 Trace fear conditioning and extinction protocol

Mice were subjected to a trace fear conditioning and extinction procedure using a custom-made PVC fear conditioning setup (50 cm X 15 cm X 21 cm). During the test days, the mice were transported in their home cages to a room adjacent to the testing room and left for 2 h before behavioral testing. We used two different contexts: In context A, the walls had white plastic circles and the floor was completely black; in context B, the walls had white vertical plastic strips and a white floor. Both chambers were covered with transparent plexiglass lids with a loudspeaker in its center point. The shock grid on the floor was made of stainless steel. Only the

grid of context A was electrified by a shock generator (World Precision Instruments, Sarasota, FL) and guided by an Arduino Uno for CS and US parameter control and footshock delivery. Mice behavior was recorded by a camera controlled by the EthoVision XT 8 software (Noldus Information Technology, The Netherlands). The apparatus was cleaned before and after each animal with 70% ethanol or 1% acetic acid for context A and context B respectively, since the mice may associate the smell with the context. After each session, mice were housed separately until the end of the test to avoid possible observational fear learning. During the Training phase of the test (Day 1), mice were allowed to explore the conditioning chamber (Context A) for 2 min before receiving five conditioning trials (baseline). Each trial consisted of a 20 s pure tone (80 dB, 2900 Hz) and a 2 s shock (0.6 mA) separated by a 20 s stimulus-free trace interval. The intertrial interval (ITI) was 120 s. Mice were removed from the chamber 120 s after the last trial. Twenty-four hours later (Day 2), mice were placed back in the conditioning chamber (Context A) for a 5 min context test. The same day (Day2) after 2 h from the context test, mice were placed in a different contest (Context B) for a Recall test consisting of a 2 min baseline period followed by four 20 s tone presentations separated by a 20 s stimulus-free trace interval with 120 s ITI. On day 3 (Early Extinction) and day 4 (Late Extinction), conditioned mice were subjected to the extinction training in context B during which they received twelve 20 s tone presentations separated by 20 s stimulus-free trace interval presentations with 120 s ITI each day.

16.4 Analysis of Freezing Behavior

Recorded videos were manually scored for freezing behavior by two separate experimenters blind to treatment conditions. Mice were considered to be freezing if no movement was detected for 2 s (defined as the complete absence of movement except for respiratory movements). Evoked freezing behavior was analyzed by calculating the percentage of time an animal spent freezing during a given phase of the test. During fear extinction, averages were calculated by pooling freezing across 2 CS presentations if not indicated otherwise.

16.5 RNA extraction and quantification (qPCR)

Tissue samples were homogenized in the cell disruption buffer (Ambion). RNA was extracted by the addiction of Phenol/guanidine-based QIAzol Lysis Reagent (Qiagen, cat. no. 79306). Chloroform was added, and the samples were shaken for 15 s. The samples were left at 20–24°C for 3 min and then centrifuged (12,000 g, 20 min, 4°C). The upper phase aqueous solution, containing RNA, was collected in a fresh tube, and the RNA was precipitated by the addition of isopropanol. Samples were mixed by vortexing, left at 20–24°C for 15 min, and then centrifuged (12,000 g, 20 min, 4°C). The supernatant was discarded, and the RNA pellet was washed in 75% ethanol by centrifugation (7500 g, 10 min, 4°C). The supernatant was discarded, and the pellet was left to dry for at least 15 min; then, it was resuspended in RNAse-free water. Total RNA concentrations were determined by NanoDrop Spectrophotometer (Thermo Scientific 2000 C). RNA quality was analyzed through a gel running (1% agarose). Total RNA was reverse transcribed using the QuantiTeck Reverse Transcription Kit (Qiagen, cat. no. 205311), and

miRNAs were reverse transcribed using the TaqMan MicroRNA reverse transcription kit (Thermo Fisher, cat. no. 4366596). Gene expression was analyzed by real-time PCR (Step one, Applied Biosystems). TaqMan inventoried assays were used for miR-29a-3p (assay ID: 002112), sno234 (assay ID:001234), and Dnmt3a (Mm00432881_m1). TaqMan assay was used for glyceraldehyde 3-phosphate dehydrogenase (Gapdh), GAPDH probe ATCCCAGAGCTGAACGG, GADPH forward CAAGGCTGTGGGCAAGGT, and GADPH reverse GGCCATGCCAGTGAGCTT. Quantitative values for cDNA amplification were calculated from the threshold cycle number (Ct) obtained during the exponential growth of the PCR products. The threshold was set automatically by the Step One software. Data were analyzed by the $\Delta\Delta$Ct methods using GAPDH or SNO234 to normalize the cDNA levels of the transcripts under investigation.

16.6 DNA extraction and validation

For the methylation analysis, we administered LNA-anti-miR29a to one hemisphere of seven mice, while the other hemisphere received an injection of the scrambled sequence, serving as an internal control. To mitigate potential lateralization effects, we randomized the side of LNA injection. The samples were stored in an ultralow freezer (-80°C) until DNA extraction. DNA was isolated from snap-frozen hippocampi using the QIAamp DNA Micro Kit (Qiagen) following the manufacturer's protocol. DNA concentration was measured with NanoDrop 2000 (Thermo Scientific), using 1 µl of input DNA. Then, dsDNA concentration was quantified using Quant-iT Picogreen dsDNA Assay (Thermo Scientific), and the distribution of DNA fragments was assessed by TapeStation 4200 (Agilent).

16.7 RRBS method

RRBS libraries were produced by Ovation RRBS Methyl-Seq with the TrueMethyl oxBS kit (Tecan, Redwood City, CA, USA) according to the manufacturer's instructions. Briefly, 100 ng of genomic DNA was digested for 1h at 37°C with the methylation-insensitive restriction enzyme MpsI. Then, fragments were ligated to methylated adapters and treated with bisulfite to convert unmethylated cytosine into uracil. PCR amplification was then performed to obtain the final DNA library. The resulting libraries were sequenced on the Illumina NovaSeq6000 with 100 bp single-end sequencing with an average of 60 million reads per sample.

16.8 RRBS data analysis

The sequencing reads were trimmed to remove the adapter and low-quality bases with Trim Galore! (www.bioinformatics.babraham.ac.uk). Then trimmed reads were aligned to the mouse reference genome mm39 with BSMAPz (github.com/zyndagj). Using the Python script methratio.py in BSMAPz, methylation ratios were extracted from the mapping output. Methylation analysis was performed using the R package methylKit (version 1.20.0) (Akalin et al., 2012). Only CpGs covered by at least 10 reads and present in every sample were retained for downstream analysis. The methylation ratio of each site was calculated by dividing the number of reads called

"C" by the total number of reads called either "C" or "T" at the specific site. The methylation score for each CpG site is represented as a β-value which ranges between 0 (unmethylated) and 1 (fully methylated). Differentially methylated CpGs (DMCs) were detected using a logistic regression model based on a Chi-square test. A false discovery rate (FDR) q value threshold of $<$ 0.05 and methylation difference of $\pm$10% between treated and control groups was used to identify significant DMCs. The promoter was defined as the region $\pm$1kb from the transcription start site. Pathway analysis was performed using the web tools WebGestalt (www.webgestalt.org) and EnrichR (maayanlab.cloud).

16.9 Statistical analysis

All the statistical analyses were performed using GraphPad Prism 8. Parametric t-test, Pearson's correlation, analysis of variance (ANOVA), and repeated measure-ANOVA (RM-ANOVA) were used. ANOVA was followed by appropriate post hoc tests. Significance was set at $P<0.05$ for all tests. Error bars represent s.e.m. in all figures.

Acknowledgements

I express my profound gratitude to all the people, both within and outside the laboratory, whose collective efforts made this research endeavor possible. A special acknowledgment is extended to my two supervisors, Prof. Tommaso Pizzorusso and Prof. Alessandro Cellerino. I am truly grateful for the opportunity to engage in this research within a dynamic and stimulating environment. Their invaluable advice and inspiration have significantly contributed to my growth during these years.

I thank Dr. Raffaele Mazziotti for his assistance, engaging discussions, and our collaborative pursuit of ambitious projects. Thanks also to Dr. Elena Putignano, for her wise suggestions and her technical and emotional support.

Gratitude is also extended to all other members of the lab. I particularly want to thank: Sara, Alexia, Giulia, Francesco, Leonardo, Valentino, Francesca T., Matteo, Elsa, Francesca D., Laura, and Paola. I have learned a lot from each of you, and your friendship has made my days productive and enjoyable. Thank you all for the challenging yet funny journey.

I am grateful to the Scuola Normale for providing me with the opportunity to be part of this exceptional community. This experience has allowed me to connect with beautiful and interesting people beyond my research domain, fostering personal growth and yielding enduring friendships.

List of Figures

List of Tables

References

Adhikari, Anna, Fiona K B Buchanan, Timothy A Fenton, David L Cameron, Julian A N M Halmai, Nycole A Copping, Kyle D Fink, and Jill L Silverman (Apr. 2022). "Touchscreen Cognitive Deficits, Hyperexcitability, and Hyperactivity in Males and Females Using Two Models of Cdkl5 Deficiency". en. In: *Hum. Mol. Genet.* 00, 00, pp. 1–19 (cit. on pp. 35, 46).

Aggius-Vella, Elena, Monica Gori, Silvia Animali, Claudio Campus, and Paola Binda (Oct. 2020). "Non-spatial skills differ in the front and rear peri-personal space". en. In: *Neuropsychologia* 147, p. 107619 (cit. on p. 16).

Ahmed, Mohsin S, James B Priestley, Angel Castro, Fabio Stefanini, Ana Sofia Solis Canales, Elizabeth M Balough, Erin Lavoie, Luca Mazzucato, Stefano Fusi, and Attila Losonczy (July 2020). "Hippocampal Network Reorganization Underlies the Formation of a Temporal Association Memory". en. In: *Neuron* 107.2, 283–291.e6 (cit. on pp. 11, 81).

Alberi, Lavinia, Sarah E Hoey, Emanuele Brai, Alessandra L Scotti, and Swananda Marathe (June 2013). "Notch signaling in the brain: in good and bad times". en. In: *Ageing Res. Rev.* 12.3, pp. 801–814 (cit. on p. 97).

Alberini, Cristina M and Eric R Kandel (Dec. 2014). "The regulation of transcription in memory consolidation". en. In: *Cold Spring Harb. Perspect. Biol.* 7.1, a021741 (cit. on p. 84).

Aleman, Tomas S, Samuel G Jacobson, John D Chico, Michele L Scott, Andy Y Cheung, Elizabeth A M Windsor, Masatoshi Furushima, T Michael Redmond, Jean Bennett, Krzysztof Palczewski, and Artur V Cideciyan (2004). *Impairment of the Transient Pupillary Light Reflex inRpe65/Mice and Humans with Leber Congenital Amaurosis*. Issue: 4 Pages: 1259 Publication Title: Investigative Opthalmology & Visual Science Volume: 45 (cit. on pp. 15, 16, 79).

Alnæs, Dag, Markus Handal Sneve, Thomas Espeseth, Tor Endestad, Steven Harry Pieter van de Pavert, and Bruno Laeng (Apr. 2014). "Pupil size signals mental effort deployed during multiple object tracking and predicts brain activity in the dorsal attention network and the locus coeruleus". en. In: *J. Vis.* 14.4 (cit. on p. 6).

Alonso, Mariana, Monica R M Vianna, Amaicha M Depino, Tadeu Mello e Souza, Patricia Pereira, German Szapiro, Haydee Viola, Fernando Pitossi, Ivan Izquierdo, and Jorge H Medina (2002). "BDNF-triggered events in the rat hippocampus are required for both short- and long-term memory formation". en. In: *Hippocampus* 12.4, pp. 551–560 (cit. on p. 97).

Amano, Taiju, Cagri T Unal, and Denis Paré (Apr. 2010). "Synaptic correlates of fear extinction in the amygdala". en. In: *Nat. Neurosci.* 13.4, pp. 489–494 (cit. on p. 54).

Amendola, Elena, Yang Zhan, Camilla Mattucci, Enrico Castroflorio, Eleonora Calcagno, Claudia Fuchs, Giuseppina Lonetti, Davide Silingardi, Alexei L Vyssotski, Dominika Farley, Elisabetta Ciani, Tommaso Pizzorusso, Maurizio Giustetto, and Cornelius T Gross (May 2014). "Mapping pathological phenotypes in a mouse model of CDKL5 disorder". en. In: *PLoS One* 9.5, e91613 (cit. on pp. 35, 49).

Amodio, Nicola, Marco Rossi, Lavinia Raimondi, Maria Rita Pitari, Cirino Botta, Pierosandro Tagliaferri, and Pierfrancesco Tassone (May 2015). "miR-29s: a family of epi-miRNAs with therapeutic implications in hematologic malignancies". eng. In: *Oncotarget* 6.15, pp. 12837–12861. ISSN: 1949-2553. DOI: 10.18632/oncotarget.3805 (cit. on p. 85).

An, Bobae, Jihye Kim, Kyungjoon Park, Sukwon Lee, Sukwoon Song, and Sukwoo Choi (July 2017). "Amount of fear extinction changes its underlying mechanisms". en. In: *Elife* 6 (cit. on p. 53).

Angulo-Chavira, Armando Quetzalcóatl, Octavio García, and Natalia Arias-Trejo (Nov. 2017). "Pupil response and attention skills in Down syndrome". en. In: *Res. Dev. Disabil.* 70, pp. 40–49 (cit. on p. 15).

Arnsten, A. F. T. and P. S. Goldman-Rakic (July 1984). "Selective prefrontal cortical projections to the region of the locus coeruleus and raphe nuclei in the rhesus monkey". In: *Brain Research* 306.1, pp. 9–18. ISSN: 0006-8993. DOI: 10.1016/0006-8993(84)90351-2 (cit. on p. 8).

Artavanis-Tsakonas, S, M D Rand, and R J Lake (Apr. 1999). "Notch signaling: cell fate control and signal integration in development". en. In: *Science* 284.5415, pp. 770–776 (cit. on p. 97).

Artoni, Pietro, Arianna Piffer, Viviana Vinci, Jocelyn LeBlanc, Charles A Nelson, Takao K Hensch, and Michela Fagiolini (Sept. 2020). "Deep learning of spontaneous arousal fluctuations detects early cholinergic defects across neurodevelopmental mouse models and patients". en. In: *Proc. Natl. Acad. Sci. U. S. A.* 117.38. Publisher: National Academy of Sciences, pp. 23298–23303 (cit. on pp. 12, 15, 16, 35, 36, 47, 79, 80).

Aston-Jones, G, J Rajkowski, P Kubiak, and T Alexinsky (July 1994). "Locus coeruleus neurons in monkey are selectively activated by attended cues in a vigilance task". en. In: *J. Neurosci.* 14.7, pp. 4467–4480 (cit. on p. 6).

Aston-Jones, Gary and Jonathan D Cohen (2005). "An integrative theory of locus coeruleus-norepinephrine function: adaptive gain and optimal performance". en. In: *Annu. Rev. Neurosci.* 28, pp. 403–450 (cit. on p. 47).

Azevedo-Santos, Isabela Freire and Josimari Melo DeSantana (Nov. 2018). "Pain measurement techniques: spotlight on mechanically ventilated patients". en. In: *J. Pain Res.* 11, pp. 2969–2980 (cit. on p. 15).

Bahi-Buisson, Nadia, Nathalie Villeneuve, Emilie Caietta, Aurélia Jacquette, Helene Maurey, Gert Matthijs, Hilde Van Esch, Andrée Delahaye, Anne Moncla, Mathieu Milh, Flore Zufferey, Bertrand Diebold, and Thierry Bienvenu (July 2012). "Recurrent mutations in the CDKL5 gene: genotype-phenotype relationships". en. In: *Am. J. Med. Genet. A* 158A.7. Publisher: Wiley, pp. 1612–1619 (cit. on p. 37).

Baldi, Elisabetta and Corrado Bucherelli (June 2015). "Brain sites involved in fear memory reconsolidation and extinction of rodents". en. In: *Neurosci. Biobehav. Rev.* 53, pp. 160–190 (cit. on p. 53).

Barkat, Tania Rinaldi, Daniel B Polley, and Takao K Hensch (July 2011). "A critical period for auditory thalamocortical connectivity". en. In: *Nat. Neurosci.* 14.9, pp. 1189–1194 (cit. on p. 12).

Barnard, K E, J J Broman-Fulks, K D Michael, R M Webb, and L L Zawilinski (Mar. 2011). "The effects of physiological arousal on cognitive and psychomotor performance among individuals with high and low anxiety sensitivity". In: *Anxiety Stress Coping* 24.2. Publisher: Anxiety Stress Coping (cit. on p. 35).

Barrett, Ruth M and Marcelo A Wood (July 2008). "Beyond transcription factors: the role of chromatin modifying enzymes in regulating transcription required for memory". en. In: *Learn. Mem.* 15.7, pp. 460–467 (cit. on p. 96).

Barry, Colin, Jessica de Souza, Yinan Xuan, Jason Holden, Eric Granholm, and Edward Jay Wang (Apr. 2022). "At-Home Pupillometry using Smartphone Facial Identification Cameras". In: *Proceedings of the 2022 CHI Conference on Human Factors in Computing Systems*. CHI '22. Issue: Article 235 event-place: New Orleans, LA, USA. New York, NY, USA: Association for Computing Machinery, pp. 1–12 (cit. on p. 13).

Bartel, David P (Mar. 2018). "Metazoan MicroRNAs". en. In: *Cell* 173.1, pp. 20–51 (cit. on p. 85).

Baumgart, Mario, Marco Groth, Steffen Priebe, Jessika Appelt, Reinhard Guthke, Matthias Platzer, and Alessandro Cellerino (May 2012). "Age-dependent regulation of tumor-related

microRNAs in the brain of the annual fish Nothobranchius furzeri". en. In: *Mech. Ageing Dev.* 133.5, pp. 226–233 (cit. on p. 96).

Baumgärtel, Karsten, David Genoux, Hans Welzl, Ry Y Tweedie-Cullen, Kyoko Koshibu, Magdalena Livingstone-Zatchej, Céline Mamie, and Isabelle M Mansuy (May 2008). "Control of the establishment of aversive memory by calcineurin and Zif268". en. In: *Nat. Neurosci.* 11.5, pp. 572–578 (cit. on p. 71).

Bear, M F and J D Daniels (1983). *The plastic response to monocular deprivation persists in kitten visual cortex after chronic depletion of norepinephrine.* Issue: 2 Pages: 407–416 Publication Title: The Journal of Neuroscience Volume: 3 (cit. on p. 9).

Beatty, J (Mar. 1982). "Task-evoked pupillary responses, processing load, and the structure of processing resources". en. In: *Psychol. Bull.* 91.2, pp. 276–292 (cit. on p. 1).

Beggiato, Matthias, Franziska Hartwich, and Josef Krems (Sept. 2018). "Using Smartbands, Pupillometry and Body Motion to Detect Discomfort in Automated Driving". en. In: *Front. Hum. Neurosci.* 12, p. 338 (cit. on p. 15).

Benarroch, Eduardo E (July 2018). "Locus coeruleus". en. In: *Cell Tissue Res.* 373.1, pp. 221–232 (cit. on p. 5).

Benetti, Roberta, Susana Gonzalo, Isabel Jaco, Purificación Muñoz, Susana Gonzalez, Stefan Schoeftner, Elizabeth Murchison, Thomas Andl, Taiping Chen, Peter Klatt, En Li, Manuel Serrano, Sarah Millar, Gregory Hannon, and Maria A Blasco (Sept. 2008). "A mammalian microRNA cluster controls DNA methylation and telomere recombination via Rbl2-dependent regulation of DNA methyltransferases". en. In: *Nat. Struct. Mol. Biol.* 15.9, p. 998 (cit. on p. 85).

Benito, Eva and Angel Barco (2015). "The neuronal activity-driven transcriptome". en. In: *Mol. Neurobiol.* 51.3, pp. 1071–1088 (cit. on p. 84).

Berti, Stefan, Gerhard Vossel, and Matthias Gamer (Oct. 2017). "The Orienting Response in Healthy Aging: Novelty P3 Indicates No General Decline but Reduced Efficacy for Fast Stimulation Rates". en. In: *Front. Psychol.* 8, p. 1780 (cit. on p. 35).

Bierwirth, Philipp and Ursula Stockhorst (Oct. 2022). "Role of noradrenergic arousal for fear extinction processes in rodents and humans". en. In: *Neurobiol. Learn. Mem.* 194, p. 107660 (cit. on p. 81).

Binda, Paola and Claudia Lunghi (Jan. 2017). "Short-Term Monocular Deprivation Enhances Physiological Pupillary Oscillations". en. In: *Neural Plast.* 2017, p. 6724631 (cit. on p. 9).

Binda, Paola, Maria Pereverzeva, and Scott O Murray (Jan. 2013a). "Attention to bright surfaces enhances the pupillary light reflex". en. In: *J. Neurosci.* 33.5, pp. 2199–2204 (cit. on p. 15).

— (May 2013b). "Pupil constrictions to photographs of the sun". en. In: *J. Vis.* 13.6 (cit. on pp. 1, 15).

— (Dec. 2014). "Pupil size reflects the focus of feature-based attention". en. In: *J. Neurophysiol.* 112.12, pp. 3046–3052 (cit. on pp. 1, 4).

Bishop, Christopher M (Aug. 2006). *Pattern Recognition and Machine Learning.* en. LLC, 233 Spring Street, New York, NY 10013, USA: Springer (cit. on p. 51).

Bitsios, P., E. Szabadi, and C. M. Bradshaw (Mar. 2004). "The fear-inhibited light reflex: importance of the anticipation of an aversive event". eng. In: *International Journal of Psychophysiology: Official Journal of the International Organization of Psychophysiology* 52.1, pp. 87–95. ISSN: 0167-8760. DOI: 10.1016/j.ijpsycho.2003.12.006 (cit. on p. 10).

Blaser, Erik, Luke Eglington, Alice S Carter, and Zsuzsa Kaldy (Mar. 2014). "Pupillometry reveals a mechanism for the Autism Spectrum Disorder (ASD) advantage in visual tasks". en. In: *Sci. Rep.* 4, p. 4301 (cit. on pp. 11, 15, 80).

Blum, Ian D, Lei Zhu, Luc Moquin, Maia V Kokoeva, Alain Gratton, Bruno Giros, and Kai-Florian Storch (Dec. 2014). "A highly tunable dopaminergic oscillator generates ultradian rhythms of behavioral arousal". en. In: *Elife* 3, pp. 1–23 (cit. on p. 35).

Bocchio, Marco, Sadegh Nabavi, and Marco Capogna (May 2017). "Synaptic Plasticity, Engrams, and Network Oscillations in Amygdala Circuits for Storage and Retrieval of Emotional Memories". en. In: *Neuron* 94.4, pp. 731–743 (cit. on p. 62).

Bohlin, Gunilla (1976). *Delayed Habituation of the Electrodermal Orienting Response as a Function of Increased Level of Arousal*. Issue: 4 Pages: 345–351 Publication Title: Psychophysiology Volume: 13 (cit. on p. 35).

Borrego, R L and R M Gardner (Feb. 1986). "Classical conditioning of pupillary constriction". en. In: *Percept. Mot. Skills* 62.1, pp. 315–322 (cit. on p. 81).

Boucsein, Wolfram (Feb. 2012). *Electrodermal Activity*. en. Springer Science & Business Media (cit. on p. 81).

Bouret, Sebastien and Susan J Sara (2004). *Reward expectation, orientation of attention and locus coeruleus-medial frontal cortex interplay during learning*. Issue: 3 Pages: 791–802 Publication Title: European Journal of Neuroscience Volume: 20 (cit. on p. 6).

Bouton, Mark E (Sept. 2004). "Context and behavioral processes in extinction". en. In: *Learn. Mem.* 11.5, pp. 485–494 (cit. on p. 53).

Boxhoorn, Sara, Nico Bast, Hans Supèr, Leonie Polzer, Hannah Cholemkery, and Christine M Freitag (May 2020). "Pupil dilation during visuospatial orienting differentiates between autism spectrum disorder and attention-deficit/hyperactivity disorder". en. In: *J. Child Psychol. Psychiatry* 61.5, pp. 614–624 (cit. on pp. 40, 41).

Braasch, D A and D R Corey (Jan. 2001). "Locked nucleic acid (LNA): fine-tuning the recognition of DNA and RNA". en. In: *Chem. Biol.* 8.1, pp. 1–7 (cit. on p. 87).

Bradley, Margaret M, Laura Miccoli, Miguel A Escrig, and Peter J Lang (July 2008). "The pupil as a measure of emotional arousal and autonomic activation". en. In: *Psychophysiology* 45.4, pp. 602–607 (cit. on pp. 36, 54, 56, 70).

Bradshaw, J (Nov. 1967). "Pupil size as a measure of arousal during information processing". en. In: *Nature* 216.5114, pp. 515–516 (cit. on p. 56).

Brai, Emanuele, Noemi Alina Raio, and Lavinia Alberi (July 2016). "Notch1 hallmarks fibrillary depositions in sporadic Alzheimer's disease". en. In: *Acta Neuropathol Commun* 4.1, p. 64 (cit. on p. 97).

Brascamp, Jan W, Gilles de Hollander, Michael D Wertheimer, Ashley N DePew, and Tomas Knapen (Aug. 2021). "Separable pupillary signatures of perception and action during perceptual multistability". en. In: *Elife* 10 (cit. on p. 9).

Breen, L A, R M Burde, and G E Mendelsohn (June 1983). "Beesting papillitis". en. In: *J. Clin. Neuroophthalmol.* 3.2, pp. 97–100 (cit. on p. 6).

Brückner, G, J Grosche, S Schmidt, W Härtig, R U Margolis, B Delpech, C I Seidenbecher, R Czaniera, and M Schachner (Dec. 2000). "Postnatal development of perineuronal nets in wild-type mice and in a mutant deficient in tenascin-R". en. In: *J. Comp. Neurol.* 428.4. Publisher: Wiley, pp. 616–629 (cit. on p. 54).

Brueckner, Bodo, Regine Garcia Boy, Pawel Siedlecki, Tanja Musch, H Christian Kliem, Piotr Zielenkiewicz, Sandor Suhai, Manfred Wiessler, and Frank Lyko (July 2005). "Epigenetic reactivation of tumor suppressor genes by a novel small-molecule inhibitor of human DNA methyltransferases". en. In: *Cancer Res.* 65.14, pp. 6305–6311 (cit. on p. 85).

Brunello, N, J Mendlewicz, S Kasper, B Leonard, S Montgomery, J Nelson, E Paykel, M Versiani, and G Racagni (Oct. 2002). "The role of noradrenaline and selective noradrenaline reuptake inhibition in depression". en. In: *Eur. Neuropsychopharmacol.* 12.5, pp. 461–475 (cit. on p. 11).

Burgos-Robles, Anthony, Ivan Vidal-Gonzalez, Edwin Santini, and Gregory J Quirk (Mar. 2007). "Consolidation of fear extinction requires NMDA receptor-dependent bursting in the ventromedial prefrontal cortex". en. In: *Neuron* 53.6, pp. 871–880 (cit. on p. 71).

Burley, Daniel T and Stephanie H M van Goozen (May 2020). "Pupil Response to Affective Stimuli: a Biomarker of Early Conduct Problems in Young Children". en. In: *J. Abnorm. Child Psychol.* 48.5, pp. 693–701 (cit. on pp. 15, 80).

Carter, Matthew E, Ofer Yizhar, Sachiko Chikahisa, Hieu Nguyen, Antoine Adamantidis, Seiji Nishino, Karl Deisseroth, and Luis de Lecea (Dec. 2010). "Tuning arousal with optogenetic modulation of locus coeruleus neurons". en. In: *Nat. Neurosci.* 13.12, pp. 1526–1533 (cit. on p. 5).

Carulli, Daniela, Tommaso Pizzorusso, Jessica C F Kwok, Elena Putignano, Andrea Poli, Serhiy Forostyak, Melissa R Andrews, Sathyaseelan S Deepa, Tibor T Glant, and James W Fawcett (Aug. 2010). "Animals lacking link protein have attenuated perineuronal nets and persistent plasticity". en. In: *Brain* 133.Pt 8, pp. 2331–2347 (cit. on pp. 54, 71, 73).

Carulli, Daniela, Kate E Rhodes, and James W Fawcett (Mar. 2007). "Upregulation of aggrecan, link protein 1, and hyaluronan synthases during formation of perineuronal nets in the rat cerebellum". en. In: *J. Comp. Neurol.* 501.1, pp. 83–94 (cit. on p. 54).

Castaldi, Elisa, Antonella Pomè, Guido Marco Cicchini, David Burr, and Paola Binda (Oct. 2021). "The pupil responds spontaneously to perceived numerosity". en. In: *Nat. Commun.* 12.1, p. 5944 (cit. on p. 1).

Cazettes, Fanny, Davide Reato, João P Morais, Alfonso Renart, and Zachary F Mainen (Jan. 2021). "Phasic Activation of Dorsal Raphe Serotonergic Neurons Increases Pupil Size". In: *Curr. Biol.* 31.1. Publisher: Cell Press, 192–197.e4 (cit. on pp. 6, 7).

Charier, David, Marie-Charlotte Vogler, Daniel Zantour, Vincent Pichot, Alexandre Martins-Baltar, Marjolaine Courbon, Frédéric Roche, François Vassal, and Serge Molliex (2019). *Assessing pain in the postoperative period: Analgesia Nociception IndexTM versus pupillometry.* Issue: 2 Pages: e322–e327 Publication Title: British Journal of Anaesthesia Volume: 123 (cit. on p. 15).

Chen, Cathy S., R. Becket Ebitz, Sylvia R. Bindas, A. David Redish, Benjamin Y. Hayden, and Nicola M. Grissom (Jan. 2021). "Divergent Strategies for Learning in Males and Females". eng. In: *Current biology: CB* 31.1, 39–50.e4. ISSN: 1879-0445. DOI: 10.1016/j.cub.2020.09.075 (cit. on p. 46).

Chen, Liang-Chieh, Yukun Zhu, George Papandreou, Florian Schroff, and Hartwig Adam (2018). *Encoder-Decoder with Atrous Separable Convolution for Semantic Image Segmentation.* Pages: 833–851 Publication Title: Computer Vision – ECCV 2018 (cit. on p. 27).

Chougule, Pratik S, Raymond P Najjar, Maxwell T Finkelstein, Nagaendran Kandiah, and Dan Milea (Apr. 2019). "Light-Induced Pupillary Responses in Alzheimer's Disease". en. In: *Front. Neurol.* 10, p. 360 (cit. on pp. 11, 15, 80).

Cocker, Kenneth D, Alistair R Fielder, Merrick J Moseley, and A David Edwards (Jan. 2005). "Measurements of pupillary responses to light in term and preterm infants". In: *Neuroophthalmology* 29.3. Publisher: Informa UK Limited, pp. 95–101 (cit. on p. 48).

Cohen, N J and V I Douglas (Mar. 1972). "Characteristics of the orienting response in hyperactive and normal children". en. In: *Psychophysiology* 9.2, pp. 238–245 (cit. on p. 41).

Connelly, Mark A, Jacob T Brown, Gregory L Kearns, Rawni A Anderson, Shawn D St Peter, and Kathleen A Neville (Dec. 2014). "Pupillometry: a non-invasive technique for pain assessment in paediatric patients". en. In: *Arch. Dis. Child.* 99.12, pp. 1125–1131 (cit. on p. 15).

Critchley, Hugo D, Christopher J Mathias, and Raymond J Dolan (Feb. 2002). "Fear conditioning in humans: the influence of awareness and autonomic arousal on functional neuroanatomy". en. In: *Neuron* 33.4, pp. 653–663 (cit. on pp. 62, 70).

Czipri, Mátyás, Jeffrey M Otto, Gabriella Cs-Szabó, Rajesh V Kamath, Csaba Vermes, Gábor Firneisz, Kevin J Kolman, Hideto Watanabe, Yefu Li, Peter J Roughley, et al. (2003). "Genetic rescue of chondrodysplasia and the perinatal lethal effect of cartilage link protein deficiency". In: *J. Biol. Chem.* 278.40. Publisher: ASBMB, pp. 39214–39223 (cit. on p. 73).

David, Michael and Paresh A Malhotra (Apr. 2022). "New approaches for the quantification and targeting of noradrenergic dysfunction in Alzheimer's disease". en. In: *Ann Clin Transl Neurol* 9.4, pp. 582–596 (cit. on p. 11).

Day, Jeremy J and J David Sweatt (Nov. 2010). "DNA methylation and memory formation". en. In: *Nat. Neurosci.* 13.11, pp. 1319–1323 (cit. on p. 96).

Day, Kenneth, Lindsay L Waite, Anna Thalacker-Mercer, Andrew West, Marcas M Bamman, James D Brooks, Richard M Myers, and Devin Absher (2013). "Differential DNA methylation with age displays both common and dynamic features across human tissues that are influenced by CpG landscape". en. In: *Genome Biol.* 14.9, R102 (cit. on p. 97).

Della Sala, Grazia, Elena Putignano, Gabriele Chelini, Riccardo Melani, Eleonora Calcagno, Gian Michele Ratto, Elena Amendola, Cornelius T Gross, Maurizio Giustetto, and Tommaso Pizzorusso (Aug. 2016). "Dendritic Spine Instability in a Mouse Model of CDKL5 Disorder Is Rescued by Insulin-like Growth Factor 1". en. In: *Biol. Psychiatry* 80.4, pp. 302–311 (cit. on p. 35).

Demarest, Scott T, Heather E Olson, Angela Moss, Elia Pestana-Knight, Xiaoming Zhang, Sumit Parikh, Lindsay C Swanson, Katherine D Riley, Grace A Bazin, Katie Angione, Lisa-Marie Niestroj, Dennis Lal, Elizabeth Juarez-Colunga, and Tim A Benke (Aug. 2019). "CDKL5 deficiency disorder: Relationship between genotype, epilepsy, cortical visual impairment, and development". en. In: *Epilepsia* 60.8, pp. 1733–1742 (cit. on p. 34).

Demontis, Ditte et al. (Jan. 2019). "Discovery of the first genome-wide significant risk loci for attention deficit/hyperactivity disorder". en. In: *Nat. Genet.* 51.1, pp. 63–75 (cit. on p. 46).

Dhingra, Deepika, Savleen Kaur, and Jagat Ram (Sept. 2019). "Illicit drugs: Effects on eye". en. In: *Indian J. Med. Res.* 150.3. Publisher: Wolters Kluwer – Medknow Publications, p. 228 (cit. on p. 6).

Diamond, Adele (2013). "Executive functions". en. In: *Annu. Rev. Psychol.* 64, pp. 135–168 (cit. on p. 46).

Diamond, J P (Jan. 2001). "The Pupil. Anatomy, Physiology and Clinical Applications". en. In: *Br. J. Ophthalmol.* 85.1, 121E (cit. on p. 9).

Dias, Brian George, Jared Vega Goodman, Ranbir Ahluwalia, Audrey Elizabeth Easton, Raül Andero, and Kerry James Ressler (Aug. 2014). "Amygdala-Dependent Fear Memory Consolidation via miR-34a and Notch Signaling". en. In: *Neuron* 83.4, pp. 906–918. ISSN: 08966273. DOI: 10.1016/j.neuron.2014.07.019 (cit. on p. 91).

Duvarci, Sevil and Denis Pare (June 2014). "Amygdala microcircuits controlling learned fear". en. In: *Neuron* 82.5, pp. 966–980 (cit. on p. 71).

Eckstein, Maria K., Belén Guerra-Carrillo, Alison T. Miller Singley, and Silvia A. Bunge (June 2017). "Beyond eye gaze: What else can eyetracking reveal about cognition and cognitive development?" eng. In: *Developmental Cognitive Neuroscience* 25, pp. 69–91. ISSN: 1878-9307. DOI: 10.1016/j.dcn.2016.11.001 (cit. on p. 7).

Ehrlich, Ingrid, Yann Humeau, François Grenier, Stephane Ciocchi, Cyril Herry, and Andreas Lüthi (June 2009). "Amygdala inhibitory circuits and the control of fear memory". en. In: *Neuron* 62.6, pp. 757–771 (cit. on p. 71).

Einhäuser, Wolfgang, James Stout, Christof Koch, and Olivia Carter (Feb. 2008). "Pupil dilation reflects perceptual selection and predicts subsequent stability in perceptual rivalry". en. In: *Proc. Natl. Acad. Sci. U. S. A.* 105.5, pp. 1704–1709 (cit. on p. 9).

El Ahmadieh, Tarek Y, Nicole Bedros, Sonja E Stutzman, Daniel Nyancho, Aardhra M Venkatachalam, Matthew MacAllister, Vin Shen Ban, Nader S Dahdaleh, Venkatesh Aiyagari, Stephen Figueroa, Jonathan A White, H Hunt Batjer, Carlos A Bagley, Daiwai M Olson, and Salah G Aoun (Jan. 2021). "Automated Pupillometry as a Triage and Assessment Tool in Patients with Traumatic Brain Injury". en. In: *World Neurosurg.* 145, e163–e169 (cit. on pp. 11, 15).

Fabbri, Muller, Ramiro Garzon, Amelia Cimmino, Zhongfa Liu, Nicola Zanesi, Elisa Callegari, Shujun Liu, Hansjuerg Alder, Stefan Costinean, Cecilia Fernandez-Cymering, Stefano Volinia, Gulnur Guler, Carl D Morrison, Kenneth K Chan, Guido Marcucci, George A Calin, Kay Huebner, and Carlo M Croce (Oct. 2007). "MicroRNA-29 family reverts aberrant methylation in lung cancer by targeting DNA methyltransferases 3A and 3B". en. In: *Proc. Natl. Acad. Sci. U. S. A.* 104.40, pp. 15805–15810 (cit. on pp. 85, 87).

Fawcett, James W., Toshitaka Oohashi, and Tommaso Pizzorusso (Aug. 2019). "The roles of perineuronal nets and the perinodal extracellular matrix in neuronal function". en. In: *Nature Reviews Neuroscience* 20.8. Number: 8 Publisher: Nature Publishing Group, pp. 451–465. ISSN: 1471-0048. DOI: 10.1038/s41583-019-0196-3 (cit. on pp. 71, 81).

Fehr, Stephanie, Meredith Wilson, Jenny Downs, Simon Williams, Alessandra Murgia, Stefano Sartori, Marilena Vecchi, Gladys Ho, Roberta Polli, Stavroula Psoni, Xinhua Bao, Nick de Klerk, Helen Leonard, and John Christodoulou (Mar. 2013). "The CDKL5 disorder is an independent clinical entity associated with early-onset encephalopathy". en. In: *Eur. J. Hum. Genet.* 21.3, pp. 266–273 (cit. on p. 34).

Felten, David L, Håkan Hallman, and Gösta Jonsson (Feb. 1982). "Evidence for a neurotrophic role of noradrenaline neurons in the postnatal development of rat cerebral cortex". In: *J. Neurocytol.* 11.1, pp. 119–135 (cit. on p. 12).

Ferry, Laure et al. (Aug. 2017). "Methylation of DNA Ligase 1 by G9a/GLP Recruits UHRF1 to Replicating DNA and Regulates DNA Methylation". en. In: *Mol. Cell* 67.4, 550–565.e5 (cit. on p. 96).

Filipowicz, Alexandre LS, Christopher M Glaze, Joseph W Kable, and Joshua I Gold (May 2020). "Pupil diameter encodes the idiosyncratic, cognitive complexity of belief updating". In: *eLife* 9. Ed. by Tobias H Donner, Timothy E Behrens, and Tobias H Donner. Publisher: eLife Sciences Publications, Ltd, e57872. ISSN: 2050-084X. DOI: 10.7554/eLife.57872 (cit. on p. 7).

Finke, Johannes B, Kati Roesmann, Tobias Stalder, and Tim Klucken (Nov. 2021). "Pupil dilation as an index of Pavlovian conditioning. A systematic review and meta-analysis". en. In: *Neurosci. Biobehav. Rev.* 130, pp. 351–368 (cit. on p. 81).

Fitzgerald, Paul J (Mar. 2014). "Is elevated norepinephrine an etiological factor in some cases of schizophrenia?" en. In: *Psychiatry Res.* 215.3, pp. 497–504 (cit. on p. 11).

Francis, Nikolas A and Patrick O Kanold (Mar. 2017). "Automated Operant Conditioning in the Mouse Home Cage". en. In: *Front. Neural Circuits* 11, p. 10 (cit. on p. 36).

Freund, Yoav and Robert E Schapire (1997). "A Decision-Theoretic Generalization of On-Line Learning and an Application to Boosting". In: *Journal of Computer and System Sciences* 55.1, pp. 119–139 (cit. on p. 51).

Frost, Shaun, Liam Robinson, Christopher C Rowe, David Ames, Colin L Masters, Kevin Taddei, Stephanie R Rainey-Smith, Ralph N Martins, and Yogesan Kanagasingam (Aug. 2017). "Evaluation of Cholinergic Deficiency in Preclinical Alzheimer's Disease Using Pupillometry". en. In: *J. Ophthalmol.* 2017, p. 7935406 (cit. on pp. 11, 15, 80).

Fuchs, Claudia, Laura Gennaccaro, Stefania Trazzi, Stefano Bastianini, Simone Bettini, Viviana Lo Martire, Elisa Ren, Giorgio Medici, Giovanna Zoccoli, Roberto Rimondini, and Elisabetta Ciani (2018). "Heterozygous CDKL5 Knockout Female Mice Are a Valuable Animal Model for CDKL5 Disorder". en. In: *Neural Plast.* 2018. Publisher: Hindawi Limited, pp. 1–18 (cit. on p. 35).

Gajardo, Abraham I J, Samuel Madariaga, and Pedro E Maldonado (2019). *Autonomic nervous system assessment by pupillary response as a potential biomarker for cardiovascular risk: A pilot study.* Pages: 41–46 Publication Title: Journal of Clinical Neuroscience Volume: 59 (cit. on p. 15).

Gallo, Francisco T, Cynthia Katche, Juan F Morici, Jorge H Medina, and Noelia V Weisstaub (Apr. 2018). "Immediate Early Genes, Memory and Psychiatric Disorders: Focus on c-Fos, Egr1 and Arc". en. In: *Front. Behav. Neurosci.* 12, p. 79 (cit. on p. 71).

Ganea, Dan Alin, Alexander Bexter, Mathias Günther, Pierre-Marie Gardères, Björn M Kampa, and Florent Haiss (Sept. 2020). "Pupillary Dilations of Mice Performing a Vibrotactile Discrimination Task Reflect Task Engagement and Response Confidence". en. In: *Front. Behav. Neurosci.* 14, pp. 1–14 (cit. on p. 36).

Gee, Jan Willem de, Olympia Colizoli, Niels A Kloosterman, Tomas Knapen, Sander Nieuwenhuis, and Tobias H Donner (Apr. 2017). "Dynamic modulation of decision biases by brainstem arousal systems". en. In: *Elife* 6 (cit. on p. 6).

Gee, Jan Willem de, Tomas Knapen, and Tobias H Donner (Feb. 2014). "Decision-related pupil dilation reflects upcoming choice and individual bias". en. In: *Proc. Natl. Acad. Sci. U. S. A.* 111.5, E618–25 (cit. on p. 6).

Gee, Jan Willem de, Konstantinos Tsetsos, Lars Schwabe, Anne E Urai, David McCormick, Matthew J McGinley, and Tobias H Donner (June 2020). "Pupil-linked phasic arousal predicts a reduction of choice bias across species and decision domains". en. In: *Elife* 9, pp. 1–25 (cit. on p. 36).

Geissler, Julia, Marcel Romanos, Ulrich Hegerl, and Tilman Hensch (Sept. 2014). "Hyperactivity and sensation seeking as autoregulatory attempts to stabilize brain arousal in ADHD and mania?" en. In: *Atten. Defic. Hyperact. Disord.* 6.3, pp. 159–173 (cit. on p. 35).

Giustino, Thomas F and Stephen Maren (Mar. 2018). "Noradrenergic Modulation of Fear Conditioning and Extinction". en. In: *Front. Behav. Neurosci.* 12, p. 43 (cit. on pp. 10, 11, 70, 81).

Gogolla, Nadine, Pico Caroni, Andreas Lüthi, and Cyril Herry (Sept. 2009). "Perineuronal nets protect fear memories from erasure". en. In: *Science* 325.5945, pp. 1258–1261 (cit. on pp. 53, 54, 70, 71).

Golovin, Randall M and Nicholas J Ward (July 2016). "Neuromodulatory influence of norepinephrine during developmental experience-dependent plasticity". en. In: *J. Neurophysiol.* 116.1, pp. 1–4 (cit. on p. 12).

Gompf, Heinrich S, Christine Mathai, Patrick M Fuller, David A Wood, Nigel P Pedersen, Clifford B Saper, and Jun Lu (Oct. 2010). "Locus ceruleus and anterior cingulate cortex sustain wakefulness in a novel environment". en. In: *J. Neurosci.* 30.43, pp. 14543–14551 (cit. on p. 6).

Granholm, Eric and Stuart R Steinhauer (Mar. 2004). "Pupillometric measures of cognitive and emotional processes". en. In: *Int. J. Psychophysiol.* 52.1, pp. 1–6 (cit. on p. 1).

Gu, Hongcang, Zachary D Smith, Christoph Bock, Patrick Boyle, Andreas Gnirke, and Alexander Meissner (Apr. 2011). "Preparation of reduced representation bisulfite sequencing libraries for genome-scale DNA methylation profiling". en. In: *Nat. Protoc.* 6.4, pp. 468–481 (cit. on pp. 85, 89).

Gulmez Karaca, Kubra, Janina Kupke, David V C Brito, Benjamin Zeuch, Christian Thome, Dieter Weichenhan, Pavlo Lutsik, Christoph Plass, and Ana M M Oliveira (Jan. 2020). "Neuronal ensemble-specific DNA methylation strengthens engram stability". en. In: *Nat. Commun.* 11.1, p. 639 (cit. on p. 97).

Guruharsha, K G, Mark W Kankel, and Spyros Artavanis-Tsakonas (Sept. 2012). "The Notch signalling system: recent insights into the complexity of a conserved pathway". en. In: *Nat. Rev. Genet.* 13.9, pp. 654–666 (cit. on p. 97).

Gustafson, Eric L and Robert Y Moore (Dec. 1987). "Noradrenaline neuron plasticity in developing rat brain: effects of neonatal 6-hydroxydopamine demonstrated by dopamine-β-hydroxylase immunocytochemistry". In: *Developmental Brain Research* 37.1, pp. 143–155 (cit. on p. 12).

Hamm, A O and R Stark (Apr. 1993). "Sensitization and aversive conditioning: effects on the startle reflex and electrodermal responding". en. In: *Integr. Physiol. Behav. Sci.* 28.2, pp. 171–176 (cit. on p. 70).

Hamm, A O and D Vaitl (Nov. 1996). "Affective learning: awareness and aversion". en. In: *Psychophysiology* 33.6, pp. 698–710 (cit. on p. 10).

Hamm, Alfons O, Mark K Greenwald, Margaret M Bradley, Bruce N Cuthbert, and Peter J Lang (Apr. 1991). "The fear potentiated startle effect". In: *Integr. Physiol. Behav. Sci.* 26.2, pp. 119–126 (cit. on p. 10).

Harris, N S, E Courchesne, J Townsend, R A Carper, and C Lord (May 1999). "Neuroanatomic contributions to slowed orienting of attention in children with autism". en. In: *Brain Res. Cogn. Brain Res.* 8.1, pp. 61–71 (cit. on p. 41).

Harrison, Neil A, C Ellie Wilson, and Hugo D Critchley (Nov. 2007). "Processing of observed pupil size modulates perception of sadness and predicts empathy". en. In: *Emotion* 7.4, pp. 724–729 (cit. on pp. 1, 4).

Hastie, Trevor, Robert Tibshirani, and Jerome Friedman (Nov. 2013). *The Elements of Statistical Learning: Data Mining, Inference, and Prediction*. en. LLC, 233 Spring Street, New York, NY 10013, USA: Springer Science & Business Media (cit. on p. 51).

Hattar, S., H. W. Liao, M. Takao, D. M. Berson, and K. W. Yau (Feb. 2002). "Melanopsin-containing retinal ganglion cells: architecture, projections, and intrinsic photosensitivity". eng. In: *Science (New York, N.Y.)* 295.5557, pp. 1065–1070. ISSN: 1095-9203. DOI: 10.1126/science.1069609 (cit. on p. 4).

Hayden, Benjamin Y, Sarah R Heilbronner, John M Pearson, and Michael L Platt (Mar. 2011). "Surprise signals in anterior cingulate cortex: neuronal encoding of unsigned reward prediction errors driving adjustment in behavior". en. In: *J. Neurosci.* 31.11, pp. 4178–4187 (cit. on p. 6).

Hayes, Taylor R and Alexander A Petrov (June 2016). "Mapping and correcting the influence of gaze position on pupil size measurements". en. In: *Behav. Res. Methods* 48.2, pp. 510–527 (cit. on pp. 21, 25).

He, Kaiming, Xiangyu Zhang, Shaoqing Ren, and Jian Sun (2016). *Identity Mappings in Deep Residual Networks*. Pages: 630–645 Publication Title: Computer Vision – ECCV 2016 (cit. on p. 27).

Hebb, D O (1955). *Drives and the C. N. S. (conceptual nervous system)*. Issue: 4 Pages: 243–254 Publication Title: Psychological Review Volume: 62 (cit. on p. 35).

Herlenius, Eric and Hugo Lagercrantz (Nov. 2004). "Development of neurotransmitter systems during critical periods". en. In: *Exp. Neurol.* 190 Suppl 1, S8–21 (cit. on p. 12).

Herry, Cyril, Stephane Ciocchi, Verena Senn, Lynda Demmou, Christian Müller, and Andreas Lüthi (July 2008). "Switching on and off fear by distinct neuronal circuits". en. In: *Nature* 454.7204, pp. 600–606 (cit. on pp. 54, 62).

Herry, Cyril and Nicole Mons (Aug. 2004). "Resistance to extinction is associated with impaired immediate early gene induction in medial prefrontal cortex and amygdala". en. In: *Eur. J. Neurosci.* 20.3, pp. 781–790 (cit. on p. 71).

Hersman, Sarah, David Allen, Mariko Hashimoto, Salvador Ignacio Brito, and Todd E Anthony (Mar. 2020). "Stimulus salience determines defensive behaviors elicited by aversively conditioned serial compound auditory stimuli". en. In: *Elife* 9 (cit. on p. 18).

Hinton, Geoffrey E (1989). "Connectionist Learning Procedures". en. In: *Artificial Intelligence 1989* 40, pp. 185–234 (cit. on p. 51).

Hoeks, Bert and Willem J M Levelt (Mar. 1993). "Pupillary dilation as a measure of attention: a quantitative system analysis". In: *Behav. Res. Methods Instrum. Comput.* 25.1, pp. 16–26 (cit. on pp. 1, 4).

Hollander, Gilles de, Eline R Kupers, Jan W Brascamp, and Tomas H Knapen (2018). "A biphasic temporal pattern in pupil size around perceptual switches in binocular rivalry".

In: *2018 Conference on Cognitive Computational Neuroscience*. event-place: Philadelphia, Pennsylvania, USA. Brentwood, Tennessee, USA: Cognitive Computational Neuroscience (cit. on p. 9).

Hopkins, Lauren S., Douglas H. Schultz, Deborah E. Hannula, and Fred J. Helmstetter (Nov. 2015). "Eye Movements Index Implicit Memory Expression in Fear Conditioning". In: *PLoS ONE* 10.11, e0141949. ISSN: 1932-6203. DOI: 10.1371/journal.pone.0141949 (cit. on p. 10).

Hourdaki, Eugenia, Stella G. Giakoumaki, Vangelis Grinakis, Katerina Theou, Maria Karataraki, and Panos Bitsios (July 2005). "Parametric exploration of the fear-inhibited light reflex". eng. In: *Psychophysiology* 42.4, pp. 447–455. ISSN: 0048-5772. DOI: 10.1111/j.1469-8986.2005.00301.x (cit. on p. 10).

Howard, Andrew, Mark Sandler, Bo Chen, Weijun Wang, Liang-Chieh Chen, Mingxing Tan, Grace Chu, Vijay Vasudevan, Yukun Zhu, Ruoming Pang, Hartwig Adam, and Quoc Le (2019). *Searching for MobileNetV3*. Publication Title: 2019 IEEE/CVF International Conference on Computer Vision (ICCV) (cit. on p. 27).

Huang, Kang, Qin Yang, Yaning Han, Yulin Zhang, Zhiyi Wang, Liping Wang, and Pengfei Wei (June 2022). "An Easily Compatible Eye-tracking System for Freely-moving Small Animals". en. In: *Neurosci. Bull.* 38.6, pp. 661–676 (cit. on p. 13).

Hugues, S, A Chessel, I Lena, R Marsault, and R Garcia (2006). "Prefrontal infusion of PD098059 immediately after fear extinction training blocks extinction-associated prefrontal synaptic plasticity and decreases prefrontal ERK2 ..." In: *Synapse*. Publisher: Wiley Online Library (cit. on p. 71).

Hurst, Jane L and Rebecca S West (Oct. 2010). "Taming anxiety in laboratory mice". en. In: *Nat. Methods* 7.10, pp. 825–826 (cit. on p. 73).

Iadanza, Ernesto, Francesco Goretti, Michele Sorelli, Paolo Melillo, Leandro Pecchia, Francesca Simonelli, and Monica Gherardelli (2020). "Automatic Detection of Genetic Diseases in Pediatric Age Using Pupillometry". In: *IEEE Access* 8, pp. 34949–34961 (cit. on pp. 11, 15, 80).

Inukai, Sachi, Alexandre de Lencastre, Michael Turner, and Frank Slack (July 2012). "Novel microRNAs differentially expressed during aging in the mouse brain". en. In: *PLoS One* 7.7, e40028 (cit. on p. 96).

Jentsch, Valerie L, Oliver T Wolf, and Christian J Merz (Jan. 2020). "Temporal dynamics of conditioned skin conductance and pupillary responses during fear acquisition and extinction". en. In: *Int. J. Psychophysiol.* 147, pp. 93–99 (cit. on p. 10).

Jepma, Marieke and Sander Nieuwenhuis (July 2011). "Pupil Diameter Predicts Changes in the Exploration–Exploitation Trade-off: Evidence for the Adaptive Gain Theory". In: *Journal of Cognitive Neuroscience* 23.7, pp. 1587–1596. ISSN: 0898-929X. DOI: 10.1162/jocn.2010.21548 (cit. on p. 7).

Jhang, Cian-Ling, Tzyy-Nan Huang, Yi-Ping Hsueh, and Wenlin Liao (Oct. 2017). "Mice lacking cyclin-dependent kinase-like 5 manifest autistic and ADHD-like behaviors". en. In: *Hum. Mol. Genet.* 26.20, pp. 3922–3934 (cit. on pp. 35, 46, 80).

Jhang, Cian-Ling, Hom-Yi Lee, Jin-Chung Chen, and Wenlin Liao (Aug. 2020). "Dopaminergic loss of cyclin-dependent kinase-like 5 recapitulates methylphenidate-remediable hyperlocomotion in mouse model of CDKL5 deficiency disorder". en. In: *Hum. Mol. Genet.* 29.14, pp. 2408–2419 (cit. on pp. 35, 46, 80).

Jones, F Nowell (1939). "The behavior of organisms: an experimental analysis". In: *The American Journal of Psychology* 52.4. Publisher: JSTOR, pp. 659–660 (cit. on p. 36).

Jones, P A (Jan. 1999). "The DNA methylation paradox". en. In: *Trends Genet.* 15.1, pp. 34–37 (cit. on p. 97).

Jones, Peter A (May 2012). "Functions of DNA methylation: islands, start sites, gene bodies and beyond". en. In: *Nat. Rev. Genet.* 13.7, pp. 484–492 (cit. on p. 97).

Jordan, Rebecca and Georg B. Keller (May 2023). "The locus coeruleus broadcasts prediction errors across the cortex to promote sensorimotor plasticity". en. In: *eLife* 12. Publisher: eLife Sciences Publications Limited. DOI: 10.7554/eLife.85111 (cit. on pp. 9, 10).

Joshi, Siddhartha, Yin Li, Rishi M Kalwani, and Joshua I Gold (Jan. 2016). "Relationships between Pupil Diameter and Neuronal Activity in the Locus Coeruleus, Colliculi, and Cingulate Cortex". en. In: *Neuron* 89.1, pp. 221–234 (cit. on pp. 6, 7, 9, 36).

Jung, Marc and Gerd P Pfeifer (Jan. 2015). "Aging and DNA methylation". en. In: *BMC Biol.* 13, p. 7 (cit. on p. 97).

Kahneman, Daniel and Jackson Beatty (1966). *Pupil Diameter and Load on Memory*. Issue: 3756 Pages: 1583–1585 Publication Title: Science Volume: 154 (cit. on pp. 1, 6).

Kaifosh, Patrick, Matthew Lovett-Barron, Gergely F Turi, Thomas R Reardon, and Attila Losonczy (Sept. 2013). "Septo-hippocampal GABAergic signaling across multiple modalities in awake mice". en. In: *Nat. Neurosci.* 16.9, pp. 1182–1184 (cit. on pp. 11, 81).

Kasamatsu, T and J D Pettigrew (Oct. 1976). "Depletion of brain catecholamines: failure of ocular dominance shift after monocular occlusion in kittens". en. In: *Science* 194.4261, pp. 206–209 (cit. on p. 9).

— (1979). "Preservation of binocularity after monocular deprivation in the striate cortex of kittens treated with 6-hydroxydopamine". In: *J. Comp. Neurol.* Publisher: Wiley Online Library (cit. on p. 9).

Kasamatsu, T, J D Pettigrew, and M Ary (Feb. 1981). "Cortical recovery from effects of monocular deprivation: acceleration with norepinephrine and suppression with 6-hydroxydopamine". en. In: *J. Neurophysiol.* 45.2, pp. 254–266 (cit. on p. 9).

Khvorova, Anastasia and Jonathan K Watts (Mar. 2017). "The chemical evolution of oligonucleotide therapies of clinical utility". en. In: *Nat. Biotechnol.* 35.3, pp. 238–248 (cit. on p. 87).

Kim, Jee Hyun, Adam S Hamlin, and Rick Richardson (Sept. 2009). "Fear extinction across development: the involvement of the medial prefrontal cortex as assessed by temporary inactivation and immunohistochemistry". en. In: *J. Neurosci.* 29.35, pp. 10802–10808 (cit. on p. 54).

Kim, Jee Hyun and Rick Richardson (July 2007). "A developmental dissociation in reinstatement of an extinguished fear response in rats". en. In: *Neurobiol. Learn. Mem.* 88.1, pp. 48–57 (cit. on p. 54).

Kluckova, Daniela, Miriam Kolnikova, Veronika Medova, Csaba Bognar, Tomas Foltan, Lucia Svecova, Andrej Gnip, Ludevit Kadasi, Andrea Soltysova, and Andrej Ficek (Oct. 2021). "Clinical manifestation of CDKL5 deficiency disorder and identified mutations in a cohort of Slovak patients". en. In: *Epilepsy Res.* 176, p. 106699 (cit. on p. 37).

Kole, Adam J, Vijay Swahari, Scott M Hammond, and Mohanish Deshmukh (Jan. 2011). "miR-29b is activated during neuronal maturation and targets BH3-only genes to restrict apoptosis". en. In: *Genes Dev.* 25.2, pp. 125–130 (cit. on p. 96).

Kolk, Sharon M and Pasko Rakic (Jan. 2022). "Development of prefrontal cortex". en. In: *Neuropsychopharmacology* 47.1, pp. 41–57 (cit. on p. 12).

Korn, Christoph W, Matthias Staib, Athina Tzovara, Giuseppe Castegnetti, and Dominik R Bach (Mar. 2017). "A pupil size response model to assess fear learning". en. In: *Psychophysiology* 54.3, pp. 330–343 (cit. on pp. 1, 4, 54, 70).

Koss, M C (Feb. 1986). "Pupillary dilation as an index of central nervous system alpha 2-adrenoceptor activation". en. In: *J. Pharmacol. Methods* 15.1, pp. 1–19 (cit. on p. 6).

Koss, Michael C., Tseggai Gherezghiher, and Akikazu Nomura (Mar. 1984). "CNS adrenergic inhibition of parasympathetic oculomotor tone". In: *Journal of the Autonomic Nervous System* 10.1, pp. 55–68. ISSN: 0165-1838. DOI: 10.1016/0165-1838(84)90067-5 (cit. on p. 9).

Krebs, Ruth M, Haeme R P Park, Klaas Bombeke, and Carsten N Boehler (Apr. 2018). "Modulation of locus coeruleus activity by novel oddball stimuli". en. In: *Brain Imaging Behav.* 12.2, pp. 577–584 (cit. on p. 15).

Krettek, J E and J L Price (Mar. 1978). "Amygdaloid projections to subcortical structures within the basal forebrain and brainstem in the rat and cat". en. In: *J. Comp. Neurol.* 178.2, pp. 225–254 (cit. on p. 71).

Kuc, Christopher, Daniel J Richard, Samantha Johnson, Leslie Bragg, Mark R Servos, Andrew C Doxey, and Paul M Craig (Dec. 2017). "Rainbow trout exposed to benzo[a]pyrene yields conserved microRNA binding sites in DNA methyltransferases across 500 million years of evolution". en. In: *Sci. Rep.* 7.1, p. 16843 (cit. on p. 87).

Kucewicz, Michal T, Jaromir Dolezal, Vaclav Kremen, Brent M Berry, Laura R Miller, Abigail L Magee, Vratislav Fabian, and Gregory A Worrell (Mar. 2018). "Pupil size reflects successful encoding and recall of memory in humans". en. In: *Sci. Rep.* 8.1, p. 4949 (cit. on p. 47).

Lähdesmäki, J, J Sallinen, E MacDonald, B K Kobilka, V Fagerholm, and M Scheinin (Aug. 2002). "Behavioral and neurochemical characterization of α2A-adrenergic receptor knockout mice". In: *Neuroscience* 113.2, pp. 289–299 (cit. on p. 12).

Larsen, Rylan S and Jack Waters (2018). *Neuromodulatory Correlates of Pupil Dilation*. Publication Title: Frontiers in Neural Circuits Volume: 12 (cit. on pp. 7, 80).

Lauder, Jean M and Floyd E Bloom (1974). *Ontogeny of monoamine neurons in the locus coeruleus, raphe nuclei and substantia nigra of the rat. I. Cell differentiation*. Issue: 4 Pages: 469–481 Publication Title: The Journal of Comparative Neurology Volume: 155 (cit. on p. 12).

Laurent, Vincent and R Frederick Westbrook (Sept. 2009). "Inactivation of the infralimbic but not the prelimbic cortex impairs consolidation and retrieval of fear extinction". en. In: *Learn. Mem.* 16.9, pp. 520–529 (cit. on p. 71).

Lavie, P (1989). "Ultradian rhythms in arousal–the problem of masking". en. In: *Chronobiol. Int.* 6.1, pp. 21–28 (cit. on p. 35).

LeDoux, J E (2000). "Emotion circuits in the brain". en. In: *Annu. Rev. Neurosci.* 23, pp. 155–184 (cit. on p. 53).

LeDoux, Joseph E (Feb. 2014). "Coming to terms with fear". en. In: *Proc. Natl. Acad. Sci. U. S. A.* 111.8, pp. 2871–2878 (cit. on p. 54).

Lee, Christian R and David J Margolis (Nov. 2016). "Pupil Dynamics Reflect Behavioral Choice and Learning in a Go/NoGo Tactile Decision-Making Task in Mice". en. In: *Front. Behav. Neurosci.* 10, p. 200 (cit. on pp. 9, 15, 36).

Lee, Tae-Ho, Jongsoo Baek, Zhong-Lin Lu, and Mara Mather (Oct. 2014). "How arousal modulates the visual contrast sensitivity function". en. In: *Emotion* 14.5, pp. 978–984 (cit. on p. 47).

Leeuw, Joshua R de (Mar. 2015). "jsPsych: a JavaScript library for creating behavioral experiments in a Web browser". en. In: *Behav. Res. Methods* 47.1, pp. 1–12 (cit. on p. 80).

Leitner, Yael (Apr. 2014). "The co-occurrence of autism and attention deficit hyperactivity disorder in children - what do we know?" en. In: *Front. Hum. Neurosci.* 8, p. 268 (cit. on p. 46).

Leknes, Siri, Johan Wessberg, Dan-Mikael Ellingsen, Olga Chelnokova, Håkan Olausson, and Bruno Laeng (Oct. 2013). "Oxytocin enhances pupil dilation and sensitivity to 'hidden' emotional expressions". en. In: *Soc. Cogn. Affect. Neurosci.* 8.7. Publisher: Oxford University Press, p. 741 (cit. on p. 6).

Leuchs, Laura, Max Schneider, Michael Czisch, and Victor I Spoormaker (Feb. 2017). "Neural correlates of pupil dilation during human fear learning". en. In: *Neuroimage* 147, pp. 186–197 (cit. on pp. 1, 4, 54, 70).

Leuchs, Laura, Max Schneider, and Victor I Spoormaker (Jan. 2019). "Measuring the conditioned response: A comparison of pupillometry, skin conductance, and startle electromyography". en. In: *Psychophysiology* 56.1, e13283 (cit. on pp. 10, 54, 56, 70, 81).

Levenson, Jonathan M, Tania L Roth, Farah D Lubin, Courtney A Miller, I-Chia Huang, Priyanka Desai, Lauren M Malone, and J David Sweatt (June 2006). "Evidence that DNA (cytosine-5) methyltransferase regulates synaptic plasticity in the hippocampus". en. In: *J. Biol. Chem.* 281.23, pp. 15763–15773 (cit. on p. 85).

Li, Haohong, Mario A Penzo, Hiroki Taniguchi, Charles D Kopec, Z Josh Huang, and Bo Li (Mar. 2013). "Experience-dependent modification of a central amygdala fear circuit". en. In: *Nat. Neurosci.* 16.3, pp. 332–339 (cit. on p. 71).

Li, Zhong, Jin-Xing Wei, Guang-Wei Zhang, Junxiang J Huang, Brian Zingg, Xiyue Wang, Huizhong W Tao, and Li I Zhang (Feb. 2021). "Corticostriatal control of defense behavior in mice induced by auditory looming cues". en. In: *Nat. Commun.* 12.1, p. 1040 (cit. on p. 18).

Liang, Jao-Shwann, Hsin Huang, Jinn-Shyan Wang, and Jyh-Feng Lu (Oct. 2019). "Phenotypic manifestations between male and female children with CDKL5 mutations". en. In: *Brain Dev.* 41.9, pp. 783–789 (cit. on p. 37).

Liao, Hsin-I, Makoto Yoneya, Shunsuke Kidani, Makio Kashino, and Shigeto Furukawa (Feb. 2016). "Human Pupillary Dilation Response to Deviant Auditory Stimuli: Effects of Stimulus Properties and Voluntary Attention". en. In: *Front. Neurosci.* 10, p. 43 (cit. on pp. 16, 21).

Lippi, Giordano, Catarina C Fernandes, Laura A Ewell, Danielle John, Benedetto Romoli, Giulia Curia, Seth R Taylor, E Paxon Frady, Anne B Jensen, Jerry C Liu, Melanie M Chaabane, Cherine Belal, Jason L Nathanson, Michele Zoli, Jill K Leutgeb, Giuseppe Biagini, Gene W Yeo, and Darwin K Berg (Dec. 2016). "MicroRNA-101 Regulates Multiple Developmental Programs to Constrain Excitation in Adult Neural Networks". en. In: *Neuron* 92.6, pp. 1337–1351 (cit. on p. 85).

Lonergan, Mary E, Georgette M Gafford, Timothy J Jarome, and Fred J Helmstetter (May 2010). "Time-dependent expression of Arc and zif268 after acquisition of fear conditioning". en. In: *Neural Plast.* 2010, p. 139891 (cit. on p. 77).

LoTemplio, S, J Silcox, K D Federmeier, and B R Payne (Dec. 2020). "Inter- and intra-individual coupling between pupillary, electrophysiological, and behavioral responses in a visual oddball task". In: *Psychophysiology*. Publisher: Psychophysiology (cit. on p. 16).

Lovell, Kathryn L (1982). *Effects of 6-Hydroxydopamine-Induced Norepinephrine Depletion on Cerebellar Development*. Issue: 4 Pages: 359–368 Publication Title: Developmental Neuroscience Volume: 5 (cit. on p. 12).

Lovett-Barron, Matthew, Patrick Kaifosh, Mazen A Kheirbek, Nathan Danielson, Jeffrey D Zaremba, Thomas R Reardon, Gergely F Turi, René Hen, Boris V Zemelman, and Attila Losonczy (Feb. 2014). "Dendritic inhibition in the hippocampus supports fear learning". en. In: *Science* 343.6173, pp. 857–863 (cit. on pp. 11, 81).

Lubin, Farah D, Tania L Roth, and J David Sweatt (Oct. 2008). "Epigenetic regulation of BDNF gene transcription in the consolidation of fear memory". en. In: *J. Neurosci.* 28.42, pp. 10576–10586 (cit. on p. 85).

Luck, Camilla C and Ottmar V Lipp (Feb. 2016). "When orienting and anticipation dissociate–a case for scoring electrodermal responses in multiple latency windows in studies of human fear conditioning". en. In: *Int. J. Psychophysiol.* 100, pp. 36–43 (cit. on p. 10).

Lugli, Giovanni, Vetle I. Torvik, John Larson, and Neil R. Smalheiser (2008). "Expression of microRNAs and their precursors in synaptic fractions of adult mouse forebrain". In: *Journal of Neurochemistry* 106.2. _eprint: https://onlinelibrary.wiley.com/doi/pdf/10.1111/j.1471-4159.2008.05413.x, pp. 650–661. ISSN: 1471-4159. DOI: 10.1111/j.1471-4159.2008.05413.x (cit. on p. 85).

Lupori, Leonardo, Valentino Totaro, Sara Cornuti, Luca Ciampi, Fabio Carrara, Edda Grilli, Aurelia Viglione, Francesca Tozzi, Elena Putignano, Raffaele Mazziotti, Giuseppe Amato,

Claudio Gennaro, Paola Tognini, and Tommaso Pizzorusso (July 2023). "A comprehensive atlas of perineuronal net distribution and colocalization with parvalbumin in the adult mouse brain". en. In: *Cell Rep.* 42.7, p. 112788 (cit. on p. 82).

Lynn, R (Sept. 2013). *Attention, Arousal and the Orientation Reaction: International Series of Monographs in Experimental Psychology*. en. Radarweg 29, 1043 NX Amsterdam, The Netherlands: Elsevier (cit. on p. 35).

Maddox, Stephanie A, Casey S Watts, and Glenn E Schafe (Jan. 2014). "DNA methyltransferase activity is required for memory-related neural plasticity in the lateral amygdala". en. In: *Neurobiol. Learn. Mem.* 107, pp. 93–100 (cit. on p. 85).

Malkani, S and J B Rosen (2000). "Specific induction of early growth response gene 1 in the lateral nucleus of the amygdala following contextual fear conditioning in rats". en. In: *Neuroscience* 97.4, pp. 693–702 (cit. on p. 71).

Maren, S. (2001). "Neurobiology of Pavlovian fear conditioning". eng. In: *Annual Review of Neuroscience* 24, pp. 897–931. ISSN: 0147-006X. DOI: 10.1146/annurev.neuro.24.1.897 (cit. on pp. 10, 11).

Maren, Stephen and Gregory J Quirk (Nov. 2004). "Neuronal signalling of fear memory". en. In: *Nat. Rev. Neurosci.* 5.11, pp. 844–852 (cit. on p. 54).

Martella, Diana, Nerea Aldunate, Luis J Fuentes, and Noelia Sánchez-Pérez (Aug. 2020). "Arousal and Executive Alterations in Attention Deficit Hyperactivity Disorder (ADHD)". en. In: *Front. Psychol.* 11, p. 1991 (cit. on p. 35).

Marzo, Aude, Jing Bai, and Satoru Otani (Dec. 2009). "Neuroplasticity regulation by noradrenaline in mammalian brain". en. In: *Curr. Neuropharmacol.* 7.4, pp. 286–295 (cit. on p. 9).

Mathis, Alexander, Pranav Mamidanna, Kevin M Cury, Taiga Abe, Venkatesh N Murthy, Mackenzie Weygandt Mathis, and Matthias Bethge (Sept. 2018). "DeepLabCut: markerless pose estimation of user-defined body parts with deep learning". en. In: *Nat. Neurosci.* 21.9, pp. 1281–1289 (cit. on pp. 13, 25).

Mathôt, Sebastiaan (Feb. 2018). "Pupillometry: Psychology, Physiology, and Function". en. In: *J Cogn* 1.1, p. 16 (cit. on pp. 1, 4, 81).

Mathôt, Sebastiaan, Jonathan Grainger, and Kristof Strijkers (Aug. 2017). "Pupillary Responses to Words That Convey a Sense of Brightness or Darkness". en. In: *Psychol. Sci.* 28.8, pp. 1116–1124 (cit. on p. 1).

Mathôt, Sebastiaan, Jean-Baptiste Melmi, Lotje van der Linden, and Stefan Van der Stigchel (2016). "The mind-writing pupil: A human-computer interface based on decoding of covert attention through pupillometry". In: DOI: https://doi.org/10.1371/journal.pone.0148805 (cit. on p. 15).

Mathôt, Sebastiaan and Stefan Van der Stigchel (Oct. 2015). "New Light on the Mind's Eye: The Pupillary Light Response as Active Vision". en. In: *Curr. Dir. Psychol. Sci.* 24.5, pp. 374–378 (cit. on p. 1).

Matsumoto, Madoka, Kenji Matsumoto, Hiroshi Abe, and Keiji Tanaka (May 2007). "Medial prefrontal cell activity signaling prediction errors of action values". en. In: *Nature Neuroscience* 10.5. Number: 5 Publisher: Nature Publishing Group, pp. 647–656. ISSN: 1546-1726. DOI: 10.1038/nn1890 (cit. on p. 7).

Mattapallil, Mary J, Eric F Wawrousek, Chi-Chao Chan, Hui Zhao, Jayeeta Roychoudhury, Thomas A Ferguson, and Rachel R Caspi (May 2012). "The Rd8 mutation of the Crb1 gene is present in vendor lines of C57BL/6N mice and embryonic stem cells, and confounds ocular induced mutant phenotypes". en. In: *Invest. Ophthalmol. Vis. Sci.* 53.6, pp. 2921–2927 (cit. on p. 49).

Mazziotti, Raffaele, Laura Baroncelli, Nicholas Ceglia, Gabriele Chelini, Grazia Della Sala, Christophe Magnan, Debora Napoli, Elena Putignano, Davide Silingardi, Jonida Tola, Paola Tognini, J Simon C Arthur, Pierre Baldi, and Tommaso Pizzorusso (May 2017a). "Mir-

132/212 is required for maturation of binocular matching of orientation preference and depth perception". en. In: *Nat. Commun.* 8, p. 15488 (cit. on pp. 3, 85, 96).

Mazziotti, Raffaele, Fabio Carrara, Aurelia Viglione, Leonardo Lupori, Luca Lo Verde, Alessandro Benedetto, Giulia Ricci, Giulia Sagona, Giuseppe Amato, and Tommaso Pizzorusso (2021). "MEYE: Web App for Translational and Real-Time Pupillometry". In: *eneuro* 8.5, pp. 1–13 (cit. on pp. 36, 40, 48, 50, 56, 75).

Mazziotti, Raffaele, Leonardo Lupori, Giulia Sagona, Mariangela Gennaro, Grazia Della Sala, Elena Putignano, and Tommaso Pizzorusso (June 2017b). "Searching for biomarkers of CDKL5 disorder: early-onset visual impairment in CDKL5 mutant mice". en. In: *Hum. Mol. Genet.* 26.12, pp. 2290–2298 (cit. on pp. 36, 47).

Mazziotti, Raffaele, Giulia Sagona, Leonardo Lupori, Virginia Martini, and Tommaso Pizzorusso (Apr. 2020). "3D Printable Device for Automated Operant Conditioning in the Mouse". en. In: *eNeuro* 7.2, pp. 1–9 (cit. on pp. 36, 46, 49).

McDonald, A J (July 1982). "Cytoarchitecture of the central amygdaloid nucleus of the rat". en. In: *J. Comp. Neurol.* 208.4, pp. 401–418 (cit. on p. 71).

McGinley, Matthew J, Stephen V David, and David A McCormick (July 2015a). "Cortical Membrane Potential Signature of Optimal States for Sensory Signal Detection". en. In: *Neuron* 87.1, pp. 179–192 (cit. on p. 35).

McGinley, Matthew J, Martin Vinck, Jacob Reimer, Renata Batista-Brito, Edward Zagha, Cathryn R Cadwell, Andreas S Tolias, Jessica A Cardin, and David A McCormick (Sept. 2015b). "Waking State: Rapid Variations Modulate Neural and Behavioral Responses". en. In: *Neuron* 87.6, pp. 1143–1161 (cit. on p. 15).

Megemont, Marine, Jim McBurney-Lin, and Hongdian Yang (Feb. 2022). "Pupil diameter is not an accurate real-time readout of locus coeruleus activity". en. In: *Elife* 11 (cit. on p. 6).

Mei, Zhen, Jiaqi Liu, Jason P Schroeder, David Weinshenker, Duc M Duong, Nicholas T Seyfried, Yujing Li, Peng Jin, Aliza P Wingo, and Thomas S Wingo (Aug. 2023). "Lowering hippocampal miR-29a expression slows cognitive decline and reduces beta-amyloid deposition in 5xFAD mice". en. In: *Res Sq* (cit. on pp. 92, 96).

Meissner, Alexander, Andreas Gnirke, George W Bell, Bernard Ramsahoye, Eric S Lander, and Rudolf Jaenisch (Oct. 2005). "Reduced representation bisulfite sequencing for comparative high-resolution DNA methylation analysis". en. In: *Nucleic Acids Res.* 33.18, pp. 5868–5877 (cit. on p. 89).

Merz, Christian Josef, Tanja Christina Hamacher-Dang, Rudolf Stark, Oliver Tobias Wolf, and Andrea Hermann (Jan. 2018). "Neural Underpinnings of Cortisol Effects on Fear Extinction". en. In: *Neuropsychopharmacology* 43.2, pp. 384–392 (cit. on pp. 54, 71).

Micieli, G., C. Tassorelli, E. Martignoni, C. Pacchetti, P. Bruggi, M. Magri, and G. Nappi (Mar. 1991). "Disordered pupil reactivity in Parkinson's disease". eng. In: *Clinical Autonomic Research: Official Journal of the Clinical Autonomic Research Society* 1.1, pp. 55–58. ISSN: 0959-9851. DOI: 10.1007/BF01826058 (cit. on pp. 7, 80).

Milad, Mohammed R and Gregory J Quirk (Nov. 2002). "Neurons in medial prefrontal cortex signal memory for fear extinction". en. In: *Nature* 420.6911, pp. 70–74 (cit. on pp. 54, 63).

Miller, Courtney A, Cristin F Gavin, Jason A White, R Ryley Parrish, Avinash Honasoge, Christopher R Yancey, Ivonne M Rivera, María D Rubio, Gavin Rumbaugh, and J David Sweatt (June 2010). "Cortical DNA methylation maintains remote memory". en. In: *Nat. Neurosci.* 13.6, pp. 664–666 (cit. on p. 85).

Miller, Courtney A and J David Sweatt (Mar. 2007). "Covalent modification of DNA regulates memory formation". en. In: *Neuron* 53.6, pp. 857–869 (cit. on p. 85).

Minichiello, L, M Korte, D Wolfer, R Kühn, K Unsicker, V Cestari, C Rossi-Arnaud, H P Lipp, T Bonhoeffer, and R Klein (Oct. 1999). "Essential role for TrkB receptors in hippocampus-mediated learning". en. In: *Neuron* 24.2, pp. 401–414 (cit. on p. 97).

Do-Monte, Fabricio H, Kelvin Quiñones-Laracuente, and Gregory J Quirk (Mar. 2015). "A temporal shift in the circuits mediating retrieval of fear memory". en. In: *Nature* 519.7544, pp. 460–463 (cit. on pp. 63, 72).

Montes-Lourido, Pilar, Manaswini Kar, Isha Kumbam, and Srivatsun Sadagopan (Feb. 2021). "Pupillometry as a reliable metric of auditory detection and discrimination across diverse stimulus paradigms in animal models". en. In: *Sci. Rep.* 11.1, p. 3108 (cit. on pp. 15, 18, 35).

Morellini, Fabio, Elena Sivukhina, Luminita Stoenica, Elena Oulianova, Olena Bukalo, Igor Jakovcevski, Alexander Dityatev, Andrey Irintchev, and Melitta Schachner (Nov. 2010). "Improved reversal learning and working memory and enhanced reactivity to novelty in mice with enhanced GABAergic innervation in the dentate gyrus". en. In: *Cereb. Cortex* 20.11, pp. 2712–2727 (cit. on p. 72).

Morita, Sumiyo, Takuro Horii, Mika Kimura, Takahiro Ochiya, Shoji Tajima, and Izuho Hatada (July 2013). "miR-29 represses the activities of DNA methyltransferases and DNA demethylases". en. In: *Int. J. Mol. Sci.* 14.7, pp. 14647–14658 (cit. on p. 87).

Morrison, J H, M E Molliver, and R Grzanna (July 1979). "Noradrenergic innervation of cerebral cortex: widespread effects of local cortical lesions". en. In: *Science* 205.4403, pp. 313–316 (cit. on p. 5).

Moseley, Brian D, Radhika Dhamija, Elaine C Wirrell, and Katherine C Nickels (Feb. 2012). "Historic, clinical, and prognostic features of epileptic encephalopathies caused by CDKL5 mutations". en. In: *Pediatr. Neurol.* 46.2, pp. 101–105 (cit. on p. 35).

Mottolese, Nicola, Beatrice Uguagliati, Marianna Tassinari, Camilla Bruna Cerchier, Manuela Loi, Giulia Candini, Roberto Rimondini, Giorgio Medici, Stefania Trazzi, and Elisabetta Ciani (Sept. 2023). "Voluntary Running Improves Behavioral and Structural Abnormalities in a Mouse Model of CDKL5 Deficiency Disorder". en. In: *Biomolecules* 13.9 (cit. on p. 80).

Mouw, Janna K, Guanqing Ou, and Valerie M Weaver (Dec. 2014). "Extracellular matrix assembly: a multiscale deconstruction". en. In: *Nat. Rev. Mol. Cell Biol.* 15.12, pp. 771–785 (cit. on p. 54).

Mu, J S, W P Li, Z B Yao, and X F Zhou (July 1999). "Deprivation of endogenous brain-derived neurotrophic factor results in impairment of spatial learning and memory in adult rats". en. In: *Brain Res.* 835.2, pp. 259–265 (cit. on p. 97).

Muhammed, Kinan, Sanjay Manohar, Michael Ben Yehuda, Trevor T.-J. Chong, George Tofaris, Graham Lennox, Marko Bogdanovic, Michele Hu, and Masud Husain (Oct. 2016). "Reward sensitivity deficits modulated by dopamine are associated with apathy in Parkinson's disease". In: *Brain* 139.10, pp. 2706–2721. ISSN: 0006-8950. DOI: 10.1093/brain/aww188 (cit. on p. 7).

Murphy, Peter R, Redmond G O'Connell, Michael O'Sullivan, Ian H Robertson, and Joshua H Balsters (Aug. 2014). "Pupil diameter covaries with BOLD activity in human locus coeruleus". en. In: *Hum. Brain Mapp.* 35.8, pp. 4140–4154 (cit. on p. 6).

Myers, K M and M Davis (Feb. 2007). "Mechanisms of fear extinction". en. In: *Mol. Psychiatry* 12.2, pp. 120–150 (cit. on p. 53).

Nabel, Elisa M and Hirofumi Morishita (Nov. 2013). "Regulating critical period plasticity: insight from the visual system to fear circuitry for therapeutic interventions". en. In: *Front. Psychiatry* 4, p. 146 (cit. on p. 81).

Napoli, Debora, Leonardo Lupori, Raffaele Mazziotti, Giulia Sagona, Sara Bagnoli, Muntaha Samad, Erika Kelmer Sacramento, Joanna Kirkpartick, Elena Putignano, Siwei Chen, Eva Terzibasi Tozzini, Paola Tognini, Pierre Baldi, Jessica Cf Kwok, Alessandro Cellerino, and Tommaso Pizzorusso (Nov. 2020). "MiR-29 coordinates age-dependent plasticity brakes in the adult visual cortex". en. In: *EMBO Rep.* 21.11. Publisher: EMBO, e50431 (cit. on pp. 3, 85, 87, 96).

Narayanan, Nandakumar S and Mark Laubach (Feb. 2017). "Inhibitory Control: Mapping Medial Frontal Cortex". en. In: *Curr. Biol.* 27.4, R148–R150 (cit. on p. 46).

Nassar, Matthew R, Katherine M Rumsey, Robert C Wilson, Kinjan Parikh, Benjamin Heasly, and Joshua I Gold (June 2012). "Rational regulation of learning dynamics by pupil-linked arousal systems". en. In: *Nat. Neurosci.* 15.7, pp. 1040–1046 (cit. on pp. 1, 56).

Nelson, Anders and Richard Mooney (May 2016). "The Basal Forebrain and Motor Cortex Provide Convergent yet Distinct Movement-Related Inputs to the Auditory Cortex". en. In: *Neuron* 90.3, pp. 635–648. ISSN: 08966273. DOI: 10.1016/j.neuron.2016.03.031 (cit. on p. 7).

Neske, Garrett T, Dennis Nestvogel, Paul J Steffan, and David A McCormick (Dec. 2019). "Distinct Waking States for Strong Evoked Responses in Primary Visual Cortex and Optimal Visual Detection Performance". en. In: *J. Neurosci.* 39.50. Publisher: Society for Neuroscience, pp. 10044–10059 (cit. on p. 47).

Ney, Luke J, Matthew O'Donohue, Yi Wang, Mikaela Richardson, Adam Vasarhelyi, and Ottmar V Lipp (Oct. 2023). "The next frontier: Moving human fear conditioning research online". en. In: *Biol. Psychol.* 184, p. 108715 (cit. on pp. 79, 81).

Nieuwenhuis, Sander (2011). "Learning, the P3, and the locus coeruleus-norepinephrine system". In: *Neural basis of motivational and cognitive control*. Publisher: Oxford University Press Oxford, UK, pp. 209–222 (cit. on p. 7).

Nieuwenhuis, Sander, Eco J De Geus, and Gary Aston-Jones (2011). "The anatomical and functional relationship between the P3 and autonomic components of the orienting response". In: *Psychophysiology* 48.2, pp. 162–175 (cit. on pp. 6, 47).

Nitecka, L and Y Ben-Ari (Dec. 1987). "Distribution of GABA-like immunoreactivity in the rat amygdaloid complex". en. In: *J. Comp. Neurol.* 266.1. Publisher: Wiley, pp. 45–55 (cit. on p. 71).

Nowicka, Dorota, Susan Soulsby, Jolanta Skangiel-Kramska, and Stanislaw Glazewski (2009). *Parvalbumin-containing neurons, perineuronal nets and experience-dependent plasticity in murine barrel cortex*. Issue: 11 Pages: 2053–2063 Publication Title: European Journal of Neuroscience Volume: 30 (cit. on p. 71).

Nunn, Nicolas, Matthew Womack, Caroline Dart, and Richard Barrett-Jolley (June 2011). "Function and Pharmacology of Spinally-Projecting Sympathetic Pre-Autonomic Neurones in the Paraventricular Nucleus of the Hypothalamus". In: *Current Neuropharmacology* 9.2, pp. 262–277. ISSN: 1570-159X. DOI: 10.2174/157015911795596531 (cit. on p. 6).

Nyström, Pär, Teodora Gliga, Elisabeth Nilsson Jobs, Gustaf Gredebäck, Tony Charman, Mark H Johnson, Sven Bölte, and Terje Falck-Ytter (May 2018). "Enhanced pupillary light reflex in infancy is associated with autism diagnosis in toddlerhood". en. In: *Nat. Commun.* 9.1, p. 1678 (cit. on pp. 12, 15, 16, 80).

O'Leary, James D, Olivia F O'Leary, John F Cryan, and Yvonne M Nolan (Dec. 2018). "A low-cost touchscreen operant chamber using a Raspberry Pi™". en. In: *Behav. Res. Methods* 50.6, pp. 2523–2530 (cit. on p. 36).

Obinata, Hirofumi, Shoji Yokobori, Yasushi Shibata, Toru Takiguchi, Ryuta Nakae, Yutaka Igarashi, Kenta Shigeta, Hisashi Matsumoto, Venkatesh Aiyagari, Daiwai M Olson, and Hiroyuki Yokota (Sept. 2020). "Early automated infrared pupillometry is superior to auditory brainstem response in predicting neurological outcome after cardiac arrest". en. In: *Resuscitation* 154, pp. 77–84 (cit. on p. 15).

Oh, Angela J, Giulia Amore, William Sultan, Samuel Asanad, Jason C Park, Martina Romagnoli, Chiara La Morgia, Rustum Karanjia, Michael G Harrington, and Alfredo A Sadun (2019). *Pupillometry evaluation of melanopsin retinal ganglion cell function and sleep-wake activity in pre-symptomatic Alzheimer's disease*. Issue: 12 Pages: e0226197 Publication Title: PLOS ONE Volume: 14 (cit. on p. 15).

Oliveira, A M M, T J Hemstedt, H E Freitag, and H Bading (Aug. 2016). "Dnmt3a2: a hub for enhancing cognitive functions". en. In: *Mol. Psychiatry* 21.8, pp. 1130–1136 (cit. on p. 97).

Oliveira, Ana M M (Oct. 2016). "DNA methylation: a permissive mark in memory formation and maintenance". en. In: *Learn. Mem.* 23.10, pp. 587–593 (cit. on p. 96).

Oliveira, Ana M M, Thekla J Hemstedt, and Hilmar Bading (July 2012). "Rescue of aging-associated decline in Dnmt3a2 expression restores cognitive abilities". en. In: *Nat. Neurosci.* 15.8, pp. 1111–1113 (cit. on pp. 87, 92, 97).

Olivia, Carter, Stoll Josef, Chatelle Camille, Koch Christof, Laureys Steven, and Einhauser Wolfgang (2013). *The use of pupil dilation to communicate with locked-in syndrome patients.* Publication Title: Frontiers in Human Neuroscience Volume: 7 (cit. on p. 16).

Olson, Heather E, Scott T Demarest, Elia M Pestana-Knight, Lindsay C Swanson, Sumaiya Iqbal, Dennis Lal, Helen Leonard, J Helen Cross, Orrin Devinsky, and Tim A Benke (Aug. 2019). "Cyclin-Dependent Kinase-Like 5 Deficiency Disorder: Clinical Review". en. In: *Pediatr. Neurol.* 97, pp. 18–25 (cit. on p. 34).

Padoa-Schioppa, Camillo and Katherine E Conen (Nov. 2017). "Orbitofrontal Cortex: A Neural Circuit for Economic Decisions". en. In: *Neuron* 96.4, pp. 736–754 (cit. on p. 6).

Pan, Jasmine, Michaela Klímová, Joseph T McGuire, and Sam Ling (Jan. 2022). "Arousal-based pupil modulation is dictated by luminance". en. In: *Sci. Rep.* 12.1, p. 1390 (cit. on p. 36).

Park, Seonghun, Do-Won Kim, Chang-Hee Han, and Chang-Hwan Im (2021). "Estimation of Emotional Arousal Changes of a Group of Individuals During Movie Screening Using Steady-State Visual-Evoked Potential". en. In: *Front. Neuroinform.* 0. Publisher: Frontiers, pp. 1–10 (cit. on p. 35).

Pfeffer, Thomas, Christian Keitel, Daniel S Kluger, Anne Keitel, Alena Russmann, Gregor Thut, Tobias H Donner, and Joachim Gross (Feb. 2022). "Coupling of pupil- and neuronal population dynamics reveals diverse influences of arousal on cortical processing". en. In: *Elife* 11, pp. 1–28 (cit. on p. 35).

Phatak, Abhijeet, Aditya Chandra Mandal, Janarthanam Jothi Balaji, and Vasudevan Lakshminarayanan (May 2023). "Direct Estimation of Pupil Parameters Using Deep Learning for Visible Light Pupillometry". In: arXiv: 2305.06425 [eess.IV] (cit. on p. 80).

Piaggio, Davide, Georgy Namm, Paolo Melillo, Francesca Simonelli, Ernesto Iadanza, and Leandro Pecchia (July 2021). "Pupillometry via smartphone for low-resource settings". In: *Biocybernetics and Biomedical Engineering* 41.3, pp. 891–902 (cit. on p. 13).

Pineles, Suzanne L, Matthew R Orr, and Scott P Orr (Sept. 2009). "An alternative scoring method for skin conductance responding in a differential fear conditioning paradigm with a long-duration conditioned stimulus". en. In: *Psychophysiology* 46.5, pp. 984–995 (cit. on p. 10).

Pitkänen, A, L Stefanacci, C R Farb, G G Go, J E LeDoux, and D G Amaral (May 1995). "Intrinsic connections of the rat amygdaloid complex: projections originating in the lateral nucleus". en. In: *J. Comp. Neurol.* 356.2, pp. 288–310 (cit. on p. 71).

Pizzorusso, Tommaso, Paolo Medini, Nicoletta Berardi, Sabrina Chierzi, James W Fawcett, and Lamberto Maffei (Nov. 2002). "Reactivation of ocular dominance plasticity in the adult visual cortex". en. In: *Science* 298.5596, pp. 1248–1251 (cit. on p. 71).

Platt, John et al. (1999). "Probabilistic outputs for support vector machines and comparisons to regularized likelihood methods". In: *Advances in large margin classifiers* 10.3. Publisher: Cambridge, MA, pp. 61–74 (cit. on p. 51).

Polack, Pierre-Olivier, Jonathan Friedman, and Peyman Golshani (July 2013). "Cellular mechanisms of brain state–dependent gain modulation in visual cortex". en. In: *Nat. Neurosci.* 16.9. Publisher: Nature Publishing Group, pp. 1331–1339 (cit. on p. 6).

Ponzio, Francesco, Andres Eduardo Lorenzo Villalobos, Luca Mesin, Claudio de'Sperati, and Silvestro Roatta (2019). *A human-computer interface based on the "voluntary" pupil accommodative response.* Pages: 53–63 Publication Title: International Journal of Human-Computer Studies Volume: 126 (cit. on p. 15).

Prehn, K, P Kazzer, A Lischke, M Heinrichs, S C Herpertz, and G Domes (June 2013). "Effects of intranasal oxytocin on pupil dilation indicate increased salience of socioaffective stimuli". In: *Psychophysiology* 50.6. Publisher: Psychophysiology (cit. on p. 6).

Privitera, Mattia, Kim David Ferrari, Lukas M von Ziegler, Oliver Sturman, Sian N Duss, Amalia Floriou-Servou, Pierre-Luc Germain, Yannick Vermeiren, Matthias T Wyss, Peter P De Deyn, Bruno Weber, and Johannes Bohacek (Aug. 2020). "A complete pupillometry toolbox for real-time monitoring of locus coeruleus activity in rodents". en. In: *Nat. Protoc.* 15.8, pp. 2301–2320 (cit. on pp. 6, 13, 16, 25, 79).

Qiyuan, J, F Richer, B L Wagoner, and J Beatty (Sept. 1985). "The pupil and stimulus probability". en. In: *Psychophysiology* 22.5, pp. 530–534 (cit. on p. 6).

Quirk, G J, G K Russo, J L Barron, and K Lebron (Aug. 2000). "The role of ventromedial prefrontal cortex in the recovery of extinguished fear". en. In: *J. Neurosci.* 20.16, pp. 6225–6231 (cit. on p. 71).

Quirk, Gregory J and Devin Mueller (Jan. 2008). "Neural mechanisms of extinction learning and retrieval". en. In: *Neuropsychopharmacology* 33.1, pp. 56–72 (cit. on p. 53).

Quirk, Gregory J, Denis Paré, Rick Richardson, Cyril Herry, Marie H Monfils, Daniela Schiller, and Aleksandra Vicentic (Nov. 2010). "Erasing fear memories with extinction training". en. In: *J. Neurosci.* 30.45, pp. 14993–14997 (cit. on p. 54).

Rae, Charlotte L, Laura E Hughes, Michael C Anderson, and James B Rowe (Jan. 2015). "The prefrontal cortex achieves inhibitory control by facilitating subcortical motor pathway connectivity". en. In: *J. Neurosci.* 35.2, pp. 786–794 (cit. on p. 47).

Rajasethupathy, Priyamvada, Sethuraman Sankaran, James H Marshel, Christina K Kim, Emily Ferenczi, Soo Yeun Lee, Andre Berndt, Charu Ramakrishnan, Anna Jaffe, Maisie Lo, Conor Liston, and Karl Deisseroth (Oct. 2015). "Projections from neocortex mediate top-down control of memory retrieval". en. In: *Nature* 526.7575, pp. 653–659 (cit. on pp. 11, 81).

Rajman, Marek and Gerhard Schratt (July 2017). "MicroRNAs in neural development: from master regulators to fine-tuners". en. In: *Development* 144.13, pp. 2310–2322 (cit. on p. 85).

Rasmussen, Carl Edward and Christopher K I Williams (Nov. 2005). *Gaussian Processes for Machine Learning*. en. Cambridge, MA 02142: MIT Press (cit. on p. 51).

Rattiner, Lisa M., Michael Davis, Christopher T. French, and Kerry J. Ressler (May 2004). "Brain-Derived Neurotrophic Factor and Tyrosine Kinase Receptor B Involvement in Amygdala-Dependent Fear Conditioning". en. In: *Journal of Neuroscience* 24.20. Publisher: Society for Neuroscience Section: Behavioral/Systems/Cognitive, pp. 4796–4806. ISSN: 0270-6474, 1529-2401. DOI: 10.1523/JNEUROSCI.5654-03.2004 (cit. on p. 90).

Reh, Rebecca K, Brian G Dias, Charles A Nelson 3rd, Daniela Kaufer, Janet F Werker, Bryan Kolb, Joel D Levine, and Takao K Hensch (Sept. 2020). "Critical period regulation across multiple timescales". en. In: *Proc. Natl. Acad. Sci. U. S. A.* 117.38, pp. 23242–23251 (cit. on p. 87).

Reimer, Jacob, Emmanouil Froudarakis, Cathryn R Cadwell, Dimitri Yatsenko, George H Denfield, and Andreas S Tolias (Oct. 2014). "Pupil fluctuations track fast switching of cortical states during quiet wakefulness". en. In: *Neuron* 84.2, pp. 355–362 (cit. on p. 9).

Reimer, Jacob, Matthew J McGinley, Yang Liu, Charles Rodenkirch, Qi Wang, David A McCormick, and Andreas S Tolias (Nov. 2016). "Pupil fluctuations track rapid changes in adrenergic and cholinergic activity in cortex". en. In: *Nat. Commun.* 7, p. 13289 (cit. on pp. 6, 7, 9, 15, 36, 70).

Reinhard, Günter and Harald Lachnit (2002). "Differential conditioning of anticipatory pupillary dilation responses in humans". eng. In: *Biological Psychology* 60.1, pp. 51–68. ISSN: 0301-0511. DOI: 10.1016/s0301-0511(02)00011-x (cit. on p. 10).

Reinhard, Günter, Harald Lachnit, and Stephan König (Jan. 2006). "Tracking stimulus processing in Pavlovian pupillary conditioning". eng. In: *Psychophysiology* 43.1, pp. 73–83. ISSN: 0048-5772. DOI: 10.1111/j.1469-8986.2006.00374.x (cit. on p. 10).

Repa, J C, J Muller, J Apergis, T M Desrochers, Y Zhou, and J E LeDoux (July 2001). "Two different lateral amygdala cell populations contribute to the initiation and storage of memory". en. In: *Nat. Neurosci.* 4.7, pp. 724–731 (cit. on p. 62).

Ressler, Kerry J, Gayla Paschall, Xiao-Liu Zhou, and Michael Davis (Sept. 2002). "Regulation of Synaptic Plasticity Genes during Consolidation of Fear Conditioning". en. In: *J. Neurosci.* 22.18. Publisher: Society for Neuroscience, pp. 7892–7902 (cit. on p. 71).

Ricciardi, Sara, Federica Ungaro, Melanie Hambrock, Nils Rademacher, Gilda Stefanelli, Dario Brambilla, Alessandro Sessa, Cinzia Magagnotti, Angela Bachi, Elisa Giarda, Chiara Verpelli, Charlotte Kilstrup-Nielsen, Carlo Sala, Vera M Kalscheuer, and Vania Broccoli (2012). "CDKL5 ensures excitatory synapse stability by reinforcing NGL-1–PSD95 interaction in the postsynaptic compartment and is impaired in patient iPSC-derived neurons". In: *Nature Cell Biology* 14.9, pp. 911–923 (cit. on p. 35).

Ripa, Roberto, Luca Dolfi, Marco Terrigno, Luca Pandolfini, Aurora Savino, Valeria Arcucci, Marco Groth, Eva Terzibasi Tozzini, Mario Baumgart, and Alessandro Cellerino (Feb. 2017). "MicroRNA miR-29 controls a compensatory response to limit neuronal iron accumulation during adult life and aging". en. In: *BMC Biol.* 15.1, p. 9 (cit. on p. 96).

Robbins, Trevor W (1997). *Arousal systems and attentional processes.* Issue: 1-3 Pages: 57–71 Publication Title: Biological Psychology Volume: 45 (cit. on p. 35).

Romberg, Carola, Sujeong Yang, Riccardo Melani, Melissa R Andrews, Alexa E Horner, Maria G Spillantini, Timothy J Bussey, James W Fawcett, Tommaso Pizzorusso, and Lisa M Saksida (Apr. 2013). "Depletion of perineuronal nets enhances recognition memory and long-term depression in the perirhinal cortex". en. In: *J. Neurosci.* 33.16, pp. 7057–7065 (cit. on p. 72).

Ronneberger, Olaf, Philipp Fischer, and Thomas Brox (Oct. 2015). "U-Net: Convolutional Networks for Biomedical Image Segmentation". en. In: *Medical Image Computing and Computer-Assisted Intervention – MICCAI 2015.* Springer, Cham, pp. 234–241 (cit. on p. 27).

Rorick-Kehn, Linda M, Jennifer W Witcher, Stephen L Lowe, Celedon R Gonzales, Mary Ann Weller, Robert L Bell, John C Hart, Anne B Need, Jamie H McKinzie, Michael A Statnick, Jeffrey G Suico, David L McKinzie, Sitra Tauscher-Wisniewski, Charles H Mitch, Randall R Stoltz, and Conrad J Wong (Oct. 2014). "Determining pharmacological selectivity of the kappa opioid receptor antagonist LY2456302 using pupillometry as a translational biomarker in rat and human". en. In: *Int. J. Neuropsychopharmacol.* 18.2 (cit. on pp. 15, 16, 79).

Ross, Jordan M and Max L Fletcher (May 2018). "Learning-Dependent and -Independent Enhancement of Mitral/Tufted Cell Glomerular Odor Responses Following Olfactory Fear Conditioning in Awake Mice". en. In: *J. Neurosci.* 38.20, pp. 4623–4640 (cit. on pp. 11, 81).

Rusconi, Laura, Lisa Salvatoni, Laura Giudici, Ilaria Bertani, Charlotte Kilstrup-Nielsen, Vania Broccoli, and Nicoletta Landsberger (Oct. 2008). "CDKL5 expression is modulated during neuronal development and its subcellular distribution is tightly regulated by the C-terminal tail". en. In: *J. Biol. Chem.* 283.44, pp. 30101–30111 (cit. on p. 35).

Ruskell, G. L. (1990). "Accommodation and the nerve pathway to the ciliary muscle: a review". en. In: *Ophthalmic and Physiological Optics* 10.3, pp. 239–242. ISSN: 1475-1313. DOI: 10.1111/j.1475-1313.1990.tb00858.x (cit. on p. 4).

Sacchetti, Benedetto, Bibiana Scelfo, Filippo Tempia, and Piergiorgio Strata (June 2004). "Long-term synaptic changes induced in the cerebellar cortex by fear conditioning". en. In: *Neuron* 42.6, pp. 973–982 (cit. on p. 62).

Sampedro-Castañeda, Marisol, Lucas L Baltussen, André T Lopes, Yichen Qiu, Liina Sirvio, Simeon R Mihaylov, Suzanne Claxton, Jill C Richardson, Gabriele Lignani, and Sila K Ultanir (Dec. 2023). "Epilepsy-linked kinase CDKL5 phosphorylates voltage-gated calcium channel Cav2.3, altering inactivation kinetics and neuronal excitability". en. In: *Nat. Commun.* 14.1, p. 7830 (cit. on p. 80).

Sara, Susan J and Sebastien Bouret (Oct. 2012). "Orienting and reorienting: the locus coeruleus mediates cognition through arousal". en. In: *Neuron* 76.1, pp. 130–141 (cit. on p. 6).

Sara, Susan J. (Mar. 2009). "The locus coeruleus and noradrenergic modulation of cognition". en. In: *Nature Reviews Neuroscience* 10.3. Number: 3 Publisher: Nature Publishing Group, pp. 211–223. ISSN: 1471-0048. DOI: 10.1038/nrn2573 (cit. on p. 7).

Sattler, Nicholas J and Michael Wehr (2020). "A Head-Mounted Multi-Camera System for Electrophysiology and Behavior in Freely-Moving Mice". en. In: *Front. Neurosci.* 14, p. 592417 (cit. on p. 13).

Savander, V, C G Go, J E LeDoux, and A Pitkänen (Oct. 1995). "Intrinsic connections of the rat amygdaloid complex: projections originating in the basal nucleus". en. In: *J. Comp. Neurol.* 361.2, pp. 345–368 (cit. on p. 71).

Schmidt, H S and L D Fortin (1982). "Electronic pupillography in disorders of arousal". In: *Sleeping and waking disorders: indications and techniques. Menlo Park, California: Addison-Wesley*, pp. 127–143 (cit. on p. 1).

Schmitt, Jeroen A J, Wim J Riedel, Eric F P M Vuurman, Monique Kruizinga, and Johannes G Ramaekers (Apr. 2002). "Modulation of the critical flicker fusion effects of serotonin reuptake inhibitors by concomitant pupillary changes". en. In: *Psychopharmacology* 160.4, pp. 381–386 (cit. on p. 6).

Schmitt, Lauren M, Stormi P White, Edwin H Cook, John A Sweeney, and Matthew W Mosconi (May 2018). "Cognitive mechanisms of inhibitory control deficits in autism spectrum disorder". en. In: *J. Child Psychol. Psychiatry* 59.5, pp. 586–595 (cit. on p. 46).

Schramm, Nicole L, Michael P McDonald, and Lee E Limbird (July 2001). "The α2A-Adrenergic Receptor Plays a Protective Role in Mouse Behavioral Models of Depression and Anxiety". en. In: *J. Neurosci.* 21.13. Publisher: Society for Neuroscience, pp. 4875–4882 (cit. on p. 12).

Sekaninova, N, M Mestanik, A Mestanikova, A Hamrakova, and I Tonhajzerova (Aug. 2019). "Novel approach to evaluate central autonomic regulation in attention deficit/hyperactivity disorder (ADHD)". en. In: *Physiol. Res.* 68.4, pp. 531–545 (cit. on p. 48).

Sevenster, Dieuwke, Tom Beckers, and Merel Kindt (Feb. 2014). "Fear conditioning of SCR but not the startle reflex requires conscious discrimination of threat and safety". en. In: *Front. Behav. Neurosci.* 8, p. 32 (cit. on p. 10).

Sg, Manohar and Husain M (Dec. 2015). "Reduced pupillary reward sensitivity in Parkinson's disease". en. In: *NPJ Parkinson's disease* 1. Publisher: NPJ Parkinsons Dis. ISSN: 2373-8057. DOI: 10.1038/npjparkd.2015.26 (cit. on p. 7).

Shepard, Kathryn N, L Cameron Liles, David Weinshenker, and Robert C Liu (Feb. 2015). "Norepinephrine is necessary for experience-dependent plasticity in the developing mouse auditory cortex". en. In: *J. Neurosci.* 35.6, pp. 2432–2437 (cit. on p. 9).

Shimaoka, Daisuke, Kenneth D Harris, and Matteo Carandini (Dec. 2018). "Effects of Arousal on Mouse Sensory Cortex Depend on Modality". en. In: *Cell Rep.* 25.11, p. 3230 (cit. on p. 47).

Shishkina, G T, T S Kalinina, and N N Dygalo (Jan. 2004). "Attenuation of α2A-adrenergic receptor expression in neonatal rat brain by RNA interference or antisense oligonucleotide reduced anxiety in adulthood". In: *Neuroscience* 129.3, pp. 521–528 (cit. on p. 12).

Shishkina, G T, T S Kalinina, N Yu Sournina, D G Saharov, V F Kobzev, and N N Dygalo (July 2002). "Effects of antisense oligodeoxynucleotide to the alpha2A-adrenoceptors on the plasma corticosterone level and on elevated plus-maze behavior in rats". en. In: *Psychoneuroendocrinology* 27.5, pp. 593–601 (cit. on p. 12).

Sievers, J, U Mangold, M Berry, C Allen, and H G Schlossberger (Dec. 1981). "Experimental studies on cerebellar foliation. I. A qualitative morphological analysis of cerebellar fissuration defects after neonatal treatment with 6-OHDA in the rat". en. In: *J. Comp. Neurol.* 203.4. Publisher: Wiley, pp. 751–769 (cit. on p. 12).

Sigal, Yaron M, Haneui Bae, Luke J Bogart, Takao K Hensch, and Xiaowei Zhuang (Apr. 2019). "Structural maturation of cortical perineuronal nets and their perforating synapses revealed by superresolution imaging". en. In: *Proc. Natl. Acad. Sci. U. S. A.* 116.14, pp. 7071–7076 (cit. on p. 71).

Silasi, Gergely, Dongsheng Xiao, Matthieu P Vanni, Andrew C N Chen, and Timothy H Murphy (July 2016). "Intact skull chronic windows for mesoscopic wide-field imaging in awake mice". en. In: *J. Neurosci. Methods* 267, pp. 141–149 (cit. on pp. 30, 50).

Smith, C I Edvard and Rula Zain (Jan. 2019). "Therapeutic Oligonucleotides: State of the Art". en. In: *Annu. Rev. Pharmacol. Toxicol.* 59, pp. 605–630 (cit. on p. 87).

Smith, M. S., U. B. Schambra, K. H. Wilson, S. O. Page, and D. A. Schwinn (Jan. 1999). "Alpha1-adrenergic receptors in human spinal cord: specific localized expression of mRNA encoding alpha1-adrenergic receptor subtypes at four distinct levels". eng. In: *Brain Research. Molecular Brain Research* 63.2, pp. 254–261. ISSN: 0169-328X. DOI: 10.1016/s0169-328x(98)00287-3 (cit. on p. 6).

Sokolov, E N (1963). "Higher nervous functions; the orienting reflex". en. In: *Annu. Rev. Physiol.* 25, pp. 545–580 (cit. on p. 35).

— (July 1990). "The orienting response, and future directions of its development". en. In: *Pavlov. J. Biol. Sci.* 25.3, pp. 142–150 (cit. on p. 35).

Solyman, Omar, Mokhtar Mohamed Ibrahim Abushanab, Andrew R Carey, and Amanda D Henderson (Feb. 2022). "Pilot Study of Smartphone Infrared Pupillography and Pupillometry". en. In: *Clin. Ophthalmol.* 16, pp. 303–310 (cit. on p. 80).

Somel, Mehmet, Song Guo, Ning Fu, Zheng Yan, Hai Yang Hu, Ying Xu, Yuan Yuan, Zhibin Ning, Yuhui Hu, Corinna Menzel, Hao Hu, Michael Lachmann, Rong Zeng, Wei Chen, and Philipp Khaitovich (Sept. 2010). "MicroRNA, mRNA, and protein expression link development and aging in human and macaque brain". en. In: *Genome Res.* 20.9, pp. 1207–1218 (cit. on p. 96).

Sotres-Bayon, Francisco and Gregory J Quirk (Apr. 2010). "Prefrontal control of fear: more than just extinction". en. In: *Curr. Opin. Neurobiol.* 20.2, pp. 231–235 (cit. on p. 71).

Sparks, Sierra, Joana Pinto, Genevieve Hayes, Manuel Spitschan, and Daniel P Bulte (Aug. 2023). "The impact of Alzheimer's disease risk factors on the pupillary light response". en. In: *Front. Neurosci.* 17, p. 1248640 (cit. on p. 80).

St John, Tanya, Annette M Estes, Stephen R Dager, Penelope Kostopoulos, Jason J Wolff, Juhi Pandey, Jed T Elison, Sarah J Paterson, Robert T Schultz, Kelly Botteron, Heather Hazlett, and Joseph Piven (July 2016). "Emerging Executive Functioning and Motor Development in Infants at High and Low Risk for Autism Spectrum Disorder". en. In: *Front. Psychol.* 7, p. 1016 (cit. on p. 46).

Steiger, H. J. and J. A. Büttner-Ennever (Jan. 1979). "Oculomotor nucleus afferents in the monkey demonstrated with horseradish peroxidase". eng. In: *Brain Research* 160.1, pp. 1–15. ISSN: 0006-8993. DOI: 10.1016/0006-8993(79)90596-1 (cit. on p. 4).

Steinwurzel, Cecilia, Silvia Animali, Guido Marco Cicchini, Maria Concetta Morrone, and Paola Binda (July 2020). "Using psychophysical performance to predict short-term ocular dominance plasticity in human adults". en. In: *J. Vis.* 20.7, p. 6 (cit. on p. 9).

Stitt, Iain, Zhe Charles Zhou, Susanne Radtke-Schuller, and Flavio Fröhlich (June 2018). "Arousal dependent modulation of thalamo-cortical functional interaction". en. In: *Nat. Commun.* 9.1, p. 2455 (cit. on p. 35).

Stoll, Josef, Camille Chatelle, Olivia Carter, Christof Koch, Steven Laureys, and Wolfgang Einhäuser (Aug. 2013). "Pupil responses allow communication in locked-in syndrome patients". en. In: *Curr. Biol.* 23.15, R647–8 (cit. on p. 16).

Storbeck, Justin and Gerald L Clore (Sept. 2008). "Affective Arousal as Information: How Affective Arousal Influences Judgments, Learning, and Memory". en. In: *Soc. Personal. Psychol. Compass* 2.5, pp. 1824–1843 (cit. on p. 35).

Strack, A. M. and A. D. Loewy (July 1990). "Pseudorabies virus: a highly specific transneuronal cell body marker in the sympathetic nervous system". eng. In: *The Journal of Neuroscience: The Official Journal of the Society for Neuroscience* 10.7, pp. 2139–2147. ISSN: 0270-6474. DOI: 10.1523/JNEUROSCI.10-07-02139.1990 (cit. on p. 4).

Strassman, A., P. Mason, F. Eckenstein, R. W. Baughman, and R. Maciewicz (Oct. 1987). "Choline acetyltransferase immunocytochemistry of Edinger-Westphal and ciliary ganglion afferent neurons in the cat". eng. In: *Brain Research* 423.1-2, pp. 293–304. ISSN: 0006-8993. DOI: 10.1016/0006-8993(87)90852-3 (cit. on p. 4).

Strauß, Maria, Christine Ulke, Madlen Paucke, Jue Huang, Nicole Mauche, Christian Sander, Tetyana Stark, and Ulrich Hegerl (Mar. 2018). "Brain arousal regulation in adults with attention-deficit/hyperactivity disorder (ADHD)". en. In: *Psychiatry Res.* 261, pp. 102–108 (cit. on p. 35).

Symonds, Joseph D et al. (Aug. 2019). "Incidence and phenotypes of childhood-onset genetic epilepsies: a prospective population-based national cohort". en. In: *Brain* 142.8, pp. 2303–2318 (cit. on p. 34).

Szabadi, Elemer (Aug. 2013). "Functional neuroanatomy of the central noradrenergic system". en. In: *J. Psychopharmacol.* 27.8, pp. 659–693 (cit. on p. 5).

— (Dec. 2018). "Functional Organization of the Sympathetic Pathways Controlling the Pupil: Light-Inhibited and Light-Stimulated Pathways". en. In: *Front. Neurol.* 9, p. 1069 (cit. on p. 6).

Tang, Sheng, Barbara Terzic, I-Ting Judy Wang, Nicolas Sarmiento, Katherine Sizov, Yue Cui, Hajime Takano, Eric D Marsh, Zhaolan Zhou, and Douglas A Coulter (June 2019). "Altered NMDAR signaling underlies autistic-like features in mouse models of CDKL5 deficiency disorder". en. In: *Nat. Commun.* 10.1, p. 2655 (cit. on p. 35).

Tervo, Dougal G. R., Mikhail Proskurin, Maxim Manakov, Mayank Kabra, Alison Vollmer, Kristin Branson, and Alla Y. Karpova (Sept. 2014). "Behavioral Variability through Stochastic Choice and Its Gating by Anterior Cingulate Cortex". English. In: *Cell* 159.1. Publisher: Elsevier, pp. 21–32. ISSN: 0092-8674, 1097-4172. DOI: 10.1016/j.cell.2014.08.037 (cit. on p. 7).

Terzic, Barbara, M Felicia Davatolhagh, Yugong Ho, Sheng Tang, Yu-Ting Liu, Zijie Xia, Yue Cui, Marc V Fuccillo, and Zhaolan Zhou (Oct. 2021). "Temporal manipulation of Cdkl5 reveals essential postdevelopmental functions and reversible CDKL5 deficiency disorder–related deficits". en. In: *J. Clin. Invest.* 131.20. Publisher: American Society for Clinical Investigation, pp. 1–14 (cit. on p. 35).

Tshimanga, Louis Fabrice, Federico Del Pup, Maurizio Corbetta, and Manfredo Atzori (Apr. 2023). "An Overview of Open Source Deep Learning-Based Libraries for Neuroscience". en. In: *NATO Adv. Sci. Inst. Ser. E Appl. Sci.* 13.9, p. 5472 (cit. on p. 79).

Tsukahara, Jason S and Randall W Engle (June 2021). "Is baseline pupil size related to cognitive ability? Yes (under proper lighting conditions)". en. In: *Cognition* 211, p. 104643 (cit. on p. 47).

Tummeltshammer, Kristen, Estée C. H. Feldman, and Dima Amso (Apr. 2019). "Using pupil dilation, eye-blink rate, and the value of mother to investigate reward learning mechanisms in infancy". eng. In: *Developmental Cognitive Neuroscience* 36, p. 100608. ISSN: 1878-9307. DOI: 10.1016/j.dcn.2018.12.006 (cit. on p. 7).

Tyler, William J, Mariana Alonso, Clive R Bramham, and Lucas D Pozzo-Miller (2002). "From acquisition to consolidation: on the role of brain-derived neurotrophic factor signaling in hippocampal-dependent learning". en. In: *Learn. Mem.* 9.5, pp. 224–237 (cit. on p. 97).

Ugalde, Alejandro P, Andrew J Ramsay, Jorge de la Rosa, Ignacio Varela, Guillermo Mariño, Juan Cadiñanos, Jun Lu, José Mp Freije, and Carlos López-Otín (June 2011). "Aging and chronic DNA damage response activate a regulatory pathway involving miR-29 and p53". en. In: *EMBO J.* 30.11, pp. 2219–2232 (cit. on p. 96).

Vallat, Raphael (2018). *Pingouin: statistics in Python*. Issue: 31 Pages: 1026 Publication Title: Journal of Open Source Software Volume: 3 (cit. on p. 31).

Varazzani, Chiara, Aurore San-Galli, Sophie Gilardeau, and Sebastien Bouret (May 2015). "Noradrenaline and dopamine neurons in the reward/effort trade-off: a direct electrophysiological comparison in behaving monkeys". en. In: *J. Neurosci.* 35.20, pp. 7866–7877 (cit. on p. 7).

Veyrac, Alexandra, Antoine Besnard, Jocelyne Caboche, Sabrina Davis, and Serge Laroche (2014). "The transcription factor Zif268/Egr1, brain plasticity, and memory". en. In: *Prog. Mol. Biol. Transl. Sci.* 122, pp. 89–129 (cit. on pp. 62, 71).

Viglione, Aurelia, Raffaele Mazziotti, and Tommaso Pizzorusso (2023). "From pupil to the brain: New insights for studying cortical plasticity through pupillometry". In: *Frontiers in Neural Circuits* 17. ISSN: 1662-5110 (cit. on pp. 5, 8, 80).

Vismara, Matteo, Nicolaja Girone, Giovanna Cirnigliaro, Federica Fasciana, Simone Vanzetto, Luca Ferrara, Alberto Priori, Claudio D'Addario, Caterina Viganò, and Bernardo Dell'Osso (Aug. 2020). "Peripheral Biomarkers in DSM-5 Anxiety Disorders: An Updated Overview". en. In: *Brain Sci* 10.8 (cit. on p. 11).

Visser, Renée M., Michelle I. C. de Haan, Tinka Beemsterboer, Pia Haver, Merel Kindt, and H. Steven Scholte (Aug. 2016). "Quantifying learning-dependent changes in the brain: Single-trial multivoxel pattern analysis requires slow event-related fMRI". eng. In: *Psychophysiology* 53.8, pp. 1117–1127. ISSN: 1540-5958. DOI: 10.1111/psyp.12665 (cit. on p. 10).

Visser, Renée M., Anna E. Kunze, Bianca Westhoff, H. Steven Scholte, and Merel Kindt (May 2015). "Representational similarity analysis offers a preview of the noradrenergic modulation of long-term fear memory at the time of encoding". eng. In: *Psychoneuroendocrinology* 55, pp. 8–20. ISSN: 1873-3360. DOI: 10.1016/j.psyneuen.2015.01.021 (cit. on p. 10).

Visser, Renée M., H. Steven Scholte, Tinka Beemsterboer, and Merel Kindt (Apr. 2013). "Neural pattern similarity predicts long-term fear memory". en. In: *Nature Neuroscience* 16.4. Number: 4 Publisher: Nature Publishing Group, pp. 388–390. ISSN: 1546-1726. DOI: 10.1038/nn.3345 (cit. on p. 10).

Voogd, Lycia D. de, Guillén Fernández, and Erno J. Hermans (July 2016). "Awake reactivation of emotional memory traces through hippocampal-neocortical interactions". eng. In: *NeuroImage* 134, pp. 563–572. ISSN: 1095-9572. DOI: 10.1016/j.neuroimage.2016.04.026 (cit. on p. 10).

Vouimba, Rose-Marie and Mouna Maroun (July 2011). "Learning-Induced Changes in mPFC–BLA Connections After Fear Conditioning, Extinction, and Reinstatement of Fear". en. In: *Neuropsychopharmacology* 36.11. Publisher: Nature Publishing Group, pp. 2276–2285 (cit. on p. 53).

Vries, Lyssa de, Lyssa de Vries, Iris Fouquaet, Bart Boets, Gunnar Naulaers, and Jean Steyaert (2021). *Autism spectrum disorder and pupillometry: A systematic review and meta-analysis*. Pages: 479–508 Publication Title: Neuroscience & Biobehavioral Reviews Volume: 120 (cit. on p. 48).

Wainio-Theberge, Soren, Annemarie Wolff, and Georg Northoff (June 2021). "Dynamic relationships between spontaneous and evoked electrophysiological activity". en. In: *Communications Biology* 4.1. Publisher: Nature Publishing Group, pp. 1–17 (cit. on p. 35).

Wainstein, G, D Rojas-Líbano, N A Crossley, X Carrasco, F Aboitiz, and T Ossandón (2017). "Pupil Size Tracks Attentional Performance In Attention-Deficit/Hyperactivity Disorder". In: *Scientific Reports* 7.1, pp. 1–9 (cit. on pp. 12, 40).

Wang, Chin-An, Talia Baird, Jeff Huang, Jonathan D Coutinho, Donald C Brien, and Douglas P Munoz (2018). *Arousal Effects on Pupil Size, Heart Rate, and Skin Conductance in an Emotional Face Task*. Pages: 1–13 Publication Title: Frontiers in Neurology Volume: 9 (cit. on p. 36).

Wang, Chin-An, Susan E Boehnke, Brian J White, and Douglas P Munoz (Mar. 2012). "Microstimulation of the monkey superior colliculus induces pupil dilation without evoking saccades". en. In: *J. Neurosci.* 32.11, pp. 3629–3636 (cit. on p. 6).

Wang, Chin-An and Douglas P Munoz (Sept. 2014). "Modulation of stimulus contrast on the human pupil orienting response". en. In: *Eur. J. Neurosci.* 40.5, pp. 2822–2832 (cit. on p. 6).

— (Aug. 2015). "A circuit for pupil orienting responses: implications for cognitive modulation of pupil size". en. In: *Curr. Opin. Neurobiol.* 33, pp. 134–140 (cit. on pp. 18, 35, 47).

Wang, Haitao et al. (Aug. 2019). "Direct auditory cortical input to the lateral periaqueductal gray controls sound-driven defensive behavior". en. In: *PLoS Biol.* 17.8, e3000417 (cit. on p. 18).

Wang, I-Ting Judy, Megan Allen, Darren Goffin, Xinjian Zhu, Andrew H Fairless, Edward S Brodkin, Steve J Siegel, Eric D Marsh, Julie A Blendy, and Zhaolan Zhou (Dec. 2012). "Loss of CDKL5 disrupts kinome profile and event-related potentials leading to autistic-like phenotypes in mice". en. In: *Proc. Natl. Acad. Sci. U. S. A.* 109.52, pp. 21516–21521 (cit. on pp. 34, 35).

Wang, Wenyuan, Ester J. Kwon, and Li-Huei Tsai (Jan. 9, 2012). "MicroRNAs in learning, memory, and neurological diseases". In: *Learning & Memory* 19.9. Company: Cold Spring Harbor Laboratory Press Distributor: Cold Spring Harbor Laboratory Press Institution: Cold Spring Harbor Laboratory Press Label: Cold Spring Harbor Laboratory Press Publisher: Cold Spring Harbor Lab, pp. 359–368. ISSN: 1072-0502, 1549-5485. DOI: 10.1101/lm.026492.112 (cit. on p. 85).

Weaving, Linda S, John Christodoulou, Sarah L Williamson, Kathie L Friend, Olivia L D McKenzie, Hayley Archer, Julie Evans, Angus Clarke, Gregory J Pelka, Patrick P L Tam, Catherine Watson, Hooshang Lahooti, Carolyn J Ellaway, Bruce Bennetts, Helen Leonard, and Jozef Gécz (Dec. 2004). "Mutations of CDKL5 cause a severe neurodevelopmental disorder with infantile spasms and mental retardation". en. In: *Am. J. Hum. Genet.* 75.6, pp. 1079–1093 (cit. on p. 35).

Weike, Almut I, Harald T Schupp, and Alfons O Hamm (Jan. 2007). "Fear acquisition requires awareness in trace but not delay conditioning". en. In: *Psychophysiology* 44.1, pp. 170–180 (cit. on p. 10).

Weinshenker, David and Jason P Schroeder (Dec. 2006). "There and Back Again: A Tale of Norepinephrine and Drug Addiction". en. In: *Neuropsychopharmacology* 32.7. Publisher: Nature Publishing Group, pp. 1433–1451 (cit. on p. 11).

Wierda, Stefan M, Hedderik van Rijn, Niels A Taatgen, and Sander Martens (May 2012). "Pupil dilation deconvolution reveals the dynamics of attention at high temporal resolution". en. In: *Proc. Natl. Acad. Sci. U. S. A.* 109.22, pp. 8456–8460 (cit. on p. 15).

Wiesel, T N and D H Hubel (Nov. 1963). "SINGLE-CELL RESPONSES IN STRIATE CORTEX OF KITTENS DEPRIVED OF VISION IN ONE EYE". en. In: *J. Neurophysiol.* 26, pp. 1003–1017 (cit. on p. 11).

Wingo, Aliza P, Mengli Wang, Jiaqi Liu, Michael S Breen, Hyun-Sik Yang, Beisha Tang, Julie A Schneider, Nicholas T Seyfried, James J Lah, Allan I Levey, David A Bennett, Peng Jin, Philip L De Jager, and Thomas S Wingo (Feb. 2022). "Brain microRNAs are associated with variation in cognitive trajectory in advanced age". en. In: *Transl. Psychiatry* 12.1, p. 47 (cit. on pp. 92, 96).

Winston, Molly et al. (Feb. 2020). "Pupillometry measures of autonomic nervous system regulation with advancing age in a healthy pediatric cohort". en. In: *Clin. Auton. Res.* 30.1, pp. 43–51 (cit. on pp. 11, 15).

Wood, Katherine C, Christopher F Angeloni, Karmi Oxman, Claudia Clopath, and Maria N Geffen (Mar. 2022). "Neuronal activity in sensory cortex predicts the specificity of learning in mice". en. In: *Nat. Commun.* 13.1, p. 1167 (cit. on pp. 11, 81).

Woods, Adam J, John W Philbeck, and Philip Wirtz (Apr. 2013). "Hyper-Arousal Decreases Human Visual Thresholds". In: *PLoS One* 8.4. Publisher: Public Library of Science, e61415 (cit. on p. 47).

Xiong, Xiaorui R, Feixue Liang, Brian Zingg, Xu-Ying Ji, Leena A Ibrahim, Huizhong W Tao, and Li I Zhang (June 2015). "Auditory cortex controls sound-driven innate defense behaviour through corticofugal projections to inferior colliculus". en. In: *Nat. Commun.* 6, p. 7224 (cit. on p. 18).

Yamada, Kota and Koji Toda (Dec. 2022). "Pupillary dynamics of mice performing a Pavlovian delay conditioning task reflect reward-predictive signals". en. In: *Front. Syst. Neurosci.* 16, p. 1045764 (cit. on pp. 10, 97).

Yiu, Yuk-Hoi, Moustafa Aboulatta, Theresa Raiser, Leoni Ophey, Virginia L Flanagin, Peter Zu Eulenburg, and Seyed-Ahmad Ahmadi (Aug. 2019). "DeepVOG: Open-source pupil segmentation and gaze estimation in neuroscience using deep learning". en. In: *J. Neurosci. Methods* 324, p. 108307 (cit. on pp. 16, 25, 79).

You, Sooyeoun, Jeong-Ho Hong, and Joonsang Yoo (Sept. 2021). "Analysis of pupillometer results according to disease stage in patients with Parkinson's disease". en. In: *Scientific Reports* 11.1. Number: 1 Publisher: Nature Publishing Group, p. 17880. ISSN: 2045-2322. DOI: 10.1038/s41598-021-97599-4 (cit. on pp. 7, 80).

Zandi, Babak, Moritz Lode, Alexander Herzog, Georgios Sakas, and Tran Quoc Khanh (June 2021). "PupilEXT: Flexible Open-Source Platform for High-Resolution Pupillometry in Vision Research". en. In: *Front. Neurosci.* 15, p. 676220 (cit. on pp. 13, 79).

Zhang, Sheng, Sien Hu, Herta H Chao, Jaime S Ide, Xi Luo, Olivia M Farr, and Chiang-Shan R Li (2014). *Ventromedial prefrontal cortex and the regulation of physiological arousal.* Issue: 7 Pages: 900–908 Publication Title: Social Cognitive and Affective Neuroscience Volume: 9 (cit. on p. 47).

Zhuang, Juntang, Tommy Tang, Yifan Ding, Sekhar Tatikonda, Nicha Dvornek, Xenophon Papademetris, and James S Duncan (Oct. 2020). "AdaBelief Optimizer: Adapting Stepsizes by the Belief in Observed Gradients". In: _eprint: 2010.07468 (cit. on p. 29).

Appendices

1 Supplmentary information for Part II

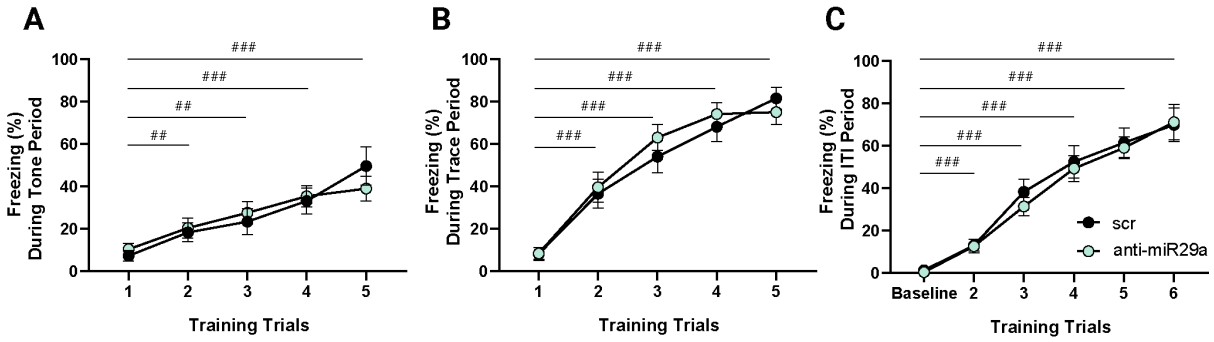

Figure S.1: **Learning curves during TFC training**. Both anti-miR29a and scr treated mice showed the same learning profile during conditioning for all the different TCF training intervals. **(A)** Freezing during Tone presentation (Two-way RM ANOVA, main effect of treatment $F(1, 19) = 8.73 \times 10^{-4}$, $p = 0.98$; main effect of trials $F(2.61, 49.71) = 23.77$, $p < 0.0001$; trials × treatment interaction $F(4, 76) = 1.21$, $p = 0.31$). **(B)** Freezing during Trace period (Two-way RM ANOVA, main effect of treatment $F(1, 19) = 0.22$, $p = 0.63$; main effect of trials $F(3.43, 65.28) = 58.40$, $p < 0.0001$; trials × treatment interaction $F(4, 76) = 0.64$, $p = 0.63$). **(C)** Freezing during ITI (Two-way RM ANOVA, main effect of treatment $F(1, 19) = 0.14$, $p = 0.70$; main effect of trials $F(2.36, 44.86) = 78.13$, $p < 0.0001$; trials × treatment interaction $F(5, 95) = 0.21$, $p = 0.95$). scr: N = 10, anti-miR29a N = 11; Tukey's multiple comparison vs s trial 1 or baseline, ## P-value < 0.01, ### P-value < 0.001. PND= Postnatal Day.

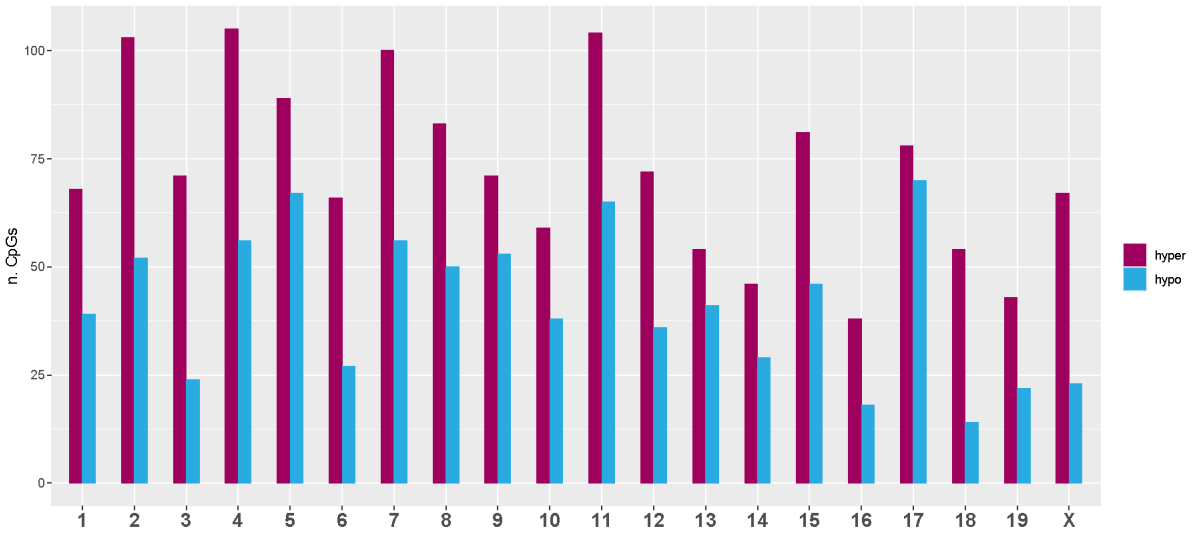

Figure S.2: **absLFC < 10 anti-miR29a vs ctr**.

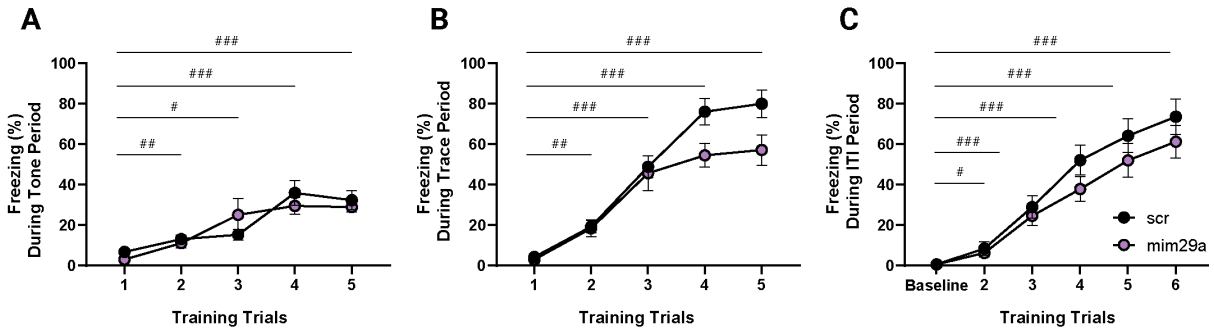

Figure S.3: **Learning curves during TFC training.** Both mim29a and scr treated mice showed the same learning profile during conditioning for all the different TCF training intervals. **(A)** Freezing during Tone presentation (Two-way RM ANOVA, main effect of treatment $F(1, 14) = 0.11$, $p = 0.75$; main effect of trials $F(2.52, 35.24) = 21.48$, $p < 0.0001$; trials × treatment interaction $F(4, 56) = 1.53$, $p = 0.20$). **(B)** Freezing during Trace period (Two-way RM ANOVA, main effect of treatment $F(1, 14) = 4.18$, $p = 0.06$; main effect of trials $F(3.79, 39.14) = 64.76$, $p < 0.0001$; trials × treatment interaction $F(4, 56) = 2.5$, $p = 0.053$). **(C)** Freezing during ITI (Two-way RM ANOVA, main effect of treatment $F(1, 14) = 0.58$, $p = 0.23$; main effect of trials $F(2.64, 36.99) = 66.44$, $p < 0.0001$; trials × treatment interaction $F(5, 70) = 0.83$, $p = 0.53$). scr: N = 10, anti-miR29a N = 11; Tukey's multiple comparison vs s trial 1 or baseline, #P-value < 0.05, ## P-value < 0.01, ### P-value < 0.001. PND= Postnatal Day.